The role of neural oscillations in the visual system and their relation to conscious perception

Miaomiao Yu

Doctor of Philosophy

University of York
Psychology

June 2020

Thesis Abstract

Neural oscillations are intrinsically linked with attention, vigilance and featural sensitivity and therefore often associated with visual perception. However, the neural oscillation literature remains conflicted on several issues. Here, I describe four experiments investigating these conflicts using a variety of experimental and analysis techniques.

We first explored the relationship between the inhibitory neurotransmitter GABA and gamma frequency oscillations in the rodent visual cortex. We found no evidence that synaptic and extrasynaptic GABA concentration altered gamma oscillations, suggesting that GABAergic inhibition cannot be linked directly to GABA concentration and instead depend on postsynaptic receptor kinetics.

The second chapter examined how spontaneous alpha activity related to performance in an orientation discrimination task. Alpha amplitude was a significant predictor of reaction time but not task accuracy. The results suggested that alpha can modulate visual perception through top-down mechanisms. Interestingly, we also found that the relationship between alpha activity and task accuracy was determined by the subject's task expertise.

The third chapter examined how *exogenous* rhythms (generated by chromatic gratings) within visual cortex may interact with ongoing *endogenous* oscillations. Univariate analysis of single EEG channels revealed significantly higher endogenous power during chromatic than achromatic stimulation. An additional multivariate classifier showed distinct patterns of activity at very high frequencies, suggesting phase coupling between exogenous and endogenous signals. This finding was extended in the final chapter, which examined the neural correlates of rapid chromatic stimulation. Robust BOLD responses were found even when stimuli flickered above the consciously perceptible frequency, indicating that the temporal filtering stage limiting perception is later than V4. Additionally, chromatic preference in 'colour area' V4 was strongly dependent on stimulus frequency.

List of Contents

List of Tables

List of Figures

Acknowledgements

This thesis would not have been possible without the input of some incredible people. First and foremost, I would like to extend the *biggest* thank you to my supervisor, Professor Alex Wade. Besides extraordinary knowledge and patience, your contagious enthusiasm created an environment that fostered creativity and made research exciting. Thank you for all your support in not only PhD work, but also my welfare and data science pursuits. I am undoubtedly a better researcher because of you.

Next, I would like to thank Professor Miles Whittington and Dr Stephen Hall, for their generosity in opening up their lab to me. Miles: for your tremendously helpful guidance and patience during our long discussions. Stephen: for being a slice preparation wizard and breaking up the long days with your humour. Despite my limited time in the Whittington lab, I have learned so much from the both of you.

I'd also like to thank my thesis advisory panel, Dr Heidi Baseler, Dr Shirley-Ann Rueschemeyer and Dr Aneurin Kennerley, for their resolute support and advice throughout the three years. I'd also like to extend an extra special thanks to Dr Andre Gouws and the entire YNiC team for their help and patience during the fMRI project (especially with the fussier than usual set-up). Additionally, I'd like to thank Dr Dan Baker, not only for your help during my PhD, but the opportunity of working as an RA during my undergraduate, which greatly strengthened my interest and confidence in research.

I'd also like to thank my colleagues in the Department of Psychology: especially Milena, Lauren, Greta and Ryan, for their help in Matlab, fMRI protocols and occasionally at the climbing wall. To my friends outside of academia, in particular Anthony, Sam P, Flinn, Ben and Oisín: you've kept me laughing through some of the toughest times and your friendships are invaluable to me. Not forgetting a heartfelt thank you to Martin: you are a 6/10 Level 0 but an incredible pillar of support for whom I am deeply grateful.

Finally, I’d like to thank my parents. Mum: for always believing in me and celebrating my achievements (no matter how small). Dad: for championing my interest in science and being my role model both as a researcher and a person. Just like you dedicated your thesis to me 27 years ago, I dedicate this thesis to you.

Author’s Declarations

I declare that this thesis is a presentation of original work and I am the sole author. This work has not previously been presented for an award at this, or any other, University. All sources are acknowledged as References.

Conference abstracts from work presented in this thesis:

1. M. Yu & A. R. Wade (2018). Frequency domain classification of chromatic SSVEP, Optical Society America (OSA) Fall Vision Meeting, 2018 and Colour Group (GB) Awards Meeting, 2018 (as an award recipient), Applied Vision Association (AVA) Christmas Meeting 2018

2. M. Yu & A. R. Wade (2017). Using EEG to measure slow modulations in the human koniocellular pathway, Applied Vision Association (AVA) Christmas Meeting 2017.

1 Chapter 1: Introduction to endogenous oscillations and their role in visual perception

1.1 Introduction to neural oscillations

Neural oscillations are periodic cycles of electrical activity originating from the central nervous system. These oscillations can be evoked through multiple mechanisms and are generally divided into two categories: *exogenous* oscillations, which are produced directly in response to external stimulation and *endogenous* oscillations, which are mostly produced by interactions between different neuronal networks. Due to the lack of a periodic regulator, endogenous oscillations are more spontaneous in nature than exogenous activity. They are thought to provide temporal frameworks for synchronising activity between spatially distinct areas of the cortex during multiple cognitive processes (Lakatos et al., 2005).

The earliest descriptions of endogenous rhythms are found in the work of Hans Berger, who made the first human electroencephalography (EEG) recording in 1924. Since then, endogenous rhythms have been explored widely in different fields, such as Parkinson's disease (Holt et al., 2019; Little & Brown, 2014) and brain-computer interfaces for both clinical and neurotypical populations (Han et al., 2019; Popescu et al., 2007; Sellers & Donchin, 2006; Silvoni et al., 2009). A main reason for the extensive research on endogenous rhythms is the idea that endogenous neural oscillations can inform us of the subject's internal state. Endogenous oscillations are typically categorised into functional bands based on their temporal frequency. Commonly, faster rhythms like *alpha (8-12Hz)*, *beta (13-25Hz)* and *gamma (25-80Hz)* are related to conscious perception, attention and sensory stimulation (Busch et al., 2004; Hanslmayr et al., 2007; Meador et al., 2002; Romei et al., 2008), while

slower rhythms, such as *delta (0.5-4Hz)* and theta are associated with sleep, memory consolidation and passive, repetitive behaviour (Cajochen et al., 1999; Rasch & Born, 2013; Vanderwolf, 1969). Studies often measure a subject's endogenous activity using neuroimaging or electrophysiology techniques and relate those measurements to that individual's experience and behaviour.

1.1.1 Production of neural oscillations

Neurons function and communicate through electrical signals, which are the transmitted when the neuron reaches critical membrane potential. An action potential is then generated: a temporarily induced change in membrane potential that can travel away from the neuron's body along the axon. Once an action potential has been generated, the neuron enters a temporary inhibitory post-synaptic potential (IPSP) state where further firing is unlikely. The neuronal membrane is regulated by inputs from both excitatory and inhibitory receptors, which, in turn, bind inhibitory and excitatory neuromodulatory chemicals released from other neurons. These receptors change the neuronal membrane potential through the influx or release of positively charged or negatively charged ions. Neurons typically have a resting potential of -70mV and action potential *threshold* of -55mV, meaning an increase in voltage towards zero (or 'depolarisation') is excitatory as it brings the neuron closer to the firing threshold. In comparison, a decrease in neuron membrane potential (also known as hyperpolarisation) would be considered as an inhibitory mechanism.

Endogenous oscillations are produced when neuronal ensembles shift between excitatory and inhibitory states even in the absence of time-locked external stimuli. Unsurprisingly, the properties of endogenous rhythms are highly dependent on the synaptic excitation to inhibition ratio (Brunel & Wang, 2003; Whittington et al., 1995). In particular, their *frequency* is determined by the amount of time required for each round of IPSP to decay, while the *amplitude* is determined by the size of the neuron cluster that is firing in synchrony. Neuronal firing can occur spontaneously and independently, but the firing of a single neuron is not detectable using non-invasive recording techniques. Endogenous oscillations measured with EEG or

magnetoencephalography (MEG) are the product of clusters of large numbers of cortical neurons firing in synchrony.

1.2 Conflicts in the literature: endogenous rhythms and visual perception

Cognitive sciences often consider endogenous rhythms to be a marker of internal state. Internal states are intrinsically linked with neuronal mechanisms, and all three parameters are regulated by inhibitory and excitatory mechanisms. Many studies describing the impact of endogenous oscillations on *visual processing* focus on *alpha (8-12Hz)* and *gamma (25-80Hz)* rhythms. Both endogenous rhythms are thought to provide temporal synchronisations between spatially distinct areas of the brain (Palva & Palva, 2011) and are regulated by sensory inputs into the system. Alpha is the dominant endogenous activity in the occipital cortex and associated with visual attention. Gamma rhythms are more task specific: predominantly studied in the hippocampus, which performs cognitive functions that often require synchronisation between distinct brain regions, such as memory retrieval (Colgin & Moser, 2010). Visual gamma oscillations are said to be involved in feature binding, where low-level components of a visual input are integrated to form a global perception (Gray et al., 1989). These rhythms provide a means of communication between clusters of neurons and visual attention modulations and those found in early visual areas are involved in feedforward mechanisms involved in bottom-up information processing (Pascal Fries, 2009; van Kerkoerle et al., 2014a).

Previous experiments have demonstrated repeatedly that performance during working memory (Chen et al., 2014), somatosensory (Gaetz et al., 2011; Monto et al., 2008) and auditory (Wehr & Zador, 2003) tasks can be manipulated by changing the amount of inhibitory drive within the system. Similarly, sensitivity to low-level visual features itself are also dependent on the level of inhibition in the neural network. Contrast level, for example, correlates positively with the frequency (Ray & Maunsell, 2011) and amplitude (Hall et al., 2005) of gamma in V1. This relationship was also found for stimulus size, where an increase in stimulus size is linked to an

increase of averaged gamma band power (Busch et al., 2004; Gieselmann & Thiele, 2008). Finally, stimulus eccentricity is also related to gamma activity: where peak gamma frequency is found with foveal stimulation and decreases as the stimulus gradually move towards the periphery (Lima et al., 2010; van Pelt & Fries, 2013).

With many of these studies suggesting a simple, monotonic relationship between gamma activity and stimulus intensity, the role of endogenous rhythm in visual perception appears relatively straightforward. However, the literature remains conflicted on several issues, which extend across neurophysiological, electrophysiological and behavioural domains. This thesis examines some of these questions. The topics that will be discussed in this introduction include the role of GABA in gamma rhythm production, the modulation of visual perception by alpha rhythms and the interaction between endogenous activity with externally driven responses.

1.2.1 The role of GABA in gamma oscillations

As previously mentioned, due to their well-documented relationship with visual mechanisms, gamma oscillations are one of the most commonly studied endogenous rhythms in visual neuroscience. The production of gamma oscillation is thought to be regulated by the chemical gamma-aminobutyric acid (GABA), one of the primary inhibitory neurotransmitters found in the mammalian nervous system. The main function of GABA is to control the timing of action potentials by temporarily 'halting' neuronal firing through a process of hyperpolarisation. GABA molecules are released by a presynaptic GABAergic interneuron into the synaptic space, where they diffuse and bind onto postsynaptic GABA receptors. This causes the opening of channels on the postsynaptic neuron membrane, specifically: chloride channels for $GABA_A$ subtype and potassium channels for $GABA_B$ subtype. In the first case, the postsynaptic neuron experiences an influx of mainly negatively charged chloride ions known as the inhibitory postsynaptic current (IPSC). As a result, the postsynaptic neuron's electrical potential becomes more fixed at chloride reversal potential (-70mV for most neurons) and the neuron is hindered in reaching action potential threshold. A single interneuron can evoke this negative electrical state or IPSP

simultaneously in multiple GABA-mediated neurons. As a result, the silenced cells all fire in synchrony once the IPSP has terminated, producing the oscillatory signals common to all neurons in the local interconnected network.

The relationship between resting GABA concentration and gamma oscillations in humans has been studied repeatedly but with conflicting results. In an influential study by Muthukumaraswamy et al. (2009), resting GABA concentration was quantified by magnetic resonance spectroscopy (MRS) and visual gamma oscillations were induced using a grating stimulus and measured with MEG. The authors found that the frequency of visual gamma oscillations correlated positively with visual cortex resting GABA concentration. Additionally, both visual gamma frequency and visual GABA concentration correlated negatively with corresponding BOLD amplitudes (see **Fig. 1.1** A – C). The same group extended their neurobiological findings by examining how they affected visual perception (Edden et al., 2009). Gamma frequency and GABA concentration were found to be significant predictors of orientation sensitivity in human observers: higher GABA concentration and gamma frequency were associated with lower orientation thresholds (see **Fig. 1.1** D – E). The authors proposed two explanations for their findings: first, inhibition which can arise from GABAergic interneurons has been linked to tighter orientation tuning in neurons. This is because the width of tuning curves is governed in part by inhibition of off-tuned responses. Secondly, gamma band rhythms are widely regarded as a critical component of feature binding, where the activity of neuronal clusters processing different visual features are synchronised, producing a global, coherent percept of a visual stimulus (Christoph, 2011; Honkanen et al., 2015; Morgan et al., 2011; Samonds & Bonds, 2005). An increase in resting GABA might reflect a more optimal environment for feature binding, which can result in a general improvement of visual task performance.

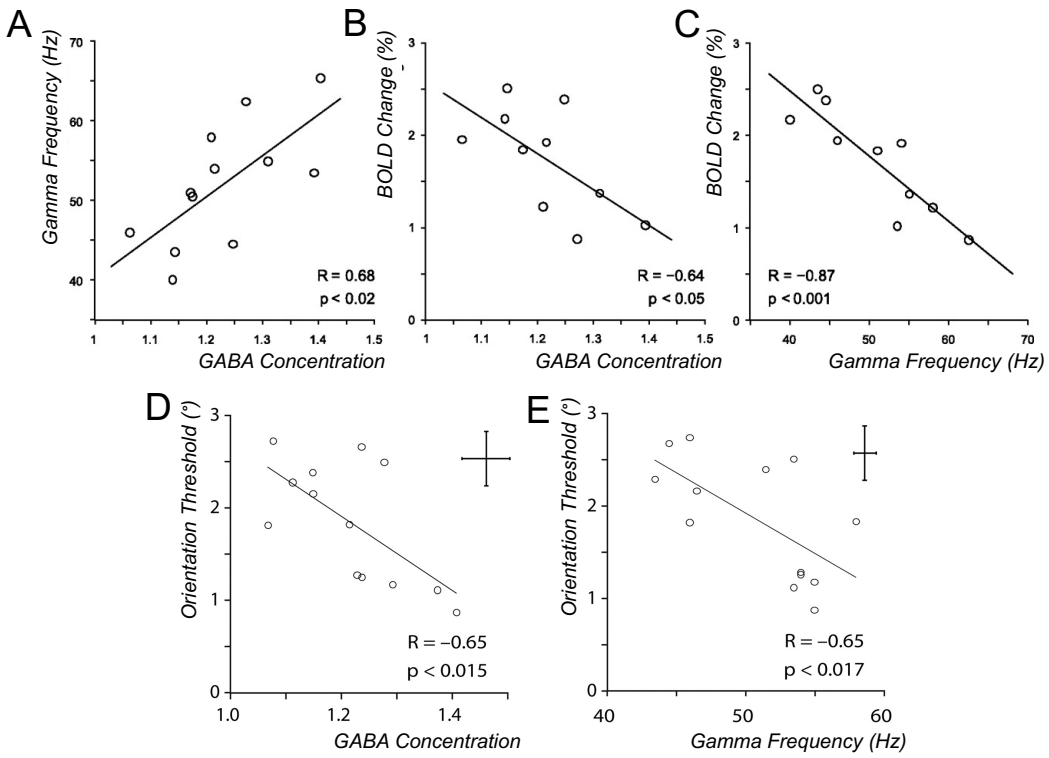

Fig. 1.1 *A – C from Muthukumaraswamy et al. (2009). Relationship between peak gamma frequency versus GABA concentration, BOLD response magnitude and GABA concentration and BOLD response magnitude and peak gamma oscillation frequency respectively. (A) shows a positive correlation between GABA level and gamma frequency. D – E from Edden et al., (2009): Orientation discrimination thresholds as a function of GABA concentration and gamma frequency respectively. Variances of the data (averaged across participants) are represented by crosshairs in the upper right corner. Variance is calculated as the average SEM for the four subjects with repeated data for gamma frequency, averaged difference between two GABA concentrations tested in the same session for GABA and averaged SEM of last ten staircase reversals for orientation thresholds.*

The striking results discussed above have not, however, been easy to replicate (Cousijn et al., 2014). Despite recruiting a larger sample of participants (12 compared to five in Muthukumaraswamy et al. (2009)) and replicating key details such as only recruiting male participants, Cousijn et al. (2014) found no significant associations between GABA concentration, glutamate concentration or GABA-glutamate ratio and gamma frequency or amplitude (see **Fig. 1.2**). The difference in findings demonstrates that while GABA has been repeatedly shown to play a critical

role in gamma rhythm production, the exact relationship between resting GABA concentration in humans and gamma oscillations is not straightforward.

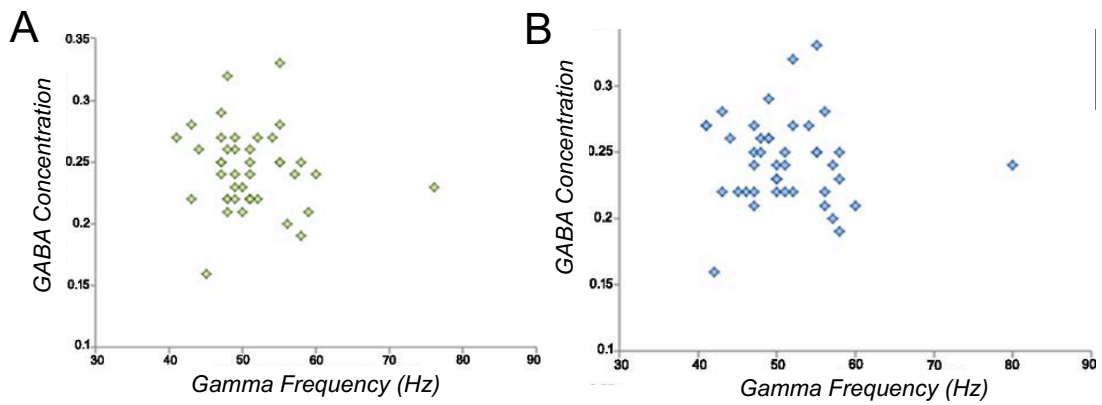

Fig. 1.2 *Adapted from Cousijn et al. (2014): Scatterplots showing no correlation between GABA concentration and (A) gamma peak frequency (Hz) based on the peak activation and (B) gamma peak frequency (Hz) in the MRS voxel where GABA was measured.*

Studies of the role of GABA in multiple sensory modalities and cognitive functions extended beyond visual cortex. But similarly, these experiments did not provide a unified framework of how GABA concentrations correlated with gamma or how this impacted on the individual's behaviour. For example, one study found that GABA and gamma *frequency* (not amplitude) within the motor cortex demonstrated a strong, linear relationship (Gaetz et al., 2011). Another study, however, found that gamma frequency was only related to GABA concentrations during encoding phase of a working memory task, and instead, gamma amplitude was correlated significantly with GABA concentrations during all stages of the working memory task (Chen et al., 2014). This correlation survived in both control and schizophrenic patients, even with lower baseline gamma amplitudes in the clinical group. A third study found no relationship between GABA or glutamate concentration, or the ratio between these two metabolites with gamma responses in the auditory cortex (Wyss et al., 2017). It is possible that the GABA-gamma relationship is simply unique to specific task demands. However, a later study which found that gamma oscillations in the visual cortex shared significant correlations with the density of $GABA_A$ receptor instead of GABA concentrations alone (Kujala et al., 2015) meant that the differing findings could also be explained by unreliable GABA measurements. Furthermore,

high between-subject variability for visual gamma frequency were common in human studies (Kujala et al., 2015; Wyss et al., 2017).

Ultimately, these conflicts reflect two unresolved issues in the field: the mechanisms of gamma production networks and methodological issues surrounding MRS. MRS is commonly criticised for being vulnerable to ‘macromolecule contamination’, where signals from macromolecules are detected and mistaken for that of the intended neurotransmitter. The aforementioned studies used different MRS sequences and voxel sizes, which may contribute to the differences in findings. Nevertheless, addressing the biology of gamma wave generation is especially critical, because while theories agree that GABA is involved in generating gamma rhythms, different computational networks conjecture almost opposite effects on gamma oscillations when GABA level is changed.

One of the primary models for producing gamma band oscillations is described in (Brunel & Wang, 2003). The authors propose intrinsic neuronal ‘loops’ consisting of excitatory pyramidal cells and inhibitory interneurons, where activation of the former prompts the simultaneous firing of multiple inhibitory interneurons. The inhibition generated then suppresses the excitatory neurons, which will produce subsequent cycles of gamma rhythms once the inhibition wears off. The frequency of the resultant gamma oscillation, known as pyramidal-interneuronal gamma (PING), is hence modulated by the ratio of excitatory to inhibitory interconnections and their excitatory postsynaptic potential (EPSP) or IPSP time frame respectively. The model anticipates that stronger inhibition would disrupt the excitation-inhibition balance and result in faster oscillations, which is supported by the results from Muthukumaraswamy et al. (2009). Additionally, the Brunel and Wang model suggests that the production of gamma oscillations does not require individual interneurons to fire at gamma band rates as this endogenous rhythm emerges from the synchronised firing of inhibitory and excitatory neuronal clusters. This is a common feature of population rhythms and has been observed in the macaque V1, where peak local field potential (LFP) amplitude corresponded to gamma frequency band independently of the spiking rate of individual neurons (Henrie & Shapley, 2005).

On the other hand, earlier studies involving hippocampal slice recordings showed that individual interneurons could transiently exhibit similar gamma band firing profiles (Traub et al., 1996; Whittington et al., 1995). When the inhibitory effect of GABA was attenuated using bicuculline (GABA antagonist), the gamma frequency of the hippocampal neurons *increased*. Mu opioids demonstrate a similar effect, reducing the probability of GABA release from presynaptic terminals receptors. As shown in Whittington et al. (1998), the administration of mu opioids can cause an increase of frequency and decrease of amplitude in endogenous oscillations. Both studies indicated that rhythm frequency is determined by inhibition strength: smaller IPSPs attenuate spiking for less time than larger IPSPs. These observations required an extension of the Brunel and Wang model and suggested that the relationship between GABA and endogenous gamma rhythm is more complex.

One of the primary methods of measuring metabolite concentrations in human electrophysiology studies is MRS. MRS uses carefully designed pulse sequences to detect a range of different metabolites within a selected voxel. When exposed to a magnetic field, different chemical nuclei exhibit different spins around their axes. This allows the metabolite to be identified based on its unique response (Tognarelli et al., 2015).

Despite being a popular GABA measuring technique, MRS has been met with several criticisms over the years. The problem can be summarised in two stages. Firstly, it is hard to optimise MRS sequences to measure glutamate or glutamatergic processes. This becomes an issue as GABA and glutamate are intrinsically linked: glutamate is the primary source of excitation for GABAergic neurons and many GABAergic functions depend on the excitatory-inhibitory balance between GABA and glutamate (Stagg et al., 2009, 2011b). Studies linking neurochemical data to behaviour should be able to account for glutamate levels as well, but this is not always the case. These concerns were mentioned in Cousijn et al.'s (2014) study, but also raised frequently in recent years (Duncan et al., 2019; Puts & Edden, 2012; Stagg, 2014; Stagg et al., 2011a), and even acknowledged in the paper they criticised (Muthukumaraswamy et al., 2009).

Secondly, GABA within a neuron exists in two 'pools': cytoplasmic, produced mainly from glutamate through tonic activation, and vesicular, which in itself is split into multiple 'sub-pools'. Only the 'readily releasable' sub-pool of vesicular GABA (usually found in close proximity to the synapse) is relevant for synaptic transmission, the others mainly exist as a reserve (Martin & Rimvall, 1993). In fact, the consensus is that cytoplasmic GABA is involved predominantly in metabolism while vesicular GABA is involved in neuronal inhibition. Small doses of GABA found outside of neurons are thought to play a role in tonic cortical inhibition (Belelli et al., 2009). A main issue of MRS is that is can only inform the *total* GABA concentration within the selected voxel and is unable to distinguish between different pools of GABA. This suggests that it is inaccurate to attribute specific behavioural or electrophysiological observations to MRS-quantified GABA.

In fact, a number of pharmacological experiments have been focused on examining the effect of GABA on gamma oscillations. Many of these involve the use of GABA agonists, which enhance postsynaptic $GABA_A$ responses directly, while others controlled the concentration of synaptic GABA using reuptake inhibitors. Since they do not alter total GABA concentration, MRS would remain insensitive to these two mechanisms. However, their roles in gamma rhythm production are extremely different. Enhancing inhibition by manipulating postsynaptic GABA receptors consistently cause a *reduction* in the frequency of gamma oscillations. In one such study, participants consumed alcohol after gamma oscillations were induced visually and motorically (Campbell et al., 2014). Alcohol both increases inhibition at $GABA_A$ receptors and decreases excitation at N-methyl-D-aspartate (NMDA) receptors and the authors, as predicted, reported a decrease in gamma frequency and increase in gamma amplitude. This finding was corroborated by Lozano-Soldevilla et al. (2014), who found that increasing dosages of lorazepam (a benzodiazepine that binds onto $GABA_A$ receptor, amplifying GABAergic inhibition) led to reduced gamma frequency. Furthermore, the moderation of gamma activity was only observed in the visual cortex, even though lorazepam did not specifically target the visual system. This suggested a unique relationship between the agonistic effects of lorazepam and visual gamma production. Additionally, the findings of these human subject studies concurred with those performed using animal models (Traub et al., 1996; Whittington et al., 1995): both showing that greater inhibition leads to IPSCs with longer decay

periods, which results in slower but stronger gamma activity (Gonzalez-Burgos & Lewis, 2012).

We might naturally assume that any method leading to a GABA increment in the cell environment would produce similar outcomes, but this is not true. The effects of GABA agonists are specifically attributed to the enhancement of postsynaptic GABA effects through activating $GABA_A$ receptors. This process is not guaranteed when we manipulate GABA concentrations by administering GABA reuptake inhibitors or increasing GABA exogenously. Furthermore, the properties of GABA receptors are dependent on the GABA receptor configurations, which are made up of three out of 19 different proteins (Olsen & Sieghart, 2008). Each unique combination is known as a subtype, with different density in different cells (Ade et al., 2008; Brickley et al., 2001; Hamann et al., 2002; Porcello et al., 2003; Santhakumar et al., 2010). Some GABA receptor subtypes drive the early phase of IPSP, while others drive the late phase of IPSP.

The response of GABA receptors to changes in synaptic GABA concentration is dependent on the subtype, and an increase in synaptic GABA only seems to affect receptors responsible for the late phase of IPSPs. This was evidenced in an early paper directly compared the effects of manipulating postsynaptic receptor kinetics and reducing reuptake of GABA (Dingledine & Korn, 1985). While *both early and late decay phases* of the IPSP were prolonged by lengthening the opening period of postsynaptic chloride channels, reducing reuptake of GABA only affected *only late decay phases*. This is important, as gamma oscillations are timed specifically by the early phases of IPSP (Gouwens et al., 2010). Clearly, the amount of GABA that actively contribute towards gamma oscillation production is highly dependent on their location as well as subtype, and our understanding of the GABA-gamma relationship should not be built entirely on studies that modulate the kinetics of postsynaptic receptors in general.

Human electrophysiology studies on the effect of reuptake inhibitors have yielded conflicting results. For example, tiagabine, a well-known GABA reuptake inhibitor, was shown to have no significant effect on the frequency or amplitude of visually evoked gamma (Muthukumaraswamy et al., 2013). The lack of impact was not

discussed in terms of the different mechanisms precipitated by GABA agonist and GABA reuptake inhibitors. Instead, the authors noted that similar observations were made in Hall et al., (2011), who attributed their observation to the variation in signal strength of movement related gamma synchronisation. Gamma synchronisation starts out strong but becomes increasingly hard to measure (Muthukumaraswamy, 2010), impairing any observable GABA driven effects. Interestingly, the same group reanalysed their data with improved methods (Magazzini et al., 2016). They then found that gamma band frequency did decrease with tiagabine, as observed in animal models and in humans using GABA agonists. The authors' interpretations of their data were driven strongly by the assumption that increasing synaptic GABA concentration would cause greater GABAergic drive. However, as previously mentioned, reuptake kinetics are downstream from the inhibitory mechanisms that control neuronal spike timings, meaning they were unlikely to have affected gamma frequency.

Additionally, human electrophysiology is limited in its granularity when assessing intrinsic neural mechanism. Gamma rhythms in human electrophysiology studies are often defined by a broadband frequency range, which only allow for *estimations* of intrinsic neural processes based on shifts in broadband endogenous power. For example, the $GABA_A$ agonist propofol can slow gamma frequency rhythms down to beta frequency rhythms (Fisahn et al., 1998; Whittington et al., 1996), causing an increase in beta band activity that is detectable by EEG. However, based purely on the EEG results, it would be unclear whether this is a direct enhancement of beta band activity, or slowing of gamma band activity to beta. Similarly, another study found that while increasing propofol did not significantly change gamma band frequency, the amplitude of visually induced gamma was increased by 60% (Saxena et al., 2013). This might be attributed to the fact that propofol acts effectively on lengthening IPSPs generated by individual interneuron networks, while gamma oscillations generated by PING are often powerful enough to remain within gamma frequency range (Faulkner et al., 1998; Whittington et al., 2000). However, this level of detail is not observable in purely MEG or EEG recordings.

Ultimately, these conflicts indicate that the effect of tiagabine on gamma oscillations should be revisited using a simpler model. The effect of GABA concentration on

visual gamma oscillations should be investigated with consideration to the following changes. First, MRS recording techniques should be bypassed, and GABA concentrations should be controlled pharmacologically instead. This would allow us to monitor both total and localised GABA concentrations, which is crucial to the second change: examining how (1) exogenously increasing 'total' GABA concentration and (2) reducing GABA reuptake changes gamma oscillations. Since studies have repeatedly shown how manipulating GABA effects at the postsynaptic site reduces gamma frequency, the focus should be on comparing such findings with the results from these two methods (which do not directly increase postsynaptic GABA functions).

1.2.2 The role of endogenous oscillations in visual perception

The rest of this introduction will describe the role of endogenous oscillations in human perception and behaviour. Endogenous rhythms can impact externally driven visual responses in two stages, the first being prior to stimulus presentation, which can affect how the stimulus is received, and the second being after stimulus onset, which can affect the stimulus-generated responses.

1.2.2.1 Prestimulus alpha activity and detection of near-threshold targets

The ability to perceive and respond to visual stimuli is dependent not only on stimulus properties, but also the internal state of the observer. This internal state can be modulated by endogenous rhythms (for example, alpha band and theta band frequencies at 8-12Hz and 4-7Hz respectively). Recent evidence reveals a relationship between these signals and well-understood cortical networks that play important roles in sensory perception and performance (Beckmann et al., 2005; Leopold et al., 2003).

The links between endogenous state and visual perception have often been studied using stimuli displayed at the observer's detection threshold: the stimulus intensity where the detection of the stimulus is just above chance (Gardner & Martin, 2000). However, at threshold, subject performance fluctuates from moment to moment. The stochastic perception of near-threshold stimuli suggests the involvement of a fluctuating modulator. Earlier works found that a lack of concentration can cause observers to miss near-threshold stimulations (Block, 1996; Rock et al., 1992), but the coherence of endogenous neuronal firing can also predict performance, for example, stronger and more synchronised neural activity in the primate visual cortex has been observed prior to successful detection of a threshold-level stimulus (Supèr et al., 2003). Clearly, the observer's internal neuronal state, especially in task-relevant cortical areas, may be crucial to near threshold percepts.

Alpha band EEG modulations are measured robustly over occipital regions and are widely regarded as an indication of both attentional state and cortical excitability. All endogenous rhythms can provide the temporal frameworks for cortical functions (Buzsáki & Draguhn, 2004), but evidence that alpha plays a unique, active role in information processing and cortical information is emerging. Generally, greater alpha activity is associated with a higher inhibitory drive (Foxe & Snyder, 2011; Pfurtscheller, 2001, 2003), which has been supported by numerous studies showing inhibitory tasks like withholding responses or suppressing task-irrelevant information to be concurrent with enhanced alpha (Jensen & Mazaheri, 2010). This led to the well-known link between alpha and attention, since cortical inhibition is also a vital component of visual attention. Both neuroimaging (Heinemann et al., 2009) and single-cell electrophysiology studies (Sundberg et al., 2012) have found that attention powerfully modulated endogenous rhythms, even in the absence of visual stimuli. In all, these findings supported the view that alpha has an active role in information processing and attention modulation (Klimesch, 2012) in addition to being a pacemaker for cognitive processes.

Hence, many of the studies examining how alpha activity predicted psychophysical performance involved experimentally manipulating the viewer's attention using visual cues. An increase in conscious attention within a specific location in the visual field causes an attenuation of alpha activity in the corresponding cortical region. This

induces a temporary bias towards processing of stimuli in the attended visual field. For example, peripheral attentional cues that successfully induced a change in alpha activity resulted in both faster and more accurate detections of visual targets in hemifields contralateral to alpha desynchronisation (Thut et al., 2006). This supported an earlier study with a similar paradigm, although in this earlier study visual cues could be valid or invalid (Sauseng et al., 2005). Sauseng et al., (2005) found that validly cued attention modulated occipital alpha activity, which subsequently improved performance in the attended hemifield.

The usage of visual cues to direct attention in their participants was criticised for incorporating a *deterministic* factor in the resulting alpha power, which compels alpha activity to increase in the contralateral hemisphere to the attended hemifield (Boncompte et al., 2016). Recent models on mechanism of attention often highlighted a spontaneity in the direction of visual attention, where strength, placement and responses of attention followed *probabilistic* representations (Koike & Saiki, 2006; Pang et al., 2008; Vul et al., 2009). Similarly, endogenous regulation of attention can occur in the absence of external visual inputs, indicating to have been exerted from higher-order cortical areas through top-down mechanisms (Kastner et al., 1999; Luck et al., 1997). Hence, it was argued that endogenous alpha that is not directed using an external visual cue should provide a more realistic representation of attentional modulations and how the visual system functions (Pang et al., 2008). Endogenous alpha modulations that are not directed by attentional cues are called ‘spontaneous’ and several studies have examined whether such endogenous activity changes correlate with performance. The results were largely consistent with that of directed attention-modulated alpha: spontaneous alpha band power averaged across ‘missed trials’ in a target detection task was significantly higher than that of detected ones, despite no difference in the overall power of other endogenous frequency bands (Ergenoglu et al., 2004). This showed that spontaneous alpha band activity correlates with the detection of low-intensity stimuli.

This effect was however, not replicated in a later study. Participants had to report whether they saw a persistent, moving target among visually identical distractors in the absence of attentional cues. The findings indicated that while alpha power was predictive of detection rate, there was no difference in the *aggregated* alpha power

for detected and undetected targets (Boncompte et al., 2016). Instead, the relationship was driven by a difference in pattern of alpha activity between contralateral and ipsilateral hemispheres. Alpha from both locations increased before stimulus presentation but enhanced ipsilateral alpha correlated positively with target detection, while enhanced contralateral alpha correlated negatively. This contradicted previous findings (Cosmelli et al., 2011; Sauseng et al., 2005; Thut et al., 2006) and was theorised to represent either involuntary shifts in attention or the participant's approximation of where the oncoming target would be.

There are also studies that do not find this negative relationship between alpha power and performance. For example, Linkenkaer-Hansen et al., (2004) found that lower alpha did not necessarily correlate with better task performance. Higher alpha band amplitudes arising from the sensorimotor cortex were linked with enhanced conscious detection and faster reaction times when observers were presented with near-threshold somatosensory stimuli (Linkenkaer-Hansen et al., 2004). The authors also found that the best performance followed strong alpha in parietal regions, which could be interpreted as the disruption or inhibition of task-irrelevant areas or involvement of the parietal region in controlling the attention required for completing the task. In all, the study revealed two things: first, alpha that is the most predictive of performance might not originate from the cortex that directly processes the stimulus. Second, alpha band power might have a non-linear relationship with cortical inhibition. This highlighted the importance of conducting trial-by-trial analysis when examining the relationship between alpha and cortical states, as this effect can be lost if the data were averaged across all trials, as in Ergenoglu et al. (2004). In fact, a later study did find that visual inputs were more likely to be perceived if they coincided with a trough in the alpha cycle or a peak in the high beta or gamma responses (Hanslmayr et al., 2007). The coupling between phase and stimulus response is strong enough to predict the outcome on a trial by trial basis and supporting the association between alpha activity and perception of transient visual stimuli without averaging across trials.

Clearly there is strong evidence for a relationship between endogenous alpha activity and visual perception. However, there is no single study that adequately addresses these following issues.

Firstly, measurements of endogenous alpha were localised to the posterior visual areas. While basing their findings on occipital alpha activity (Sauseng et al., 2005), the same group had previously found posterior alpha activity to be controlled by prefrontal regions in an earlier study (Sauseng et al., 2005). The role of prefrontal cortex in attention modulation had been repeatedly demonstrated (Nobre et al., 2004; Rosen et al., 1999; Small et al., 2003), but this new finding was the first to link posterior alpha band power with this process. This prompted the question of whether alpha band activity calculated across the scalp would more accurately reflect the observer's attentional state, or other task-related networks, than occipital alpha alone.

Secondly, performance interacts with reaction time. Faster reaction times could indicate a more alert, vigilant internal state but speeding up reactions might also lead to worse performance. Reaction time is also associated with endogenous activity. As mentioned, Hanslmayr et al. (2007) demonstrated that enhanced alpha activity inhibited visual perception, while enhanced beta and gamma activity improved it. This difference in relationship of alpha and non-alpha endogenous activity with perception was later extended to response time, where macaques performing a visuomotor task showed a significant correlation between increased prestimulus alpha activity and longer reaction time (Zhang et al., 2008). The authors also found increased beta activity in the frontal cortex was associated with shorter response times and that regions that are part of the same network tend to show similar relationships between endogenous states and external performance. Even so, only some studies in this field had considered response time as a measurement of task performance alongside accuracy. A more comprehensive investigation might look at both simultaneously.

Finally, previous studies found a hemispheric dissociation where receiving a visual cue in one hemifield not only decreased alpha activity in the contralateral occipital region (Sauseng et al., 2005; Thut et al., 2006), but also induced a resynchronisation of alpha activity in the ipsilateral cortex (Kelly et al., 2006; Worden et al., 2000). Considering conflicting results of previous experiments (Boncompte et al., 2016; Cosmelli et al., 2011), it would be interesting to investigate whether contralateral

desynchronisation and ipsilateral resynchronisation of alpha activity persists especially in the absence of a visual cue, and if the alpha-perception relationship is stronger in either hemifield as compared to the whole brain.

1.2.2.2 Interaction between endogenous oscillations and visually evoked responses

In addition to informing about the observer's internal state before stimulus onset, endogenous oscillations can also interact with visually evoked responses. Some studies have indicated that steady-state potentials, instead of being purely stimulus-driven responses, are endogenous rhythms that have been phase-locked to the external rhythm (Makeig et al., 2002; Sayers et al., 1974). The exogenous and endogenous frequency do not have to match to produce powerful entrainments: the most efficient stimulus frequency depends on the stimulus features. For example, responses to face stimuli are the most optimal at 6Hz (Alonso-Prieto et al., 2013). These findings suggested a top-down influence of visual perception by endogenous rhythms, as well as the need to investigate endogenous entrainment using a wide range of stimulus frequencies.

Previous investigations of endogenous-exogenous interactions often consisted of attempting to phase-lock the endogenous component to a periodic stimulus and measuring performance in simple visual detection tasks (Hanslmayr et al., 2007; Spaak et al., 2014). These studies rarely involved the use of chromatic visual inputs, which, we argue below, may have an important relationship to some endogenous rhythms.

The human visual system is trichromatic, and the properties of visual pathways that process chromatic information have been studied extensively. The human retina contains three classes of cones, namely short- (S), medium- (M) and long- (L). Each cone type has a different spectral sensitivity profile: S-cones optimally absorb light at a wavelength of 420nm, M-cones 530nm and L-cones 570nm. The signals from these cones are combined at the retinal ganglion cell (RGC) stage to form additive and opponent channels. These are an *achromatic luminance channel* (L+M), which

processes signals from L and M cones in an additive way (S cone signals do not contribute to luminance)*, an isoluminant blue-yellow* system (S-(L+M)) that is modulated by on- and off- S-cone inputs, and an *isoluminant red-green* pathway (L-M), which processes L and M signals in an antagonistic way (MacLeod & Boynton, 1979; Perry et al., 1984; Shapley & Perry, 1986). These channels define the axes of three dimensions of the DKL and MacLeod Boynton colour spaces (De Valois et al., 2000; Derrington et al., 1984; MacLeod & Boynton, 1979).

The signals from these channels are projected from the retina to anatomically distinct layers in the lateral geniculate nucleus (LGN). The relationship between anatomically defined channels (parvo-, magno- and koniocellular pathways) and the functional chromatic channels is not entirely straightforward. Large parasol RGCs primarily input into the magnocellular (MC) layers in the LGN which carries almost entirely achromatic information. But the midget RGCs which drive parvocellular (PC) LGN layers carry both L-M and L+M signals information, and small bistratified ganglion cells which both project to the koniocellular (KC) layers and can carry S-cone initiated signals may also have inputs from other cone types (Dacey, 2000; Dacey & Lee, 1994; Lee et al., 1988). While achromatic, blue-yellow and red-green signals do not map perfectly onto the MC, KC and PC pathways respectively, it is true that PC and KC neurons respond preferentially to red-green chromatic signals and opponent blue-yellow signals respectively (Kaiser et al., 1990; Kremers et al., 1993; Lee et al., 1988; Lee, 2011).

The chromatic properties of LGN layers allow these anatomical visual pathways to be reasonably isolated using coloured stimuli. This means that entrainment between stimulus-evoked responses within the LGN and endogenous activity could, in principle, be used as a marker to reveal functional and physiological connections between LGN and the oscillating structure. The LGN is located in the posterior region of the thalamus, and therefore initial investigations began with the other structures in the thalamus. The thalamus plays an essential role in regulating sleep-wake rhythms and consciousness, producing a characteristic slow oscillation that corresponds to delta and theta frequency bands (Coulon et al., 2012) and previous research has shown that midbrain structures, such as the superior colliculus that regulate vigilance and eye movement, have strong connections with KC layers but

not PC or MC (Casagrande, 1994; Feig & Harting, 1994; Harting et al., 1991; Hendry & Reid, 2000).

More relevant to our work here, we note that a marmoset study had previously demonstrated a relationship between LGN activity and the thalamus (Cheong et al., 2011a). Multi-electrode recordings showed that KC activity experienced more fluctuations than PC or MC neurons. However, activity of individual KC neuron was highly synchronised (**Fig. 1.3** A – C) and fluctuations were highly coordinated over a time period of 15s (**Fig. 1.3** D). Both observations implicated the presence of an endogenous oscillation that modulated the activity of KC neurons exclusively.

Additionally, the authors found that KC spike rates were inversely correlated with slow (<10Hz) endogenous activity in the absence of external stimulation (**Fig. 1.3** E and F). This correlation was unique to both KC and slow endogenous rhythms: PC and MC spike rates did not correlate with <10Hz signals, and KC spike rates were unaffected by endogenous activity above 10Hz. This finding extended the first by showing that KC neurons were synchronised to a slow, rhythmic modulation that is normally characteristic of the superior colliculus within the midbrain.

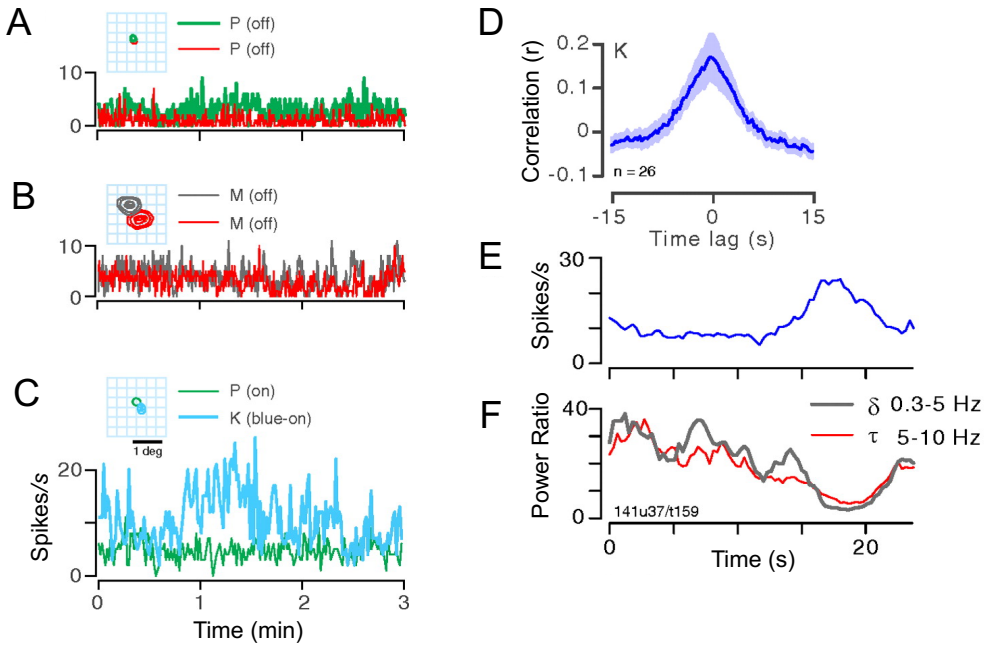

Fig. 1.3 *Figures adapted from Cheong et al., (2011). The spike rates of (A) two P cells, (B) two M cells and (C) one K cell and one P cell. KC responses showed greater fluctuation over time period as opposed to MC or PC neurons. (D) Strong correlation between spike rates of two neurons selected from KC layer. (E) Activity recorded from a KC neuron and (F) relative power of delta (0.3-5Hz) and theta (5-10Hz) activity (to EEG power between 10-50Hz). Power of low frequency endogenous activity show a distinct inverse correlation with KC spike rate in (E).*

This paper prompted us to ask if non-invasive techniques could also provide insights with regards to deep cortical responses in humans. Since the responses were unique to *KC* neurons, we wondered if S-cone driven responses would display signs of association with slow endogenous activity. In addition, we asked if responses to other chromaticities might also exhibit similar interactions with other endogenous activities. We could not measure signals from the LGN directly, but if interactions were occurring there, we might be able to measure their effects in cortex by examining non-linear response terms in the EEG.

A system processing signals of different frequencies can produce *intermodulation terms* when these frequencies interact in a nonlinear manner. Intermodulation terms manifest as power at the low-order sums and differences of the interacting frequencies. Depending on the frequencies of the endogenous activity and stimulus,

these nonlinear responses can appear almost anywhere across a wide frequency range.

Considering that high temporal frequency responses in the system can come from an interaction between flickering stimuli and endogenous activity, we ask a follow-up question: can the network support high temporal frequency responses driven directly by external stimuli? To investigate this question, we first reviewed the literature on the temporal response profiles of the visual system.

As previously mentioned, visual signals are projected into distinct layers in the LGN. This early separation of information naturally led to assumptions that processing would remain segregated until the signals terminate in higher visual areas. For example, many earlier works documented an apparent dichotomy between stimulus properties and corresponding processing streams, where motion and luminance were processed in dorsal regions and chromatic information were processed in ventral areas (Goodale & Milner, 1992; Mishkin et al., 1983; Mishkin & Ungerleider, 1982; Zeki, 1990). Eventually, the topographical details of these areas were mapped out using fMRI (McKeefry & Zeki, 1997): a region on the ventral occipitotemporal cortex was activated by presentation of colourful stimuli, independently of V3 and dorsal V5. This area was mapped out in even greater detail in a later study (Bartels & Zeki, 2000) (**Fig. 1.4**).

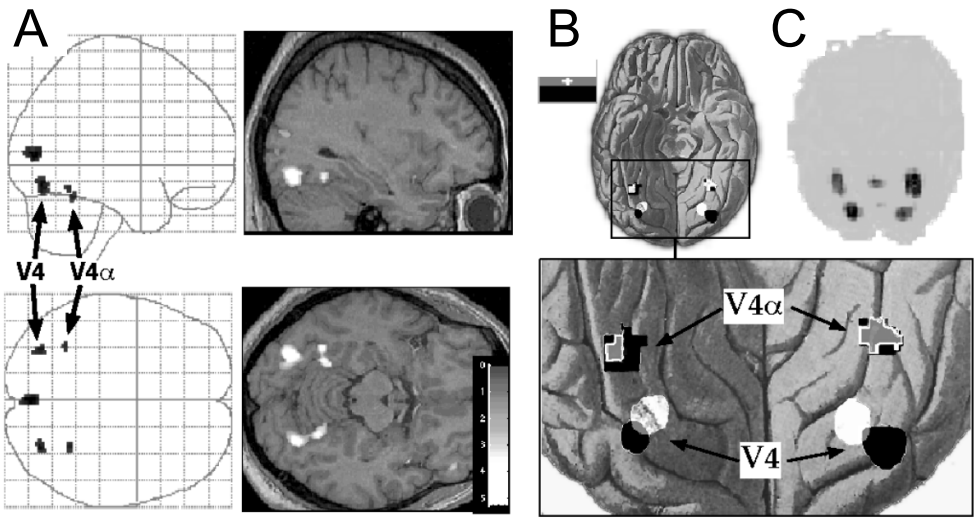

Fig. 1.4 *Fusiform gyrus regions that are responsive towards colour. Area V4 and area V4α from posterior and anterior regions respectively. Both areas show retinotopic organisation. (A) SPM of comparison between chromatic and achromatic stimulation on glass-brain projection (left) and anatomical images (right). (B) Comparing upper (white) and lower (black) visual field responses of chromatic stimulation against achromatic stimulation. (C) ICA separated the entire V4 complex (V4 and V4α). Figure adapted from Bartels & Zeki (2000), based on a reanalysis of data from McKeefry & Zeki (1997).*

The clear functional distinction between these higher-order areas inspired more research on human contrast sensitivity to chromatic and achromatic stimuli through a variety of neuroimaging methods, some with more complex chromatic stimuli to test additional cognitive responses (Brewer et al., 2005; Engel et al., 1997a; Liu & Wandell, 2005; Wade et al., 2008). Some research resulted in new definitions of visual areas, such as V8 (Hadjikhani et al., 1998) which bore similarities with V4α in Bartels & Zeki, (2000) (**Fig. 1.4**).

The precortical chromatic channels also inherit unique temporal sensitivity profiles, where the chromatic pathways largely respond more to slower temporal modulations as compared to achromatic pathways (Kelly, 1983). Temporal sensitivities differ between chromatic channels as well: psychophysical studies have shown that a 10Hz isoluminant red-green flicker is easily visible, but an isoluminant blue-yellow flicker at the same frequency would be almost invisible.

Many of these studies have verified the temporal properties of the early visual pathways, but two aspects of the chromatic response profiles are still debated. Firstly, colour and luminance processing pathways are not entirely distinct. Achromatic information, for example, can be carried via both P- and MC pathways (Derrington et al., 1984; Derrington & Lennie, 1984; Leventhal et al., 1981; Perry et al., 1984; Reid & Shapley, 2002). In contrast, MC neurons have exhibited properties of PC neurons, producing first-harmonic responses to slower red-green stimuli and strong second harmonic responses to faster ones (Lee & Sun, 2009). The chromatic information transmitted by MC neurons may not be limited to red-green signals: conflicting reports with regards to MC neurons carrying S-cone isolating signals have also been found (Chatterjee & Callaway, 2002; Sun et al., 2006). Moreover, the motion of a purely chromatic stimulus can be perceived consciously. Some argued that this was due to the transmission of chromatic information through the MC pathway to neurons in MT (Cavanagh & Anstis, 1991; Thiele et al., 1999). Evidence has also shown that the PC neurons inputs into area MT, although to a lesser extent than MC (Maunsell et al., 1990).

Furthermore, the processing of temporal information is partly determined by stimulus colour, in addition to other visual features such as contrast, eccentricity and spatial frequency (Hartmann et al., 1979; Hecht & Verrijp, 1933; Tyler, 1985). But even under optimal conditions, the conscious perception of individual flicker attenuates above specific temporal frequencies. This threshold is known as the critical flicker fusion frequency (CFFF) and is approximately 50Hz for luminance, 15-25Hz for chromatic red-green and 10Hz for S-cone isolating stimuli (Eskew et al., 1994; Holcombe & Cavanagh, 2001; Kelly, 1983; Lee et al., 1990; Matin, 1968; Wisowaty, 1981). Clearly, visual inputs are temporally filtered at some stage before perception, but where are the anatomical locations of the filtering stages? Considering how chromatic pathways have a more limited temporal response range than luminance processing channels, it is likely that filtering occurs after the segregation of chromatic and achromatic signals.

Initially, it was proposed that rapid signals were filtered at the earliest opportunity, as a way to conserve energy in the visual system. The temporal sensitivities of precortical structures were investigated, and it became clear that some filtering does

occur in precortical visual structures. Studies revealed that phasic and tonic ganglion cells were highly responsive to flicker between 20-40Hz (Lee et al., 1990) while LGN neurons were optimally activated by a lower, more limited frequency range between 4-10Hz (Derrington & Lennie, 1984; Solomon et al., 1999). However, this did not mean that fast signals are entirely filtered out in the LGN. Firstly, MC responses are transient and can convey motion information to later visual areas. The middle temporal (MT) cortical area, for example, receives much stronger MC inputs than PC (Maunsell et al., 1990). Secondly, earlier work on the filtering of rapid signals measured response heterogeneity across individual neurons (Tolhurst et al., 1983; Werner & Mountcastle, 1963). This was based on the idea that high variations in one stage's neuronal activity would weaken the signal and make it harder to transmit to subsequent visual areas. Despite the relative heterogeneity of cell types and ganglion cell connections in the retina, single cell activity in both LGN and retina were found to be relatively homogenous within layers (Croner et al., 1993; Gur et al., 1997; Schiller & Colby, 1983). This suggested that the signal was not weakened and was likely conveyed to higher-order visual areas. In summary, while the temporal range that LGN neurons respond to is noticeably smaller than that found in the RGCs, evidence suggests that some rapid signals are still present in cortex.

Additionally, another study found the majority of sampled colour opponent cells within numerous V1 layers exhibited frequency matched responses up to 30Hz and for three cells up to 60Hz (Gur & Snodderly, 1997). This implied that rapid signals not only reach the cortex, but that the early visual cortex is capable of processing these rapid signals. The final stages of temporal filtering for these signals might therefore occur even later in the visual stream, possibly in extrastriate visual areas.

One method of tracing these rapid signals involved measuring psychophysical thresholds after adaptation. Isoluminant flicker modulating at beyond the CFFF was invisible (Farrell et al., 1987; Zlody, 1965), but prolonged adaptation to such invisible flicker nevertheless produced adaptation effects (Shady et al., 2004) (see **Fig. 1.5** for visualisation). Similar adaptation effects were found for both chromatic and achromatic conditions, and adaptation showed particular interocular transfer implicating the involvement of multiple filtering stages up to and including the cortex.

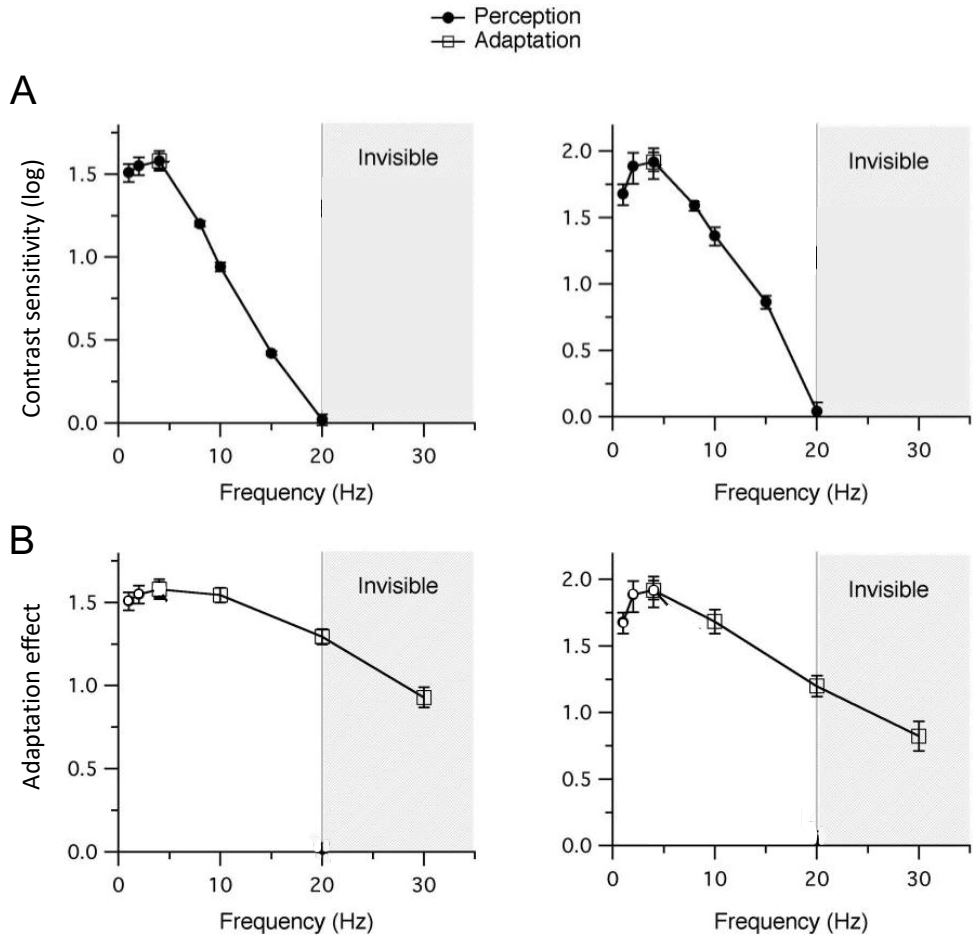

Fig. 1.5 *(A). Log scaled contrast sensitivity to increasing frequency in chromatic red-green flicker. The two figures show data collected from two subjects. Contrast sensitivity was used here as a measurement of conscious perception. Higher contrasts were required to maintain conscious perception as the flicker frequency increases. However, conscious perception of flicker stops at 20Hz for both subjects, after which the stimuli entered the 'invisible' frequency range. (B) Adaptation effect as a function of adapter flicker frequency. Adaptation effect was obtained by having subjects fixate on a flickering stimulus for two minutes, then measuring the level of contrast they require to see a probe. The figures showed that adapter flicker of 5Hz generated high adaptation effects, which gradually weakened as frequency was increased to 10Hz and 20Hz. This effect continues even when the adapter flicker entered the 'invisible' range of 30 Hz: demonstrating that participants showed adaptation effects despite not being able to consciously perceive the flicker. This demonstrated cortical modulations of this fast flicker. Figures adapted from Shady et al. (2004).*

Since, to a first approximation, adaptation to high frequency flicker only happens in the cortex (exception being Solomon et al., (2004)), evidence of invisibly fast flicker leading to this process revealed two things. First, the magnitude of the effect caused

by invisible flicker can be estimated from the extent of adaptation. In this case, the modulation transfer function followed a similar trajectory in both visible and invisible zones, which suggested that the degree of adaptation effect caused by invisible flicker appeared comparable to that of visible flicker. Secondly, imperceptibly fast signals reach the cortex and are not filtered out entirely in precortical region, refuting earlier theories.

One of the most comprehensive neuroimaging studies on this topic (Jiang et al., 2007) examined chromatic red-green flicker at various frequencies and contrasts. The authors measured responses in several visual areas (V1, V2, V3/VP, V3a, hV4/V4v and the region anterior to hV4, labelled VO) and found that all visual areas apart from VO produced comparable BOLD responses to full contrast flicker, regardless of temporal frequency (**Fig. 1.6** A). While all flicker frequencies generated standard contrast response functions in all visual areas (BOLD signal decreases with contrast), responses to 30Hz flicker in VO never rose above baseline, regardless of contrast (**Fig. 1.6** C). Overall, the findings indicated that we should expect 'invisible' fast flicker to generate responses in visual areas up to V4, although magnitude of responses might gradually attenuate as flicker frequency increases.

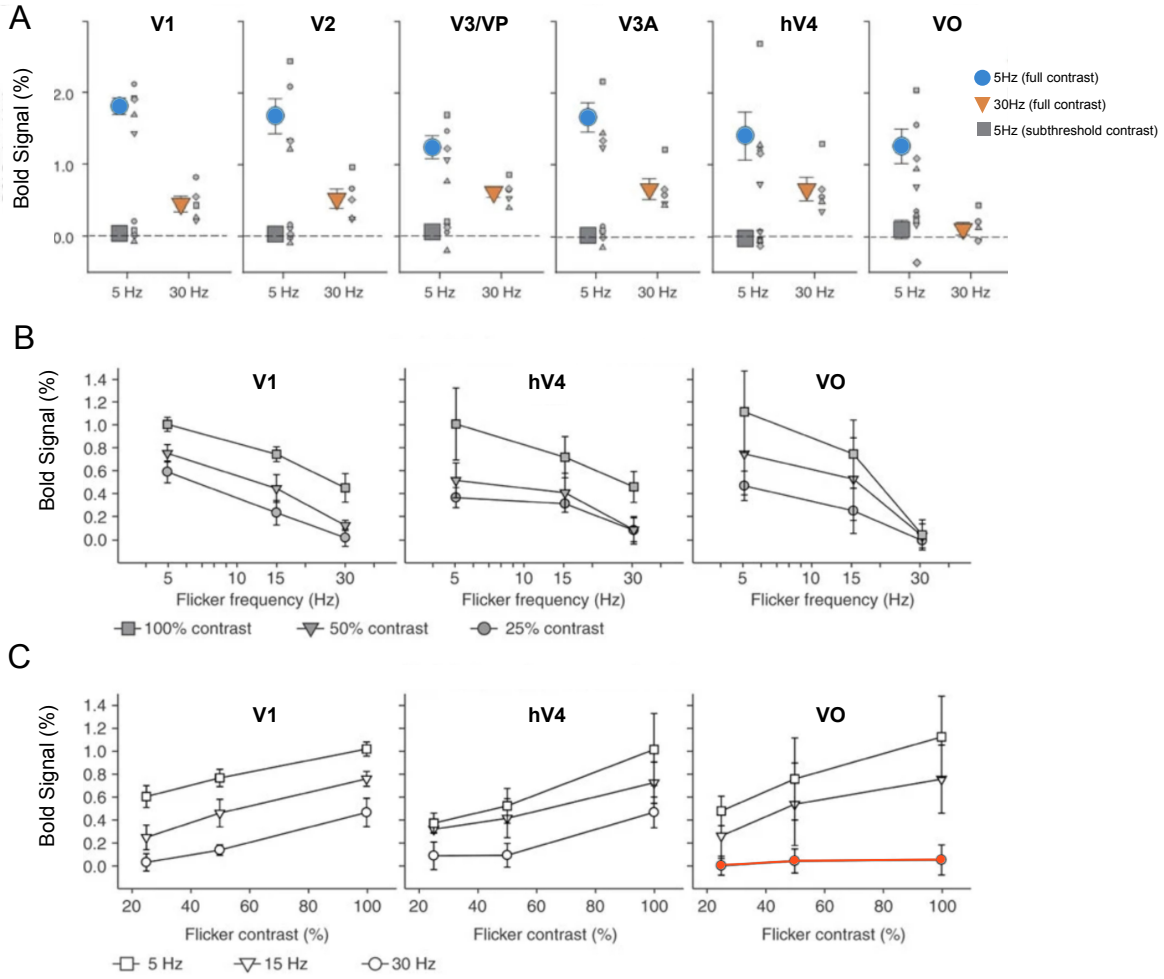

Fig. 1.6 *(A) Chromatic red-green flicker at 5 Hz (consciously perceptible 'visible' frequency) and 30 Hz (imperceptible 'invisible' frequency) produced statistically significant increases in BOLD responses in comparison to static control in the primary visual cortex, V2, V3A and V4. VO (anterior to hV4) was the only area that showed a distinction between the two stimuli, responding greatly to the visible flicker only. To ensure that the responses are truly dependent on temporal frequencies, the authors included a 5 Hz chromatic flicker with subthreshold contrast in the paradigm. This flicker while being slow enough for conscious perception, is perceptually indistinguishable from a 30 Hz 'invisible' chromatic flicker due to its low contrast. None of the areas which responded powerfully to the latter did so for this subthreshold flicker: demonstrating that the temporal frequency was critical in driving the responses. Rapidly modulating inputs are able to generate rapidly modulating signals beyond the primary visual cortex. (B) The averaged BOLD signal plotted as a function of stimulus frequency for three tested contrast levels (25, 50 and 100%) in visual areas V1, hV4 and VO. Increasing temporal frequency resulted in a decrease in BOLD responses for all visual areas. (C) The average BOLD signal plotted as a function of stimulus contrast level for three tested frequencies (5, 15, and 30Hz). The relationship between response magnitude, frequency and contrast are similar for all visual areas, with the exception of VO, which showed no significant responses at 30Hz regardless of contrast. Error bars indicate ± 1 SEM. Figures adapted from Jiang, Zhou, & He (2007).*

Historically, relatively little attention has been paid to the temporal characteristics of the KC pathway. This might be due to the earlier idea of chromatic information being conveyed exclusively by the PC system (Troscianko et al., 1996). The KC neurons are relatively temporally low-pass and 'sluggish': S-cone driven responses typically peak below 10Hz (Engel et al., 1997b). This temporal low-pass nature is reflected in cortical responses as well: a recent study (Spitschan et al., 2016) found that V1 and V2/V3 responded more to faster, achromatic signals (luminance, 16Hz) than slower, chromatic signals (red-green, 8Hz), matching observations in psychophysics performance. MT is the most responsive to fast flicker regardless of chromaticity and while S-cone responses were limited to V1 and V2/V3, peaking at lower frequencies (around 4-8Hz) (**Fig. 1.7**).

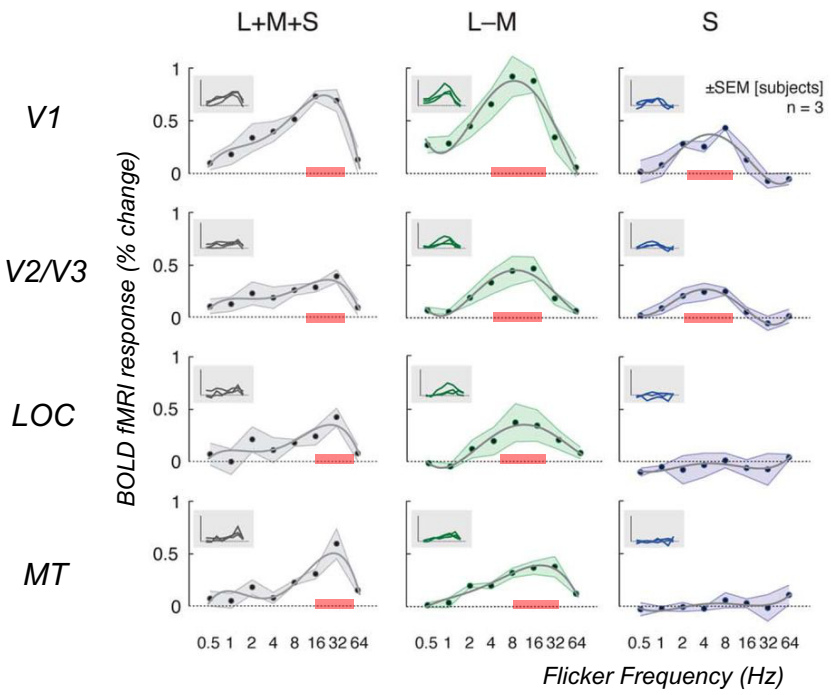

Fig. 1.7 *BOLD fMRI responses in V1, V2/V3, lateral occipital cortex (LOC) and MT plotted against flicker frequencies (Hz) for cone pathways. The temporal transfer functions are plotted for L+M+S, L-M and S. Shaded region indicates +/- 1 SEM across the three subjects. Solid line is a fourth-order polynomial fit to the data and red bars highlight the frequency range of peak BOLD responses. Figure adapted from Spitschan et al. (2016).*

However, some psychophysical experiments have shown that S-cone signals *can* convey significant information about motion at more rapid modulation rates (Cavanagh & Anstis, 1991; Dougherty et al., 1999; Lee & Stromeyer, 1989). S-cone isolating and purely luminance stimuli moving at 12Hz generated comparable patterns of neural activity around 200ms after stimulus onset, with a surprising, additional early response in the S-cone condition at approximately 50-90ms (Morand et al., 2000). This suggests that S-cone signals may have a fast, privileged way of accessing lateral visual cortex (perhaps area MT) (Barberini et al., 2005; Dobkins & Albright, 1994; Seidemann et al., 1999; Sincich & Horton, 2005; Thiele et al., 1999; Wandell et al., 1999). S-cone signals serve different purposes in different cortical regions. Those in colour-processing areas contribute to colour perception, while it is possible that S-cone inputs to other locations provide information about ambient light intensity - perhaps aiding shape, edge and motion processing (Conway, 2014). An earlier neuroimaging study supported this theory, showing that while responses within the LGN to both chromatic flicker (red-green and S-cone isolating) were similar (attenuating at 12Hz), their cortical temporal response functions differed (D'Souza et al., 2011). Specifically, normalised S-cone driven BOLD responses within MT showed a marked increase with increasing temporal frequency up to 10Hz as compared to luminance or red-green stimuli (**Fig. 1.8**). The activation of V3a was higher than that of earlier areas like V1, but not as great as MT. This finding added to the growing body of evidence suggesting that S-cone driven signal pathways have the potential to signal relatively fast modulations.

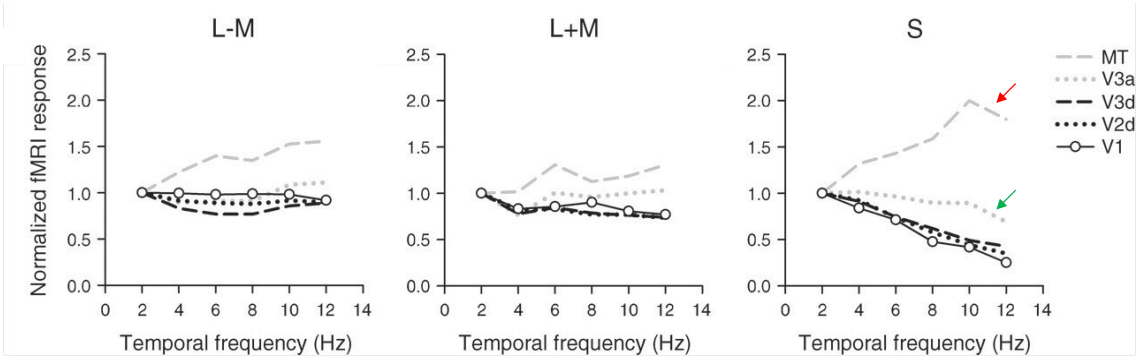

Fig. 1.8 *Adapted from D'Souza et al. (2011): Normalised fMRI responses in V1, V2d, V3d, V3a (denoted by green arrow) and MT (denoted by red arrow) to red-green, luminance and S-cone isolating stimuli. S-cone isolating stimulus generated a marked increase fMRI response at higher temporal frequencies, reaching a peak at 10Hz for MT and V3a. This was not seen in any other chromatic conditions.*

1.3 Rationale for the current thesis

The current literature clearly demonstrates the involvement of endogenous oscillations in cognitive functions. Certain aspects, such as occipital alpha modulation using attentional cues and the role of GABA in gamma rhythm, have been validated repeatedly. But with the rapid expansion of research in this field, several important questions still need to be addressed.

Firstly, the relationship between resting GABA concentration and gamma frequency remains inconsistent, especially in human studies. These experiments often estimate GABA concentrations using MRS, but an increasing amount of evidence is suggesting that total GABA concentration within a voxel is not proportionate to the amount of GABA actually involved in gamma production. Secondly, endogenous alpha activity can predict an observer's detection of a near-threshold target. However, such experiments often induce alpha using attentional cues. It remains unclear if this quality of alpha activity would persist if alpha were measured spontaneously, and whether spontaneous alpha shared different relationships with task accuracy and response time. Similarly, we wanted to know if the *function* of

alpha activity was consistent between individuals. Thirdly, the relationship between endogenous oscillations and colour vision remains relatively unexplored. Precortical visual pathways have well-established temporal and spatial tuning profiles and can be reasonably isolated using chromatic inputs. Any interactions between endogenous activity and chromatic inputs can act as markers for the mechanisms underpinning endogenous activity. Finally, 'invisibly' rapid flicker had previously caused adaptation effects within the cortex, but fMRI studies had only modulated chromatic stimuli up to 30Hz. We aimed to examine the neural correlates of responses driven directly by rapid stimuli.

Each chapter in this thesis was therefore designed to address these issues using alternative experimental or analysis paradigms. The first chapter investigated the relationship between GABA concentration and gamma oscillations. This involved increasing extrasynaptic and synaptic GABA concentrations through pharmacological agents in rodent cortex slice preparations. The second chapter investigated whether spontaneous alpha activity in humans prior to stimulus presentation was predictive of their accuracy and response time in an orientation discrimination task. In the third chapter, we modulated achromatic and chromatic flicker selected along the Macleod-Boynton colour axes and looked for signatures of interaction between exogenous and endogenous activity. This was performed first through a univariate analysis using averaged EEG power, then through a multivariate analysis using both phase and amplitude information. Lastly, we conducted an fMRI experiment examining the filtering stages of very rapid chromatic flicker within the visual cortex. This extended both the findings of the third chapter (showing entrainment at very high frequencies) as well as previous fMRI experiments with more limited temporal and chromatic ranges.

We specified five research questions, namely:

1. Does increasing synaptic or extrasynaptic GABA concentrations change gamma oscillation properties?
2. Can spontaneous alpha activity predict task performance?
3. What does alpha represent?

4. Do endogenous activity and stimulus driven activity interact? Specifically, with regards to chromatic stimulation from the axes of Macleod Boynton.
5. Does the human visual cortex respond to very rapid stimulation? Where are the signals filtered out?

2 Chapter 2: The effects of GABA and tiagabine on kainate-induced gamma oscillations in rodent visual cortex slices

2.1 Abstract

GABA is an inhibitory neurotransmitter that has an established role in the production of resting-state and stimulus-induced gamma band (> 25Hz) neural oscillations in animals (Bartos et al., 2007; Buzsáki & Wang, 2012; Chen et al., 2014). Higher concentrations of resting GABA are often associated with faster gamma rhythms in the visual cortex (Edden et al., 2009; Muthukumaraswamy et al., 2009), but a more recent study found no correlation between the two (Cousijn et al., 2014). Likely explanations for these conflicting results include fundamental disagreements about the mechanisms of gamma production (Brunel & Wang, 2003; Traub et al., 1996), limitations in the spatial resolution of GABA measurement techniques (Duncan et al., 2019; Puts & Edden, 2012; Stagg et al., 2011; Stagg, 2014), and the inherently low signal-to-noise ratio (SNR) of gamma oscillations in extracranial measurements of neural rhythms (Yuval-Greenberg & Deouell, 2009, 2011).

To address these issues, the current experiment investigated the relationship between GABA and gamma oscillations using *in vitro* recording techniques. This simpler, reduced system simultaneously allows for greater control over the paradigm and fewer uncontrolled variables, which leads to more straightforward data interpretation as compared to in vivo and other non-invasive studies. Gamma rhythms were induced in rodent primary visual cortex slices using kainate (Fisahn, 2005), after which we either (a) increased GABA concentration by exogenous

application to the slice bathing medium or (b) administered tiagabine: a GABA reuptake inhibitor. Our null hypothesis, consistent with the results of Cousijn et al. (2014), was that we would observe no changes to gamma oscillations despite the increased net concentration of GABA in the slice, as the modification of extracellular GABA does not guarantee a change in releasable *synaptic* GABA concentration (the most critical for gamma production networks). On the other hand, tiagabine is predicted to cause a *decrease* in gamma frequency as it retains the rodent's pre-existing GABA in the synaptic space, prolonging the time postsynaptic neurons are inhibited and delaying each round of synchronised neuronal firing (Roepstorff & Lambert, 1994; Thompson & Gähwiler, 1992). However, it has also been argued that an increase in synaptic GABA will not change gamma frequency, as its effects are limited to the late phase of IPSP (Dingledine & Korn, 1985).

The results supported our first hypothesis: we found no significant linear relationship between gamma frequency or amplitude when increasing extracellular GABA concentration. On the other hand, we found that only two of four animals showed a gradual decrease in frequency after the application of tiagabine, while the others were either ambiguous or showed a slight increase. Longer recordings of the slices showed that frequency (and amplitude) fluctuated greatly for at least an hour after tiagabine administration. In a follow-up analysis, we observed that kainate-induced gamma band oscillations showed a negative relationship between frequency and amplitude and that this changed to a positive relationship after applying tiagabine.

Our findings validated concerns raised in Cousijn et al. (2014): that experiments examining the effects of GABA must differentiate between releasable synaptic GABA and non-synaptic GABA. However, the conflicting outcomes following tiagabine administration indicated we must consider other sources and mechanisms of GABA action on visual gamma oscillations, such as extracellular GABA, homeostatic mechanisms that moderate excessive GABA as well as the role of GABA-induced postsynaptic currents in spike probability timing. The fluctuations in gamma frequency and amplitude also suggest caution when interpreting readings taken across long experiments.

2.2 Introduction

GABA is an inhibitory neurotransmitter that plays a vital role in the production of gamma oscillations within the visual cortex. Presynaptic neurons release GABA molecules into the synaptic space, where they might attach onto corresponding postsynaptic GABA receptors. Successful attachment causes the postsynaptic membrane potential to shift towards chloride reversal potential (-70mV), which decreases firing rate in postsynaptic neurons temporarily. When the inhibition wears off, the 'halted' neurons will fire together, producing gamma oscillations.

This mechanism is relatively straightforward, but the relationship between GABA concentration and gamma oscillations is not. An assumption held frequently by human or non-human primate MEG studies is that *higher concentration of GABA would cause greater inhibition and result in stronger and faster gamma oscillations*. One of the most prominent studies in this field was conducted by Muthukumaraswamy et al., (2009), where gamma activity was induced in subjects and resting GABA concentration was measured using MRS. The authors found a positive correlation between gamma frequency and resting GABA concentration, which supported the theory. This finding was soon extended by another experiment showing that GABA concentration also predicted orientation sensitivity within subjects (Edden et al., 2009). These findings unanimously supported a simple, linear relationship between gamma and GABA concentration and demonstrated how this might affect visual performance. Yet, replications of this result had been difficult. A study aimed at replicating these findings found no significant associations between GABA concentration with gamma frequency as well as no relationship between glutamate or GABA-glutamate ratio and gamma frequency (Cousijn et al., 2014). Such disputes were not limited to the visual cortex: the relationship between GABA concentration and gamma oscillations within the motor cortex (Gaetz et al., 2011), working memory (Chen et al., 2014) and auditory cortex (Wyss et al., 2017) have also varied between experiments.

A literature review suggested that these conflicts comprised two issues. Firstly, there are multiple computational models explaining the process of gamma production,

where outcomes are sometimes in direct opposition to one another. For example, the model described in Brunel & Wang, (2003) states that gamma rhythms are produced by intrinsic loops between excitatory and inhibitory drives. In contrast, a second model described by (Traub et al., 1996; Whittington et al., 1995) proposed that individual inhibitory interneurons can form loops irrespective of excitatory pyramidal cells. The first model predicts that the frequencies of resultant rhythms are tightly regulated by the ratio of excitation to inhibition and increasing inhibitory drive would cause an increase in frequency, while the second asserts that an increase in inhibitory drive would be followed by a decrease in oscillation frequency. Both models have been supported by evidence from human and rodent experiments (Muthukumaraswamy et al., 2009; Whittington et al., 1998), and the lack of consensus means that the effect of increased inhibition on endogenous frequency remains unclear.

Secondly, studies are expressing concerns about measuring inhibitory drive using MRS (Cousijn et al., 2014; Duncan et al., 2019; Muthukumaraswamy et al., 2009; Puts & Edden, 2012). These included fundamental technical issues, such as a lack of standardisation in MRS sequences across studies, the sequences not being optimised to measure other metabolites (e.g. glutamate) involved in rhythmogenesis, and its vulnerability to metabolite contamination.

But more importantly, MRS measures the *total* GABA concentration within a selected voxel, which is not an accurate estimation of inhibitory drive. GABA is divided into several ‘pools’ within a neuron such as cytoplasmic or vesicular. Out of these pools, only a subset of vesicular GABA is released during synaptic transmission (Martin & Rimvall, 1993), where *some* of them stimulate inhibitory processes that lead to gamma oscillations. This disparity between the amount of GABA that actually contributes to inhibitory potentials and the total GABA concentration within a voxel highlights how unsuitable MRS measurements are for inferring inhibitory drive.

Additionally, the process is made more complicated by the fact that gamma oscillations are driven by *early* phases of IPSP (Gouwens et al., 2010), which unlike late phases are *not* affected by an increase of synaptic GABA concentration (Dingledine & Korn, 1985). This finding is widely supported by the literature. Multiple

pharmacological studies that successfully manipulated inhibitory drive often involved the application of GABA agonists (Campbell et al., 2014; Gonzalez-Burgos & Lewis, 2012; Lozano-Soldevilla et al., 2014). GABA agonists directly affected postsynaptic GABA receptors and increases inhibition of subsequent neurons. These studies found that by directly enhancing GABAergic process at the postsynaptic receptors, gamma activity reduced in frequency but increased in amplitude. On the other hand, studies that have used GABA reuptake inhibitors have produced less consistent results. A study that administered tiagabine to its subjects found no significant effect on frequency and amplitude of gamma oscillations (Muthukumaraswamy et al., 2013), which was congruous with earlier papers (Dingledine & Korn, 1985; Gouwens et al., 2010). However, a later reanalysis of the same dataset reported that tiagabine caused a decrease in gamma frequency (Magazzini et al., 2016). This observation was explained by likening increased synaptic GABA concentration to increased postsynaptic GABA dynamics, which highlighted two important matters. First, synaptic GABA concentration does not provide a robust assessment of postsynaptic kinetics, and second, that this assumption is still held by researchers.

Together, these issues illustrated the complexity of gamma production and consequently a need to examine the GABA-gamma relationship. The current study aimed to understand the relationship between GABA concentration and gamma oscillations originating from the visual cortex. Instead of MRS, we used an *in vitro* rat model, which permitted direct and precise control over GABA concentrations. While the current research question does not require us to work with GABA agonists, previous success in using animal models for pharmacological studies justify the use of rodent models: comparable effects of benzodiazepines were observed in both human (Lozano-Soldevilla et al., 2014) and animal (Faulkner et al., 1998; Traub et al., 1996; Whittington et al., 1995) models. Gamma band oscillations were evoked using kainic acid, a glutamate agonist. To validate the MRS-related concerns of previous studies, we introduced GABA in increasing dosages to the cortical slices while simultaneously recording extracellular field potential in the animal's primary visual cortex in this first part of the study. Our aim was to investigate whether increasing the total GABA concentration would modulate gamma oscillations. We hypothesised that increasing GABA concentration would *not* increase gamma

frequency, as GABAergic effects are only enhanced if the additional GABA successfully activate postsynaptic receptors.

In addition to disproving that total GABA concentration is correlated with gamma frequency, we investigated how gamma was affected by GABA reuptake inhibitors and whether the effect would be different from experiments that directly manipulated postsynaptic kinetics (Campbell et al., 2014; Lozano-Soldevilla et al., 2014). In the second part of the study, we administered one fixed dosage of the GABA reuptake inhibitor tiagabine, a selective and potent inhibitor of GABA transporter (GAT-1) on the presynaptic neuron (Magazzini et al., 2016; Muthukumaraswamy et al., 2013). Since reuptake inhibitors only prolong the late phase of IPSP (which does not affect gamma production), we predicted that tiagabine would not change gamma band frequency and amplitude.

2.3 Methods

2.3.1 Rodent model

We obtained coronal slices with a thickness of 450μm from the visual cortex of 18 adult male Wistar rats (weighing approximately 200g). During the experiment, the slices were maintained in an interface chamber flushed with oxygenated (95%/5% O_2/CO_2) artificial cerebrospinal fluid (ACSF), which is composed of (in mM) 126 NaCl, 3 KCl, 1.25 NaH_2PO_4, 0.6 $MgSO_4$, 1.2 $CaCl_2$, 24 $NaHCO_3$ and 10 glucose, at 34°C. All experimental procedures were performed under the United Kingdom Home Office government licence with local ethical review board approval and conformed to regulations described in the UK Animals (Scientific Procedures) Act (ASPA), 1986.

2.3.2 Drugs

This experiment used Kainic acid (1-500nM), GABA and (3*R*)-1-[4,4-Bis(3-methyl-2-thienyl)-3-butenyl]-3-piperidinecarboxylic acid hydrochloride (tiagabine

hydrochloride). All drugs were applied to the bathing solution (i.e. 50ml of oxygenated ACSF) circulating the interface chamber. In order to generate gamma oscillations, kainate (0.8μM, or 40μl of 1mM concentration in a 50ml volume of bathing solution) was always applied first after slices were prepared and stabilised. We then waited for the slices to reach equilibrium, which takes between 60-90 minutes. GABA or tiagabine was introduced to the bathing medium upon detecting gamma band oscillations. Slice preparations that failed to oscillate after the allotted time were discarded at this point.

GABA and tiagabine solutions were made at the start of each experimental week. For GABA solution, we mixed 103.12μg of GABA with 1ml deionised water, producing a solution of 1mM concentration. Tiagabine solution was made by mixing 3.75mg in 1ml deionised water, producing a solution of 10mM concentration. Kainic acid was obtained from Sigma-Aldrich (Poole, UK) and GABA and tiagabine were obtained from Tocris Bioscience (Avonmouth, UK).

2.3.3 Extracellular recording

We performed extracellular recording at a sampling frequency of 2000Hz using one micropipette (2-5 MΩ) filled with ACSF per slice. Data were acquired from within layer IV in the primary visual cortex (V1) of prepared cortical slices (see **Fig 2.1**) using the Axograph X software package (Axon Instruments, Foster City, CA). A bandpass filter of 0.1 to 200Hz was applied during data acquisition. Each recording lasted for 60 s normally with the only exception being the last session, where we took longer recordings of 60 minutes. This was performed on two slice preparations taken from one rat, using two micropipettes on the same slice approximately 3mm apart. The first micropipette (E1) recorded from layer II/III and the second from layer IV (E2).

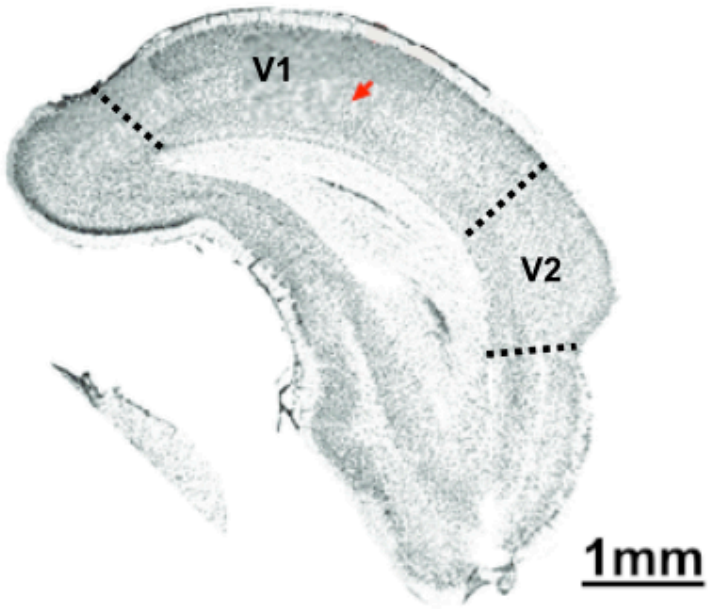

Fig. 2.1 *Adapted from Yan et al. (2011): Histology diagram of single slice of a rat visual cortex with V1 and V2 labelled. The current experiment recorded from layer IV within V1, which is indicated by the red arrow.*

2.3.4 Experimental procedure

Slices were prepared at the start of each experimental day and left to rest at room temperature in an oxygenated, ACSF filled chamber for approximately 1 hour. We then brought the slices up to 34°C and placed our prepared micropipettes on the recording sites in V1 (see Extracellular Recording for detail). We took one to three initial recordings to obtain baseline activity before applying the kainate solution. The cortical slices were further monitored every approximately 15 minutes for 60 to 90 minutes until gamma band oscillations were detected. We did not proceed further if the slice showed no evidence of gamma band oscillation after 90 minutes.

To test the effect of GABA, we administered a dosage of GABA every 60 minutes after establishing gamma oscillations. Experimental duration was less than six hours for each slice. The exact concentrations tested are listed in **Table 2.1**. We took one recording 60 minutes after each GABA administration to allow sufficient time for the agent to take effect.

Table 2.1 *The GABA concentrations (μM) tested on six separate experimental sessions.*

Experimental Session (Date)	GABA Concentrations tested (μM)
Session 1 (07/03/17)	10, 100, 500, 1000
Session 2 (21/03/17)	200, 500, 1000, 2000
Session 3 (04/04/17)	100, 200, 500, 1000, 2000
Session 4 (12/06/17)	10, 20, 50, 100
Session 5 (13/06/17)	1, 2, 5, 10, 20
Session 6 (16/06/17)	1, 2, 5, 10

To examine the effect of tiagabine, we administered a single 10μM dosage of tiagabine (50μl of 10 mM solution in a 50ml bath) after confirming the presence of gamma oscillations. We then took one recording every 15 minutes (for 90 minutes) after administering tiagabine to monitor the condition of the slices. This was repeated for all tiagabine experimental sessions but one, where we recorded for 60 continuous minutes after tiagabine administration.

Out of the 18 experimental sessions, six tested the effect of GABA and the remaining twelve tested the effect of tiagabine.

2.3.5 Data analysis

Data were analysed using Matlab 9.4 (R2018a, MathWorks Inc., Natick, MA, USA). Electrophysiology recordings were fast Fourier transformed (FFT) and results were plotted in the frequency domain. To extract the peak frequency and amplitude from each recording, we used Matlab's default curve fitting tool *fit* with the following parameters: *fittype: 'gauss1', fitoptions: 'Method', 'NonlinearLeastSquares'*. We restricted the data range of curve fitting function to optimise the procedure for both speed and accuracy after visualising the amplitude spectrum (frequency: 15-70 Hz and amplitude: 0.10-*inf* μV). As an example, we plotted the frequency domain data from one 60s recording in blue dots and the reconstructed fitted curved in red (**Fig. 2.2**).

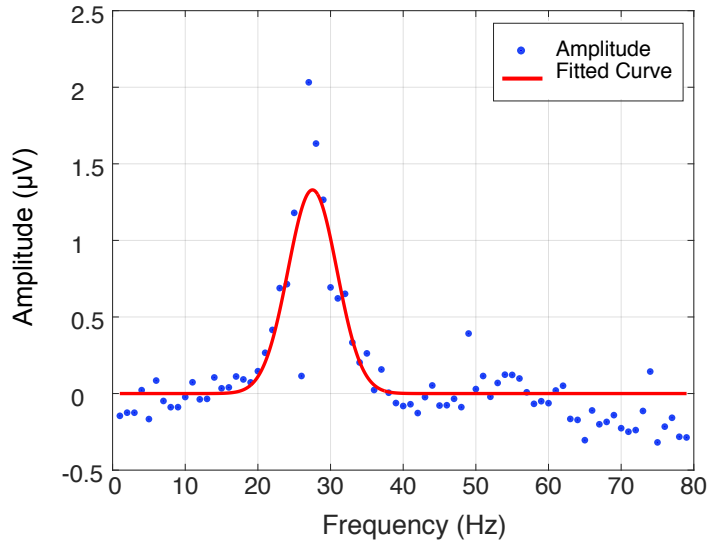

Fig. 2.2 *Data from one electrophysiology recording plotted in the frequency domain. This particular curve fit explained 0.74 or 74% of the variance and has a peak frequency of 27.5Hz and an estimated amplitude of 1.33μV.*

We excluded any recording where the fitted curve had an r^2 (variance explained) of less than .10, or 10% – in other words, where there was no significant peak present in the gamma range. This left us with N = 5 out of six for GABA sessions and N = 5 (including the session where recordings lasted 60 minutes) out of twelve for the tiagabine recordings. We obtained the peak frequency (Hz) and the corresponding amplitude (μV) of these recordings and plotted them in the figures below.

2.4 Results

2.4.1 Overview of data

Recordings prior to the addition of kainate often appeared as 1/f noise with a peak at mains noise frequency (50Hz). Biologically relevant peaks are formed after adding kainic acid and allowing slice preparations to reach equilibrium. Frequency domain figures revealed that kainate-generated gamma oscillations were often centred around 25-35Hz (example seen in **Fig. 2.3**, left).

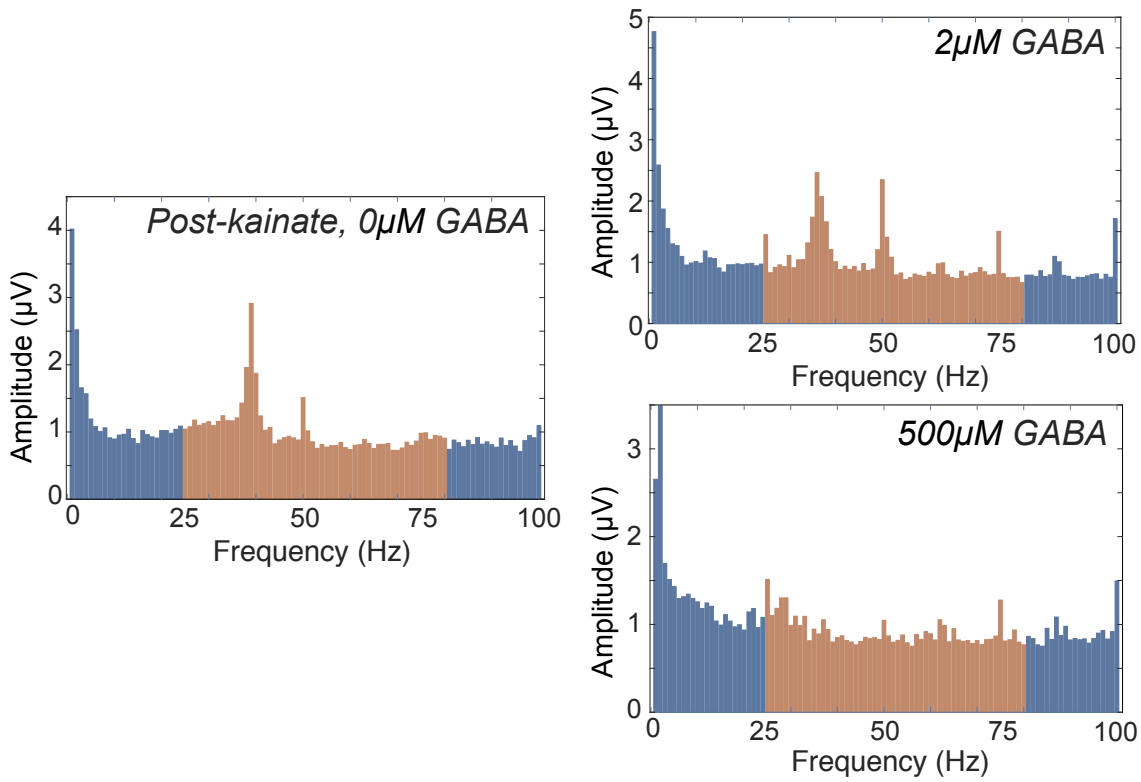

Fig. 2.3 *Amplitude spectrums (ranging 1-100Hz) for three selected electrophysiology recordings. Orange bars highlight the gamma frequency range 25-80Hz. Left figure shows kainate-generated gamma oscillations emerging as a peak centred at 28Hz prior to administering GABA (control). Top right figure shows the same peak after administering 2μM GABA and bottom right figure shows activity of a different slice after administering 500μM GABA.*

2.4.2 The effect of increasing GABA dosages on gamma oscillations

A linear mixed-effects model with GABA concentration as the predictor and gamma *frequency* as the dependent variable showed an overall non-significant effect: $F(1, 45) = 1.33$, $p = .254$, marginal $R^2 = .028$, conditional $R^2 = .028$). To examine whether GABA altered the amplitude of peak frequency (as opposed to the frequency itself) of the gamma oscillations, we ran a second linear mixed-effects model with GABA concentration as the predictor and the amplitude of peak gamma frequency as the

dependent variable and also found an overall non-significant effect of GABA: F(1, 44.79) = 0.08, p = .780, marginal R^2 < .01, conditional R^2 = .11) (see **Fig. 2.4**).

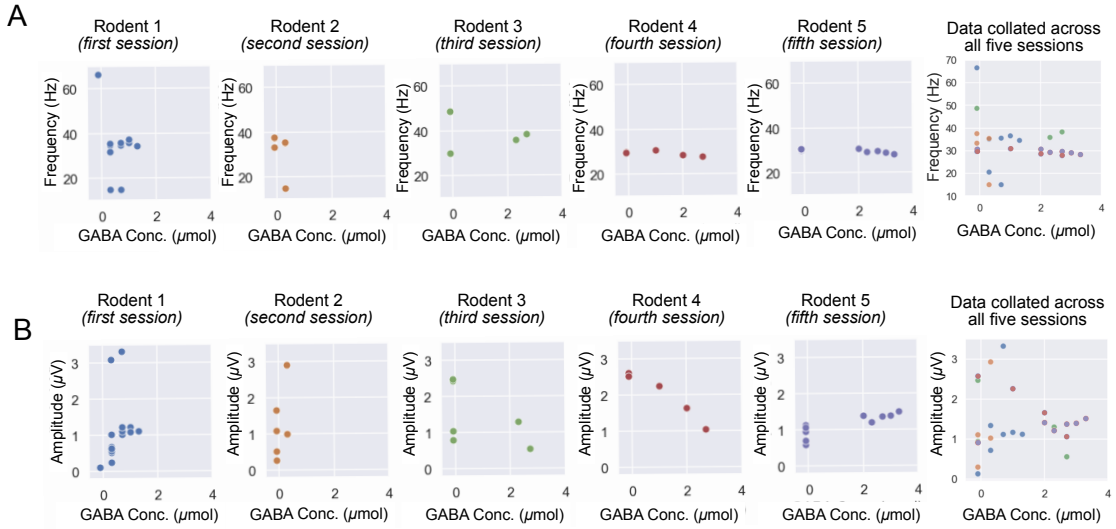

Fig. 2.4 *(A) Frequency (Hz) of endogenous rhythms measured in the visual cortex as a function of log-scaled GABA concentration. (B) PSD (μV) of signal peak frequency shown in (A). The last column displays data collated across all five sessions. Peak frequencies and corresponding amplitudes rendered onto the same figure and different colours are used to indicate data from each of the five sessions. Overall, we found that GABA concentration did not consistently cause an increase peak gamma band frequency or amplitude.*

2.4.3 The effect of tiagabine on gamma oscillations

Similar to the previous analysis, we only analysed data from recordings where the fitted curve explained more than 10% total variance. This restricted our sample to four separate sessions. Peak frequencies and amplitudes of these recordings were not normally distributed. Median peak frequency increased for two samples and decreased for two samples, while median amplitude increased for one sample and decreased for three. Descriptive statistics are summarised in **Table 2.2**.

Table 2.2 *Median and interquartile range (IQR) of peak frequency and amplitude before and after tiagabine application.*

	Between kainate and tiagabine application		After tiagabine application	
	Frequency	*Amplitude*	*Frequency*	*Amplitude*
Session 1	Median = 37.73, IQR = 2.88	Median = 0.63, IQR = 0.25	Median = 45.68, IQR = 1.54	Median = 0.56, IQR = 0.01
Session 2	Median = 34.13, IQR = 0.64	Median = 0.41, IQR = 0.03	Median = 26.88, IQR = 2.86	Median = 0.28, IQR = 0.06
Session 3	Median = 45.66, IQR = 1.85	Median = 0.41, IQR = 0.15	Median = 40.46, IQR = 1.09	Median = 0.52, IQR = 0.09
Session 4	Median = 40.04, IQR = 17.04	Median = 0.95, IQR = 1.37	Median = 52.35, IQR = 6.49	Median = 0.60, IQR = 0.25

We made violin plots to visualise these inconsistent changes to frequency and amplitudes before and after tiagabine administration (**Fig 2.5)**. This provided further insights, especially with changes to amplitudes in Session 4. Changes in amplitudes are also inconsistent: with two showing attenuation, one showing an increase and another showing virtually no changes. These conflicts implied that GABA reuptake inhibitor tiagabine did not ensure increased postsynaptic GABAergic drive.

What is the reason for this heterogeneity? Our readings are taken over short intervals at relatively arbitrary times before and after the administration of the pharmacological agent. To examine how stable were our measurements over time, we plotted the frequency and amplitude extracted from each recording as a function of time (**Fig 2.5)**. We noted that the two observed *decreases* in frequency were consistent and relatively monotonic after the administration of tiagabine. However, we noted the general presence of significant pre- and post-administration changes in both frequency and magnitude, suggesting that multiple measurements of these quantities are necessary to obtain reliable readings.

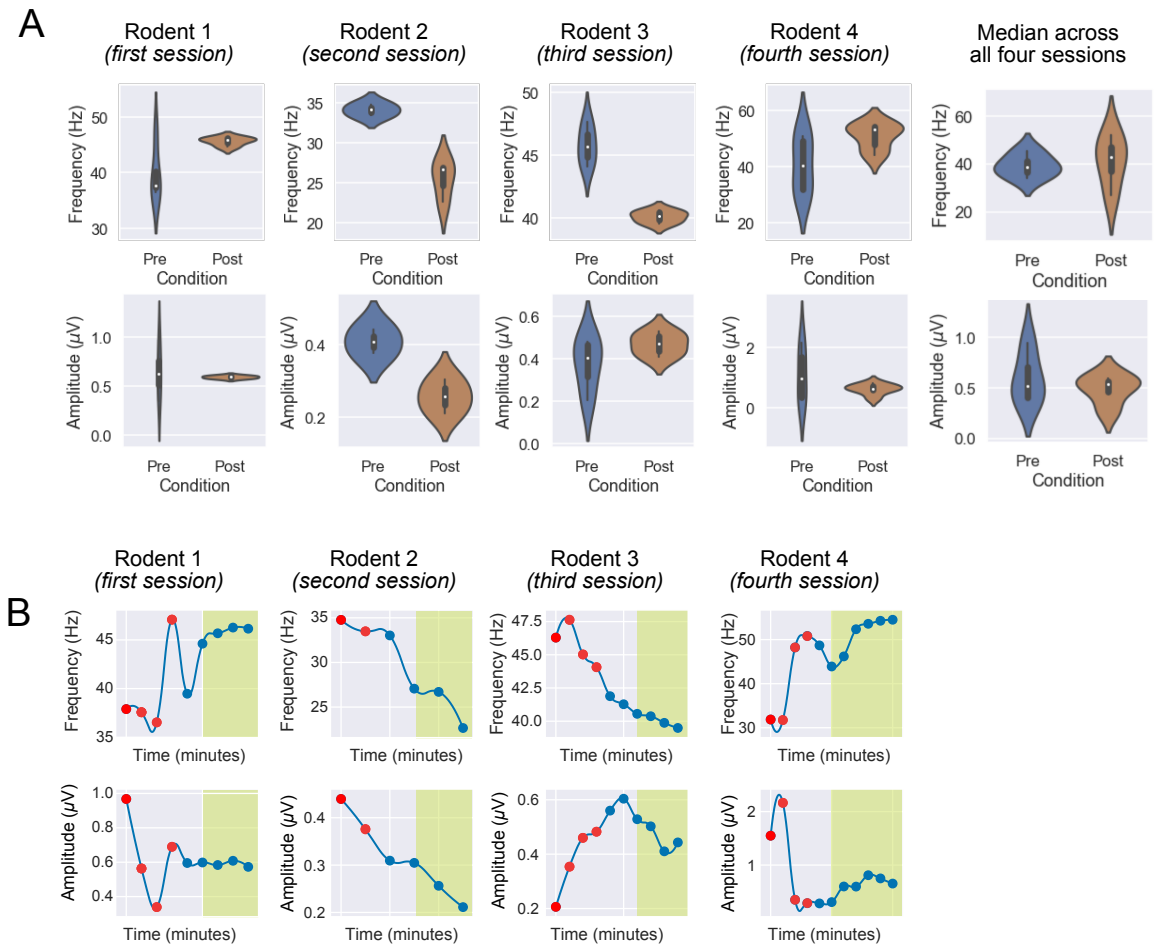

Fig. 2.5 *(A) Violin plots of frequency (Hz) and amplitude (μV) before tiagabine application (blue) and after (orange). Out of four rats, two showed a decrease in frequency and two showed an increase after tiagabine application. Similarly, three rats decreased in amplitude and one rat increased. Violin plots in the last column show the distribution of median frequencies and amplitudes for before and after tiagabine application. (B) The frequency and amplitude of V1 slice recorded during experiment. Each dot represents a single reading taken from the slice. Specifically, red dots indicate the pre-tiagabine, post-kainate recordings and blue line and dots illustrate the results of subsequent recordings. The figure demonstrates how frequency and amplitude changes as a function of time. Green shaded regions indicate periods 30 minutes after tiagabine administration (i.e. minimum time needed for slice preparations to equilibrate). Two out of four rodents showed decreases in gamma frequency after tiagabine administration while all four showed decreases in amplitude.*

To visualise how tiagabine modulated visual gamma oscillations during the equilibration period, we recorded two slice preparations using two micropipettes each for 60 minutes. One minute of data every three minutes was extracted and processed. The reconstructed fitted curves showing peak frequency and amplitude

were plotted in **Fig. 2.6** A. These values were then plotted across time in **Fig. 2.6** B, revealing fluctuations of both signal properties. However, we did not observe any significant relationship between the activity recorded within the same cortical slice: Spearman's rho revealed non-significant correlations for both slice one (frequency: r = 0.15, p = .561; amplitude: r = -0.45, p = .060) and slice two (frequency: r = -0.21, p = .413; amplitude: r = 0.01, p = .964), as seen in the last column of **Fig. 2.6** B.

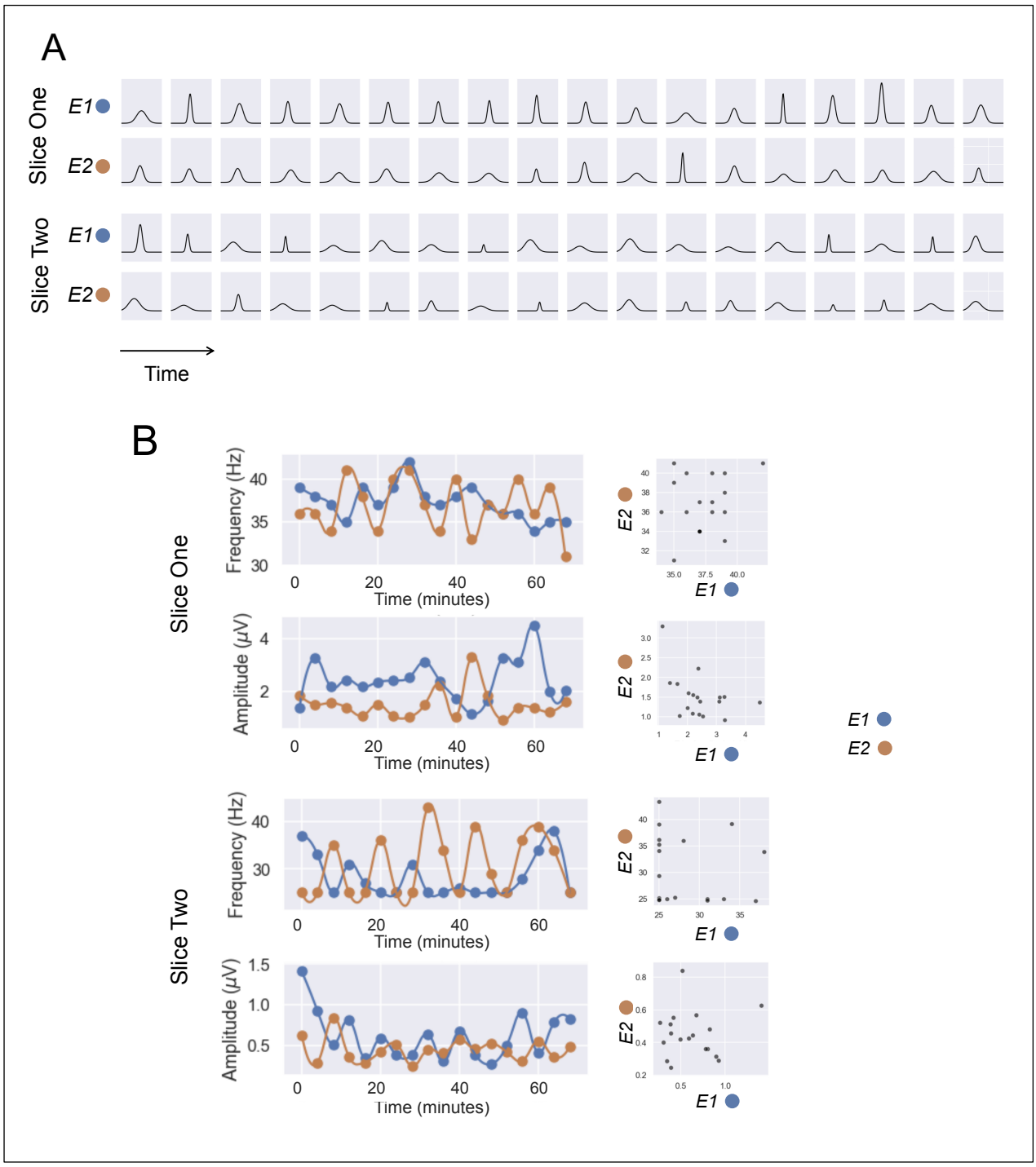

Fig. 2.6 *Data from two slices of cortex taken from a single rat. Data were collected continuously for 60 minutes immediately after applying tiagabine. We extracted 60 seconds of data every three minutes and fitted curves to this data using the same parameters as earlier analyses. We then reconstructed the curves based on the output parameters, shown in (A). (B) showed changes in frequency (Hz) and amplitude (μV) as a function of time from the reconstructed activity, with blue indicating data from the first micropipette (E1) and orange from the second micropipette (E2). The figures showed that both frequency and amplitude fluctuate continuously after administering tiagabine. To more clearly illustrate the relationship of frequency and amplitude recorded from E1 and E2, we plotted each data point on scatterplots. The scatterplots indicated that the LFPs were uncorrelated.*

Finally, we ran Spearman's rho correlations collectively on all measurements of frequencies and amplitudes and found that prior to the addition of tiagabine, frequency and amplitude were negatively correlated ($r = -.47$, $p = .026$) and positively correlated after ($r = .75$, $p < .001$) (**Fig. 2.7**).

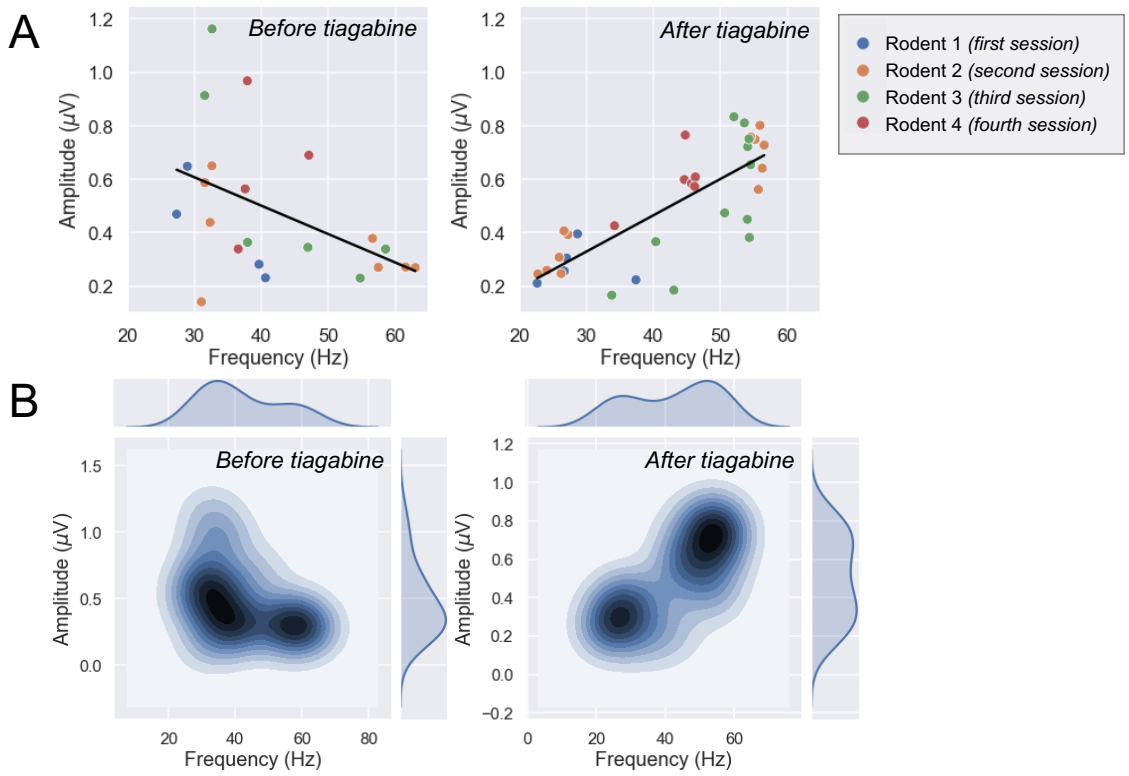

Fig. 2.7 (A) Scatterplot illustrating correlation between frequency and magnitude before adding tiagabine and after adding tiagabine. Colour of dots indicate different rodents (or experimental sessions). (B) The same data as in (A) but plotted as a kernel density estimate. In both plots, we observed gamma oscillation exhibit a clear negative relationship between frequency and amplitude prior to tiagabine administration and a clear positive relationship after.

2.5 Discussion

We increased GABA concentration in slice preparations of rodent visual cortex pharmacologically to examine the effect on endogenous gamma oscillations. We found no significant changes in frequency or amplitude of kainate induced gamma activity suggesting that total GABA concentration (as measured, for example, by MRS) does not necessarily correlate with gamma production. As a follow-up, we reduced GABA reuptake without changing the total GABA concentration using tiagabine. As increasing synaptic GABA concentration does not necessarily enhance

postsynaptic potentiation, we expected tiagabine to also have no effect on gamma frequency. The data showed inconsistent results with two cases of gamma frequency decrease, one ambiguous, and one increase. On the whole, there was no clear effect of tiagabine on gamma frequency, leading to our conclusion that gamma oscillations are *not* critically dependent on the total or synaptic GABA concentration.

2.5.1 The movement of GABA molecules after exogenous application of GABA

As previously mentioned, the involvement of GABA molecules in GABAergic processes are highly dependent on their locations within the cell environment. When GABA is applied in abundance as in first part of this study, a large proportion of it gathers in the extrasynaptic space, which allows access to extrasynaptic receptors such as $GABA_B$ and $GABA_A$ tonic receptors containing alpha- and delta-subunits (Brickley & Mody, 2012; Richardson et al., 2011). Despite reaching a higher *total* GABA concentration as compared to the control, the concentration of synaptic GABA is hardly affected. In other words, the observations made from administering GABA solution are likely caused by kinetics of extrasynaptic GABA receptors. In contrast, GABA reuptake inhibition *does not* alter the total GABA concentration within the slice preparations but significantly increases the amount of synaptic GABA. Interestingly, some of this excess GABA can leak into extrasynaptic spaces when synaptic concentration becomes sufficiently high (Scanziani, 2000). This means that any changes to gamma activity from tiagabine should mainly come from an increase in synaptic GABA and spill-over to extrasynaptic GABA. It should be also noted that synaptic GABA pools are much smaller than extrasynaptic pools, meaning we cannot obtain a fair estimate of synaptic GABA concentration from total concentration.

The lack of effect on gamma frequency suggests that the mechanisms involved in gamma rhythmogenesis are not significantly regulated by overall GABA concentration. So, what happens instead? While inhibitory currents mediated by postsynaptic $GABA_A$ receptors are phasic in nature and are characterised by shorter

IPSPs, extrasynaptic $GABA_A$ receptors mediate *tonic* inhibitions, which are characterised by more persistent, longer IPSPs. Tonic inhibition occurs when extrasynaptic $GABA_A$ receptors are exposed to a sufficiently high level of GABA. In general, $GABA_A$ receptors containing delta-subunit or alpha5-subunit are the primary drivers of tonic inhibition. Activation of delta-subunit $GABA_A$ receptors can cause hyperpolarisation which decreases probability of neuronal firing (Farrant & Nusser, 2005; Nusser & Mody, 2002). Or, in certain cases, these receptors can evoke shunting, where an inhibitory current occurring in close proximity to an excitatory current causes the cell to be less receptive to the excitatory current. This cancels the excitatory effect. Tonic inhibition has been demonstrated to decrease the frequency of gamma oscillations caused by phasic excitation-inhibition, or at least those induced through NMDA receptor activation (Mann & Mody, 2010). While this is observed in the data of Sessions 2 and 3 examining tiagabine, the overall effect was not reliable enough to be conclusive. Additionally, studies have found that tonic conductance generated by alpha-subunit $GABA_A$ receptors modulate spiking rates of pyramidal neurons in the hippocampus (Caraiscos et al., 2004; Glykys & Mody, 2007). This indicated that tonic conductance more accurately reduces the neuronal baseline excitability without net effect on the dynamics.

2.5.2 Effects of increasing synaptic GABA concentration

Similarly, the GABAergic drive is determined predominantly by GABA receptors and not the GABA concentration (Dingledine & Korn, 1985). Having more available GABA is only impactful if the excessive synaptic GABA reach and activate the postsynaptic sites. Neurons have homeostatic GABA regulation mechanisms that protect the normal GABAergic functions from excessive synaptic GABA. Increasing GABA concentration can cause channels to open for a longer time, owing to a shift in opening ‘types’ from brief to more sustained states (Macdonald & Olsen, 1994). However, this effect is temporary and the GABA receptors become desensitised to excessive GABA after a period of time (Cash & Subbarao, 1987). Presynaptic GABA receptors might also stop releasing GABA (Olsen & DeLorey, 1999), leading to a

decrease in synaptic GABA and restoring normal IPSP durations. It is likely that gamma activity will change if GABA were modulated in the appropriate locations and dosages, but this detail was not considered in this part of the study, or MRS in general.

2.5.3 Correlation between gamma amplitude and frequency

We first observed that gamma frequency and amplitude were negatively correlated before tiagabine administration and positively correlated after. This data contradicted the observations made in Muthukumaraswamy et al. (2009), which stated that gamma frequency and amplitude were uncorrelated. Further investigations using kernel density plots revealed that this change in correlation originates from a shift in peak frequency. While there are two peak frequencies (approximately 25-35Hz and 50-60Hz) throughout the experiment, kainate-induced gamma was dominated by the lower gamma frequency range and while activity measured after adding tiagabine were dominated by the higher band.

A recent computational model demonstrated that our observations can be explained by neuronal clusters with different postsynaptic potential time scales, even within the same network (Keeley et al., 2016). Other work suggest that the activity centred at these two frequency bins most likely originated from different subtypes of interneuron networks. The slower rhythms are mediated by somatostatin-expressing interneurons, while faster rhythms are mediated by parvalbumin-expressing interneurons (Chen et al., 2017). Largely, the evidence argued somatostatin interneurons' critical role in visually induced gamma oscillations (Hakim et al., 2018; Veit et al., 2017) and parvalbumin's critical role in faster networks with great precision in spike timings (Cardin et al., 2009; Kohus et al., 2016). In other words, the shift in peak frequency might depend on the engagement of different subtypes of interneuron.

Like many human studies examining visual gamma rhythms, the current experiment made no distinction between slower and faster rhythms within the gamma range. This can have a significant effect on our findings, because low and high gamma activity are sensitive to reuptake inhibitors in different ways. As mentioned in the introduction, reducing uptake of GABA molecules has a greater effect GABA receptor subtypes with slower kinetics, such as delta-subunit containing GABA receptors. These subtypes dominate the late phase IPSP, or IPSCs further from the peak, leading to a greater effect on frequency for lower frequencies (longer period length rhythms) than higher ones. The two distinct gamma peaks might also explain the large between-subject variability within gamma frequencies in many human EEG and MEG studies.

Any study of gamma rhythms is further complicated by the fact that gamma oscillations are often nested in the activity of slower frequency bands. Nesting refers to the amplitude regulation of faster oscillations by the phase of slower endogenous rhythms. The phase-coupling between gamma and theta activity had been demonstrated repeatedly (Belluscio et al., 2012; Bragin et al., 1995; Colgin et al., 2009; Lundqvist et al., 2011), including studies which found interneurons evoking inhibitory potentials in hippocampal pyramidal cells at theta frequency, despite receiving excitatory pulses at gamma frequency (Gillies et al., 2002; Gloveli et al., 2005). Interestingly, tiagabine is extremely effective in amplifying theta rhythms (Feld et al., 2013; Taranto-Montemurro et al., 2017). This means that the observations we made in gamma band amplitude might be a consequence of tiagabine's modulation of theta rhythms, and not directly from the reduction of GABA uptake. It is difficult to know the impact this process had on the current data, especially considering how the slice works exhibited two distinct gamma rhythms.

2.5.4 Future directions

So far, the non-significant effects of exogenously applied GABA and GABA reuptake inhibitors on gamma activity refute the assumption that overall GABA concentration is a reliable indication of actual GABAergic processes. But additionally, the data also highlighted some issues that should be considered in future experiments, namely the

fluctuations in gamma frequency and amplitude over time and physiological limitations of slice work.

We observed persistent fluctuations in gamma band frequency and amplitude over the course of an hour after tiagabine administration (shown in **Fig. 2.6** B). As our slice preparations were stable physically, we suspect that these fluctuations are caused by complex interactions between multiple homeostatic processes. The peak frequency and amplitude observed at any moment may reflect whichever mechanism was dominant at time of data acquisition, which highlighted the fact that readings were highly dependent on when the slice preparations were sampled. The constructed trajectories of gamma activity in **Fig 2.5** might overlook more fine-grained modulations of the slices. Aside from allowing sufficient time for slices to stabilise, studies should take multiple readings at matched time points to obtain a more accurate picture of the slice's behaviour.

In vitro pharmacological studies allow us to measure neuronal responses for long periods of time and control the pharmacological environment. However, they come with certain limitations. The current experiment cannot provide information about the role of long-range endogenous networks that are involved either in non-visual areas of the brain or visual neuron clusters separated by slicing. Gamma band rhythms are widely regarded as a means of synchronising activation of spatially discrete groups of neurons (Schoffelen et al., 2005; Womelsdorf et al., 2007) and many vital, precortical visual structures, such as the retina, rely heavily on GABA (Wu & Maple, 1998; Yang, 2004). It is possible that GABAergic drive was disrupted or highly abnormal due to networks being confined to one slice alone. Slice work is also time sensitive: the physiological health of the slices inevitably deteriorates over the course of the experiment, decreasing reliability in later readings. In fact, a significant amount of data was rejected due to poor variance explained by the curve fitting function. These issues can be overcome with larger sample sizes, or *in vivo* techniques.

2.5.5 Conclusion

We demonstrated that gamma oscillations can remain unchanged during an increase in GABA concentration in both extrasynaptic and synaptic spaces. The non-significant and inconsistent effects of exogenously applied and GABA reuptake inhibitors on gamma activity respectively highlights two important issues. Firstly, it refutes the assumption that overall GABA concentration is a reliable indication of actual GABAergic processes. Gamma production is highly dependent on the kinetics of $GABA_A$ receptors themselves and not on concentration. Although this information is commonly acknowledged in neurophysiology, it is often omitted in human and non-human primate neuroimaging studies. GABA-dependent processes are often linked directly with GABA estimation carried out using MRS, a technique that cannot distinguish between synaptic, extrasynaptic and unreleased cytoplasmic GABA. This confounds the results on two levels: not identifying GABA based on their location and not differentiating GABA receptor kinetics from GABA concentration. The current findings highlighted the need to consider this in the future.

The second issue involves distinguishing between gamma activity arising from different neuronal subpopulations. We found evidence for the shift of peak frequency from 25-35Hz to 50-70Hz after administering tiagabine. Furthermore, GABA reuptake produced highly inconsistent results across the sample: two showed decreases in gamma frequency, one increase and one ambiguous. On one hand, this might be the product of numerous physiological defence mechanisms regulating the excessive synaptic GABA. However, it might also reflect different responsivity profiles of lower or higher gamma to reuptake inhibitors. Future experiments on this phenomenon should consider monitoring networks involving different interneuron subtypes separately.

3 Chapter 3: Can prestimulus alpha power predict performance accuracy and reaction time in an orientation discrimination task?

3.1 Abstract

Endogenous oscillations of the alpha frequency band are often found in the occipital cortex and have been shown to modulate visual perception. While the literature generally agrees on alpha activity desynchronising (i.e. decreases in power) with visual attention, an increasing number of studies have questioned the cortical specificity of this relationship as well as whether other features of the alpha activity, like phase, might be more predictive of behaviour and perception than power. The current study examines the strength and consistency of the relationship between alpha band activity and visual perception. Specifically, we asked if the amplitude of prestimulus alpha power or scalp-level differences in alpha activity pattern can predict psychophysical performance in a low-level orientation discrimination task.

Seven healthy participants completed a long series of four-alternative forced choice (4AFC) orientation discrimination tasks where they were selected the spatial location of an 'odd one out' tilted grating (with the mean target tilt set at each participant's personal orientation threshold). EEG responses were recorded during the psychophysics session and alpha power in the 500ms preceding stimulus onset was computed as the predictor variable for subsequent analyses. To analyse both large-scale and visual responses separately, we worked with data computed from two groups of electrodes: all 64 EEG sensors and occipital sensors (POz, Oz, O1, O2).

We found significant but inconsistent relationships between prestimulus alpha power with score and response time across the seven participants. Subsequent linear mixed effects models revealed that as a group, prestimulus alpha computed across all 64 EEG sensors significantly predicted reaction time but not scores. Interestingly, we found that a significant correlation between participant's orientation thresholds and degree to which prestimulus alpha predicted performance. We also found no difference between how response time correlated with prestimulus alpha activity measured in the contralateral and ipsilateral hemisphere (respective of the hemifield where the target appeared).

We then asked if the pattern (rather than the localised amplitude) of alpha band activity across the entire head could predict psychophysical performance and trained a support vector machine (SVM) with a linear kernel using responses computed from all EEG channels. We found that the machine was significantly more accurate in classifying hits and misses when trained on EEG activity centred at the alpha frequency range approximately 500-1250ms after stimulus onset. The timing of this high classification performance implied that the result was likely due to a change in the participant's emotional or vigilance state, pending their most recent performance. It also confirmed our previous finding, that spontaneous prestimulus alpha was not predictive of the score.

Overall, spontaneous prestimulus alpha power predicted reaction time on a group level, but not score. However, we also found an interaction between prestimulus alpha effects and overall orientation thresholds suggesting the presence of significant individual differences relating to expertise. This suggests a need to regulate participant's sensitivity to relevant visual features in similar future studies. Lastly, we found that the pattern of alpha band activity after stimulus onset can strongly predict the outcome of the trial, which might be due to a change in internal state based on the participant's most recent performance or feedback.

3.2 Introduction

Alpha activity can be measured within the visual cortex and has been regarded as a marker for attention and cortical excitability for decades (Block, 1996; Rock et al., 1992). Both properties are essential to visual function and has led to increasing amount of research examining the role of alpha in visual perception. More recent studies have evidenced that attention is a robust driver of alpha (Heinemann et al., 2009; Klimesch, 2012; Sundberg et al., 2012) but also that alpha is more generally an indication of cortical inhibition, and is prevalent during tasks that require the subject to actively suppress information (Foxe & Snyder, 2011; Jensen & Mazaheri, 2010; Pfurtscheller, 2001, 2003).

The association between alpha and attention has prompted many studies to induce higher alpha using attentional cues. The subject's attention is directed to a specific location within the visual field, causing a decrease in alpha activity within the cortical area corresponding to the visual field. Items presented in the attended visual field have a higher chance of being detected than the unattended visual field (Sauseng et al., 2005; Thut et al., 2006). Despite a clear association between better performance and alpha desynchronisation, the use of attentional cues was criticised by many studies for being artificial. Visual attention in natural circumstances is spontaneous and its strength and direction follow more probabilistic distributions than when cued (Koike & Saiki, 2006; Pang et al., 2008; Vul et al., 2009). As a result, an increasing amount of research is investigating the relationship between *spontaneous alpha* (alpha activity measured without cues) and visual perception instead.

The relationship between spontaneous alpha and detection of low-intensity stimuli has not been as consistent: one study demonstrated similar trends as attention modulated alpha (Ergenoglu et al., 2004) while another did not (Boncompte et al., 2016). The latter observation was, however, made based on aggregated alpha power. When alpha power in the two hemispheres were considered separately, the authors found contralateral alpha activity negatively correlated with detection rate while ipsilateral alpha activity positively correlated with detection rate. This result implied that the relationship between alpha and visual perception was consistent but would rely on random shifts in attention without a cue.

On the other hand, higher alpha power can also precede improved task performance. This was evidenced within the sensorimotor cortex, where detection and response time towards a haptic stimulus was linked with higher alpha band power (Linkenkaer-Hansen et al., 2004). Interestingly, the authors found that alpha activity within the parietal cortex was even more predictive of performance than alpha measured from the sensorimotor cortex. This suggested that alpha activity was likely inhibiting task-irrelevant cortical areas, and implied that the activity that most strongly predict task performance is not necessarily found in task-relevant cortical areas. This was supported by a later study which found that prefrontal regions significantly modulated occipital alpha activity during a visual task (Sauseng et al., 2005). Both findings drove at the possibility that alpha activity measured across the scalp is a stronger indication of performance than alpha activity measured from a single task-relevant region.

Additionally, very few studies have examined response time in conjunction with task success. Response time can inform us of the individual's vigilance state and clearly interacts with task accuracy (hasty responses can produce more 'mistakes'). A strong positive relationship had been demonstrated between prestimulus alpha power and response time (Zhang et al., 2008), suggesting that in addition to inhibition and attention, alpha is also indicative of vigilance state. We believed that a more comprehensive model predicting task performance using alpha should consider both task accuracy as well as response time.

Our understanding of the alpha-performance relationship can hence be extended by investigating how endogenous alpha activity measured from either parieto-occipital region or across the scalp might predict visual task performance. Task performance should also be broken down into accuracy and response time and considering recent theories about attention (Koike & Saiki, 2006; Pang et al., 2008; Vul et al., 2009), alpha activity should not be driven using visual cues. Additionally, spontaneous alpha from either hemisphere should be analysed separately, considering the hemispheric dissociation found in previous experiments (Kelly et al., 2006; Sauseng et al., 2005; Thut et al., 2006; Worden et al., 2000). This might reveal a difference between the relationship of hemispheric or aggregated alpha with task performance.

The current experiment investigated the relationship between spontaneous prestimulus alpha power and performance in an orientation discrimination task. We conducted our analyses separately for alpha activity localised to the occipital region and alpha activity computed from all available sensors. We first asked if prestimulus alpha power significantly and consistently predicted accuracy and response time on a trial-by-trial basis. We also examined if the modelled relationship differed between contralateral and ipsilateral electrodes. Lastly, we trained an SVM classifier with a linear kernel to predict the outcome of a trial given the pattern of electrical activity across all sensors.

3.3 Methods

3.3.1 Participants

We recruited seven neurotypical participants (age range: 22 to 47 years, three female) from the University of York. All participants had normal or corrected-to-normal visual acuity and all participants but ARW were naïve to the aims of the experiment. All procedures were approved by the University of York Department of Psychology Ethics Committee and all subjects' informed consent was obtained prior to data collection.

3.3.2 EEG recording and apparatus

The stimuli were displayed on a gamma corrected 22.5" ViewPixx display monitor (VPixx Technologies, Saint-Bruno, Canada) at 1920 x 1200 pixels resolution. The monitor has a 120 Hz screen refresh rate and mean luminance of 250 cd/m^2. Calibrations were done using a NIST-traceable Jaz USB photospectrometer with 2nm resolution (Ocean Optics, Dunedin, FL). Participants viewed the screen from 57 cm, resulting in the four stimuli subtending 5° visual angle vertically and horizontally.

We recorded electrophysiology data using 64-channel Waveguard EEG caps and ASA analysis software from ANT Neuro (ANT Neuro, Netherlands) using a 10/20 montage. Vertical electrooculogram data were collected using self-adhesive electrodes placed above the left eyebrow and on the left cheek of participants. The EEG data were sampled at 1000 Hz with a notch filter at 50Hz. The electrode impedance was kept below 10 kΩ. An Arduino Uno (Arduino Inc.) was used to convert serial output from the display system to TTL, generating triggers synchronised to each trial onset.

3.3.3 Stimulus design

Stimuli were created using Psykinematix Visual Psychophysics GPU 2.0.1 software (KyberVision, Japan). The task was designed to test the participant's orientation discrimination abilities using a four-alternative forced choice paradigm. In each trial, four Gabor gratings were shown at the same time in four corners of a square extending 5° visual angle. The choices were presented spatially instead of temporally so as to reduce any effect of memory on the performance, and four choices were used instead of two to reduce the effect of guessing (performance at chance reduced to 25% from 50%) and internal bias.

Prior to the experiment, each participant's orientation discrimination threshold was obtained using a Bayesian staircase paradigm. The task for obtaining threshold was identical to that of the main experiment: the participants were instructed to select the interval containing the grating that was not vertical using the keyboard. Keys 'q', 'a', 'p' and 'l' indicated top left, bottom left, top right and bottom right intervals respectively. The tilted grating had a 0.25 probability for appearing in any of the four locations (see **Fig. 3.1** A for visualisation). A low contrast dot in the centre of the screen indicated the start of a new trial. This was followed by a pre-stimulus delay of approximately 650ms and presentation of stimuli for 200ms. The participant then had approximately 500ms to respond and was given feedback (high beep tone for right interval selected, low beep tone for wrong) (see **Fig. 3.1** B for visualisation). There was a 200ms inter-stimulus interval (ISI) between each trial. Each trial (excluding ISI) lasted approximately 1400ms.

The orientation of the gratings during the initial threshold blocks ranged from vertical (0°) to diagonal (45°), tilting anti-clockwise and gradually converged on a threshold value after 40 trials. We repeated this task three times and calculated the average threshold tilt value which was subsequently used in the experiment. Participants then completed 1400 continuous trials for the main experiment.

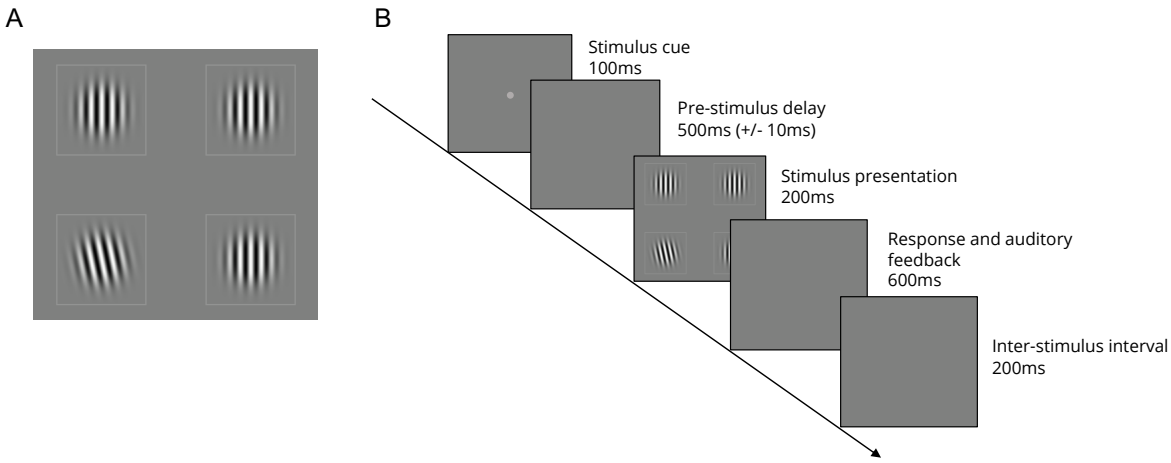

Fig. 3.1 *(A) Example of a single trial during the experiment. In this case, the bottom-left interval contains the tilted grating and participants who correctly identify this target should press 'a'. (B) Breakdown of the components within a single trial: stimulus cue, prestimulus delay, stimulus presentation, response period and ISI.*

3.3.4 EEG data processing and artifact removal

The data were processed in Matlab 9.4 (R2018a, MathWorks Inc., Natick, MA, USA). Approximately 1% of triggers were faulty and not recorded by the EEG system. We identified the affected trials by locating the triggers which were more than 1.2 times the expected duration apart from each other and removed them from the final data analysis.

EEG data were preprocessed using the FieldTrip toolbox for EEG/MEG-analysis (Oostenveld et al., 2011). Continuous EEG data were bandpass filtered between 2Hz and 40Hz. We then applied independent component analysis (ICA) (Bell & Sejnowski, 1995) using the Fieldtrip command *ft_componentanalysis* on the

remaining data to identify noisy components caused by muscle movements. All components were inspected visually and those clearly manifesting blink- or cardiac artifacts were removed before reconstructing the time series.

The processed EEG data were then segmented into trials, each containing 1650 samples (750ms pre-stim and 900ms after stimulus onset). We Fourier transformed the 500 samples (or 500ms) of EEG data prior to stimulus onset and computed the RMS amplitude of the frequencies between 8Hz and 12Hz inclusive as an estimate of alpha power during this period. EEG data were then averaged across four sets of electrodes for the univariate analyses: (1) across all 64 channels, (2) across the four posterior-most electrodes, covering the occipital cortex (Oz, O1, O2 and POz), (3) across occipital electrodes on the left hemisphere (O1, PO3, PO5) and (4) across occipital electrodes on the right hemisphere (O2, PO4, PO6).

3.3.5 Psychophysics data processing

We measured psychophysical performance on two attributes: task accuracy and reaction time. To calculate epoched scores, we ran a sliding window (with a window size of 10 trials) along a vector of responses (‘hits or ‘misses’) and calculated the proportion of ‘hit’ trials out of ten. For ease of analysis, we binned reaction time into 12 ‘reaction time categories’ ranging from 200ms to 800ms with a bin size of 50ms. As an example: a reaction time of 430ms would be classed as category ‘5’.

3.3.6 Data analysis

To investigate the relationship between prestimulus alpha and psychophysical performance, we first built linear regression models based each participant’s data. To do this, we grouped each participant’s psychophysical performance by bins and obtained the corresponding average prestimulus alpha power. This was followed up by a linear model based on the grand average prestimulus alpha at each bin (across all participants).

We used a generalised linear mixed effect model for the final analysis. The linear mixed effect model is similar to a linear regression model but allows for both fixed effects (in this case, the relationship between prestimulus alpha and psychophysical performance) and random effects (participants) of variables. The linear mixed effect model, unlike an ANOVA or linear regression, also includes all unaggregated observations from each participant, which makes it a powerful statistical test that is able to explain a higher proportion of variance.

Simple linear regressions were modelled in IBM SPSS Statistics for Macintosh (version 25.0) and linear mixed effect models were modelled in R (version 3.4.3, R Core Team, 2013) using the *lmer* function in *lme4* (Bates et al., 2015) and *summary* and *anova* functions in *lmerTest* (Kuznetsova et al., 2017) to obtain p-values through Likelihood Ratio Tests (LRT). Lastly, we calculated the proportion of variance explained by fixed effects only (marginal R^2) and proportion of variance explained by fixed and random effects (conditional R^2) using the *r.squaredGLMM* function in the *MuMIn* package (version 1.43.15, Barton, 2014).

3.4 Results

The results are organised in three parts. We first describe some initial visualisations of the data, followed by univariate analyses involving EEG responses averaged across visual electrodes. Lastly, we present the findings of a multivariate classification paradigm, predicting 'hits' and 'misses' with prestimulus alpha patterns.

We plot epoched alpha power (standardised within individual participants) recorded at occipital visual electrodes (**Fig. 3.2** A), binned scores (**Fig. 3.2** B) and reaction time (**Fig. 3.2** C) across the duration of the experiment. All three variables appeared to vary significantly during the experiment and are uncorrelated across subjects. We also plot single trial data for the same electrodes averaged across individual trials for each subject in **Fig. 3.2** D, which shows a distinct visually evoked component at the point of stimulus onset (which starts at approximately 750ms and ends at approximately 950ms within each trial). Using **Fig. 3.2** D, we estimated that the visually evoked potential (VEP) averages fewer than 8 cycles per second. This

indicates that it is slower than alpha range and will not be a confounding factor when we calculate alpha power later. We also plot prestimulus and poststimulus alpha power collected at each electrode for each possible score bin. The results show a strong positive correlation between pre- and poststimulus alpha power suggesting that our estimate of poststimulus alpha power is not entirely controlled by the deterministic VEP (**Fig. 3.2** E).

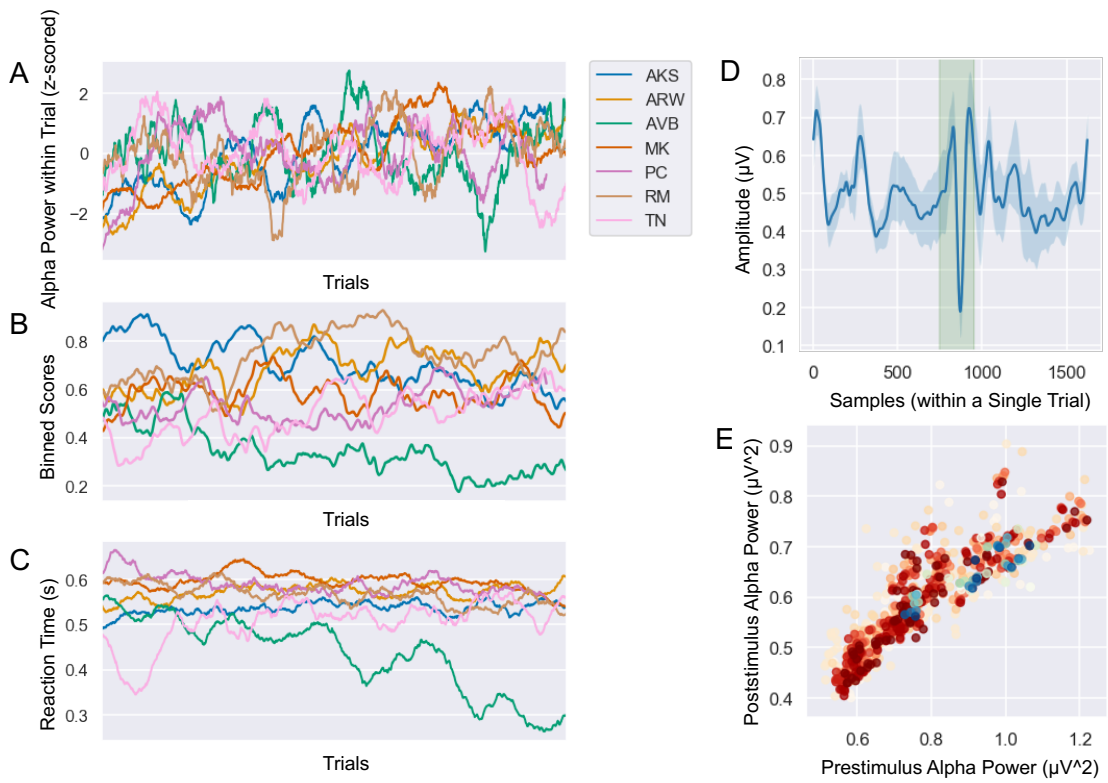

Fig. 3.2 *(A) Standardised alpha power, (B) binned scores and (C) reaction time across all trials for each of the participant. We observed great variation in these metrics across the experimental session. (D) Time series of averaged alpha power recorded at occipital visual electrodes (Oz, O1, O2 and POz), averaged across all participants for each trial. Blue shaded area denotes error of 1 SEM and green shaded area denotes stimulus presentation. We observe a stereotypical VEP is generated by the stimulus presentation. (E) Correlation plot between prestimulus and poststimulus alpha power. Blue denotes visual electrodes; gradient indicates scores with higher scores presented in darker colours. Figure shows a high correlation between pre- and poststimulus alpha levels.*

3.4.1 Univariate analyses: linear regression and mixed effect model

Mean alpha power varies across subjects and we are concerned primarily with deviations from the mean. We therefore calculated the *standardised* alpha power within each participant by z-scoring the raw alpha power. The z-scored alpha power formed the predictor variable in the following models. We fitted linear regression models to each participant's data separately as well as the group mean, using standardised alpha power to predict either binned scores or reaction time (**Fig. 3.3** and **Fig. 3.4** respectively).

3.4.1.1 Statistical analysis of binned scores

First, we asked whether there was a statistical relationship between alpha power and task accuracy. Task accuracy, or binned score, was defined by the proportion of correctly identified intervals out of ten trials.

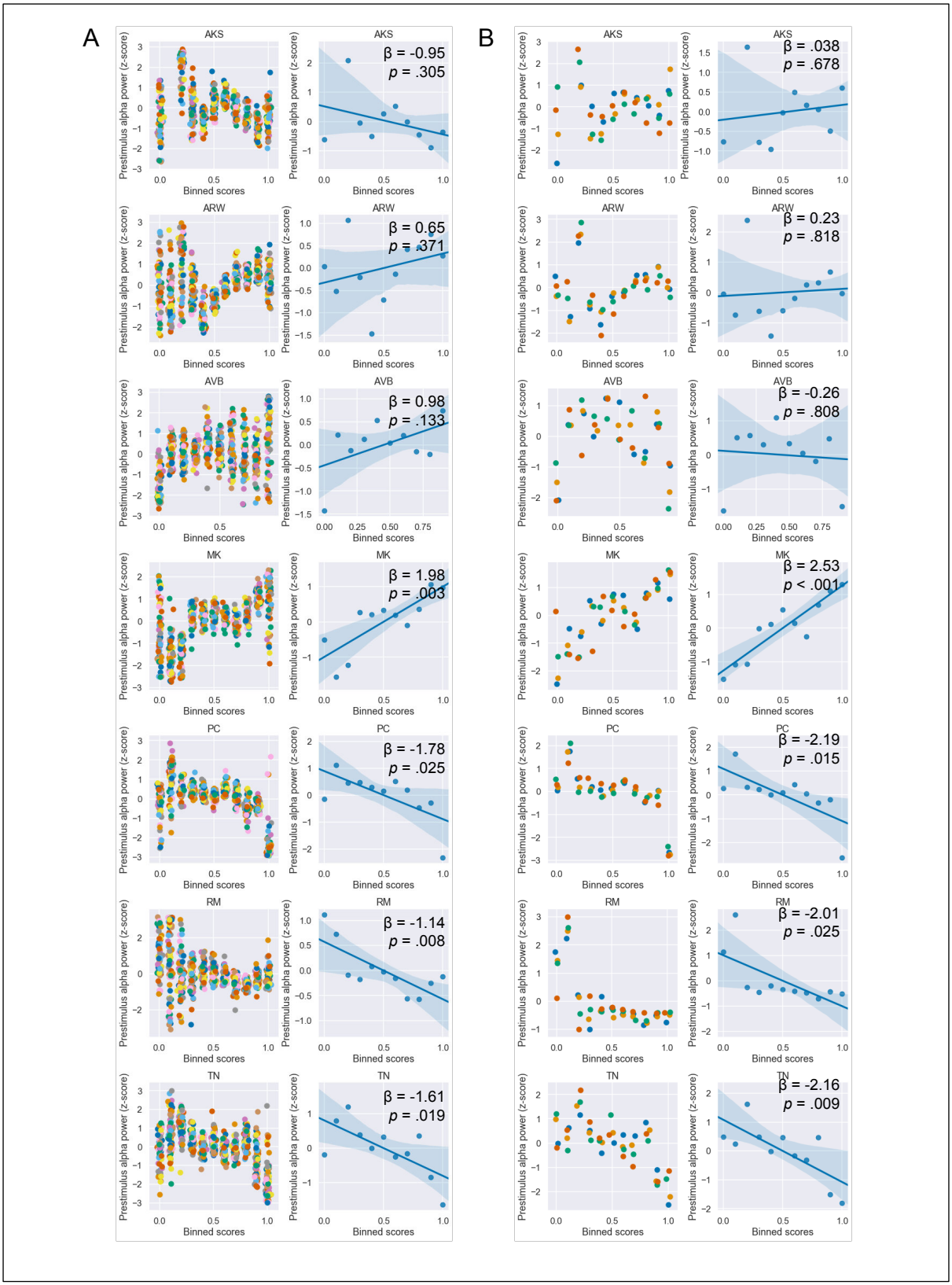
A
B
AKS
ARW
AVB
MK
PC
RM
TN
Prestimulus alpha power (z-score)
Binned scores
β = -0.95
p = .305
β = 0.65
p = .371
β = 0.98
p = .133
β = 1.98
p = .003
β = -1.78
p = .025
β = -1.14
p = .008
β = -1.61
p = .019
β = .038
p = .678
β = 0.23
p = .818
β = -0.26
p = .808
β = 2.53
p < .001
β = -2.19
p = .015
β = -2.01
p = .025
β = -2.16
p = .009

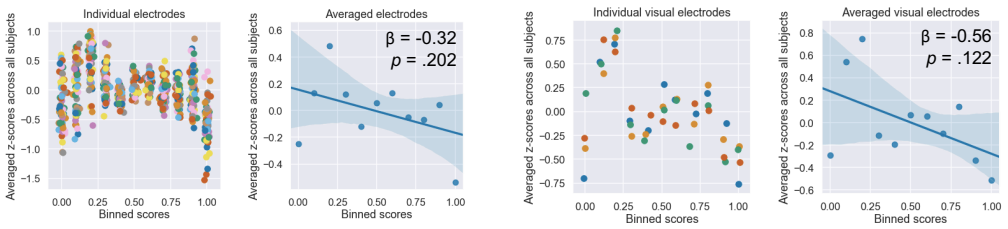

Fig. 3.3 *Scatterplots of the relationship between performance accuracy on the orientation discrimination task and the alpha power in the 500ms period before stimulus onset from (A) all 64 electrodes or (B) occipital visual electrodes only. Each electrode is denoted by a single colour. Left column represents responses at individual electrode and contains a jitter of 0.25 standard deviation (range * .01) for better visualisation. Right columns show averaged alpha power at each binned score from those electrodes with a best fit straight line. Shaded region represents bootstrapped 95% confidence interval.*

3.4.1.1.1 Linear regression models

3.4.1.1.1.1 Individual data

We ran separate linear regression models for each participant's data. We found four out of seven models significantly predicted binned scores using prestimulus alpha power for both data averaged across all electrodes (*AKS:* R^2 = *.13,* $F(1,8) = 1.20$, p = .305; *ARW*: R^2 = *.09,* $F(1,9) = .89$, p = .371; *AVB*: R^2 = *.26,* $F(1,8) = 2.80$, p = .133; *MK*: R^2 = *.65,* $F(1,9) = 16.81$, p = .003; *PC*: R^2 = *.45,* $F(1,9) = 7.22$, p = .025; *RM*: R^2 = *.56,* $F(1,9) = 11.56$, p = .008; *TN*: R^2 = *.47,* $F(1,9) = 8.08$, p = .019) and visual electrodes (*AKS:* R^2 = *.02,* $F(1,8) = 0.19$, p = .023; *ARW*: R^2 = *.01,* $F(1,9) = 0.06$, p = .818; *AVB*: R^2 = *.01,* $F(1,8) = 0.06$, p = .808; *MK*: R^2 = *.83,* $F(1,9) = 43.86$, p = <.001; *PC*: R^2 = *.50,* $F(1,9) = 9.05$, p = .015; *RM*: R^2 = *.45,* $F(1,9) = 7.27$, p = .025; *TN*: R^2 = *.55,* $F(1,9) = 11.03$, p = .009). Details of linear regression models based on each participant's data can be found in Appendices (**Table 3.6** and **Table 3.7**).

3.4.1.1.1.2 Group averaged data

The standardized alpha power across (**Table 3.1**) all electrodes or (**Table 3.2**) visual electrodes only were averaged across all seven participants and a simple linear

regression was computed to predict binned scores based on this averaged prestimulus alpha power. We found that averaged prestimulus alpha power was not a significant predictor of binned scores for either sets of electrodes (all electrodes: R^2 = .17, $F(1,9) = 1.89$, p = .202; visual electrodes: R^2 = .24, $F(1,9) = 2.91$, p = .122).

Table 3.1 *Details of the linear regression model for data averaged across all participants (all electrodes).*

Variable	b	SE	β	*t*	p
Intercept (Constant)	0.28	0.14		1.12	.290
Standardised alpha power	-0.32	0.24	-.417	-1.38	.202

Table 3.2 *Details of the linear regression model for data averaged across all participants (visual electrodes).*

Variable	b	SE	β	*t*	p
Intercept (Constant)	0.28	0.19		1.44	.183
Standardised alpha power	-0.56	0.33	-.49	-1.71	.122

3.4.1.1.2 Linear mixed effect model

We ran two linear mixed effects models on the combined data of all seven participants using standardised prestimulus alpha power as the fixed effect predictor, participant as the random effect and binned score as the dependent variable. Prestimulus alpha power in the first model is calculated from all electrodes across the scalp, while the second model was built from responses in the occipital region. As the relationship between alpha and performance clearly vary between participants, we allowed for random intercept as well as random slope. The inclusion of random effects of participant resulted in a greater proportion of variance explained (from < 1% to 35%), as shown by the increase in conditional R^2 from marginal R^2.

Both linear mixed effects models revealed non-significant effects of prestimulus alpha power on binned score (all electrodes: $F(1, 9947) = 0.76$, $p = .384$, marginal $R^2 < .001$, conditional $R^2 = .36$; visual electrodes only $F(1, 9947) = 0.43$, $p = .510$, marginal $R^2 < .01$, conditional $R^2 = .35$). This showed that prestimulus alpha power did not predict binned scores in a linear manner.

3.4.1.2 Statistical analysis of reaction time

Performance can interact with reaction time: hasty decisions will produce shorter reaction times but might also increase error rate. On the other hand, alpha power might primarily alter reaction times while participants maintain the same performance level. To investigate this possibility, we repeated the regression analysis using reaction time as the dependent variable.

3.4.1.2.1 Linear regression models

3.4.1.2.1.1 Individual data

We ran separate linear regression models for each participant's data with reaction time as the outcome variable. We found one out of seven models significantly predicted reaction time using responses recorded at all electrodes (AKS: $R^2 = .75$, $F(1,10) = 29.37$, $p < .001$; ARW: $R^2 = .06$, $F(1,10) = 0.67$, $p = .432$; AVB: $R^2 = .13$, $F(1,10) = 1.54$, $p = .242$; MK: $R^2 = .17$, $F(1,8) = 1.63$, $p = .237$; PC: $R^2 = .25$, $F(1,10) = 3.24$, $p = .102$; RM: $R^2 = .25$, $F(1,10) = 3.31$, $p = .099$; TN: $R^2 = .10$, $F(1,10) = 1.13$, $p = .312$) and visual electrodes (AKS: $R^2 = .75$, $F(1,10) = 29.18$, $p < .001$; ARW: $R^2 = .02$, $F(1,10) = 0.16$, $p = .701$; AVB: $R^2 = .04$, $F(1,10) = 0.40$, $p = .543$; MK: $R^2 = .26$, $F(1,8) = 2.86$, $p = .130$; PC: $R^2 = .16$, $F(1,10) = 1.96$, $p = .192$; RM: $R^2 = .29$, $F(1,10) = 4.08$, $p = .071$; TN: $R^2 = .42$, $F(1,10) = 7.14$ $p = .023$). Details of linear regression models can be found in Appendices (**Table 3.8** and **Table 3.9**).

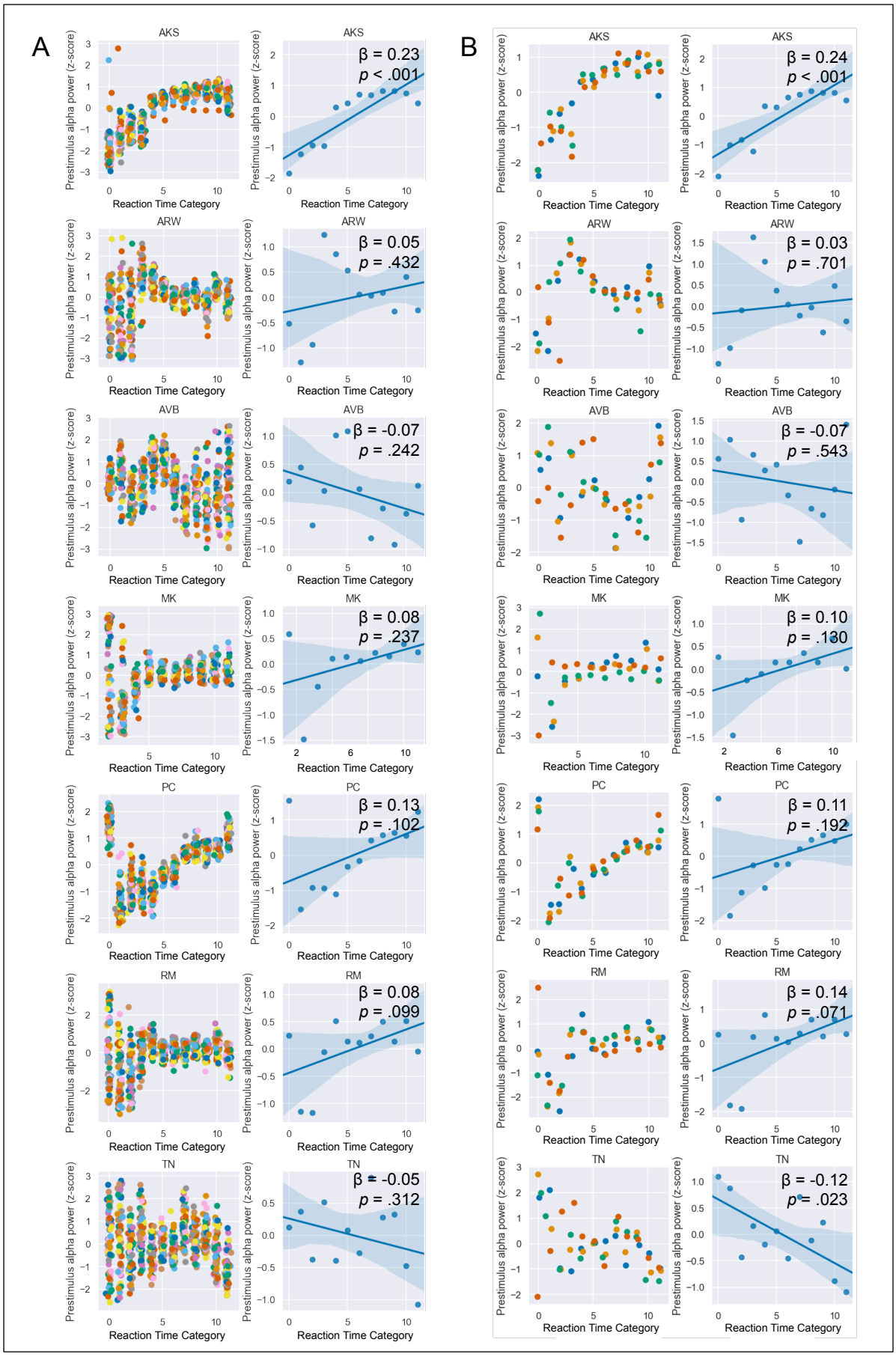
A
B
AKS
ARW
AVB
MK
PC
RM
TN
Prestimulus alpha power (z-score)
Reaction Time Category
β = 0.23
p < .001
β = 0.24
p < .001
β = 0.05
p = .432
β = 0.03
p = .701
β = -0.07
p = .242
β = -0.07
p = .543
β = 0.08
p = .237
β = 0.10
p = .130
β = 0.13
p = .102
β = 0.11
p = .192
β = 0.08
p = .099
β = 0.14
p = .071
β = -0.05
p = .312
β = -0.12
p = .023

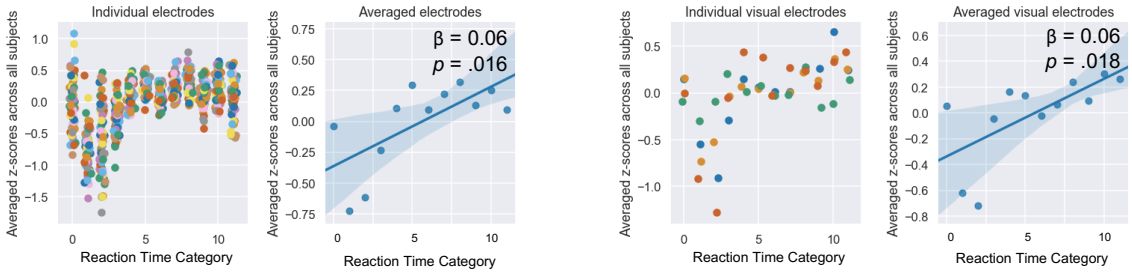

Fig. 3.4 *Scatterplots of the relationship between reaction time for the orientation discrimination task and the alpha power in the 500ms period before stimulus onset from (A) all 64 electrodes or (B) occipital visual electrodes only. Each electrode is denoted by a single colour. Left column represents responses at individual electrode and contains a jitter of 0.25 standard deviation (range * .01) for better visualisation. Right columns show averaged alpha power at each binned score from those electrodes with a best fit straight line. Shaded region represents bootstrapped 95% confidence interval.*

3.4.1.2.1.2 Group averaged data

We ran a similar linear regression model to predict reaction time based on averaged prestimulus alpha power. We found that in prestimulus power was a significant predictor of reaction time for both sets of electrodes (all electrodes: R^2 = .45, $F(1,10)$ = 8.29, p = .016; visual electrodes: R^2 = .442, $F(1,10)$ = 7.91, p = .018) (see **Table 3.3** and **Table 3.4**).

Table 3.3 *Details of the linear regression model for data averaged across all participants (all electrodes).*

Variable	b	SE	β	*t*	p
Intercept (Constant)	-0.36	0.15		-2.50	.031
Standardised alpha power	0.06	0.02	.67	2.88	.016

Table 3.4 *Details of the linear regression model for data averaged across all participants (visual electrodes).*

Variable	b	SE	β	*t*	p
Intercept (Constant)	-0.34	0.14		-2.43	.035
Standardised alpha power	0.06	0.02	.67	2.81	.018

3.4.1.2.2 Linear mixed effect model

Similar to binned scores, we ran two linear mixed effect models to examine how prestimulus alpha (from all electrodes and from visual electrodes only) predicted reaction time with the allowance of random intercept and random slope. The models revealed that prestimulus alpha power summed over the entire scalp was a significant predictor of reaction time: $F(1, 9571.40) = 7.78$, $p = .005$, marginal $R^2 = .001$, conditional $R^2 = .22$), but this effect was not found for alpha rhythms in the occipital cortex $F(1, 9581.40) = 3.07$, $p = .080$, marginal $R^2 < .001$, conditional $R^2 = .23$) (see **Table 3.5** for detail).

Table 3.5 *Details of the significant linear mixed effect model predicting reaction time from prestimulus alpha.*

Variable	b	SE	β	*t*	p
Intercept (Constant)	0.54	0.01		26.07	<.001
Standardised alpha power	0.02	<0.01	-0.13	2.79	.005

3.4.2 Relationship between alpha power and orientation threshold

We decided to run an additional analysis looking at how the direction and strength of relationship between prestimulus alpha and task accuracy might change in accordance with orientation discrimination threshold. The relationship between alpha and psychophysical performance is represented by the standardised coefficient (beta) produced by the linear regression models described previously. We ran a Pearson's correlation and found a strong significant correlation between orientation discrimination threshold and unstandardised coefficients for binned scores ($r = -.86$, $p = .014$) but not for reaction time ($r = .18$, $p = .692$). This effect was only significant for all electrodes, but not for responses gathered at visual electrodes only ($r = -.65$, $p = .111$; $r = .01$, $p = .982$; see **Fig. 3.5**).

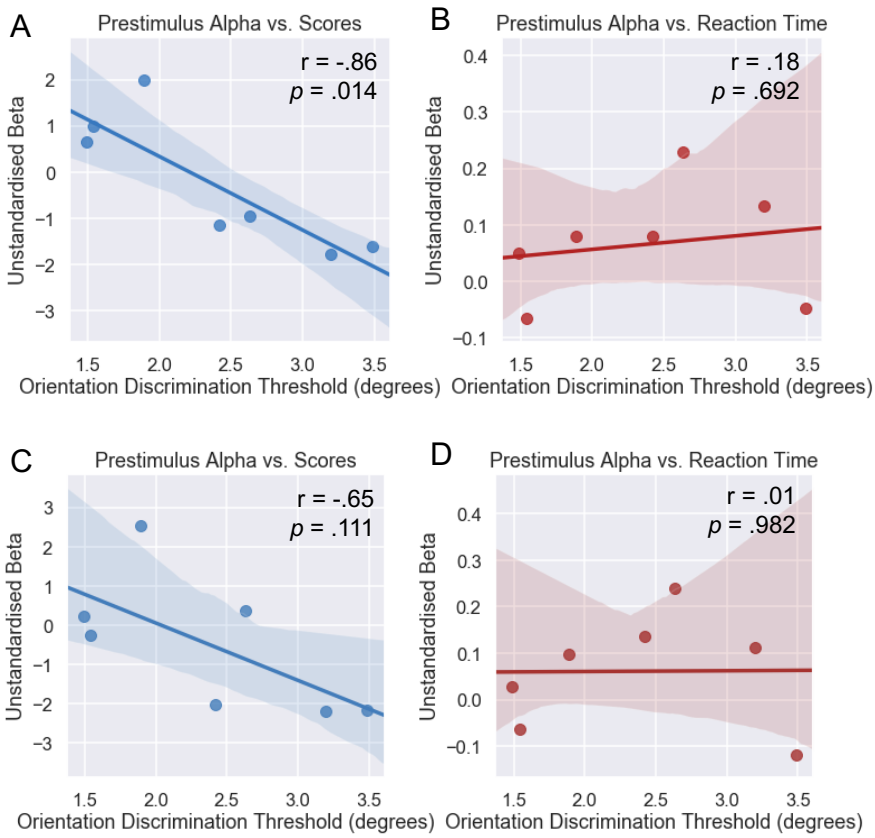

Fig. 3.5 *Standardised coefficients (betas) from linear regression models and participant's corresponding orientation discrimination threshold (measured in tilt °). Participants who require smaller tilts to detect differences have lower orientation discrimination thresholds (i.e. higher sensitivity to changes in orientation). We found an association between participant's orientation discrimination threshold and direction of relationship between alpha power and scores: participants with higher orientation discrimination thresholds exhibit more negative correlations between prestimulus alpha and scores for responses gathered from all electrodes (A) but not responses gathered from visual electrodes only (C). Similarly, no significant correlation was found between alpha and reaction time with orientation discrimination thresholds (B and D).*

3.4.3 Laterality of alpha power modulation

Previous studies on alpha and attention often involve cuing the participant to one hemifield then comparing how alpha from the hemisphere contralateral or ipsilateral to the target differed in predicting performance (Kelly et al., 2006; Sauseng et al., 2005; Thut et al., 2006; Worden et al., 2000). To investigate whether this distinction is important with *spontaneous* alpha, we separated targets based on their location

(left or right hemifield) before analysing responses from the corresponding contralateral and ipsilateral occipital regions. We asked if the relationship between behaviour and alpha power depended on the laterality of the sensors (ipsi- vs contra-lateral). The results are plotted per participant and summarised below (**Fig. 3.6**).

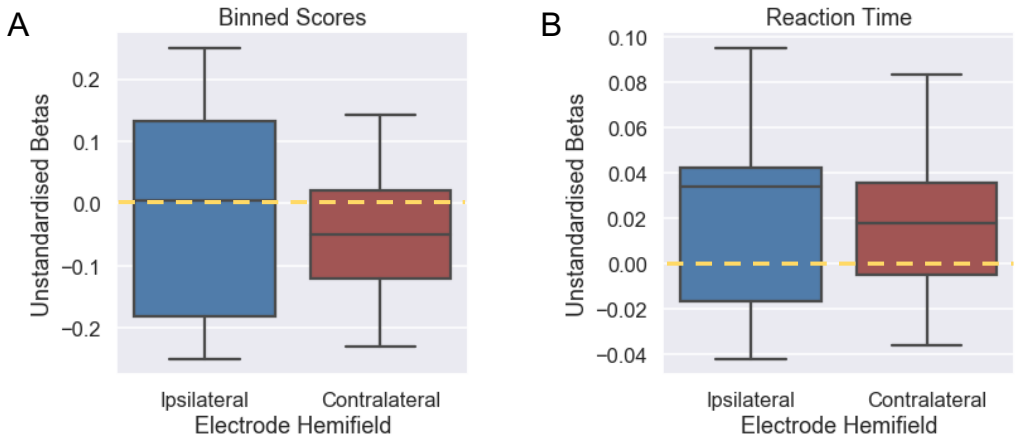

Fig. 3.6 *Box plots indicate the relationship (quantified by unstandardized beta from linear regression models) between binned scores (left) and reaction time (right) with alpha band responses found in either the ipsilateral (blue) or the contralateral (red) electrodes. Paired sample t-tests revealed that contralaterally measured alpha power did not predict performance differently from ipsilaterally measured alpha power for binned scores and reaction times.*

Similar to the previous analysis on orientation thresholds, we quantified the relationship between alpha and behaviour using the unstandardised beta from each participant's linear regression model. We ran two-tailed paired sample t-tests and found that unstandardised betas for both alpha predicting binned scores: $t(13) = -0.99$, $p = .339$ and alpha predicting reaction time: $t(13) = 0.17$, $p = .869$ were non-significant. Together with a visualisation of the data in **Fig. 3.6**, the data showed that neither contralateral nor ipsilateral spontaneous alpha power predicted behavioural data.

3.4.4 Multivariate analysis: SVM

The data above are based on univariate measures of mean alpha from defined sets of electrodes (all 64 sensors or occipital electrodes POz, Oz, O1, O2). However, it is

possible that performance is related more to the *pattern* of alpha amplitudes across the scalp: Perhaps, for example, the relative amplitudes of frontal and occipital alpha are more informative than their absolute levels? To address this, we asked whether we could classify performance ('hits' versus 'misses') based on the multivariate alpha amplitudes at different points across a trial – using the alpha power computed in a sliding 500ms window.

We ran a SVM using the 'libsvm' function (Chang & Lin (2011); software available at https://www.csie.ntu.edu.tw/~cjlin/libsvm/), with a linear kernel function and calculated classification accuracy using a leave-one-out cross validation methods. The task of the pattern classifier was to predict performance (correct / incorrect) on each trial. To avoid bias effects, we bootstrapped the data by randomly selecting an equal sample of 108 'hits' and 108 'misses' without replacement, arranging them into subgroups of 18 values each and using the mean of each subgroup. We repeated this process 100 times and obtained the averaged classification accuracy (percentage correct) at each output frequency across the frequency range per subject per bin. The chance (guessing) level was 50% as there were two possible outcomes. The data plotted are the averaged performance measures across all subjects.

Fig. 3.7 A shows the mean accuracy of the pattern classification algorithm for 500ms bins starting at -2000ms before the stimulus onset and ending approximately 2000ms after with the trial occurring at 0ms. **Fig. 3.7** B shows the result of the same procedure applied to datasets with scrambled labels.

We find that classification is significantly *above* chance for bins in the frequency band centred on 11Hz at time points between approximately 100 and 800ms *after* stimulus onset. As these data are based on the incoherently averaged power during each bin, we do not know whether poststimulus performance is driven by the phase locked VEP or the phase randomised endogenous alpha power.

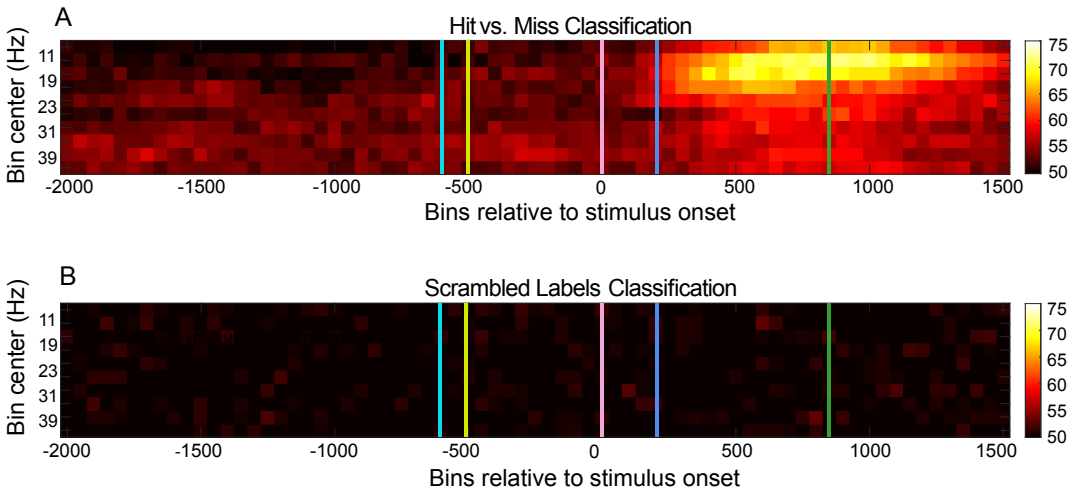

Fig. 3.7 (A). Heatmap of classification accuracy for incoherently averaged EEG data. This method of averaging is phase-insensitive and preserves phase-randomised endogenous band power. Coloured lines indicate stimulus epochs: cyan -100ms stimulus cue, lime green - start of 500ms prestimulus delay, pink - 200ms stimulus display, blue - start of 600ms response period and green - start of 200ms ISI. High accuracies were found when training the machine on signals of around 11Hz found 400 to 1200ms after stimulus onset, corresponding mostly to response period and ISI immediately after. (B) Heatmap with the same parameter as (A) but with scrambled labels ('hits' and 'misses' randomly chosen). Classification accuracy was consistently as chance level across the frequency range and bins tested.

3.5 Discussion

Prestimulus alpha power of each participant was used to predict binned scores and reaction time. We found that approximately half the participants showed significant relationships between prestimulus alpha power and scores. Because this effect had different polarities for different subjects, it was not significant at the group level. In addition, we found a significant relationship between alpha and reaction time at the group level.

A visualisation of **Fig 3.3** revealed that some participants' alpha power correlated positively with scores while others correlated negatively. This relationship was stable across different electrode groups (all and occipital). We quantified each participant's relationship between prestimulus alpha and psychophysical performance by the linear regression's unstandardized beta values (i.e. slope of the model) and found

that these were significantly modulated by the participant's orientation thresholds. In contrast, orientation threshold values did not change prestimulus alpha's prediction of response time. Finally, we grouped response by visual electrodes contralateral or ipsilateral to the visual hemifield where target was presented. While we did not observe any differences between contralateral and ipsilateral responses within subjects, we observed that contralaterally recorded prestimulus alpha appeared to have more positive relationships with reaction time.

We found a peak of classification accuracy approximately 500-1250ms after stimulus onset in the alpha frequency range (centred at 11Hz). Interestingly, classification accuracy was at chance in the 500ms prior to stimulus onset, which implies that while averaged prestimulus alpha power *amplitude* corresponded to task performance in some participants, there was no distinct *spatial pattern* of activity prior to hits or misses.

To summarise, we find that psychophysical performance was not consistently predicted by prestimulus alpha at a group level, but subsequent experiments should consider differences in alpha-based modulations based on the subject's sensory thresholds. Unlike attention-driven alpha activity, spontaneous alpha measured from both contralateral and ipsilateral sensors did not differ significantly in terms of predicting task behaviour. The spatial pattern of alpha band activity approximately 500ms after stimulus onset accurately predicted hits and misses. Since this activity occurs after the stimulus presentation, it is unlikely to reflect attention or arousal and may, instead, be driven by the auditory feedback component of the psychophysical trial.

3.5.1 Relationship between expertise and alpha

Perceptual learning is the process where an individual gradually improves in low-level visual task performance after ample practice. While task aspects like study design (Kuai et al., 2005) and feedback (Aberg & Herzog, 2012; Petrov et al., 2006)

strongly influence the rate of perceptual learning, participants who have had more practice are more likely to perform better during future hyperacuity tasks.

Assuming orientation discrimination to be a measurement of task expertise or experience, the strong relationship between orientation discrimination *thresholds* and unstandardised *betas* might be evidence for task-expert dependent internal state. Repetitive tasks in predictable conditions are correlated with increased engagement of the default mode network (Vatansever et al., 2017). Participants who have been trained by similar experiments before might enter an 'autopilot' mental state during the current experiment, which produces rapid, accurate responses. This is only possible in task experts who are extremely familiar with the task, while those who are unfamiliar with the task exert more effortful conscious attention.

One explanation for the inconsistencies between participants' alpha–psychophysical performance relationships might be that prestimulus endogenous power indicates conscious awareness. Conscious awareness is not necessarily reflected in task performance: a recent study showed that prestimulus endogenous signals were strong predictors of self-reported awareness scores (lower awareness associated with higher prestimulus alpha) but not participant's accuracy in a contrast discrimination task (Samaha et al., 2017). Similarly, reaction time might be more dependent on vigilance, which does not necessarily correspond to alpha power (van Dijk et al., 2008). Furthermore, although cortical excitability might be most strongly reflected in alpha band activity, there is no reason alpha rhythms should modulate stimulus-driven activity differently from endogenous neural noise (Samaha et al., 2017). Any effect alpha activity has on stimulus-driven responses should also influence the global neural noise, resulting in no difference in the SNR.

Contradictory alpha–performance relationships may be related to the source of the alpha activity. Local field potential and multiunit recordings have shown that alpha generated in V2 and V4 came from all examined layers: supragranular (superficial), granular, and infragranular (deep), while alpha generated in the inferotemporal cortex was found only in supragranular and infragranular layers (Bollimunta et al., 2011). The functional correlates of alpha varied with regards to where the primary alpha generator was located: those predominantly generated in the deep layers (as

for the visual areas) reflected functional inhibition, while those generated in the superficial layers (as with inferotemporal cortex) corresponded to cortical excitability. These spatial differences may explain some of the differences in findings across the EEG literature.

Considering the strong evidence for alpha modulating visual performance, we take into account two differences in methods that might have contributed to our current observations. First, previous literature has shown that the power spectrum of the period right before stimulus onset is significantly smaller with better performance (Busch et al., 2009). Unsurprisingly, this included alpha band activity, where summed power was much greater for instances where participants failed to identify the stimulus. This effect was the most robust at approximately -600ms to -300ms before stimulus onset, indicating the possibility that there is a more optimal time period for extracting prestimulus alpha. However, a smaller sampling window would further decrease the frequency resolution of the frequency domain data, making it difficult to isolate alpha band signals precisely. Secondly, previous studies also drew a distinction between the functions of lower frequency and higher frequency alpha (Pfurtscheller, 2003; Pfurtscheller et al., 2000). Only alpha activity of frequency between 10-12Hz correlated significantly to memory performance, surprisingly with greater alpha power correlating positively with performance (Vogt et al., 1998). Additionally, a recent study had observed that performance following higher and lower alpha power were virtually identical, while intermediate alpha power reliably predicted accuracy and reaction time (Linkenkaer-Hansen et al., 2004). The current experiment did not make a distinction between frequency bands within the alpha range, which might have concealed an association between alpha and performance that is exclusive to higher, intermediate or lower alpha. Post-hoc selection of subdivided alpha bands is also potentially susceptible to statistical multiple comparisons errors.

Although contralateral and ipsilateral alpha power was not significantly different within each participant, we found that contralateral alpha power exhibited a significantly positive relationship with reaction time. Since no visual prestimulus cues were provided in this experiment, this finding revealed the strong association

between spontaneous alpha power, as opposed to attention-modulated alpha power, with reaction time.

The SVM classification results confirmed that prestimulus alpha contains little information about subsequent trial performance (hits and misses). While the region of very high classification accuracy *is* centred around the alpha frequency band, it occurs approximately 500ms to 1250ms *after* stimulus onset. The timing of the high classification accuracy implied some dependency on the outcome of the trial just passed, which leads to our proposal that the high classification accuracies were caused by performance- or feedback-dependent changes in the participant's internal state after completing each trial.

A recent study has shown that emotional states can significantly alter alpha in the frontal cortex (Rajabi et al., 2017). In addition, numerous studies have evidenced the interconnections between vigilance (Davis & Whalen, 2001), motivation (Begleiter et al., 1983; Hömberg et al., 1981) and stress (Hancock & Warm, 1989) with endogenous state and maintenance of long-term attention (Oken et al., 2006). Hence, we interpreted the classification results as a change in internal state following task performance reflected in alpha band activity. Unfortunately, we do not know exactly how feedback or perceived performance alters the internal state of each participant. Successful trials might lead to a brief 'relaxation' – or an increase in motivation. Conversely, after a miss, some subjects might experience in decline in motivation while others feel the need to 'do better'.

3.5.2 Future Directions

3.5.2.1 Phase

An aspect of alpha oscillation this study did not consider is the phase. Literature suggest that the likelihood of perceiving a near-threshold target depends on the phase of the endogenous oscillation at the time of visual input – possibly because alpha power reflects modulations in mean population membrane potentials. Along

with amplitude, the phase of endogenous rhythms also reflect local electrical field potentials (Buzsáki & Draguhn, 2004). In fact, the phase of slower oscillations regulates both the rate at which neurons fire as well as several faster oscillations. This means that depending on the endogenous phase at which near-threshold inputs arrives, the responses generated by the system can be enhanced or attenuated, which then affects the likelihood this stimulus would be perceived (Schroeder & Lakatos, 2009). One example of this is in the Active Visual Sensing Hypothesis (Leszczynski & Schroeder, 2019): where phases of endogenous oscillations are reset using saccades, which ensures high excitability when the observer fixate, giving the visual input arriving in that moment a better chance of being perceived.

Due to the fast, temporally precise nature of the visual system, some authors argue that alpha phase offers a more appropriate modulation of visual perception than alpha amplitudes. Alpha band activity is linked with information transmission from the LGN to the visual cortex. Observer's sensitivity to changes in the stimulus is synchronised with the phase of endogenous alpha rhythms. The relationship is strong enough to predict observer's performance on discriminating near-threshold stimuli: phase angles could predict 'hits' and 'misses' and alpha band signals were strongest at approximately 500ms prior to stimulus presentation (Busch et al., 2009)

3.5.2.2 Frequency

Reaction time is also correlated with alpha *frequency* measured from contralateral electrodes and faster alpha band rhythms coincided with quicker and more accurate visual perception of stimuli presented in quick succession (Samaha & Postle, 2015). This clearly demonstrates the stochastic conscious perception of the observer at certain time points during stimuli presentation, depending on the frequency of alpha signals. While the current study did not find an association between alpha power and task accuracy, these studies imply that alpha phase and frequency might be more appropriate at predicting trial success.

Some recent studies contend that psychophysical performance indicates changes in internal decision criterion and not spontaneous fluctuations in threshold. In a yes/no

task, lower alpha power correlated with more liberal decision criterion. Participants reported stimulus detection more often, but not necessarily more accurately (Limbach & Corballis, 2016). Similarly, participants' self-reported confidence correlated negatively with alpha power, independent of task accuracy (Samaha et al., 2017). Responses to constant stimulus properties is determined by a dynamic, varying internal criterion and endogenous state. A valuable future endeavour could involve constructing a variable for internal bias in order to distinguish between shifts in criterion from shifts in visual perception (Roy et al., 2018).

Many studies suggest that attention-modulated alpha effects may be exerted through top-down control and are a direct product of the system's anticipation and preparation for an incoming stimulus. This naturally strengthens the relationship between prestimulus alpha and successful detection of near-threshold stimuli (Busch et al., 2009; Ergenoglu et al., 2004; Romei et al., 2008; van Dijk et al., 2008). Instead, our findings offered insights to mechanisms behind spontaneous alpha modulation of psychophysical behaviour. An observer's relationship between prestimulus alpha and task performance can be dependent on how familiar they are with the task. Future experiments should account for the observer's expertise before associating endogenous states with behaviour.

3.5.3 Conclusion

In conclusion, we examined whether prestimulus alpha power significantly predicted task performance in a 4AFC orientation discrimination paradigm. We found that firstly, the relationship between prestimulus alpha and performance varied greatly between participants. Follow-up analyses revealed that (1) this relationship was significantly dependent on the participant's orientation discrimination for scores, but not reaction time and (2) prestimulus alpha did significantly predicted reaction time. Interestingly, the relationships were only significant for whole brain alpha power and not for occipital cortex. This implied the involvement of other non-visual cognitive networks that modulate alpha band activity. Lastly, we found evidence that the scalp-level pattern of activity in a time period after stimulus onset was highly predictive of

hits and misses. This is likely due to a change in the participant's mood and vigilance following feedback on performance for the most recent trial.

4 Chapter 4: Frequency domain classification of chromatic SSVEP signals

4.1 Abstract

Periodic visual stimuli generate time-locked, ‘frequency-tagged’ steady state visually evoked potentials (SSVEPs) at the scalp. The amplitudes of these responses at harmonics of the input frequency provide a rich source of information about the neuronal computation that are driven by exogenous inputs. The human brain also generates endogenous rhythms: spontaneous, ongoing oscillations of neuronal population responses that generate broader but robust peaks in the EEG power spectrum. Such oscillations are typically invisible in an SSVEP analysis because phase information of endogenous rhythms is random from moment to moment. As a result, their time-locked amplitude averages to near-zero.

In this study, we ask whether information about chromaticity is present at frequencies other than the low-order harmonics of the inputs that are typically studied. This could happen for two reasons. First, we examine whether endogenous activity is modulated by visual inputs and if so, if that modulation depends on chromaticity. If there are nonlinear interactions between inputs and endogenous rhythms, then information about the chromaticity of a periodic stimulus might be present at non-harmonics of the input. Second, we ask whether information about the chromaticity of the input is present in higher order harmonics of the input above the critical flicker fusion (CFF) threshold. If so, then it is possible that ‘invisible’ information about flickering inputs is maintained in the visual system with very high temporal precision even in the absence of awareness.

We presented square-wave contrast modulating (on-off) stimuli composed of sinusoidal chromatic contrast gratings defined along the three axes of the Macleod-Boynton colour space (achromatic luminance, isoluminant L-M and S-cone isolating). The stimuli flickered at three modulation frequencies (5, 12 and 16 Hz) while we recorded each subject's steady-state responses using a 64-channel EEG system. For each input frequency condition, we examined the response spectrum from posterior electrodes using both an incoherent (phase insensitive) and coherent (phase sensitive) analysis pipeline. We also used the pattern of complex frequency domain responses to train a support vector machine (SVM) (*libsvm* with linear basis function kernels) to classify chromaticity.

The results contained two surprising findings. Firstly, each stimulus chromaticity generated a different level of endogenous EEG power across a wide range of frequencies. In particular, theta and alpha band power were elevated significantly in isoluminant chromatic conditions compared to achromatic conditions.

The multivariate analysis revealed that the SVM was able to categorise stimulus colour at a range of individual frequencies extending, in some cases, beyond the CFFF. The importance of this finding is two-fold: the significant classifications we found at the input frequencies (and subsequent harmonics) demonstrated that slowly flickering stimuli generate harmonics that extend up to very high frequencies. Specifically, we found instances of achromatic flicker driving response in the visual system up to 100Hz and isoluminant chromatic flicker up to 50Hz. These are far above CFFF for their respective colours. On the other hand, the significant classifications we found at non-input and non-harmonic frequencies indicated phase-locked intermodulation terms. We theorised that these were generated by non-linear interactions between chromatically driven responses and more prominent endogenous theta and alpha rhythms.

4.2 Introduction

The brain produces *endogenous* rhythms, which are defined as ongoing, internal neural oscillations that persist (and are sometimes amplified) in the absence of

external visual input. Endogenous rhythms are functionally categorised by their frequencies (*delta* 1-4 Hz, *theta* 4-8 Hz, *alpha* 8-12 Hz, *beta* 12-25 Hz, *gamma* 25-80 Hz), with established roles in attention (Klimesch et al., 2007), feature-binding and visual working memory (Berens et al., 2008; Honkanen et al., 2015). On the other hand, the visual system also constantly receives external sensory inputs, which undergo various stages of temporal and spatial filtering as they travel from the sensor to the cortex. These sensory inputs generate *exogenous* rhythms of neural activity that are *stimulus-locked*, meaning that inputs with a stable temporal structure would generate electrical activity that inherit that temporal structure. As a result, we can tag, identify and recover responses to a periodic input by conducting spectral analyses and looking at the input frequency and corresponding harmonics (Norcia et al., 2015).

Many studies have evidenced that endogenous and exogenous signals interact in some capacity during visual processing. Earlier works suggested SSVEP to be phase-locked endogenous activity (Makeig et al., 2002; Sayers et al., 1974) but the mechanisms of these entrainments largely remain an active area of research (Keitel et al., 2014). More recent studies suggested that occipital alpha activity was modulated by a 10Hz periodic stimuli (Klimesch et al., 2007; Spaak et al., 2014), and entrainment of alpha can subsequently impact detection of near-threshold stimuli by both amplitude and phase (Busch et al., 2009; Graaf et al., 2013). The evidence suggests that cortical rhythms are modulated by periodic inputs, and understanding this interaction using non-invasive techniques will give us better insights into how these neural mechanisms work.

The chromatic and temporal properties of LGN layers have been extensively modelled (Baseler & Sutter, 1997; Derrington & Lennie, 1984; D'Souza et al., 2011; Liu & Wandell, 2005; Livingstone & Hubel, 1987; Mullen et al., 2010). Activation of precortical pathways can provide greater insights into the interactions between exogenous and endogenous signals. This paradigm was used in a primate study, which showed spike activity of KC neurons to inversely correlate with slow endogenous waves between 0.5-10Hz (Cheong et al., 2011). The authors found that stimulus-driven spike rates in koniocellular neurons were negatively correlated with the amplitudes of slow endogenous waves within *delta* and *theta* ranges (defined as

0.5-5Hz and 5-10Hz respectively in this particular study). Modulation of koniocellular activity persisted both in the absence and presence of visual stimulation, suggesting that both stimulus-driven and endogenous koniocellular activity were coupled to slow deep brain rhythms. This finding supported previously discovered physiological connections between the superior colliculus structures and the koniocellular pathway that were unique to this cell type (Casagrande, 1994; Feig & Harting, 1994; Harting et al., 1991; Hendry & Reid, 2000). It also demonstrated the potential in studying deep brain responses using non-invasive methods. The interactions were restricted to one precortical pathway with a unique, chromatic signature, which prompted the question of whether chromatic SSVEP signals generated by other colours (or purely luminance stimuli) would reveal similar couplings with endogenous activities.

The current experiment investigated the relationship between endogenous activity and isoluminant chromatic responses in the human visual system. Chromatic processing channels have well-established temporal low-pass natures, which we expect would regulate the standard temporal responses of colour-selective neurons. On the other hand, since endogenous activity can modulate as fast as 80Hz, we wondered if we could find signatures of chromatic interactions within a wider frequency range.

We aimed to answer two research questions. Firstly, we asked over what range of frequencies can we detect the effects of achromatic and isoluminant chromatic flickering stimuli? Specifically, we examined stimulus-driven responses in terms of significant power at the flicker's (1F) frequency and subsequent harmonics (*n*F - i.e. multiples of the input frequency). Secondly, we asked if the flickering stimuli interacted with endogenous rhythms. This analysis was carried out in two ways. We began by identifying any modulations of endogenous rhythms within *incoherently averaged* EEG responses. This analysis is sensitive to non-phase-locked interactions between the two frequency sources – for example, a general amplification of an ongoing alpha rhythm by the presence of an exogenous input. Secondly, we repeated the analysis while maintaining the complex (phase-sensitive) information in the signals throughout the averaging procedure. This analysis is very sensitive to phase-locked interactions (because the phase-randomised noise

components are expected to average to zero) but blind to phase-randomised interactions of the type examined in the first analysis.

Because the visual system contains nonlinear (for example, threshold nonlinearity) as well as linear stages, even pure sine-wave inputs generate higher harmonics (McKeefry et al., 1996). In addition, non-linear interactions between neuronal signals generate ‘intermodulation’ terms: signals at the sums and differences of the signal frequencies (Norcia et al., 2015; Regan & Regan, 1988) between inputs and endogenous rhythms are therefore also expected to contain multiple temporal components.

In the current study, we examined the effect of stimulus colour on individual output frequencies within the power spectrum. Because endogenous frequencies are not tightly confined to a single frequency, we looked for ‘hillocks’ of significance that might indicate intermodulation terms, specifically between 5-10Hz endogenous signals and S-cone driven responses. We also removed stimulus-driven responses at input frequency and harmonics and examined the effect of stimulus colour on broadband endogenous EEG power.

Finally, considering how evidence of entrainment might be contained in amplitude and phase information spread across multiple EEG sensors, we used a sensitive SVM pattern classifier to compare classification accuracies for magnitude (phase removed) data and complex (phase retained) data.

4.3 Methods

4.3.1 Participant

We recruited 16 neurotypical subjects (age range: 18 to 45-year-old, eight female) from the University of York. All participants had normal or corrected-to-normal visual acuity and normal colour vision as tested by Ishihara plates (24 plates edition). All

procedures were performed after obtaining approval from the Department of Psychology Ethics Committee.

4.3.2 EEG recording and apparatus

Scalp EEG responses were recorded at a sampling rate of 1KHz using the ASA software and 64-channel Waveguard EEG caps from ANT Neuro (ANT Neuro, Netherlands) with a standard 10/20 montage array. The data were notch filtered in hardware at 50Hz at acquisition to remove line noise.

The stimuli were displayed using a gamma corrected 22.5” display monitor (ViewPixx, VPixx Technologies) at the spatial resolution of 1920 x 1200 pixels, with a 120 Hz refresh rate and mean luminance of 250 cd/m^2. The calibration was made with NIST-traceable Jaz USB photospectrometer with a 2nm resolution. Subjects viewed the display from 57cm. The displayed subtended 37.5° of visual angle horizontally.

4.3.3 Stimulus design

Stimuli were created in Matlab with the Psychophysics Toolbox extensions (Brainard, 1997; Kleiner et al., 2007; Pelli, 1997) and consisted of horizontally oriented, phase randomised 1 cycle/degree sinusoidal gratings. These gratings varied along two features: temporal frequency (square wave modulation at 5, 12 and 16 Hz) and chromaticity (luminance, S-cone isolating and red-green). Stimuli were created using the Stockman-Sharpe 10° cone fundamentals (Stockman & Sharpe, 2000) to compute cone excitation. Chromaticity of coloured stimuli varied on a subject-by-subject basis to ensure isoluminance using values measured by a pre-experiment heterochromatic minimum flicker task (Lee et al., 1988). Stimuli were windowed using a Gaussian envelope (full width at half maximum = 30°). To avoid changes in the isoluminant settings caused by macular pigment, the central 2° was replaced by a grey Gaussian blob (see **Fig. 4.1** A for visualisation).

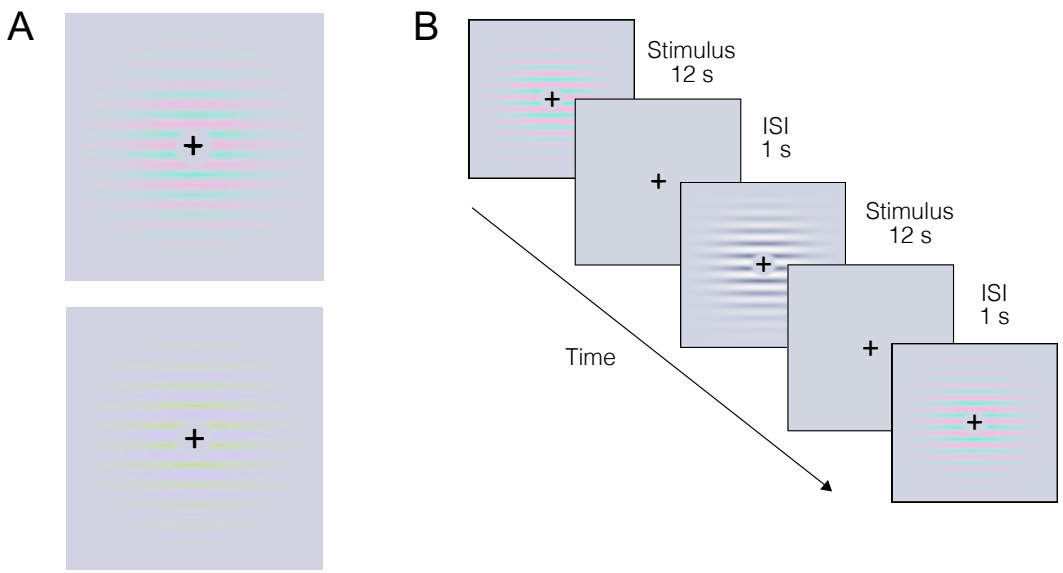

Fig. 4.1 *(A) Red-green (top) and S-cone isolating (bottom) stimuli presented during the experiment. (B) Experimental paradigm showing three trials and two ISI with red-green and luminance stimuli as examples.*

4.3.4 Experimental Procedure

Participants were instructed to fixate the centre of the screen and perform a free-running central fixation task (detecting changes to the shape of a small fixation target) to ensure that they maintained an approximately constant attentional state throughout the experiment. Stimuli were displayed in trials of 12s with 1s inter-stimulus intervals (ISI) (see **Fig. 4.1** B). There were 15 repetitions of all nine conditions.

4.3.5 EEG data processing

The 12-second EEG responses to each trial were segmented into 1s bins. The first and last bin were discarded to remove onset and offset transients, leaving 150 bins of data per condition for each subject (15 repetitions of ten bins per trial).

Our research questions required analysis of both magnitude and complex data. This meant that after Fourier transformation we had to average each bin coherently or incoherently, according to the question we were investigating.

4.3.5.1 Incoherent averaging

Incoherent averaging computes the mean of the Fourier amplitude spectrum without consideration of the phase information (by taking the magnitude of each component). Because phase-randomised noise is maintained in this analysis, this reduces the SNR of the resultant frequency domain data but is helpful in identifying constant, phase-randomised components within the signal.

4.3.5.2 Coherent averaging

Coherent averaging computes the mean of the complex Fourier transform of each bin. This maintains information about the phase of the signal at each frequency. Because phase-randomised noise will average away under this analysis, any phase-locked signals evoked by periodic stimuli have high SNR. In other words, coherent averaging reveals the presence of exogenously driven signals (and endogenous signals that are phase-locked to the input) while removing the influence of endogenous rhythms and noise.

We model these interactions in **Fig. 4.2**.

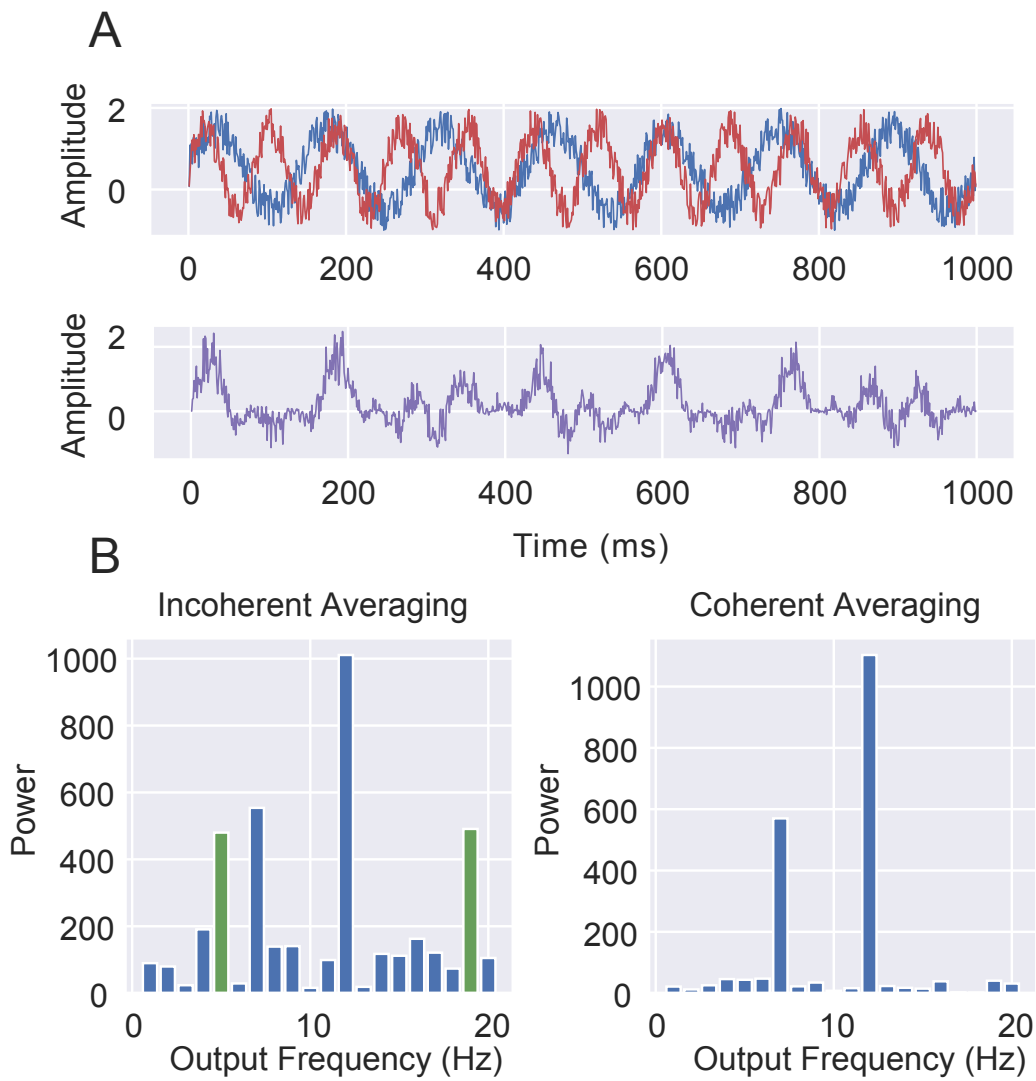

Fig. 4.2 *An example of a synthetic signal containing a 7Hz phase-locked component (blue) and a 12Hz phase-randomised component (red): represented separately and the resulting combined signal after a weak, non-linear interaction (purple). (B) Signal in (A) after Fourier transformation and incoherent averaging or coherent averaging. Incoherent averaging reveals intermodulation terms at the sums and differences of the dominant frequencies (i.e. 5 and 19Hz), generated by the non-linear interaction denoted in green. Coherent averaging averages away phase-randomised intermodulation terms but reveals the phase-locked input and its harmonics with high SNR.*

In our experiments, we generated inputs at 5, 12 and 16Hz. Based on the stimulus and endogenous frequency that interacted with koniocellular activity (Cheong et al.,

2011), we summarised the possible frequency range of intermodulation terms in the table below (**Table 4.1**).

Table 4.1 *Predicted intermodulation term frequencies based on input signal frequency and 5-10Hz endogenous activity.*

Stimulus Frequency	Predicted Intermodulation Terms	
5Hz	*Sum*	10-15Hz
	Difference	1-5Hz
12Hz	*Sum*	17-22Hz
	Difference	2-7Hz
16Hz	*Sum*	21-26Hz
	Difference	6-11Hz

4.3.6 Data analysis

We ran three analyses on the data. The first analysis was a repeated measured ANOVA, looking for an effect of stimulus colour on broadband endogenous power, The second analysis was similar to the first, but examining the effect of stimulus colour on the EEG power at individual output frequencies (within a range of 1-100Hz) instead of broadband power. This additional level of detail also allowed us to examine evidence of intermodulation terms in the power spectrum and stimulus-driven responses at the input frequency and harmonics. Finally, we ran a multivariate classification analysis on the complex data to understand if entrainment could be evidenced in the spatial pattern of magnitude and phase information across the scalp.

4.3.6.1 ‘Broadband’ EEG power analysis

We ran a repeated measures ANOVA examining the effects of chromatic conditions on each endogenous frequency band. To compute the power of endogenous frequency bands, we removed EEG magnitudes at stimulus temporal frequency and corresponding harmonics. We then calculated the root mean square (RMS) power

within the frequency ranges of interest: *theta (4-7Hz), alpha (8-12Hz), beta (13-25Hz) and gamma (25-80Hz)*. *Delta (1-3.5Hz)* band data was excluded from the analysis as our recordings had a typical 1/f noise profile meaning that they contained relatively high levels of low-frequency noise.

4.3.6.2 'Narrowband' EEG power analysis

We examined how each of the nine combinations of temporal frequency and chromaticity affected EEG power measured in the frequency domain (1-100Hz). This was performed for both coherently and incoherently averaged EEG power: the former showed stimulus-locked responses and the latter to identify non-phase-locked intermodulation terms that would indicate an interaction between the input rhythm and endogenous activity between 5-10Hz.

4.3.6.3 SVM classification

We analysed the nine conditions individually for each participant. Each condition yielded 150 one-second bins of EEG data per participant. To obtain confidence intervals on our classification results, we bootstrap resampled our data by first randomly shuffling the bins then averaging them in groups of five. This resulted in 30 averaged bins per condition, which we then fast Fourier transformed and classified based on individual frequency components.

We asked the classifier to identify stimulus colour (luminance, S-cone isolating or red-green) based on the averaged bins of evoked responses for each temporal frequency (5, 12 or 16 Hz). Confidence intervals were obtained through bootstrapping, which consisted of 1000 independent trials. Within each trial, datapoints were first shuffled before we computed classification accuracy using a ten-fold cross validation procedure. The dataset was divided into ten parts before training the machine on nine and testing it with the remaining novel dataset to establish an accuracy. The resulting accuracy score represents that of a single participant, a single temporal frequency and a single comparison of chromaticity. The analysis was conducted at each frequency between 1-100Hz for all three

chromaticities. We also performed pairwise comparisons to examine any effects between one colour condition and another.

4.4 Results

4.4.1 Univariate analyses

Each bin of raw EEG data was Fourier transformed and the amplitudes were averaged coherently (preserving amplitude and phase information) and incoherently (preserving amplitude information only). We plotted the power spectra from 1-100Hz in **Fig. 4.3**. The data demonstrated several expected signatures of the chromatic SSVEP, such as stronger responses at the fundamental frequency of stimulus that decreased in the second harmonic. We also observed higher SNR in coherently averaged data as well as a persistent alpha peak in incoherently averaged power.

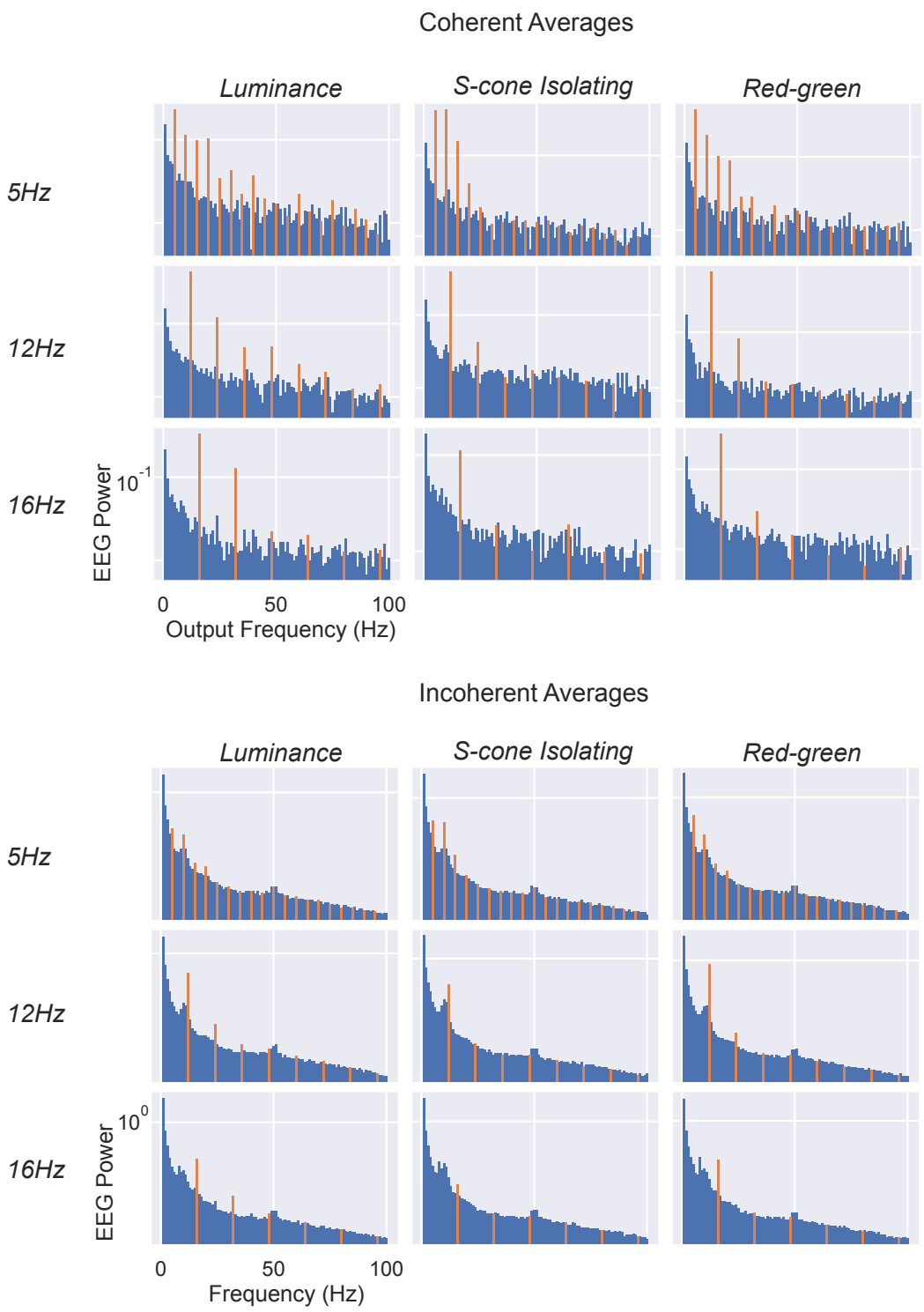

Fig. 4.3 *Spectrum of log transformed (-log10) group mean EEG power, averaged coherently (top) and incoherently (bottom). Orange bars denote the harmonics of input frequencies. As we expected, we observed higher SNR in the coherently averaged power spectrum and a bump of high EEG power at alpha frequency range in the incoherently averaged power spectrum.*

4.4.1.1 ‘Broadband’ EEG Power Analysis

We removed EEG responses at input frequencies and harmonics to stimulus-driven responses before calculating the RMS of incoherently averaged power within *theta, alpha, beta* and *gamma* bands. We then performed a repeated measures ANOVA on the data, asking if there were any main effects of endogenous band or stimulus colour on the magnitude of EEG responses. Mauchly’s test indicated that the data for colour did not violate assumptions of sphericity ($p = .294$). However, the data for endogenous bands and interaction between stimulus colour and endogenous band did ($p < .001$ for both cases), resulting in the using of Greenhouse-Geisser corrections for the effects of these two features.

We found a significant main effect of endogenous band: $F(1.50, 22.47) = 77.63$, $p < .001$, partial $\eta 2 = 0.84$ which reflects the 1/f nature of the EEG signal. More interestingly, we also found a significant effect of stimulus colour: $F(2, 30) = 16.27$, $p < .001$, partial $\eta 2 = 0.52$ as well a significant interaction between colour and frequency band: $F(2.55, 38.18) = 10.77$, $p < .001$, partial $\eta 2 = 0.42$ (see **Fig. 4.4**). We performed *post hoc* analyses using paired-sample t-tests, where we compared the responses to each stimulus colour within an endogenous frequency band. The data revealed that within every endogenous band tested, RMS EEG responses to luminance flicker were significantly *lower* than the response to S-cone isolating flicker (*theta*: $t(15) = -2.53$, $p = .023$; *alpha*: $t(15) = -6.52$, $p < .001$; *beta*: $t(15) = -4.04$, $p = .001$; *gamma*: $t(15) = -4.96$, $p < .001$) and red-green flicker (*theta*: $t(15) = -4.07$, $p = .001$; *alpha*: $t(15) = -6.34$, $p < .001$; *beta*: $t(15) = -5.45$, $p < .001$; *gamma*: $t(15) = -2.66$, $p = .018$). In contrast, no significant differences were found between the two chromatic conditions (*theta*: $t(15) = 0.18$, $p = .860$; *alpha*: $t(15) = -1.64$, $p = .123$; *beta*: $t(15) = -1.55$, $p = .141$; *gamma*: $t(15) = 0.32$, $p = .753$).

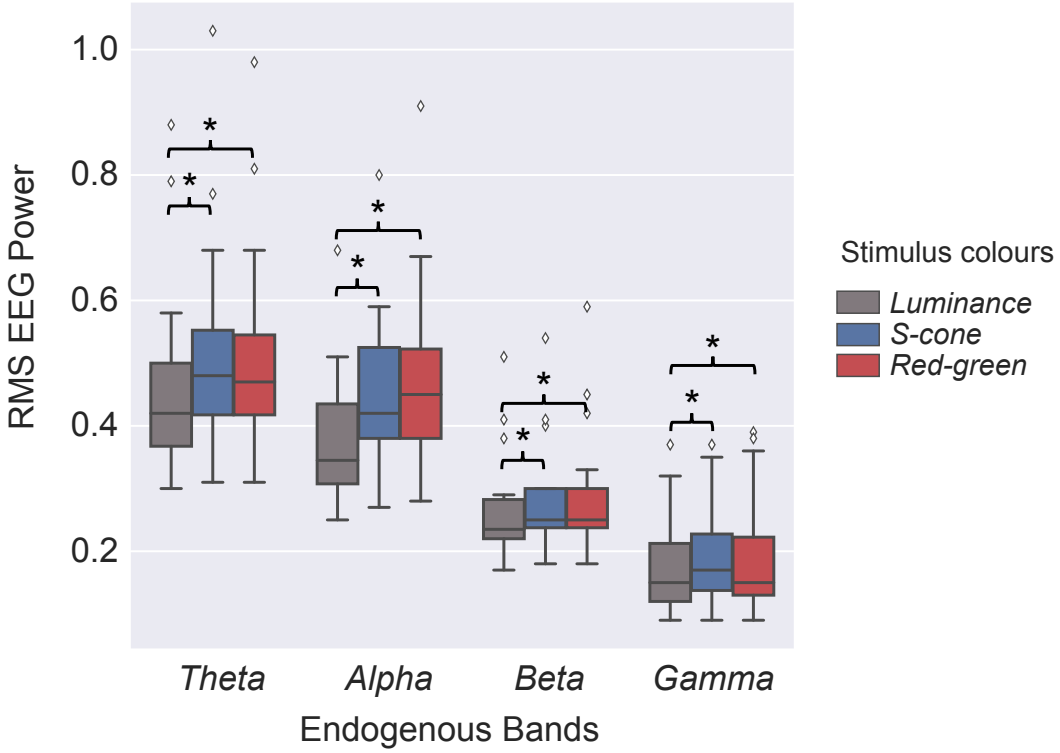

Fig. 4.4 *Boxplots of RMS EEG power of endogenous theta, alpha, beta and gamma bands averaged across participants as a function of stimulus chromaticity. We found significant main effects of endogenous band, colour as well as a significant interaction. Post hoc comparisons revealed significant differences between luminance and either chromatic conditions within an endogenous band, denoted by asterisks.*

As a control, we ran the same ANOVA on four frequency bands composed of frequencies that are randomly selected from 1-80 Hz (with no overlaps). The ANOVA revealed no effects of colour and interaction between colour and endogenous frequency bands on EEG power ($p = .487$ and $p = .431$ respectively).

4.4.1.2 'Narrowband' EEG Power Analysis

We then ran one-way repeated measures ANOVA on the EEG power at output frequencies (1-100Hz) individually, again examining whether there was a significant main effect of stimulus colour on the EEG power. Unlike the previous analysis, which was only performed on incoherently averaged EEG power, this analysis was carried out on both coherently and incoherently averaged EEG power. We had two aims for

this analysis: first, it allowed us to identify any broader peaks of EEG power at the sums and differences of the input and endogenous frequencies that might indicate non-linear interactions between the two signals. These broad peaks or 'hillocks' would have been masked within broadband endogenous power. Secondly, by not removing the responses at harmonics of the stimulus frequency, we can provide statistical evidence for the stimulus-driven responses we observe in **Fig. 4.3**.

We were particularly interested in the coherently averaged responses at the fundamental stimulus frequency and its harmonics, which would inform us of the presence of neural signals driven by the stimulus (red bars in **Fig. 4.5**). We were also interested in finding clusters of high significance, which might indicate intermodulation terms originating from nonlinear interactions with endogenous frequency bands.

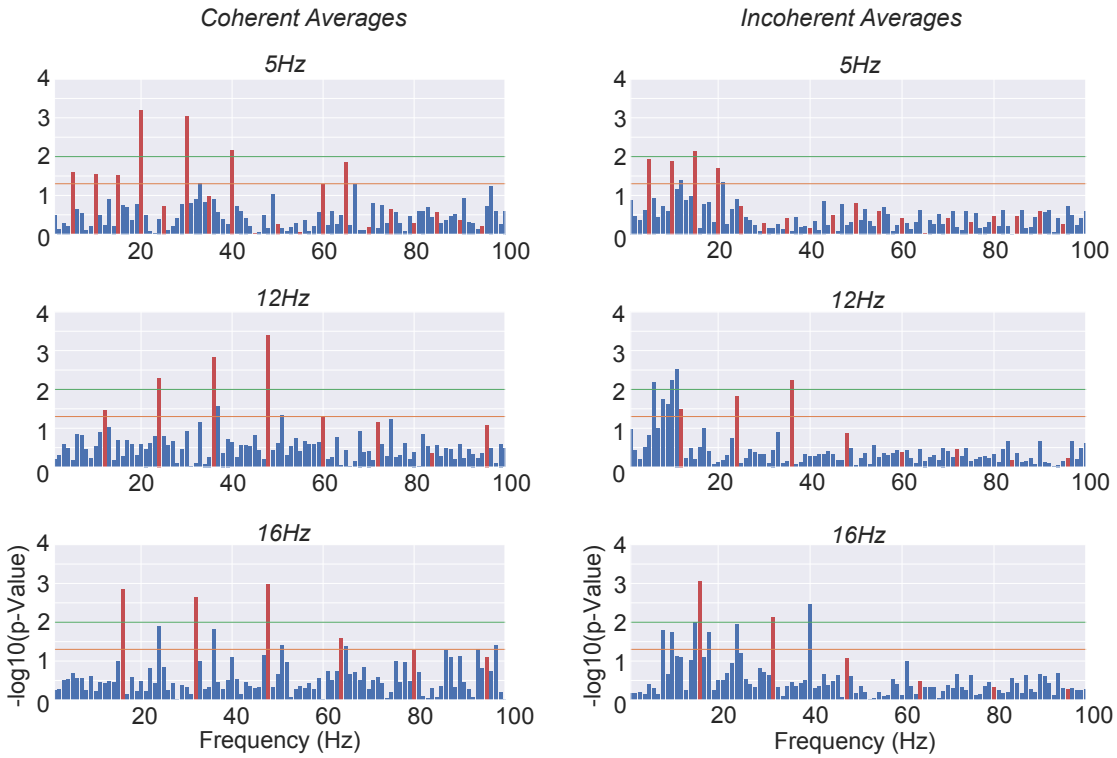

Fig. 4.5 *Log transformed (*-log10*) p-values produced by one-way ANOVAs looking for significant main effects of stimulus chromaticity on EEG power. This was performed separately for coherently averaged and incoherently averaged EEG power. Red bars indicated harmonics of stimulus temporal frequency. Orange line indicated where* p-*value = .05 and green line indicated where* p-*value = .01. Intermodulation terms may appear as groups or 'hillocks' of significant* p-*values in the incoherently averaged EEG power spectrum. We observed this in alpha frequency range for 12Hz flicker, but not for 5Hz or 16Hz flicker.*

4.4.1.2.1 Coherently averaged EEG power

Lower-bound estimates were used if Mauchly's test revealed violations of sphericity. We found significant effects of colour on EEG power at the first four harmonics regardless of stimulus temporal frequency, as well as at isolated non-harmonic frequencies. Post-hoc comparisons revealed significant differences in responses between luminance and coloured flicker (details are summarised in Appendices **Table 4.2**). This data trend was visible in **Fig. 4.3**: high frequency luminance and red-green flicker produced higher responses than S-cone isolating flicker.

4.4.1.2.2 Incoherently averaged EEG power

Analyses of incoherently averaged EEG power revealed similar results to those found for coherently averaged data in terms of stimulus-driven EEG responses. However, the lower SNR meant that in 12Hz and 16Hz conditions, responses were significant only up to the third and second harmonics respectively. We found a cluster of significant EEG power for 12Hz flicker at approximately the alpha frequency range. Post hoc tests revealed no significant differences between stimulus colours at any frequency despite the significant main effect (details are summarised in Appendices **Table 4.3**).

4.4.2 Multivariate analysis

In the previous sections we observed strong effects of stimulus colour on the EEG power at the flicker frequency F and nF as well as broadband endogenous power but did not find evidence of intermodulation terms in the incoherently averaged spectrum. The analysis here was extended using a multivariate classification paradigm. The paradigm was conceptually similar to time-domain multivariate pattern analysis EEG signal processing in King & Dehaene (2014), but instead of performing our analysis across time points, we asked if the pattern of activity at each sensor changed consistently with stimulus colour at any given *frequency.* Given the univariate results, we expected significant classifications up to the fourth harmonic of stimulus frequencies.

We used an SVM classification paradigm (*libsvm* with a linear kernel) to analyse the distribution of activity across the scalp. We adopted a conservative approach in this analysis: we first asked whether a three-way classification was significant at each frequency. Significance would indicate some consistent difference between responses patterns as a function of chromaticity (similar to looking at main effects in ANOVAs). Then, at frequencies where three-way classification was significant, we performed pairwise analyses. This allowed us to examine all three comparisons between stimulus colours (luminance and S-cone isolating, luminance and red-

green, S-cone isolating and red-green) and understand which colours were contributing to the effect of colour (analogous to *post hoc* comparisons).

The data revealed that three-way classification of complex EEG data was significantly above chance at multiple harmonics of the stimulus frequencies, as well as clusters of non-harmonic frequencies. The highest frequencies of significant classification were close to 50Hz for 5Hz flicker and 100Hz for 12 and 16Hz flicker respectively – far higher than the CFFF of any stimulus colour (**Fig. 4.6**).

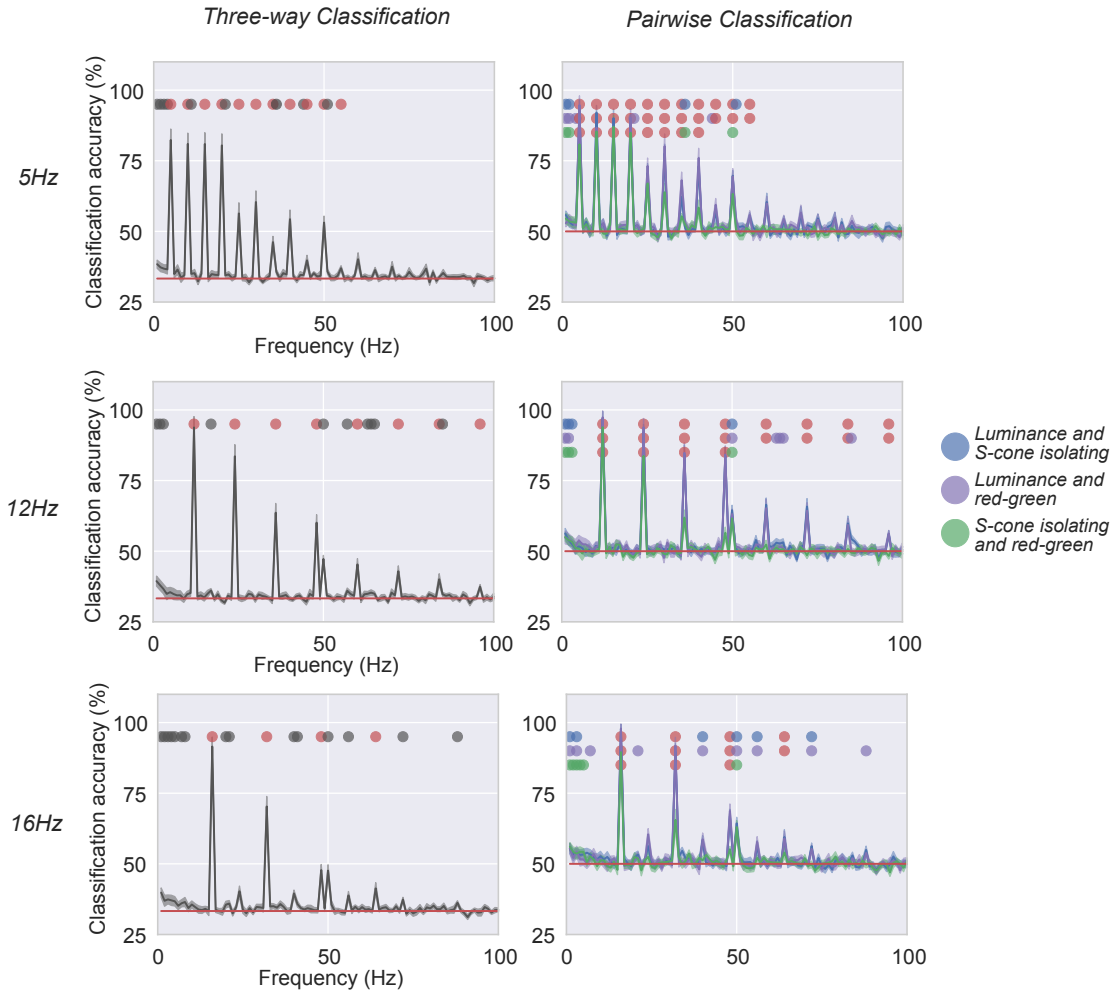

Fig. 4.6 *Mean and SEM of classification accuracy plotted across output frequencies for three-way comparisons (left) and pairwise comparisons (right). Scatter points along the top of the figure indicated the frequencies where accuracy was significantly above chance: 33.3% for three-way, 50% for pairwise (indicated by the red line) after Bonferroni corrections. Red scatter points indicated harmonics of stimulus frequency. Frequencies where pairwise classification was significant but three-way classification was not had been discarded in the diagram.*

4.4.2.1 Visualisation of variations in pattern of electrical activity

Significant classification accuracies indicated that each stimulus colour evoked a distinct pattern of electrical activity. However, the classification paradigm itself did not provide information on the source where this distinct pattern had emerged. In

order to visualise the multivariate results, we performed an additional set of t-tests using the complex data recorded at each of the 64 sensors.

Because the 12Hz stimulation paradigm appeared to provide the richest set of responses, we simplified our analysis by restricting to just this paradigm. We compared each sensor's electrical pattern and asked if there was a significant difference between the stimulus colours. This was repeated for all three pairings of stimulus colours at nine frequencies: fundamental frequency (i.e. 12Hz) up to the eighth harmonic with an additional non-harmonic frequency (75Hz) as control. The t-tests were performed on an individual basis for each participant before being averaged across the group using Fisher's Method to attain a group mean. All p-values were adjusted using Benjamini-Hochberg corrections (Benjamini & Hochberg, 1995) for multiple comparisons before being averaged.

We found that 12Hz flicker of different colours evoked significantly distinct patterns of activity across the scalp (see **Fig. 4.7** for example of one participant). The difference between luminance and either chromatic flicker was clearly significant up to the eighth harmonic, while the difference between chromatic flicker was significant only up to the fourth harmonic. Distinct patterns of electrical activity were mainly found in the occipital and parietal regions for comparisons between S-cone isolating and red-green conditions, but more evenly distributed across the scalp in luminance versus chromatic comparisons. Meanwhile, the control at 75Hz showed no significant difference between stimulus colours.

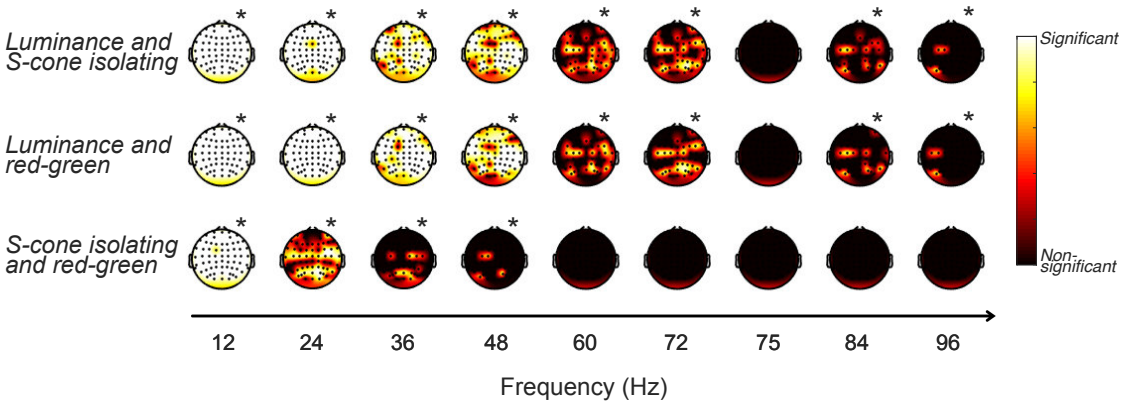

Fig. 4.7 Scalp topography showing responses generated by stimulus colour. Significance was denoted using colour: lighter colours indicated higher significance and darker colour indicated low significance. Asterisks indicated significant t-test results ($p < .05$). We found that the pattern of activity generated by luminance flicker differed greatly with both chromatic S-cone isolating and chromatic red-green flicker up to the eighth harmonic. Chromatic conditions were only significantly different within themselves up to the fourth harmonic. This analysis allowed us to visualise the source of distinct complex responses that led to significant classification accuracies within the SVM analyses.

4.5 Discussion

Overall, across all experiments, we found significant EEG power both at the fundamental frequency (F) and higher harmonics of the input (nF) - including at frequencies beyond CFFF. This demonstrated that external visual stimuli could drive and entrain responses in the visual system at high frequency. We also found significant effects of stimulus colour on broadband endogenous power, even with stimulus-driven responses removed. While this implied an interaction between exogenous and endogenous activity, we did not find any strong evidence of intermodulation terms within the incoherently averaged (phase-insensitive) power spectrum. However, after broadening the data pool to include all 64 sensors and phase information, we could classify stimulus colours with significant accuracies at harmonic and certain clusters of non-harmonic frequencies. After visualising the pattern of electrical activity using scalp topography, we concluded that these results

indicated entrainment of endogenous activity and exogenously driven signals. However, evidence for this entrainment was only available when we considered phase information in addition to magnitude, and the disparity was greater between achromatic and either colour than between the two chromatic conditions themselves – suggesting that the classifier was essentially driven by the presence of absence of signal in the achromatic condition.

In general, we found evidence in coherently averaged EEG signals that chromatic inputs evoked strong responses in all three experimental conditions up to the fourth harmonic. Further post hoc comparisons showed signatures of the visual pathways driven by each stimulus colour. For example, luminance stimuli generated greater EEG responses when modulated at higher temporal frequencies, showing distinct frequency doubling responses for 16Hz flicker. These were typical of magnocellular responses: large receptive fields of parasol ganglion cells are associated with greater sensitivity to high contrast, low spatial frequencies and high temporal frequencies (Dacey, 2000). In contrast, this dominant second harmonic component was not prominent in chromatic conditions. Higher EEG responses were found for slower S-cone isolating stimuli consistent with the temporal low-pass nature of the koniocellular pathway, where neurons fire preferentially to sustained as opposed to transient stimulation. The optimal stimulation frequency for S-cone isolating stimuli was at centred around 10 Hz, due to the disparity in the temporal properties of centre and surround fields of midget cells (Derrington et al., 1984). Overall, we observed stronger second harmonic component in achromatic as compared to chromatic responses, which being well-established trait of the luminance processing channel (McKeefry et al., 1996), validated our methodology. Additionally, we could infer the quality of stimulus calibration: the difference in responses towards S-cone isolating and luminance stimuli suggested that the colour processing channels were successfully isolated with minimum luminance leakage.

4.5.1 ‘Broadband’ EEG: significant interactions between stimulus colour and broadband endogenous power

We found that mean EEG signals averaged incoherently across endogenous frequency bands (ignoring multiples of the input frequencies) were modulated by stimulus colour. More specifically, chromatically evoked responses were greater than achromatic responses within each endogenous frequency band. This effect was strongest within the alpha range, which might be related to its dominance within the occipital region (Groppe et al., 2013). While statistically significant, the difference between chromatic and achromatic responses were noticeably reduced in activity with higher frequencies, such as gamma. Since other parameters such as stimulus frequency were controlled, the results implied that this interaction between endogenous frequencies and colour might originate from the visual pathways.

This theory was proposed in an earlier literature review (Sewards & Sewards, 1999). With increasing evidence demonstrating the involvement of alpha and gamma activity in visual awareness (Adrian & Matthews, 1934; Schanze & Eckhorn, 1997; Young et al., 1992), the authors proposed that the involvement of these endogenous rhythms must be matched with visual processing in terms of the temporal qualities (Nealey & Maunsell, 1994; Van Essen & Gallant, 1994). Alpha band activity, being the slower of the two, would dominate parvocellular pathway. In contrast, the magnocellular layers might be associated with faster gamma band activity. The current results are consistent with these hypotheses: chromatic stimuli producing higher alpha band activity as they are processed by the same precortical layers, with the effect weakening with more rapid endogenous activity.

4.5.2 ‘Narrowband’ EEG: no intermodulation terms in incoherently averaged EEG data

There were significant effects of stimulus colour on incoherently averaged EEG power at approximately alpha frequency range in response to 12Hz flicker. This did not coincide with any of our predicted intermodulation term frequency ranges in **Table 4.1**. The hillocks were inconsistent between stimulus frequencies, and no effect was found for 5Hz flicker, which in theory should generate stronger responses due to the low-pass nature of S-cone processing channels. Intermodulation terms should also result in higher EEG power at both the sums and differences of two original frequencies: meaning we should see two peaks in the frequency domain, not one. Finally, the results could be accounted for by an overlap between the frequencies of alpha activity (dominant in occipital lobe) and the stimulus. Linear summation of the endogenous power and fundamental component power might have resulted in higher EEG power. Considering these details, we conclude that there were no intermodulation terms in the incoherently average power spectrum.

This, however, did not necessarily mean that there being no stimulus-driven modulation of endogenous rhythms. The lack of intermodulation terms might be explained by several factors. Firstly, entrainment with slower endogenous rhythms might be more difficult in the current experiment. The previous study that observed a correlation between S-cone signals and slow endogenous activity had administered surgical anaesthesia to the marmosets (Cheong et al., 2011). Anaesthesia enhances slower endogenous rhythms (Chauvette et al., 2011), which can cause their relationship with koniocellular spike rates to be more pronounced. In contrast, the current experiment instructs participants to maintain attention using a fixation task. The awake brain is not only less prone to generating slow rhythms, but likelier in generating beta and gamma rhythms due to the potentiation processes required in communication between the cortex and geniculate (Wróbel, 2000). This shift in dominant EEG activity frequency range could make it more difficult to detect and entrain slower endogenous rhythms. Lastly, detecting interaction through amplitude can be tricky depending on the coupling strength between oscillators. Weak entrainment might not produce detectable changes in the amplitude of the synchronised rhythm (Kuramoto, 1984).

4.5.3 Multivariate analysis: significant classification of complex EEG data

We found that three-way (and pairwise) classifications using complex data from all 64 sensors were highly accurate at most harmonics of the stimulus frequency and even within sporadic clusters of non-harmonic frequencies. Significant classification accuracies at stimulus frequency and harmonics suggested that flickering stimuli of relatively slow flicker rate could drive the visual system robustly at rates far higher than the CFF threshold, reinforcing our earlier results. Further analyses showed that different stimulus colours generated different spatial patterns of electrode responses at particular frequencies. This effect persisted at high harmonics (again, beyond CFFF) but not for a control frequency (75Hz) that was not a harmonic of the input. The SVM was highly accurate in distinguishing luminance generated responses from those for either chromatic condition but was unable to accurately classify responses to S-cone isolating and red-green stimuli after approximately 50Hz. This supported the broadband EEG power analysis and suggested that activity from chromatic and luminance channels interact uniquely with endogenous frequency bands. We also observed that the difference in pattern between luminance and colour extended across the scalp while the difference between the two colours were concentrated mainly in the occipital region. This indicated that achromatic and chromatic processing might extend and involve different cortical areas beyond the visual cortex.

The clusters of significantly accurate classification at *non-harmonics* indicated phase-locked components between endogenous activity and stimulus-driven responses. Similar observations had been made previously: rhythmic visual inputs were shown to reset endogenous oscillations with the entrained hemifield (Spaak et al., 2014). The entrained signal was strong enough to predict behaviour (i.e. the detection of near-threshold targets), and the effect phase sensitive. Spaak et al found entrainment of alpha activity specifically but significant classification accuracies in the current experiment were found at high frequencies (>50Hz). Similarly robust, high frequency cortical responses had been demonstrated before

(Shady et al., 2004), and considering the frequency range, our results might indicate *gamma* phase resetting. Gamma oscillations are prevalent in layer 4 of V1 during earlier stages of visual processing and provides a feedforward mechanism from V1 to V4 (van Kerkoerle et al., 2014). While it is difficult to confirm this theory, the results showed how phase information could be valuable in understanding signal entrainment. It offered another dimension of information, which was not available in phase-insensitive, incoherently averaged EEG power.

4.5.4 Conclusion

We found evidence that luminance and isoluminant chromatic flicker drives the visual system powerfully, not only at the fundamental frequency but also at multiple harmonics. The robust stimulus-driven responses interacted significantly with broadband endogenous EEG power, most strongly with alpha band activity. The effect of stimulus colour on alpha band power persisted when we examined each frequency bin individually. However, we did not find intermodulation peaks or consistent evidence of interaction between endogenous band and stimulus-driven responses in the Fourier domain of incoherently averaged data. This did not necessarily demonstrate a lack of interaction between exogenous and endogenous activity, as entrainment might be evidenced in phase information rather than amplitude alone.

Multivariate classifications using both phase and amplitude information produced high accuracies of classifying stimulus colours at certain clusters of output frequencies. The high temporal frequency of these signals (far beyond CFFF) suggests two conclusions. First, despite the irregularity of significant classification accuracies: the high frequencies at which they occur (in coherently averaged data) demonstrated phase-locked components and phase-resetting of endogenous rhythms by the flickering stimuli. Second, chromaticity of stimuli affects each endogenous band activity differently: chromatic stimuli (S-cone isolating and red-green) generated higher alpha power. This suggested that endogenous rhythms are driven uniquely by different visual pathways. Our study also offered a novel method

of identifying entrainment between endogenous and exogenous rhythms that incorporated complex data.

5 Chapter 5: Neural responses to visible and invisible chromatic flicker.

5.1 Abstract

Temporal contrast sensitivity is either bandpass (luminance) or lowpass (chromatic) with sensitivity typically decreasing as the rate approaches an upper bound: the critical flicker fusion frequency (CFFF). Stimuli modulating faster than the CFFF are not consciously perceived. Yet, both behavioural and neuroimaging studies have shown that such imperceptible fast flicker was able to drive neural activity in multiple visual areas. While these results are robust, the existing studies are limited in two ways. Firstly, the stimulus frequencies used in these studies were often restricted by the framerate of their display equipment (for example, the Nyquist limit of a 60Hz refresh rate monitor is 30Hz). However, the occipital cortex appears capable of responding at much higher frequencies (>100Hz), as evidenced in both the previous chapter (*Classification of chromatic steady-state visually evoked potentials (SSVEP)*) and some recent literature. This makes the neural modulations of very rapid flicker an interesting but unexplored topic. Secondly, due to the temporal low-pass nature of the koniocellular (KC) pathway, most previous studies included only luminance and/or chromatic red-green stimuli. However, there is evidence to show that the KC system shares unique interconnections with motion sensitive areas, implicating that rapid modulations of S-cone stimuli can, in theory, drive the visual system through these alternate pathways.

We ran a functional magnetic resonance imaging (fMRI) block design study, where participants viewed a five-primary LED light source (subtending 1.56° of visual angle) which could generate flicker at arbitrary frequencies – in principle up to 500Hz. High contrast stimuli with a Gaussian spatial profile were modulated at five

temporal frequencies (2, 8, 32, 64 and 125Hz) and along three different directions in MacLeod-Boynton space (luminance, S-cone isolating and red-green) with an additional 2 Hz subthreshold contrast condition for each colour. To extend our understanding of the neural correlates of fast chromatic flicker, we examined the mean amplitude of BOLD responses in V1, V3a and V4 in three participants. We asked if (1) responses to flicker modulating at beyond CFFF were significantly greater than the null condition for all chromaticities and (2) if rapid S-cone isolating stimuli (32Hz and above) evoked a greater response in V3a than in V1. Additionally, we were also interested in understanding how the chromatic preference of a visual area interacted with the stimulus frequency within the slow visible range.

Despite the small stimulus size, we found that faster flicker evoked measurable responses, especially in higher-order visual areas. Red-green stimuli elicited the strongest neural responses, although we also found evidence of S-cone responses above 32Hz modulation. V3a responses were stronger than responses in V1 and V4, but this was true of all three stimulus colours, meaning V3a did not show a unique preference for rapid S-cone signals. Overall, despite clear heterogeneity in responses across subjects, we found some limited evidence for responses to super-threshold flicker frequencies that tended to be outside the primary visual cortex.

Finally, we observed that relative responses to chromatic and achromatic flicker in V1 and V4 depended on stimulus frequency. Again, these differences varied across subjects but indicated that attempts to classify areas according to their chromatic sensitivity might be overly simplistic: ‘colour areas’ might not appear to be chromatically selective and vice-versa depending on the temporal properties of the retinal input.

5.2 Introduction

The human visual system is highly robust in processing inputs of varying intensity and features. The types of feature processed by a visual neuron is dependent on its physiological properties. For example, parasol RGC have large receptive fields and

thicker myelination, which support their low spatial resolution and fast responses respectively. Midget RGC have smaller receptive fields and processes L and M cone signals in an opponent manner, which result in a higher spatial resolution and the ability to carry red-green chromatic signals.

The RGC and LGN layers they project to also differ in terms of how they respond to a pulsating stimulus. MC neurons that receive mostly parasol RGC input respond to both stimulus-on and off sequences while PC neurons where most midget RGC project respond in a more tonic manner (Shapley & Perry, 1986). Temporal response functions therefore depended on stimulus chromaticity. Responses to chromatic stimuli generally peak at lower temporal frequencies while responses to achromatic stimuli peak at higher temporal frequencies. Achromatic stimuli also produce a distinct second harmonic component in the frequency domain as compared to chromatic stimuli, due to their transient nature (McKeefry et al., 1996).

Nevertheless, individual flicker of a temporally modulated stimulus cannot be perceived consciously past a certain temporal frequency threshold, even under optimal conditions. This threshold, or CFFF, is dependent on the chromaticity of the stimulus. Luminance channels are able to consciously perceive flicker up to 50Hz, while chromatic channels have lower thresholds: approximately 25Hz for red-green and 10Hz for S-cone isolating (Eskew et al., 1994; Holcombe & Cavanagh, 2001; Kelly, 1983; Lee et al., 1990; Matin, 1968; Wisowaty, 1981). The disparity between input and perception indicates that fast temporal information is filtered out at certain stages within the visual pathway. The disparity between chromatic and achromatic temporal sensitivity spectrums indicates that filtering arises after chromatic channels are separated.

Many earlier works investigated precortical visual areas as filtering stages, with the argument that there is no evolutionary purpose to process signals that would ultimately be excluded. Studies revealed that RGC are able to respond to a wider frequency range than LGN neurons (Derrington & Lennie, 1984; Lee et al., 1990; Solomon et al., 1999), which suggests temporal information is filtered between the two structures. However, another study evidenced that V1 neurons respond at

stimulus-matched frequencies up to 60Hz (Gur & Snodderly, 1997), which implicated rapid signals not only reach the cortex but are likely filtered out in higher-order areas.

This argument had been further supported with behavioural evidence, in particular using adaptation effects. Adaptation is defined as an attenuation in sensitivity to visual stimulus after prolonged exposure and takes place in the cortex, making it a marker for where the adaptive signal travels within the visual system. A study in 2004 found that flicker modulating above CFFF caused adaptation effects despite the absence of conscious perception (Shady et al., 2004), therefore indicating that rapid temporal frequencies are not filtered prior to V1. This effect was supported by a chromatic orientation adaption study (Vul & MacLeod, 2006), where chromatic gratings above CFFF caused orientation aftereffects despite not being seen.

These findings were supplemented by a neuroimaging study examining responses to chromatic red-green stimuli (Jiang et al., 2007). A comparison of the visual areas revealed distinct BOLD responses to 30Hz red-green flicker from V1 to hV4. BOLD amplitude decreased at higher frequencies as compared to slower contrast-matched flicker. This observation was congruent with the earlier adaptation studies where strength of adaptation decreased as the adapting flicker rate increased (Shady et al., 2004). Both observations suggested that responses to flicker are reduced as frequency increase within the ‘invisible’ range, similar to the trajectory within the ‘visible’ range. The only area where response matched conscious perception was VO, suggesting this is where processing of temporal information above CFFF terminates.

Overall, these studies provided valuable insights into how temporal signals are processed within the cortex. However, we propose two ways the results can be made more comprehensive. Firstly, the neuroimaging experiment should be repeated with more chromaticities, specifically luminance (achromatic) and S-cone isolating (blue-yellow). As compared to the chromatic red-green channel, the KC channel processing S-cone signals had received less attention. KC responses are widely regarded as ‘sluggish’, with lower and more limited temporal response range (Casagrande, 1994; Engel et al., 1997; Spitschan et al., 2016). However, several more recent findings have indicated not only that S-cone signals can convey motion

information, but that they may do so through an alternate pathway (Cavanagh & Anstis, 1991; Dobkins & Albright, 1994; Dougherty et al., 1999; D'Souza et al., 2011; Morand et al., 2000; Thiele et al., 1999). This unique temporal response function of KC neurons should be included in the investigation of chromatic filtering stages within the visual cortex.

Secondly, the modulation range of the neuroimaging study was somewhat limited. Extrapolating from our findings in Chapter 4, entrainment can occur at frequencies far beyond 50Hz, but few attempts have been made to drive the visual system directly at such high frequencies. Directly driving the visual cortex at high frequencies can provide further insight into the temporal filtering occurring at each visual area, instead of the general responsiveness of the occipital region. Additionally, considering the upper limit of reported CFFF for red-green inputs is 25Hz (Kelly, 1983), a modulation of 30Hz might be on the brink of conscious perception for some participants. For a more definite 'invisible' frequency range, we might include frequencies that are many times higher than the CFFF.

Our current study investigated the activity in visual areas V1, V3a and V4 when observers fixate on chromatic and achromatic targets flickering at one of a wide variety of frequencies – including frequencies that appeared to be invisible. We aimed to extend the existing work in two ways: first, expanding the frequency range. Previous experiments have typically used LCD monitors and projectors for stimulus display, which were limited in the maximum temporal frequency they could render: the maximum (Nyquist) stimulus frequency is half the monitor's refresh rate. Here, we trialled the use of an LED-based colour display device, which allowed us to modulate our stimuli well beyond 100Hz. Secondly, we selected stimulus chromaticities from all three axes of the Macleod-Boynton colour space. Given the evidence for potential high-frequency S-cone driven responses outside V1, (D'Souza et al., 2011; Stockman et al., 1991), we wondered if we could infer a unique sensitivity to faster S-cone signals in V3a responses as compared to other visual areas.

We were primarily interested in neural responses to stimuli modulating beyond the CFFF. For each stimulus chromaticity, we asked if responses to these invisible rapid

flicker were greater than a control, which had the same cue and trial structure but no flicker. We also asked if rapid S-cone isolating signals drove V3a more strongly than V1 and V4. Finally, we asked whether the chromatic preference of a visual area interacted with stimulus frequency. We expected that interaction between stimulus colour and frequency would entail the preference in area V4 for colour at certain flicker rates but not others.

5.3 Methods

5.3.1 Participants

We recruited three participants (one female; aged 24 - 48 years old) from the Department of Psychology at the University of York. Two out of three participants (RE and MS) were naïve to the study. All participants had normal colour vision (*tested using Ishihara plates, 24 plates edition*) and normal or corrected-to-normal visual acuity.

We obtained each participant's personal CFFF for each stimulus chromaticity prior to scanning. Participants completed 70 trials of two-interval forced choice task Bayesian staircase paradigm, where they had to indicate the target with the flicker. Participants' CFFF ranged from 36.3-49Hz for luminance stimuli, 20.5-23Hz for S-cone isolating stimuli and 24.8-27.1Hz for red-green stimuli, ensuring that the frequency range tested included both perceptible and consciously imperceptible stimuli for all participants. We also acquired the participant's contrast threshold for stimuli of all colours at 2Hz. This value was halved and used to customise subthreshold contrast visual inputs for each participant. Each participant then completed four 1-hour scanning sessions. The experiment was approved by the York Neuroimaging Centre Board of Ethics and all participants gave written informed consent before taking part in any experimental procedures.

5.3.2 Apparatus

All stimuli were developed and ran from Matlab 8.5.0 (2015a, The MathWorks Inc., Natick, MA, USA). An Arduino Due device (Arduino LLC) was used to transmit stimulus specifications from Matlab to a Prizmatix FC5-LED projector (Prizmatix Ltd, Israel). The projector contained five LED outputs, each relayed by a fibre optic cable branch. All outputs were merged into a single fibre optic cable (12mm, plastic core, 2mm diameter), which feeds into an IS-200 integrating sphere (Thorlabs, Inc., Newton, NJ) through a CCSA1 cosine corrector (Thorlabs, Inc., Newton, NJ). The integrating sphere mixes the LED outputs perfectly to produce one homogenised light, which was finally projected onto a 3x3cm sheet of volumetric light shaping diffuser (Luminit, CA) using a structurally identical fibre optic cable as before. A square of black paper with a 6mm hole was attached onto the diffuser on the same side as the fibre optic to remove aberrations around the edges of the projected light. Attentional task responses were made using a five-button fibre-optic response pad (Current Designs, Philadelphia, PA). The experiment was controlled from a Shuttle PC with Intel Core i7-4790K processor at 4.0 GHz and an NVIDIA GeForce GTX970 graphics card with 4 GB DDR5 memory.

5.3.3 Stimulus design

Stimuli were created using the silent substitution method (Estévez & Spekreijse, 1982), which involves controlling stimulus primaries (LED outputs in this case) in a way that activate selected cones in isolation. Cones that are not activated are effectively silenced. This required us to first determine a transformation matrix between the LED outputs amplitudes and how they drove each cone type, then inversing this matrix to compute the LED amplitude required. For example, for a red-green stimulus, we would multiply the inverted matrix by the cone activations of our target: *[L, M, S]* activation levels of *[1, -2, 0].*

The transformation matrix was first calculated between the LED primaries' spectra and cone fundamentals. Both were sampled to within the same wavelength range

and step size (390-720nm and 1nm respectively). LED_n values denoted the intensity of each LED output and L, M and S values denoted sensitivity of each cone type. This transform matrix was inverted using the pseudoinverse function (*pinv*) in Matlab.

$$LED2Cone = \begin{pmatrix} L_{\lambda 390nm} & \cdots & \cdots & L_{\lambda 720nm} \\ M_{\lambda 390nm} & \cdots & \cdots & M_{\lambda 720nm} \\ S_{\lambda 390nm} & \cdots & \cdots & S_{\lambda 720nm} \end{pmatrix} \times \begin{pmatrix} LED1_{\lambda 390nm} & \cdots & nLED_{\lambda 390nm} \\ \vdots & \vdots & \vdots \\ \vdots & \vdots & \vdots \\ LED1_{\lambda 720nm} & \cdots & nLED_{\lambda 720nm} \end{pmatrix}$$

$$Cone2LED = LED2Cone^{-1}$$

The LED spectra were calibrated using a NIST-traceable Jaz USB photospectrometer with a 2nm resolution (Ocean Optics, Dunedin, FL). Calibrations were performed on the LED output (at maximum amplitude) projected onto the light diffuser. Stockman and Sharpe (2000) L-, M- and S-cone 2° cone fundamentals in 0.1nm step size were obtained from the CVRL website (www.cvrl.org). The data were resampled for 1nm step size between wavelength range 390-720 nm.

The stimulus temporal modulation was performed using the Pulse Width Modulation (PWM) technique, where LEDs are dimmed and brightened rapidly during stimulus presentation. The perceived brightness of the LED is dependent on the proportion of bright to dim periods over the presentation. This method is commonly implemented in experiments using microcontrollers. The current study utilised an Arduino Due, which has 12 analogue inputs, providing 4096 different intensity values at a modulation rate of 200Hz.

To compute the final intensities, we multiplied the transform matrix Cone2LED by a vector denoting cone activation ratios for each opponent pathway of the Macleod-Boynton colour space, where *[L, M, S] = [1 1 1]* for L+M+S, *[0 0 1]* for S-cone isolating and *[1 -2 0]* for L-M. Background or null LED is to *[0.5 0.5 0.5]*. After determining the chromaticity, luminance, S-cone isolating, and red-green stimuli were scaled to modulate at the appropriate contrast levels: 85%, 69% and 14% respectively for full contrast conditions and half of each participant's threshold or approximately 1.5%, 1.5% and 0.5% respectively for subthreshold contrast

conditions. We modulated stimuli at the following temporal frequencies: 2Hz, 8Hz, 32Hz, 64Hz and 125Hz.

5.3.4 MRI parameters

5.3.4.1 Anatomical imaging

T1-weighted anatomical data were collected on a GE 3T Signa HDx Excite MRI scanner with a 8-channel whole-head phased-array coil (MRI Devices Corporation) using standard parameters (TR = 7.8ms; TE = 3.0ms; flip angle = 20°; FOV = 290 x 290 mm^2; matrix size = 256 x 256; voxel resolution = 1.13 x 1.13 x 1.0 mm^3, 176 slices in total).

5.3.4.2 Functional imaging

Functional imaging data were collected on the same GE MRI scanner with a 16-channel posterior surface coil (Nova Medical, Wilmington, MA) to improve SNR in the occipital region. The scan sequence was identical for each of the four experimental sessions the participants completed. Firstly, we completed a proton density (PD) anatomical scan to register functional data to MNI space, using a prescription identical to that used in the functional scans (TR = 2000ms; TE = 30ms; flip angle = 80°; FOV = 240 x 240 mm^2; matrix size = 128 x 128; voxel resolution = 2 x 2 x 2.5 mm^3, 26 slices). Slices were taken semi-axially, covering the occipital lobe and the ventral surface along the temporal lobe.

This was followed by six blocks of gradient-echo EPI scans, each with 12 runs of flickering stimuli (TR = 2000ms; TE = 30ms; flip angle = 80°; FOV = 240 x 240 mm^2; matrix size = 128 x 128; voxel resolution = 2 x 2 x 2.5 mm^3, 26 slices). Each block started with three ‘dummy’ volumes (lasting 3 TRs) to allow signals to reach magnetic equilibrium.

5.3.5 fMRI procedure and task

Participants completed both the temporal threshold and the contrast threshold tasks prior to scanning. The stimulus was viewed from a distance of 22cm and subtended1.56° of visual angle. Lights within the scanning room were switched off or concealed before starting the experiment to maximise stimulus visibility.

Stimuli were presented in a block design, with each block consisting of 10 TRs (20s) of stimulus presentation followed by a 5 TRs (10s) interstimulus interval (ISI). The stimulus presented in each block was randomly chosen from 19 shuffled conditions (full contrast: 2Hz luminance, 2Hz S-cone isolating, 2Hz red-green, 8Hz luminance, 8Hz S-cone isolating, 8Hz red-green, 32Hz luminance, 32Hz S-cone isolating, 32Hz red-green, 64Hz luminance, 64Hz S-cone isolating, 64Hz red-green, 125Hz luminance, 125Hz S-cone isolating, 125Hz red-green, subthreshold contrast: 2Hz luminance, 2Hz S-cone isolating, null condition) prior to the scan. Each fMRI scan consisted of ten blocks, taking 6 minutes 30s. In each session, a participant would complete six scans.

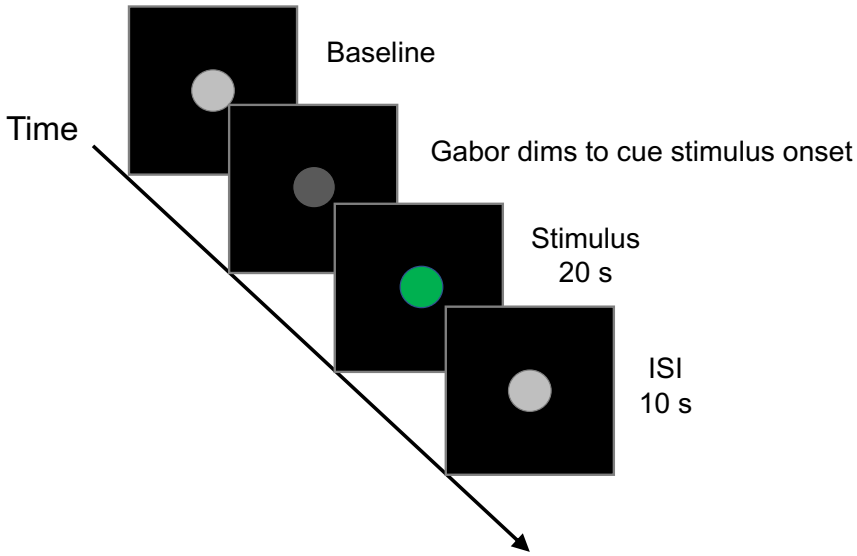

Fig. 5.1 *Stimulus configuration for a single block. First, baseline light is presented, followed by a brief dimming as part of the attentional task. This is succeeded by ten blocks of stimulus presentation, each one lasting 10 TRs (or 20 s) and a 5 TRs (10 s) ISI.*

To maintain the participant's attention, the LED output was programmed to dim briefly just before the stimulus presentation on randomly selected trials. Participants were asked to push any button on the response pad upon observing this.

5.3.6 Regions of interest (ROI)

5.3.6.1 Mapping of ROI

The participants had all completed retinotopic scanning prior to the current experiment using the standard retinotopic mapping procedure of rotating wedge and expanding ring stimuli. V1, V3a and V4 were identified using phase reversal techniques. Areas immediately adjacent to stimulus-driven regions can produce negative BOLD responses (Wade & Rowland, 2010) and combining responses from positive and negative regions can lower the apparent response to the stimulus. In addition, penumbral cones (those in the shadow of blood vessels) can cause

significant noise (Spitschan et al., 2015) because they generate errors in the estimates of cone excitation spectra. To address these issues, we first limited each visual area to the central 3° of visual field (where blood vessels are rare or absent). We then ran a contrast to identify regions within this area that were responsive to 2-64Hz modulations of all three colours in comparison to the control condition. These areas were selected as our final regions of interest.

5.3.6.2 Analysis of ROI

We analysed data from individual participant in Matlab 8.5.0 (2015a, The MathWorks Inc., Natick, MA, USA) using the mrVista software (https://web.stanford.edu/group/vista/cgi-bin/wiki/index.php/Software; Vista Lab, Stanford University). Three dummy volumes included at the start of each scan were discarded and motion correction was performed within each scan. We used the FAST-corrected and BET-extracted PD scans within each session as a reference to align functional data with the participant's anatomical detail using an information maximisation algorithm (Nestares & Heeger, 2000). Cortical grey and white matter boundaries were reconstructed using Freesurfer v5.3 and we limited BOLD activity in subsequent analyses within the grey matter.

We suspected that a sudden onset of bright light in the dark scanning room might generate atypical BOLD responses. Hence, the first trial of each scan was coded as a separate condition regardless of stimulus properties. We also discarded the sixth scan for participant *RE* due to an artefact that persisted after motion compensation.

We combined the functional data from all four experimental sessions for each participant before running a general linear model (GLM) analysis on the combined sequences for all 20 (19 + 1) conditions. We modelled the time course from each ROI using the stimulus matrix convolved with a weighted hemodynamic response function (the 'difference of Gammas' hemodynamic response function from the SPM 8 toolbox (http://www.fil.ion.ucl.ac.uk/spm/)). This produced a beta weight per condition within each ROI. We then subtracted the beta weight of the control condition from the beta weights of the rest. The GLM also yielded the percentage of

variance explained for each ROI per participant. We excluded one set of beta weights (MS, V3a) from further analysis as it explained less than 2% of variance.

5.4 Results

5.4.1 Overview of the data

We ran a GLM on the data combined across all four sessions for participants separately and estimated the mean amplitudes (beta weights) in each condition. Mean amplitude for the null condition was then subtracted from the beta values of all conditions. The results are plotted in **Fig. 5.2**, **Fig. 5.3** and **Fig. 5.4** for ARW, RE and MS respectively). We observed some signatures of chromatic BOLD responses, such as greater responses to slow flickering, high contrast stimuli that attenuates with increasing frequencies.

We ran one-sample t-tests comparing null adjusted mean amplitudes of each condition to the test value of 0 (i.e. null condition) for participants separately (see **Fig. 5.2**, **Fig. 5.3** and **Fig. 5.4** and **Table 5.1, Table 5.2, and Table 5.3 in** Appendices for detailed statistics). We found high inter-subject variances in responses, but participants largely responded significantly to low temporal frequency high contrast stimuli.

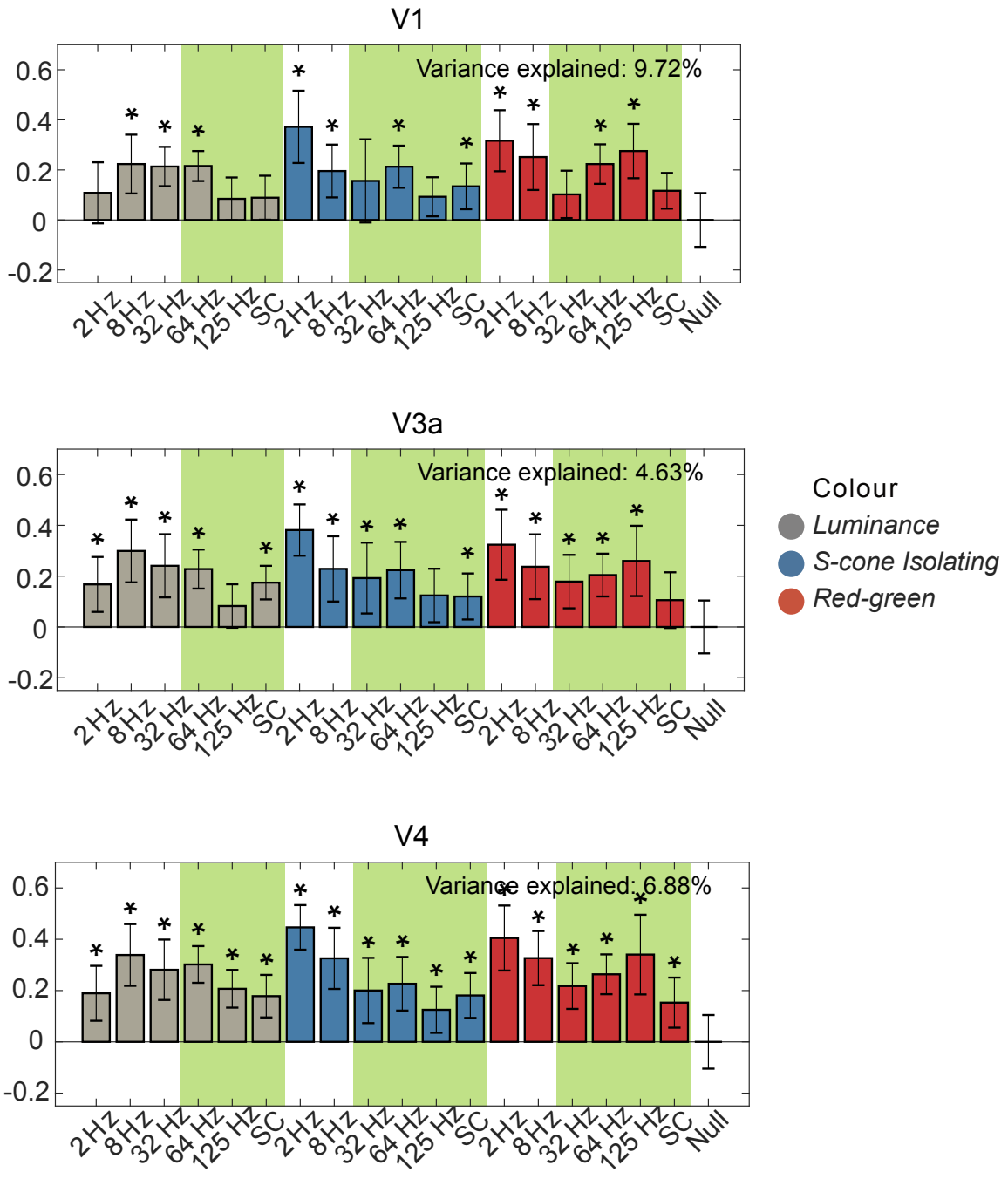

Fig. 5.2 *BOLD amplitude (GLM betas) recorded at ARW's ROIs with null subtracted. Error bars denote ±1 SE. Green shaded area denotes conditions where either temporal frequency or contrast is below threshold and participant cannot consciously perceive the stimuli. Asterisks denote conditions with significant difference between amplitudes and the control (i.e. 0% BOLD).*

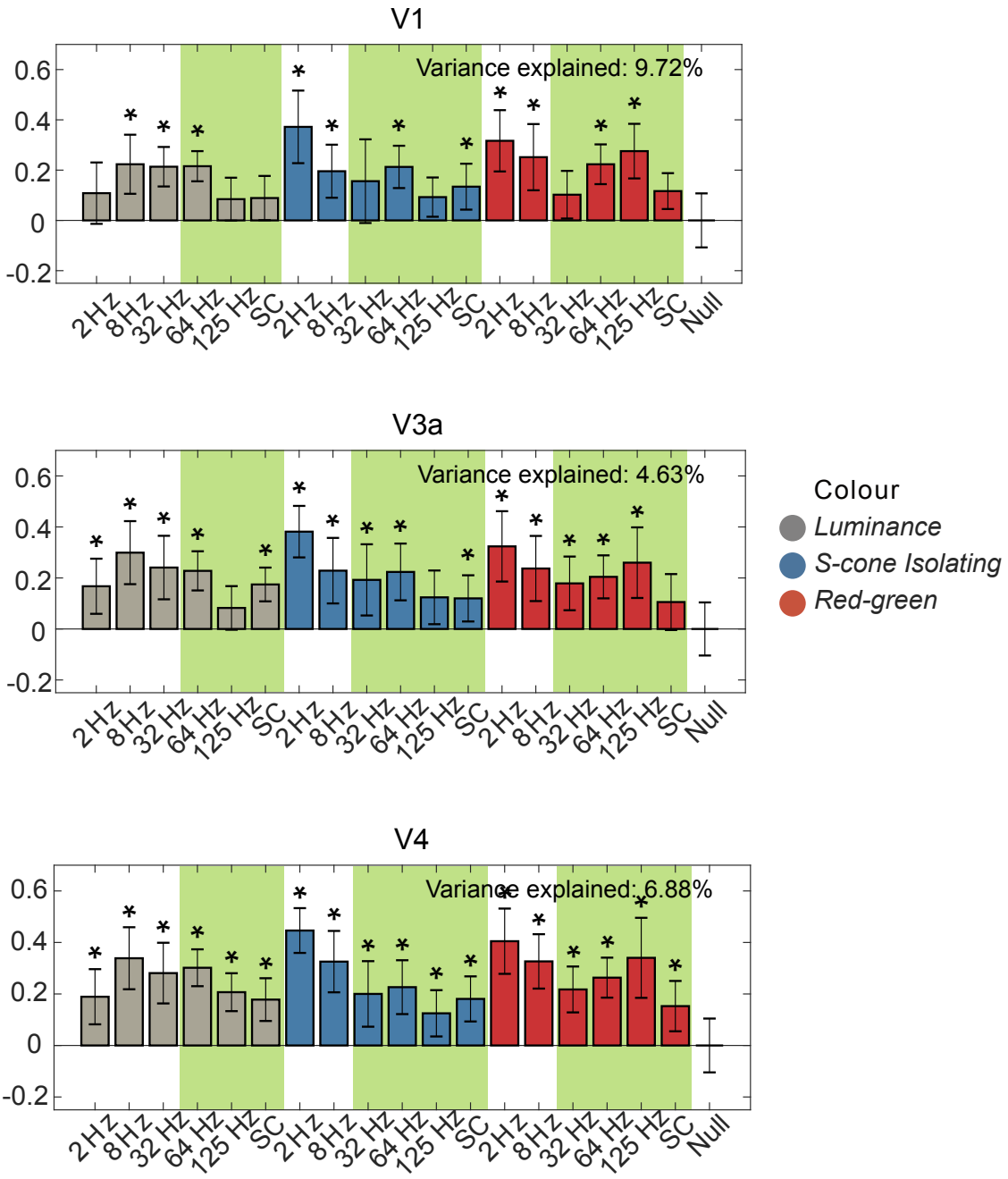

Fig. 5.3 *BOLD amplitude (GLM betas) recorded at RE's ROIs with null subtracted. Error bars denote ±1 SE. Green shaded area denotes conditions where either temporal frequency or contrast is below threshold and participant cannot consciously perceive the stimuli. Asterisks denote conditions with significant difference between amplitudes and the control (i.e. 0% BOLD).*

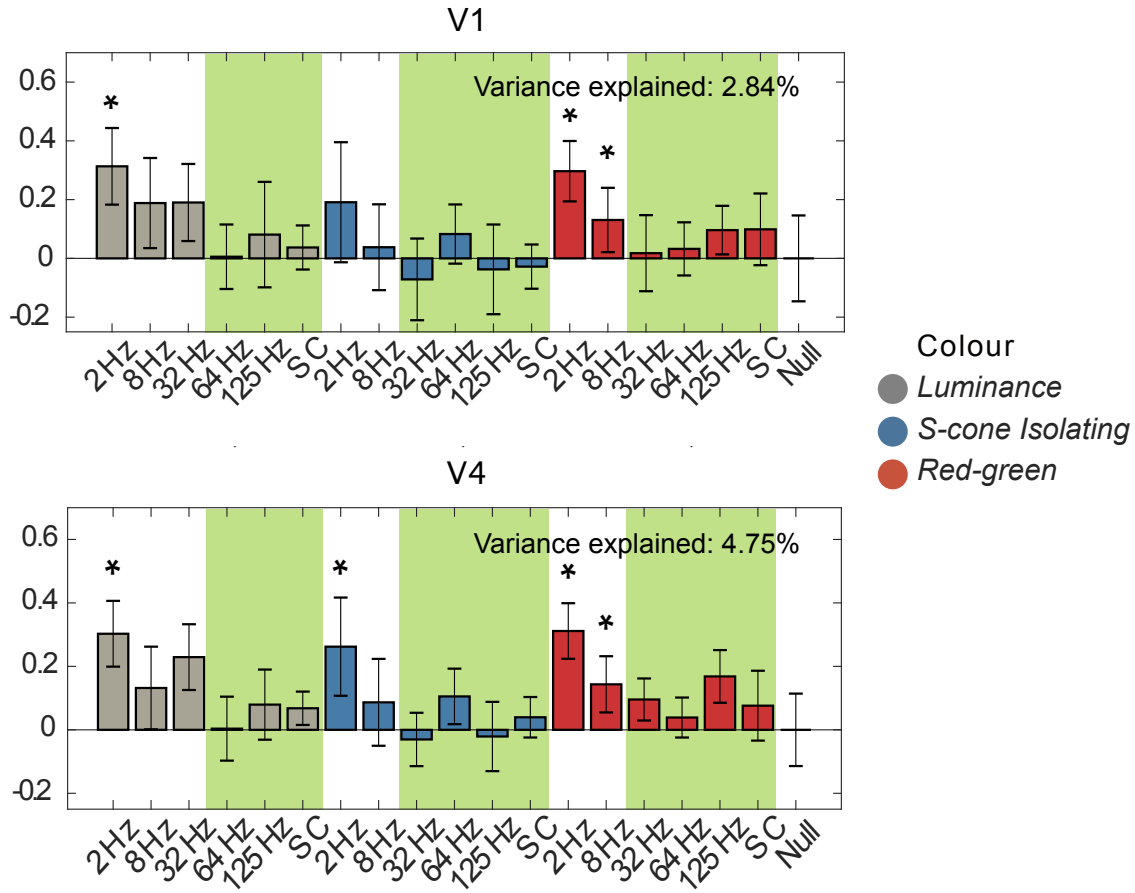

Fig. 5.4 *BOLD amplitude (GLM betas) recorded at MS's ROIs with null subtracted. Error bars denote ±1 SE. Green shaded area denotes conditions where either temporal frequency or contrast is below threshold and participant cannot consciously perceive the stimuli. Asterisks denote conditions with significant difference between amplitudes and the control (i.e. 0% BOLD).*

5.4.2 Neural responses to 'visible' stimuli

In general, we observed a relationship between contrast sensitivity and temporal frequency, where responses to high contrast stimuli were stronger for lower temporal frequencies and decreased as the flicker became faster. We plotted the group averaged amplitudes for 'visible' stimuli at 2Hz for full and subthreshold contrast conditions. Expectedly, full contrast conditions evoked higher BOLD amplitudes for flicker of all stimulus colours than subthreshold conditions.

5.4.3 Neural responses to ‘invisible’ stimuli

Based on our research questions, we first compared the data for ‘invisible’ flicker conditions to contrast and chromatically matched ‘visible’ flicker to find out if visible flicker generated significantly greater BOLD activity. We then examined if responses to invisible flicker were greater than the null condition. Lastly, we compared the responses between the two ‘invisible’ frequencies (32 and 64Hz) in chromatic conditions to determine if responses simply decline with increasing temporal frequencies. These conditions were chosen to match and extend on the findings in Jiang, Zhou, & He (2007)’s paper.

We found for purely luminance stimuli, visible flicker at 2Hz consistently generated greater responses than invisible flicker of 64Hz in all visual areas. We also observed this trend in chromatic conditions, where both 32 and 64Hz flicker produced much smaller responses than 2Hz flicker. Flicker modulate at above CFFF also produced higher BOLD responses than the null conditions. Within the invisible frequency range for chromatic flicker, BOLD responses increased with higher temporal frequencies. All means and standard deviations are summarised in **Table 5.4** in the Appendices. All comparisons can be visualised in **Fig. 5.5**.

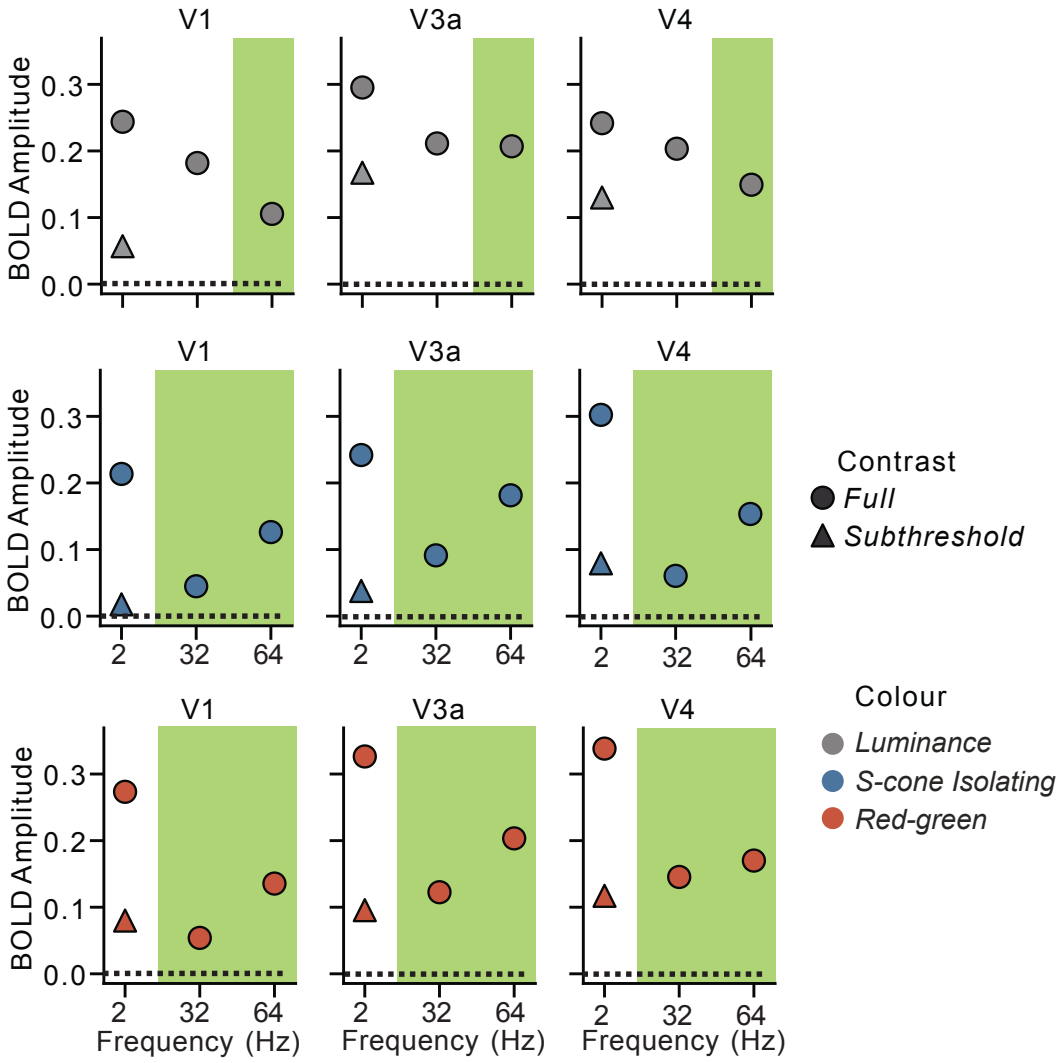

Fig. 5.5 *Mean amplitude (beta weights) from GLMs averaged across three participants. Green shaded region denotes the 'invisible' frequency range where flicker rate is above participants' CFFF. The data showed that full contrast 2Hz stimuli consistently evoked greater BOLD responses than subthreshold contrast stimuli. As compared to full contrast 2Hz flicker, responses towards full contrast 'invisible' flicker were always weaker for purely luminance stimuli (64Hz). This attenuation was also observed for all 32Hz chromatic flicker, but chromatic responses showed unexpected increases at 64Hz.*

5.4.4 Neural responses to rapid S-cone flicker

We also asked if BOLD responses to S-cone isolating stimuli evoked greater BOLD amplitudes in V3a as compared to the other temporal frequencies. The results

showed that while S-cone driven responses were indeed greater in V3a than V1 and V3, this trend was also observed for luminance and red-green driven responses. This finding was depicted in **Fig. 5.6**.

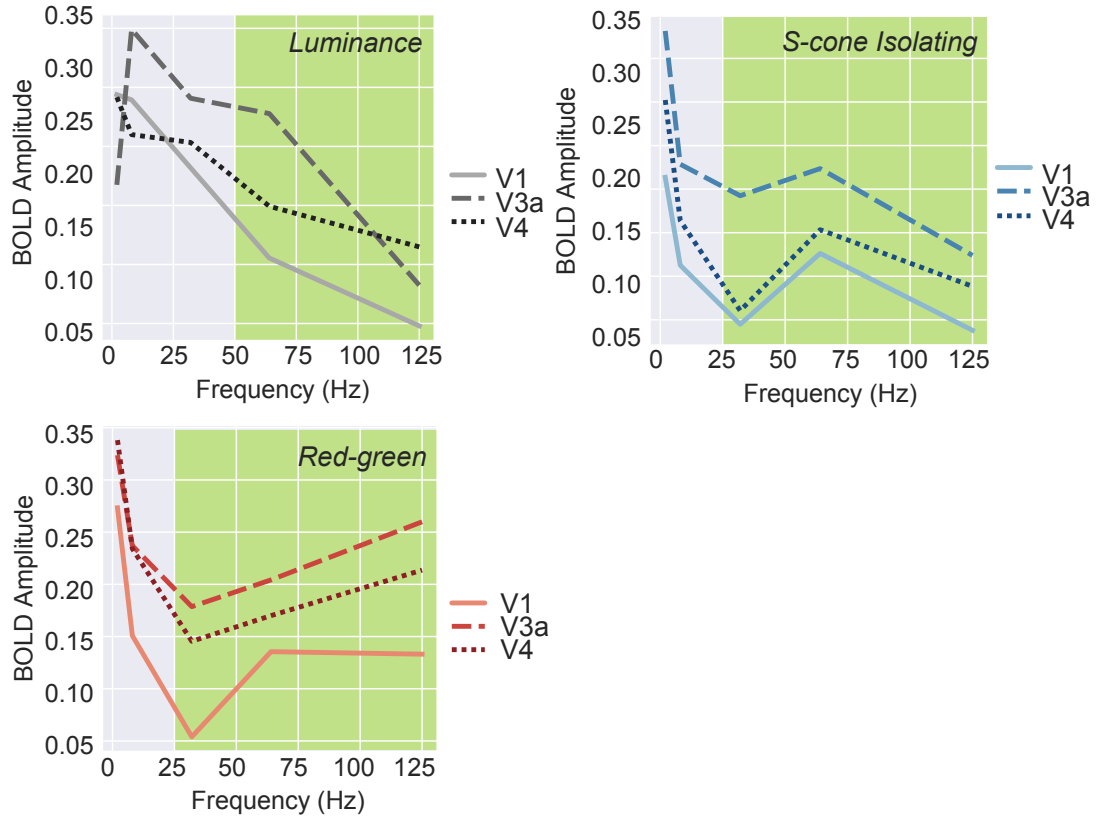

Fig. 5.6 *Mean amplitude (beta weights) in V1, V3a and V4 averaged across ARW and RE (MS V3a data excluded) for S-cone isolating stimuli. Grey lines represent data for luminance flicker, blue lines represent data for S-cone isolating flicker and red represent data for red-green flicker. Green shaded region denotes the 'invisible' frequency range where flicker rate is above participants' CFFF. V3a was consistently more responsive than V1 across all chromaticities. In general, BOLD amplitudes decreased as a function of increasing temporal frequencies, with the exception of red-green flicker. We also saw an increase in BOLD amplitude to rapid S-cone isolating flicker at 64Hz. However, this was not unique to V3a, implying a bottom-up amplification of neural responses that affects all the activity of all visual areas.*

5.4.5 Interaction between stimulus frequency and colour in V1 and V4

We examined the mean amplitude in V1 and V4 for 2Hz and 8Hz stimuli and asked if there was an interaction between colour and temporal frequency. The results indicated that responsiveness to a chromatic stimulus was dependent on the temporal frequency. In **Fig. 5.7**, for example, responses to 2Hz chromatic stimuli are greater than that for 2Hz achromatic stimuli in both V1 and V4. However, this difference became less distinct with 8Hz stimuli, where responses to all three chromaticities were almost identical in V4.

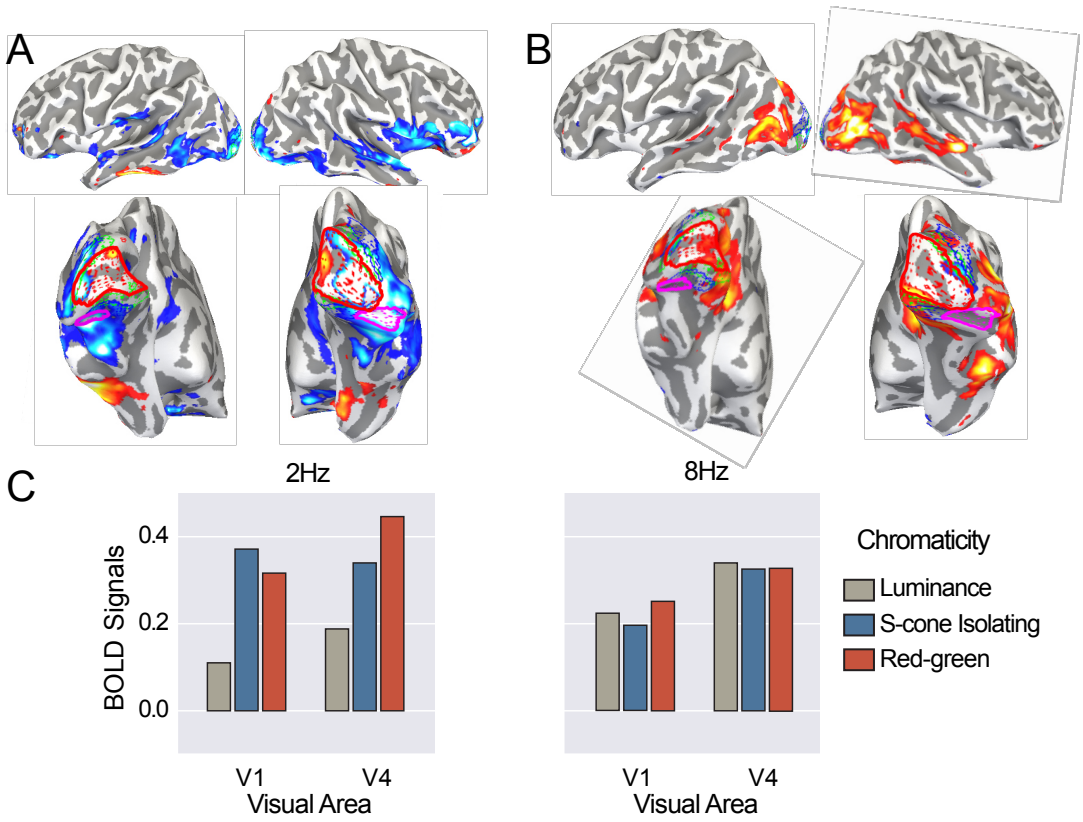

Fig. 5.7 *Participant ARW's data rendered onto a brain surface mesh using mrMeshPy, showing neural responses as a result of running contrast between luminance and chromatic (S-cone isolating and red-green) conditions for (A) 2Hz flicker and (B) 8Hz flicker. Cool tones indicate greater activation for chromatic than luminance stimuli and warm tones indicate greater activation for luminance than chromatic stimuli. Visual areas are denoted by coloured outlines: V1 in red, V2 in green, V3a in blue and V4 in pink. Visual areas outlined here are identified based on retinotopic mapping and are not restricted to the central 3 degrees. (C) Averaged BOLD signals across visual areas for the conditions illustrated above.*

This was not the case for the other participants, who showed greater responses to 2Hz luminance and red-green stimuli in both V1 and V4. This response pattern was also observed for 8Hz stimuli in RE (**Fig. 5.8**), but MS showed a distinct preference for luminance stimuli in V1 and chromatic red-green stimuli in V4 (**Fig. 5.9**).

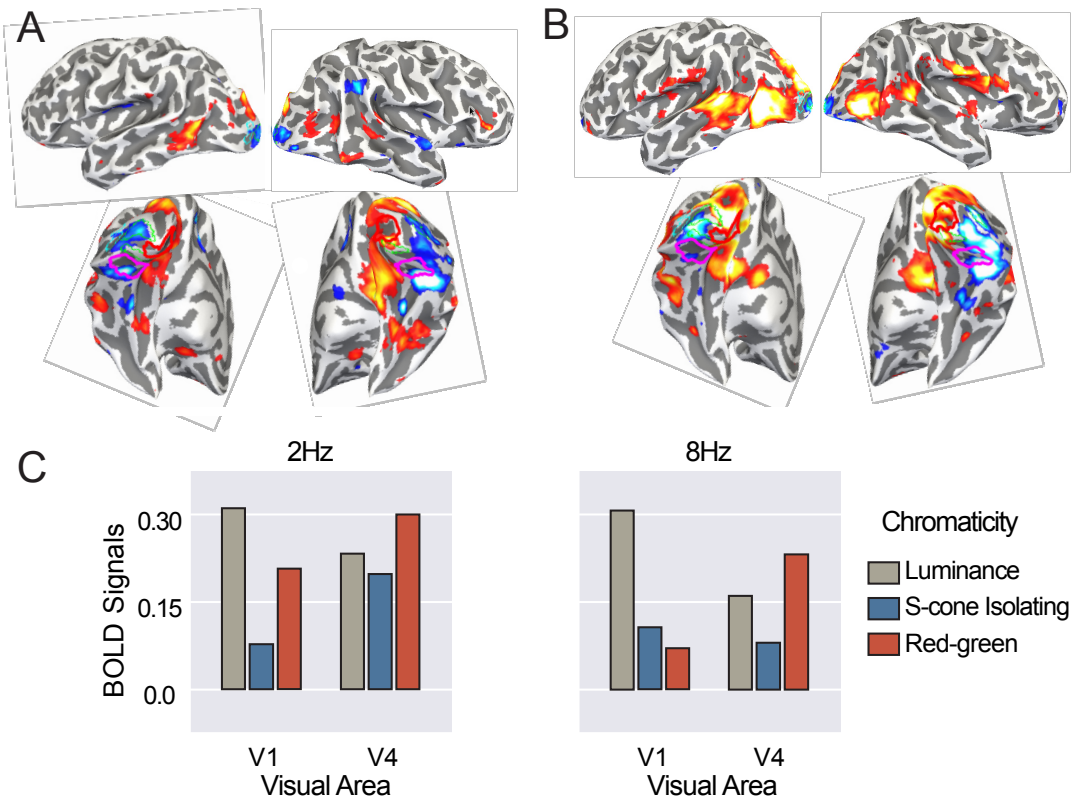

Fig. 5.8 *Participant RE's data rendered onto a brain surface mesh using mrMeshPy, showing neural responses as a result of running contrast between luminance and chromatic (S-cone isolating and red-green) conditions for (A) 2Hz flicker and (B) 8Hz flicker. Blue indicate greater activation for chromatic than luminance stimuli and orange tones indicate greater activation for luminance than chromatic stimuli. Visual areas are denoted by coloured outlines: V1 in red, V2 in green, V3a in blue and V4 in pink. Visual areas outlined here are identified based on retinotopic mapping and are not restricted to the central 3 degrees. (C) Averaged BOLD signals across visual areas for the conditions illustrated above.*

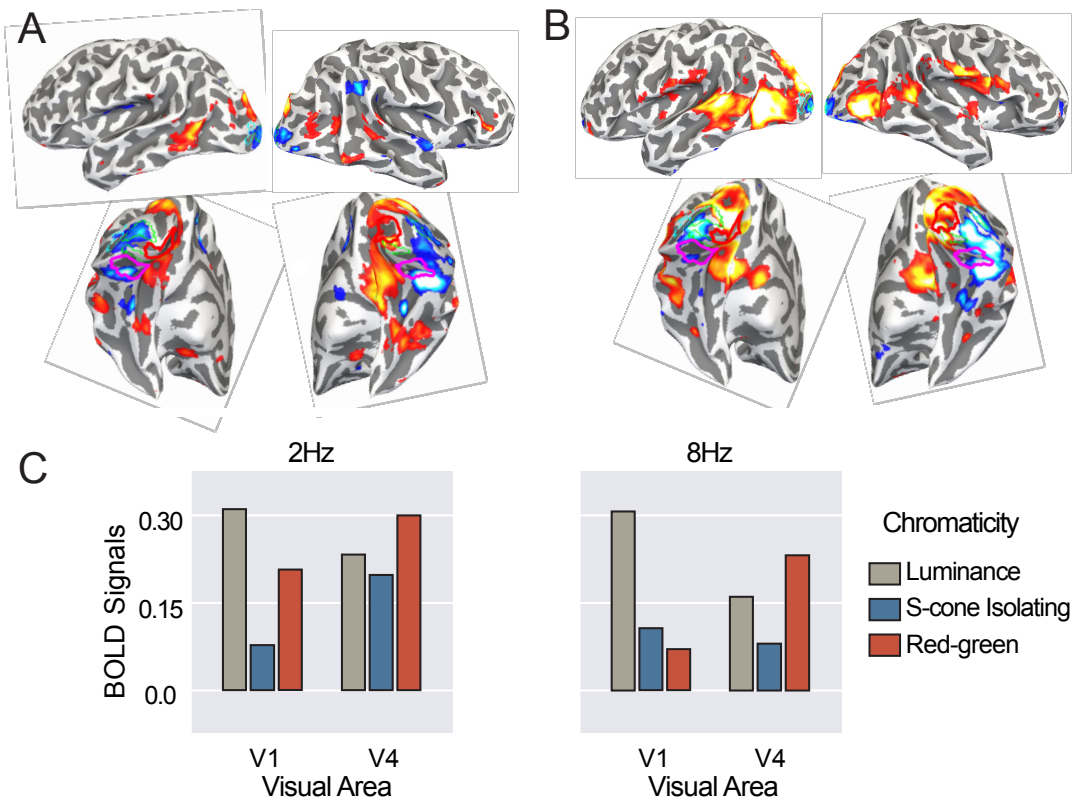

Fig. 5.9 *Participant MS's data rendered onto a brain surface mesh using mrMeshPy, showing neural responses as a result of running contrast between luminance and chromatic (S-cone isolating and red-green) conditions for (A) 2Hz flicker and (B) 8Hz flicker. Blue tones indicate greater activation for chromatic than luminance stimuli and orange tones indicate greater activation for luminance than chromatic stimuli. Visual areas are denoted by coloured outlines: V1 in red, V2 in green, V3a in blue and V4 in pink. Visual areas outlined here are identified based on retinotopic mapping and are not restricted to the central 3 degrees. (C) Averaged BOLD signals across visual areas for the conditions illustrated above.*

BOLD activation averaged across all three participants showed that luminance (mean = 0.24, SD = 0.12) and chromatic flicker (mean = 0.24, SD = 0.11) at 2Hz generated a roughly 1:1 ratio in V1. This pattern of BOLD activation was also found in V4 for 8Hz conditions (luminance: mean = 0.21, SD = 0.11, chromatic: mean = 0.20, SD = 0.11). In contrast, chromatic 2Hz flicker (mean = 0.32, SD = 0.09) evoked higher BOLD amplitudes in V4 than achromatic ones (mean = 0.24, SD = 0.06) and achromatic 8Hz flicker (mean = 0.24, SD = 0.06) evoked higher BOLD amplitudes in V1 than chromatic ones (mean = 0.13, SD = 0.08) (**Fig. 5.10**).

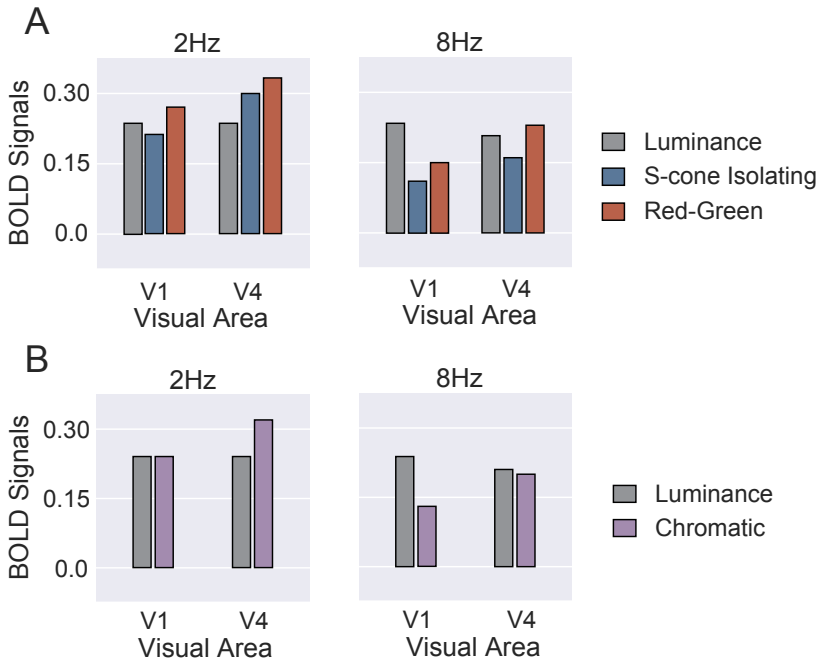

Fig. 5.10 *Group averaged BOLD signals across visual areas for 2 and 8Hz achromatic and chromatic flicker: (A) showing all three chromaticities separately and (B) showing luminance and coloured stimuli.*

5.5 Discussion

BOLD responses to chromatic and achromatic stimuli have been extensively researched, but often with a stimulus modulation frequency range that is limited by the framerate of the display system. The current study overcame this obstacle using a novel 5-primary LED system to generate our stimuli. We were primarily interested in whether flicker modulating above CFFF generated clear BOLD responses as compared to null conditions. But, additionally, we also searched for evidence that fast S-cone signals enhanced activity in motion sensitive, non-chromatic areas like V3a, and whether responses of V1, V3a and V4 to chromatic inputs changed with the temporal frequency of the stimulus.

5.5.1 BOLD responses to 'visible' and 'invisible' stimuli

Overall, we found some evidence of high temporal frequency flicker driving V1, V3a and V4. Both individual and group averaged responses showed that high contrast, low frequency stimuli generated higher BOLD amplitudes as compared to low contrast, high frequency stimuli. However, on an individual basis, we found one participant (ARW) that responded significantly to multiple 'invisible' flicker conditions, demonstrating a high heterogeneity in the results. The comparisons between group averaged data suggested that selected 'invisible' flicker conditions (32, 64Hz for S-cone isolating and red-green, 64Hz for luminance) evoked responses that were smaller than colour- and contrast-matched 'visible' 2Hz conditions, but greater than null. We also found that although responses to fast S-cone isolating stimuli were generally greater in V3a than V1 and V4, this trend was not unique to S-cone isolating stimuli. Lastly, we found a clear interaction between temporal frequency and stimulus colour in visual areas. Specifically, chromatic preference was demonstrated by V4 responses only for 2Hz flicker, and 8Hz luminance responses were much higher than chromatic responses.

We also noted that the red-green stimuli, which were used in the previous fMRI study by Jiang et al. (2007), often generated the strongest responses. Our data also showed that grouped averaged responses to invisible flicker in V4 were greater than those in the null condition. This suggested that signals modulating above the CFF were not filtered out before V4, which was consistent with the findings of the previous study.

On the other hand, we observed a much higher level of variability between subjects than expected (**Fig. 5.2**, **Fig. 5.3** and **Fig. 5.4**), suggesting that the situation might not be that simple. While two out of three subjects showed non-significant BOLD responses to high frequency flicker, one subject (ARW) showed robust responses to invisible flicker: some of which were similar or even higher than the colour-matched

visible stimuli. We considered possible mechanisms that might have caused significant responses to invisible flicker aside from bottom-up visual processing.

One possibility would be that the activity we measured for chromatic stimuli was partially due to luminance 'leakage' or 'splatter' (Spitschan et al., 2014). We modulated the stimuli at very high contrasts (i.e. the maximum provided by the relatively pure LED primaries). This made the resultant flicker more salient, but with an increased probability that they were not rendered perfectly at isoluminance. Normally, isoluminant flicker modulating above CFFF would fuse and appear perceptually identical to the background. A stimulus 'splatter', however, could provide an additional chromatic filter to a perceptually invisible flicker. Additionally, the mechanisms of the early visual system are not perfectly linear, such as retinal computation (Chichilnisky & Kalmar, 2002; Schwartz & Rieke, 2011). This means that even if our estimates of cone spectral sensitivities were perfectly accurate, the non-linearities in the visual pathway might lead to residual 'DC' colour perception when the mean luminance of alternating flicker does not sum to zero (Rider et al., 2018; Stockman et al., 2017).

Furthermore, the ventral stream is linked with top-down colour imagery in addition to bottom-up stimuli (Chao & Martin, 1999). Direct interactions between perception and memory have been evidenced repeatedly (Hansen et al., 2006; Olkkonen et al., 2008). Greyscale images of objects with conventional colour schemes (e.g. bananas) could also induce chromatic biases, moving the achromaticity baseline closer towards the implied colour (Lee & Mather, 2019). In a similar way, static images that contained motion cues may activate motion sensitive cortical areas (Kourtzi & Kanwisher, 2000) as well as evoke motion aftereffects (Winawer et al., 2008). Attention to subthreshold motion may even be sufficient in driving motion areas (Huk & Heeger, 2002). We extrapolate from these findings that tiny flashes of colour leakage can theoretically lead to an amplified response in visual areas if the observer was cued to *think* about colour or remember colour stimuli rather than consciously perceiving it. Although the current stimuli were void of semantic information, it is possible that a hint of colour drove the visual system through similar top-down mechanisms.

On the other hand, if luminance leakage were contributing to the high BOLD responses in 'invisible' conditions, we would expect to see even bigger responses towards achromatic luminance stimuli, which we do not (**Fig. 5.2**). Additionally, luminance 'splatter' is determined by the bit depth of signal specification: with the RMS cone contrast of isoluminant patterns being about 7%, our estimates of luminance 'splatter' for red-green stimuli would be no more than 1% contrast even with a 5% error. Even if responses were contaminated by luminance splatter, it would be by a negligible amount. Furthermore, the GLMs conducted using ARW's data consistently produced the highest variance explained amongst the participants, suggesting that the finding was robust despite being unusual. The small sample size and lack of group level statistical testing made it difficult to speculate further, but in general, the data indicated that responses to rapid signals were possible and might be more prevalent if experiment was repeated with more subjects and focused on fewer frequencies.

We aimed to extend the findings of Jiang et al. (2007) by investigating how BOLD signal amplitudes changed with increasing frequency within in the invisible range. Despite not being tested for significance, the BOLD responses for 64Hz chromatic flicker were consistently higher than that for 32Hz (see **Fig. 5.5**). This conflicted with our predictions based on the attenuated adaptation effects (Vul & MacLeod, 2006), where within the 'invisible' range, a faster flicker would drive the visual system less powerfully than a slower flicker, and also with our general intuition that faster flicker must drive the visual system less strongly than slower ones in general.

If the increase at 64Hz is real, what could cause it? One possibility is an interaction with an existing endogenous rhythm – perhaps gamma. Visual detection reaction times have previously shown strong correlations with the gamma activity within V4 (Womelsdorf et al., 2006, 2007; Womelsdorf & Fries, 2007), adding to a growing pool of evidence for the role of gamma activity in attention synchronisation (Engel et al., 2001; Steinmetz et al., 2000). A more recent experiment demonstrated that this effect can be essentially emulated by exogenously driving the visual system at gamma frequency range. The authors found that flicker of gamma range frequencies beyond CFFF (>50Hz) was able to direct attention, which resulted in better target detection and discrimination (Bauer et al., 2009). Interestingly, this effect was limited

to the mid-gamma range and not found for flicker below 35Hz, in accord to the range most suitable for the enhancement of postsynaptic kinetics (Fries et al., 2001). The current findings offer some weak support to this theory, as responses to 32Hz flicker and greater responses to 64Hz flicker through attention direction in the absence of conscious awareness.

Finally, we saw more larger 'invisible' BOLD responses in V4 than in earlier visual areas. This indicated that signals were not strongly temporally filtered prior to arriving in V4. Instead, responses becoming significantly higher than null in V4 than V1 suggested an amplification of signals progressing through the visual areas. Our data contradicted some previous findings which showed V4 activation to be restricted by the temporal frequency of stimuli (D'Souza et al., 2011; Mullen et al., 2010) but agreed broadly with Jiang et al. (2007)'s findings of significant 'invisible' flicker responses on the ventral surface. Instead, rapid chromatic and achromatic signals were likely filtered out in later extrastriate areas, possibly VO (Jiang et al., 2007).

5.5.2 Rapid S-cone flicker

Curiously, we observed higher BOLD responses to rapid S-cone isolating stimuli (>2Hz) in V3a when compared to V1 or V4. Although we initially suspected that this might have been a genuine effect, we found that activation within V3a was the strongest regardless of chromaticity. This implied that rapid S-cone signals did not preferentially activate V3a as compared to other visual areas. Instead, our data bore some resemblance to the temporal response functions described in D'Souza et al., (2011). The authors showed that V3a responses normalised to that of 2Hz were higher than V1 responses across the entire tested frequency range (up to 12Hz). This was supported by a more recent study using repetitive transcranial magnetic stimulation (rTMS), which showed that speed perception of both S-cone isolating and red-green signals were disadvantaged when rTMS was applied to V3a and MT (McKeefry et al., 2010). Area V3a's ability to process motion information in chromatic signals are not limited to S-cone isolating stimuli as previously thought (Lee & Stromeyer, 1989; Morand et al., 2000).

5.5.3 Interaction between stimulus frequency and colour in V1 and V4

Our data also showed an interaction between stimulus colour and temporal frequency. We found a strong preference for chromatic flicker in V4, a well-known 'colour' area, but only when flicker frequency was at 2Hz. At 8Hz, the BOLD amplitude evoked by achromatic and chromatic stimuli were almost identical. In contrast, we found that luminance flicker at 8Hz generated noticeably higher response in V1 as compared to V4, which was consistent with luminance channel's ability to process motion (Livingstone & Hubel, 1987). The finding supported multiple studies that demonstrated the distinct temporal properties of chromatic and luminance processing channels (D'Souza et al., 2011; Liu & Wandell, 2005; Spitschan et al., 2016). The present-day chromatic retinotopic mapping are usually conducted with 2Hz stimuli and the Mondrian pattern in seminal research was shown at 1Hz (McKeefry & Zeki, 1997). Had it been shown at a faster frequency, perhaps the region in the fusiform gyrus would not have been as active.

5.5.4 Future directions

The current experiment extended our understanding of the temporal response functions in multiple visual areas by modulating the stimuli at much higher frequencies than before. However, it is clear that the experiment could be altered to produce more robust results in the future. Firstly, we experienced an unexpectedly high level of inter-subject variability. While our main interest was in responses generated by flicker above CFFF, we expected to see standard contrast response functions clearly across the data of all participants for the slower, perceptible frequency range. This was true of our chromatic responses, which were almost always greater at 2Hz than 8Hz (consistent with a temporal low-pass filter). However, we also observed instances where our expectations were not met, for example: non-significant V1 responses to fast luminance stimuli (MS, 32Hz) and non-significant V4 responses to slow S-cone isolating stimuli (RE, 2Hz). The lack of

clear signatures for chromatic flicker indicated that results of subsequent analyses might not be robust and reliable.

Taking into account the overall low variance explained by the GLMs, future experiments should aim to create more powerful stimulation. This can be achieved by increasing the stimulus size or intensity. The current stimulus extended 1.56° visual angle, while those in previous experiments ranged from 3-3.5° (Jiang et al., 2007; Shady et al., 2004) to 21° in the neuroimaging study that established the S-cone temporal frequency response functions in V3a and MT (D'Souza et al., 2011). Since a smaller stimulus size would indicate fewer strongly activated voxels, the signal we obtained after averaging across the voxel group would inevitably be weaker. We also experienced some difficulties when defining ROIs. Overlaps between the regions activated during the stimulus presentation and predefined visual areas were small. In fact, the dataset with >2% variance explained (MS, V3a) revealed no overlap between the left hemisphere ROI and activated area. We suspected that this might be due to tiredness causing a lack of central fixation, which can lead to not just a lack of foveal activation, but foveal suppression if fixation moved into the peripheral visual field. Foveal stimuli are restricted by the difference in cone fundamentals between foveal and peripheral vision (Stockman & Sharpe, 2000), so future experiments might consider using larger annulus stimuli. Additionally, decreasing the number of frequencies tested and recruiting more participants for shorter testing periods would also provide a more sensible trade-off between testing time and reliability of results and allow us to compute more robust group statistics.

5.5.5 Conclusion

In conclusion, we found substantial responses to high temporal frequency modulations in group averaged data. Additionally, red-green flicker drove the visual system more robustly than the other chromaticities and responses in V4 were more significant than responses in V1, which indicated amplification of the initial V1 neural responses. On an individual basis, however, only one subject exhibited significant responses to invisible rapid flicker. This might be a 'real' effect but could also

implicate some input from top-down mechanisms. Despite the high inter-subject variability and low variance explained, we believe that rapid, invisible signals can drive the visual cortex. Future endeavours should consider recruiting a larger sample size and more focused temporal frequency range to conduct statistical testing.

We also found that all three chromaticities activated V3a most strongly, which meant that we could not conclude V3a processing rapid S-cone driven signals through an alternate pathway. Significant rapid S-cone responses found by previous experiments in MT may originate from a direct input to that area rather than being found throughout the motion processing pathway. Lastly, we observed that visual areas exhibited different chromatic sensitivity depending on the frequency of the stimulus (2 or 8Hz): the chromatic preference in V4 was clear with 2Hz flicker but absent at 8Hz.

6 Chapter 6: General discussion

6.1 Summary of key findings

The general objective of this thesis was to understand the relationship between cortical rhythms and visual perception. Currently, the research on endogenous activity remains conflicted on several fundamental issues, including their production and their functions. The study of rhythmic cortical activity extends across multiple disciplines, and so to address these questions, our work approached the topic from several directions. Specifically, we investigated the mechanisms of endogenous rhythmogenesis and involvement of endogenous activity with visual perception and stimulus-driven responses. Our key research questions included changes to visual cortex gamma activity after modulating synaptic and extrasynaptic GABA concentration, predicting psychophysical performance using prestimulus alpha activity and looking for signatures of interaction between chromatic SSR and endogenous rhythms in general. Finally, we examined the neural correlates of periodic, high frequency responses using fMRI, examining the filtering stages of very fast visual input.

We demonstrated in the first experimental chapter that gamma oscillations in slice preparations of rodent visual cortex were not affected by increasing GABA concentration either extrasynaptically (through application of GABA solution) or synaptically (using GABA reuptake inhibitor tiagabine). The data also revealed substantial fluctuations in both frequency and amplitude of gamma rhythms after administering tiagabine and that ‘gamma-band’ endogenous activity was consistently centred at two distinct frequencies. The findings implicated three things. Firstly, voxel-based GABA concentration cannot be accurate estimations of GABAergic drives: GABA production, storage and usage are deeply interlinked and can only be quantified accurately by considering postsynaptic GABA receptor kinetics. Secondly, the properties of gamma oscillations are extremely time-sensitive (at least in slice preparations), which makes it important to standardise or indicate *when* recordings

were taken across different studies. Lastly, gamma activity can include subtypes of distinct frequency bands which arise from different networks and have different reactivity to chemical agents. These subtleties are often disregarded in human electrophysiology and neuroimaging studies, which inevitably contribute to inconsistencies in the literature regarding the GABA-gamma relationship.

The second experimental chapter looked at predicting psychophysical performance using alpha activity. As previous studies often modulated alpha activity using attentional cues, this chapter focused on spontaneous alpha, which was more stochastic in nature. We found that spontaneous alpha power predicted reaction time but *not accuracy* during an orientation discrimination task. Surprisingly, trial success ('hits' and 'misses') could only be predicted by the pattern of alpha activity *after* stimulus presentation, and the relationship between alpha power and task accuracy changed as a function of the subject's orientation discrimination threshold. Overall, the results suggested that spontaneous alpha is a more accurate marker of vigilance than of feature sensitivity. Alpha activity might also indicate emotional state as the timing of high classification accuracy corresponded to when subjects received feedback. Finally, prior experience might engage different cortical networks that oscillate at the same frequency band. This highlights the importance of controlling for the subject's task experience in future psychophysics experiments.

The third chapter explored endogenous oscillations and their interactions with stimulus driven responses. The stimuli in question were chosen from the three axes of the Macleod-Boynton colour space (MacLeod & Boynton, 1979): luminance achromatic and isoluminant chromatic blue-yellow and red-green. The data exhibited several SSVEP signatures, such as strong responses at fundamental frequencies and stronger second harmonic components in luminance than chromatic responses (McKeefry et al., 1996). Robust responses were often evident at high order harmonics of the inputs, suggesting the presence of nonlinearities in the visual system.

We also found an effect of stimulus colour on the four broadband EEG power tested: theta, alpha, beta, gamma, with alpha being the strongest. However, the power spectrum did not reveal clear intermodulation terms that would be the signatures of

nonlinear interactions between S-cone isolating signals and sub-alpha range (<10Hz) activity. Considering the possibility that the interaction was too weak to be seen in the power spectrum, we extended the data to include phase information and trained a classifier to predict stimulus colour based on the pattern of activity across the scalp. We found clusters of high classification accuracies and post hoc tests revealed that differences in electrical activity mostly emerge from comparisons between either chromatic conditions with the achromatic condition. Overall, the results did not support any distinct relationship between koniocellular and endogenous sub-alpha range activity (Cheong et al., 2011). However, complex data revealed unique patterns of activity at non-harmonic frequencies above CFFF, which indicated that (1) phase information can offer more insight about signal interactions than amplitude data alone and (2) phase coupling occurs and differs specifically between endogenous rhythms and pathways processing either chromatic or achromatic.

The high frequencies of significant classification accuracies demonstrated that the brain can sustain rapid phase-locked signals in response to external stimulation. Together with previous psychophysical and neuroimaging evidences (Jiang et al., 2007; Shady et al., 2004), we extended this finding in the fourth chapter. We presented rapid flicker to the observers directly and examined BOLD activation in three visual areas that we expected to have very different chromatic response profiles (V1, V3a and V4). Chromatic and achromatic flicker was selected from the Macleod-Boynton colour space and modulated across five temporal frequencies using a 5-primary LED system with no framerate restrictions. Even without conscious perception, many flicker beyond CFFF drove V1, V3a and V4 robustly, with red-green responses being the most powerful in both ‘visible’ and ‘invisible’ frequency ranges. There was no indication of bias towards rapid S-cone signals however, suggesting that potential MT responses to fast S-cone inputs might occur through a more direct pathway (D’Souza et al., 2011; Morand et al., 2000). Finally, the ratio of chromatic to achromatic contrast sensitivity was clearly dependent on temporal frequency: V4 responses were only greater for chromatic than achromatic inputs at 2Hz. This finding supports the idea that chromatic and achromatic inputs stimuli may be multiplexed in some areas commonly thought to be highly specialised for colour

and that it may be more appropriate to talk about neuronal chromatic sensitivity in the context of temporal (and perhaps also spatial) frequency.

6.2 Future directions

This thesis addressed a wide range of research questions pertaining to endogenous rhythms. Using a wide variety of measurement techniques and analysis methods, the results highlight the complexity of neural oscillations at multiple levels. Measurements of endogenous rhythms are often modulated by external stimulation, and they do not necessarily share simple linear relationships with neurochemical agents used to regulate them. Furthermore, the function and mechanisms inferred from endogenous activity are not determined solely by their frequency. Incorporating these details will inevitably improve the consistency and accuracy of future studies.

To avoid misinterpreting measurements of endogenous oscillations, future projects should use more precise methods when measuring or manipulating endogenous drive. This might involve finding more suitable markers for neuronal activity. For example, GABAergic inhibition is almost entirely driven by postsynaptic receptor kinetics, which can be more accurately inferred from postsynaptic $GABA_A$ receptor density than voxel-based concentration. Manipulating GABAergic process is more efficient through appropriate pharmaceutical agents like GABA agonists as they directly affect postsynaptic kinetics. As biological systems have homeostatic defence mechanisms that resist changes in membrane potentials, it is impossible to monitor endogenous rhythms perfectly. Nonetheless, these methods would produce more realistic estimates of endogenous activity than some of the current techniques.

The data also illustrated some unexpected sensitivities of endogenous activity to attention and task expertise. We reported high inter-subject variability in two datasets (Chapter 3 and Chapter 5), which we suspect were influenced by the subject's prior experience with the task and their engagement during the experiment. Specifically, subjects who were highly familiar with visual psychophysics showed evidence of correlation between stronger alpha activity and more accurate visual discrimination (Chapter 3), as well as more robust BOLD responses to high rates of chromatic

flicker (Chapter 5). Neural responses can be amplified through top-down attentional modulations (Pessoa et al., 2003) which meant that the more robust responses might be caused by simply being more attentive during the task. This is a question to be addressed with more formal assessments of prior experiences, attention and interest. Nevertheless, the current work demonstrated a need for controlling for these factors.

The result also challenges the idea that the *function* of endogenous activity is clearly defined by its *frequency*. We showed that gamma band oscillations can be slowed down to beta frequency by increasing inhibition (Fisahn et al., 1998; Whittington et al., 1996), but there is no clear consensus on whether this signal would be considered 'gamma' by its origin, or 'beta' by its oscillatory rate. Similarly, a decrease in alpha power can signify increased attention (Klimesch, 2012) or decreased inhibition of task-irrelevant areas (Pfurtscheller & Lopes da Silva, 1999), thus having opposite consequences on the subject's performance. In fact, multiple networks can oscillate within the same frequency band. High and low gamma for example, have different behavioural correlates and postsynaptic potentials despite being in within the gamma range (>25Hz).

Moreover, endogenous oscillations might not be related to cognitive processes at all. Gamma band activity is commonly acknowledged as being a temporal guideline to many cognitive functions. But there is also compelling evidence to suggest the time courses of gamma oscillations are more tightly linked with micro-saccades in the eyes instead of neural oscillatory activity (Bosman et al., 2009; Yuval-Greenberg et al., 2008; Yuval-Greenberg & Deouell, 2009, 2011). Frequency and amplitude of endogenous activity are also extremely time-sensitive: as shown in Chapter 3, the timeframe for this fluctuation can be as short as three minutes. Reporting and standardising time intervals between sampling (and, potentially, measuring eye movements) would be helpful in future human experiments.

6.3 Final conclusions

This thesis addressed several key issues regarding endogenous oscillations and high frequency responses in the visual system. Our main findings are summarised as:

1. Involvement of GABA in the production of gamma oscillations is not dependent on concentration alone (synaptically or extrasynaptically). We cannot meaningfully infer GABAergic inhibitory drive from the total GABA concentration measured within a voxel.
2. Spontaneous alpha power prior to visual stimulation is a good indicator of how *fast* the subject would respond, but not how *accurately*. This suggests that spontaneous alpha activity, unlike attention-modulated alpha, might be more associated with vigilance than orientation sensitivity.
3. Alpha activity might be related to task expertise, indicating activation of default mode network in experts and disengagement with the task in novices.
4. Interaction between endogenous activity and stimulus-driven responses was observed in averaged broadband EEG power and complex data.
5. Very rapid modulations can drive the visual cortex powerfully. Responses to flicker above CFFF were smaller as compared to slower, high contrast flicker, but still robust, indicating that high temporal frequencies are partially filtered before V4 but terminate in even higher-order areas. Response towards stimulus chromaticity is dependent on temporal frequency within the visible range.

These findings provided a clearer depiction of how endogenous rhythms work with regards to visual processing and how they interact with visual inputs. Existing conflicts in the literature were revisited using multiple techniques and analyses. We found that while there is a pivotal association between endogenous activity and visual perception, the strength and characteristic of this association are highly dependent on physiological and behavioural factors. The current work also extended research on the temporal filtering stages within the visual cortex using a novel multi-primary LED display system and found evidence of invisible rapid signals as high as V4. This implicated that neuronal processes up to extrastriate areas can be modulated unconsciously by flicker beyond CFFF.

Abbreviations

4AFC	Four-alternate forced choice
ACSF	Artificial cerebrospinal fluid
ANOVA	Analysis of variance
ASPA	Animals Scientific Procedures Act
BOLD	Blood oxygen level-dependent
CFF	Critical flicker fusion
CFFF	Critical flicker fusion frequency
DC	Direct current
DKL space	Derrington, Krauskopf and Lennie colour space
EEG	Electroencephalography
EPSP	Excitatory postsynaptic potential
fMRI	Functional magnetic resonance imaging
FFT	Fast Fourier transform
FOV	Field of view
GABA	Gamma aminobutyric acid
GAT-1	Gamma aminobutyric acid transporter 1
GLM	Generalised linear model
hV4	Fourth visual area in humans
ICA	Independent component analysis
IPSC	Inhibitory postsynaptic current
IPSP	Inhibitory postsynaptic potential
ISI	Interstimulus interval
KC	Koniocellular
L or L-cone	Cones with peak sensitivity *long* wavelengths (~564nm)
LED	Light-emitting diode
LFP	Local field potentials
LGN	Lateral geniculate nucleus
LRT	Likelihood ratio test
M or M-cone	Cones with peak sensitivity *medium* wavelengths (~534nm)
MC	Magnocellular

MEG	Magnetoencephalography
mM	Millimolar
MRI	Magnetic resonance imaging
MRS	Magnetic resonance spectroscopy
MT/V5	Middle temporal area in primates or V5
NMDA	N-methyl-D-aspartate receptor
PC	Parvocellular
PD	Proton density
PING	Pyramidal-interneuron network gamma
rTMS	Repetitive transcranial magnetic stimulation
RGC	Retinal ganglion cell
RMS	Root mean square
ROI	Region of interest
S or S-cone	Cones with peak sensitivity *short* wavelengths (~420nm)
SEM	Standard error of the mean
SNR	Signal to noise ratio
SPM	Statistical parametric mapping
SSVEP	Steady-state visually evoked potential
SVM	Support vector machine
TE	Echo time
TR	Repetition time
V1	Primary visual cortex
V2	Second visual area
V3	Third visual complex
VP	Ventral posterior area or ventral V3
V3a	Visual area V3a
V4	Fourth visual area
VO	Ventral occipital lobe, anterior to hV4
VEP	Visually evoked potential

References

Aberg, K. C., & Herzog, M. H. (2012). Different types of feedback change decision criterion and sensitivity differently in perceptual learning. *Journal of Vision*, *12*(3). https://doi.org/10.1167/12.3.3

Ade, K. K., Janssen, M. J., Ortinski, P. I., & Vicini, S. (2008). Differential Tonic GABA Conductances in Striatal Medium Spiny Neurons. *The Journal of Neuroscience*, *28*(5), 1185–1197. https://doi.org/10.1523/JNEUROSCI.3908-07.2008

Adrian, E. D., & Matthews, B. H. C. (1934). The Berger rhythm: potential changes from the occipital lobes in man. *Brain*, *57*(4), 355–385. https://doi.org/10.1093/brain/57.4.355

Alonso-Prieto, E., Belle, G. V., Liu-Shuang, J., Norcia, A. M., & Rossion, B. (2013). The 6 Hz fundamental stimulation frequency rate for individual face discrimination in the right occipito-temporal cortex. *Neuropsychologia*, *51*(13), 2863–2875. https://doi.org/10.1016/j.neuropsychologia.2013.08.018

Bartels, A., & Zeki, S. (2000). The architecture of the colour centre in the human visual brain: New results and a review. *The European Journal of Neuroscience*, *12*(1), 172–193. https://doi.org/10.1046/j.1460-9568.2000.00905.

Barberini, C. L., Cohen, M. R., Wandell, B. A. & Newsome, W.T. (2005). Cone signal interactions in direction-selective neurons in the middle temporal visual area (MT). *Journal of Vision*, 5(7): 603-21. https://doi.org/ 10.1167/5.7.1

Bartos, M., Vida, I., & Jonas, P. (2007). Synaptic mechanisms of synchronized gamma oscillations in inhibitory interneuron networks. *Nature Reviews. Neuroscience*, *8*(1), 45–56. https://doi.org/10.1038/nrn2044

Baseler, H. A., & Sutter, E. E. (1997). M and P Components of the VEP and their Visual Field Distribution. *Vision Research*, *37*(6), 675–690. https://doi.org/10.1016/S0042-6989(96)00209-X

Bates, D., Mächler, M., Bolker, B., & Walker, S. (2015). Fitting Linear Mixed-Effects Models Using lme4. *Journal of Statistical Software*, *67*(1), 1–48. https://doi.org/10.18637/jss.v067.i01

Bauer, F., Cheadle, S. W., Parton, A., Müller, H. J., & Usher, M. (2009). Gamma flicker triggers attentional selection without awareness. *Proceedings of the National Academy of Sciences*, *106*(5), 1666–1671. https://doi.org/10.1073/pnas.0810496106

Beckmann, C. F., DeLuca, M., Devlin, J. T., & Smith, S. M. (2005). Investigations into resting-state connectivity using independent component analysis. *Philosophical Transactions of the Royal Society of London. Series B, Biological Sciences*, *360*(1457), 1001–1013. https://doi.org/10.1098/rstb.2005.1634

Begleiter, H., Porjesz, B., Chou, C. L., & Aunon, J. I. (1983). P3 and stimulus incentive value. *Psychophysiology*, *20*(1), 95–101. https://doi.org/10.1111/j.1469-8986.1983.tb00909.x

Belelli, D., Harrison, N. L., Maguire, J., Macdonald, R. L., Walker, M. C., & Cope, D. W. (2009). Extrasynaptic GABAA receptors: Form, pharmacology, and function. *The Journal of Neuroscience: The Official Journal of the Society for Neuroscience*, *29*(41), 12757–12763. https://doi.org/10.1523/JNEUROSCI.3340-09.2009

Bell, A. J., & Sejnowski, T. J. (1995). An information-maximization approach to blind separation and blind deconvolution. *Neural Computation*, *7*(6), 1129–1159. https://doi.org/10.1162/neco.1995.7.6.1129

Belluscio, M. A., Mizuseki, K., Schmidt, R., Kempter, R., & Buzsáki, G. (2012). Cross-frequency phase-phase coupling between θ and γ oscillations in the hippocampus. *The Journal of Neuroscience: The Official Journal of the Society for Neuroscience*, *32*(2), 423–435. https://doi.org/10.1523/JNEUROSCI.4122-11.2012

Benjamini, Y., & Hochberg, Y. (1995). Controlling the False Discovery Rate: A Practical and Powerful Approach to Multiple Testing. *Journal of the Royal Statistical Society: Series B (Methodological)*, *57*(1), 289–300. https://doi.org/10.1111/j.2517-6161.1995.tb02031.x

Berens, P., Keliris, G. A., Ecker, A. S., Logothetis, N. K., Tolias, A. S., Berens, P., Keliris, G. A., Ecker, A. S., Logothetis, N. K., & Tolias, A. S. (2008). Comparing the feature selectivity of the gamma-band of the local field potential and the underlying spiking activity in primate visual cortex. *Frontiers in Systems Neuroscience*, *2*, 2. https://doi.org/10.3389/neuro.06.002.2008

Block, N. (1996). How can we find the neural correlate of consciousness? *Trends in Neurosciences*, *19*(11), 456–459. https://doi.org/10.1016/s0166-2236(96)20049-9

Bollimunta, A., Mo, J., Schroeder, C. E., & Ding, M. (2011). Neuronal Mechanisms and Attentional Modulation of Corticothalamic Alpha Oscillations. *Journal of Neuroscience*, *31*(13), 4935–4943. https://doi.org/10.1523/JNEUROSCI.5580-10.2011

Boncompte, G., Villena-González, M., Cosmelli, D., & López, V. (2016). Spontaneous Alpha Power Lateralization Predicts Detection Performance in an Un-Cued Signal Detection Task. *PLOS ONE*, *11*(8), e0160347. https://doi.org/10.1371/journal.pone.0160347

Bosman, C. A., Womelsdorf, T., Desimone, R., & Fries, P. (2009). A Microsaccadic Rhythm Modulates Gamma-Band Synchronization and Behavior. *Journal of Neuroscience*, *29*(30), 9471–9480. https://doi.org/10.1523/JNEUROSCI.1193-09.2009

Bragin, A., Jandó, G., Nádasdy, Z., Hetke, J., Wise, K., & Buzsáki, G. (1995). Gamma (40-100 Hz) oscillation in the hippocampus of the behaving rat. *The Journal of Neuroscience: The Official Journal of the Society for Neuroscience*, *15*(1 Pt 1), 47–60.

Brainard, D. H. (1997). The Psychophysics Toolbox. *Spatial Vision*, *10*(4), 433–436.

Brewer, A. A., Liu, J., Wade, A. R., & Wandell, B. A. (2005). Visual field maps and stimulus selectivity in human ventral occipital cortex. *Nature Neuroscience*, *8*(8), 1102–1109. https://doi.org/10.1038/nn1507

Brickley, S. G., Revilla, V., Cull-Candy, S. G., Wisden, W., & Farrant, M. (2001). Adaptive regulation of neuronal excitability by a voltage-independent potassium conductance. *Nature*, *409*(6816), 88–92. https://doi.org/10.1038/35051086

Brickley, Stephen G., & Mody, I. (2012). Extrasynaptic GABA(A) receptors: Their function in the CNS and implications for disease. *Neuron*, *73*(1), 23–34. https://doi.org/10.1016/j.neuron.2011.12.012

Brunel, N., & Wang, X.-J. (2003). What Determines the Frequency of Fast Network Oscillations With Irregular Neural Discharges? I. Synaptic Dynamics and Excitation-Inhibition Balance. *Journal of Neurophysiology*, *90*(1), 415–430. https://doi.org/10.1152/jn.01095.2002

Busch, N. A., Debener, S., Kranczioch, C., Engel, A. K., & Herrmann, C. S. (2004). Size matters: Effects of stimulus size, duration and eccentricity on the visual gamma-band response. *Clinical Neurophysiology*, *115*(8), 1810–1820. https://doi.org/10.1016/j.clinph.2004.03.015

Busch, N. A., Dubois, J., & VanRullen, R. (2009). The Phase of Ongoing EEG Oscillations Predicts Visual Perception. *Journal of Neuroscience*, *29*(24), 7869–7876. https://doi.org/10.1523/JNEUROSCI.0113-09.2009

Buzsáki, G., & Draguhn, A. (2004). Neuronal oscillations in cortical networks. *Science (New York, N.Y.)*, *304*(5679), 1926–1929. https://doi.org/10.1126/science.1099745

Buzsáki, G., & Wang, X.-J. (2012). Mechanisms of Gamma Oscillations. *Annual Review of Neuroscience*, *35*(1), 203–225. https://doi.org/10.1146/annurev-neuro-062111-150444

Cajochen, C., Foy, R., & Dijk, D. J. (1999). Frontal predominance of a relative increase in sleep delta and theta EEG activity after sleep loss in humans. *Sleep Research Online: SRO*, *2*(3), 65–69.

Campbell, A. E., Sumner, P., Singh, K. D., & Muthukumaraswamy, S. D. (2014). Acute effects of alcohol on stimulus-induced gamma oscillations in human primary visual and motor cortices. *Neuropsychopharmacology: Official Publication of the American College of Neuropsychopharmacology*, *39*(9), 2104–2113. https://doi.org/10.1038/npp.2014.58

Caraiscos, V. B., Elliott, E. M., You-Ten, K. E., Cheng, V. Y., Belelli, D., Newell, J. G., Jackson, M. F., Lambert, J. J., Rosahl, T. W., Wafford, K. A., MacDonald, J. F., & Orser, B. A. (2004). Tonic inhibition in mouse hippocampal CA1 pyramidal neurons is mediated by alpha5 subunit-containing gamma-aminobutyric acid type A receptors. *Proceedings of the National Academy of Sciences of the United States of America*, *101*(10), 3662–3667. https://doi.org/10.1073/pnas.0307231101

Cardin, J. A., Carlén, M., Meletis, K., Knoblich, U., Zhang, F., Deisseroth, K., Tsai, L.-H., & Moore, C. I. (2009). Driving fast-spiking cells induces gamma rhythm and controls sensory responses. *Nature*, *459*(7247), 663–667. https://doi.org/10.1038/nature08002

Casagrande, V. A. (1994). A third parallel visual pathway to primate area V1. *Trends in Neurosciences*, *17*(7), 305–310.

Cash, D. J., & Subbarao, K. (1987). Desensitization of gamma-aminobutyric acid receptor from rat brain: Two distinguishable receptors on the same membrane. *Biochemistry*, *26*(24), 7556–7562. https://doi.org/10.1021/bi00398a004

Cavanagh, P., & Anstis, S. (1991). The contribution of color to motion in normal and color-deficient observers. *Vision Research*, *31*(12), 2109–2148. https://doi.org/10.1016/0042-6989(91)90169-6

Chang, C.-C., & Lin, C.-J. (2011). LIBSVM: A library for support vector machines. *ACM Transactions on Intelligent Systems and Technology*, *2*(3), 1–27. https://doi.org/10.1145/1961189.1961199

Chao, L. L., & Martin, A. (1999). Cortical regions associated with perceiving, naming, and knowing about colors. *Journal of Cognitive Neuroscience*, *11*(1), 25–35. https://doi.org/10.1162/089892999563229

Chatterjee, S., & Callaway, E. M. (2002). S cone contributions to the magnocellular visual pathway in macaque monkey. *Neuron*, *35*(6), 1135–1146. https://doi.org/10.1016/s0896-6273(02)00874-7

Chauvette, S., Crochet, S., Volgushev, M., & Timofeev, I. (2011). Properties of Slow Oscillation during Slow-Wave Sleep and Anesthesia in Cats. *The Journal of Neuroscience*, *31*(42), 14998–15008. https://doi.org/10.1523/JNEUROSCI.2339-11.2011

Chen, C.-M. A., Stanford, A. D., Mao, X., Abi-Dargham, A., Shungu, D. C., Lisanby, S. H., Schroeder, C. E., & Kegeles, L. S. (2014). GABA level, gamma oscillation, and working memory performance in schizophrenia. *NeuroImage : Clinical*, *4*, 531–539. https://doi.org/10.1016/j.nicl.2014.03.007

Chen, G., Zhang, Y., Li, X., Zhao, X., Ye, Q., Lin, Y., Tao, H. W., Rasch, M. J., & Zhang, X. (2017). Distinct Inhibitory Circuits Orchestrate Cortical beta and gamma Band Oscillations. *Neuron*, *96*(6), 1403-1418.e6. https://doi.org/10.1016/j.neuron.2017.11.033

Cheong, S. K., Tailby, C., Martin, P. R., Levitt, J. B., & Solomon, S. G. (2011). Slow intrinsic rhythm in the koniocellular visual pathway. *Proceedings of the National Academy of Sciences of the United States of America*, *108*(35), 14659–14663. https://doi.org/10.1073/pnas.1108004108

Chichilnisky, E. J., & Kalmar, R. S. (2002). Functional asymmetries in ON and OFF ganglion cells of primate retina. *The Journal of Neuroscience: The Official Journal of the Society for Neuroscience*, *22*(7), 2737–2747. https://doi.org/20026215

Christoph, H. (2011). Feature-binding and attention are reflected in human EEG gamma-band oscillations. *Frontiers in Human Neuroscience*, *5*. https://doi.org/10.3389/conf.fnhum.2011.207.00014

Colgin, L. L., Denninger, T., Fyhn, M., Hafting, T., Bonnevie, T., Jensen, O., Moser, M.-B., & Moser, E. I. (2009). Frequency of gamma oscillations routes flow of information in the hippocampus. *Nature*, *462*(7271), 353–357. https://doi.org/10.1038/nature08573

Colgin, L. L., & Moser, E. I. (2010). Gamma oscillations in the hippocampus. *Physiology (Bethesda, Md.)*, *25*(5), 319–329. https://doi.org/10.1152/physiol.00021.2010

Conway, B. R. (2014). Color signals through dorsal and ventral visual pathways. *Visual Neuroscience*, *31*(2), 197–209. https://doi.org/10.1017/S0952523813000382

Cosmelli, D., López, V., Lachaux, J.-P., López-Calderón, J., Renault, B., Martinerie, J., & Aboitiz, F. (2011). Shifting visual attention away from fixation is specifically associated with alpha band activity over ipsilateral parietal regions. *Psychophysiology*, *48*(3), 312–322. https://doi.org/10.1111/j.1469-8986.2010.01066.x

Coulon, P., Budde, T., & Pape, H.-C. (2012). The sleep relay—The role of the thalamus in central and decentral sleep regulation. *Pflügers Archiv - European Journal of Physiology*, *463*(1), 53–71. https://doi.org/10.1007/s00424-011-1014-6

Cousijn, H., Haegens, S., Wallis, G., Near, J., Stokes, M. G., Harrison, P. J., & Nobre, A. C. (2014). Resting GABA and glutamate concentrations do not predict visual gamma frequency or amplitude. *Proceedings of the National Academy of Sciences*, *111*(25), 9301–9306. https://doi.org/10.1073/pnas.1321072111

Croner, L. J., Purpura, K., & Kaplan, E. (1993). Response variability in retinal ganglion cells of primates. *Proceedings of the National Academy of Sciences*, *90*(17), 8128–8130. https://doi.org/10.1073/pnas.90.17.8128

Dacey, D. M. (2000). Parallel Pathways for Spectral Coding in Primate Retina. *Annual Review of Neuroscience*, *23*(1), 743–775. https://doi.org/10.1146/annurev.neuro.23.1.743

Dacey, D. M., & Lee, B. B. (1994). The ‘blue-on’ opponent pathway in primate retina originates from a distinct bistratified ganglion cell type. *Nature*, *367*(6465), 731–735. https://doi.org/10.1038/367731a0

Davis, M., & Whalen, P. J. (2001). The amygdala: Vigilance and emotion. *Molecular Psychiatry*, *6*(1), 13–34. https://doi.org/10.1038/sj.mp.4000812

De Valois, R. L., Cottaris, N. P., Mahon, L. E., Elfar, S. D., & Wilson, J. A. (2000). Spatial and temporal receptive fields of geniculate and cortical cells and directional selectivity. *Vision Research*, *40*(27), 3685–3702. https://doi.org/10.1016/S0042-6989(00)00210-8

Derrington, A. M., Krauskopf, J., & Lennie, P. (1984). Chromatic mechanisms in lateral geniculate nucleus of macaque. *The Journal of Physiology*, *357*, 241–265.

Derrington, A. M., & Lennie, P. (1984). Spatial and temporal contrast sensitivities of neurones in lateral geniculate nucleus of macaque. *The Journal of Physiology*, *357*, 219–240. https://doi.org/10.1113/jphysiol.1984.sp015498

Dingledine, R., & Korn, S. J. (1985). Gamma-aminobutyric acid uptake and the termination of inhibitory synaptic potentials in the rat hippocampal slice. *The Journal of Physiology*, *366*, 387–409. https://doi.org/10.1113/jphysiol.1985.sp015804

Dobkins, K. R., & Albright, T. D. (1994). What happens if it changes color when it moves? The nature of chromatic input to macaque visual area MT. *The Journal of Neuroscience*, *14*(8), 4854–4870.

Dougherty, R. F., Press, W. A., & Wandell, B. A. (1999). Perceived speed of colored stimuli. *Neuron*, *24*(4), 893–899. https://doi.org/10.1016/s0896-6273(00)81036-3

D’Souza, D. V., Auer, T., Strasburger, H., Frahm, J., & Lee, B. B. (2011). Temporal frequency and chromatic processing in humans: An fMRI study of the cortical visual areas. *Journal of Vision*, *11*(8), 8–8. https://doi.org/10.1167/11.8.8

D'Souza, Dany V., Auer, T., Strasburger, H., Frahm, J., & Lee, B. B. (2011). Temporal frequency and chromatic processing in humans: An fMRI study of the cortical visual areas. *Journal of Vision*, *11*(8), 8–8. https://doi.org/10.1167/11.8.8

Duncan, N. W., Zhang, J., Northoff, G., & Weng, X. (2019). Investigating GABA concentrations measured with macromolecule suppressed and unsuppressed MEGA-PRESS MR spectroscopy and their relationship with BOLD responses in the occipital cortex. *Journal of Magnetic Resonance Imaging*, *50*(4), 1285–1294. https://doi.org/10.1002/jmri.26706

Edden, R. A. E., Muthukumaraswamy, S. D., Freeman, T. C. A., & Singh, K. D. (2009). Orientation discrimination performance is predicted by GABA concentration and gamma oscillation frequency in human primary visual cortex. *The Journal of Neuroscience: The Official Journal of the Society for Neuroscience*, *29*(50), 15721–15726. https://doi.org/10.1523/JNEUROSCI.4426-09.2009

Engel, A. K., Fries, P., & Singer, W. (2001). Dynamic predictions: Oscillations and synchrony in top-down processing. *Nature Reviews Neuroscience*, *2*(10), 704–716. https://doi.org/10.1038/35094565

Engel, S., Zhang, X., & Wandell, B. (1997). Colour tuning in human visual cortex measured with functional magnetic resonance imaging. *Nature*, *388*(6637), 68–71. https://doi.org/10.1038/40398

Ergenoglu, T., Demiralp, T., Bayraktaroglu, Z., Ergen, M., Beydagi, H., & Uresin, Y. (2004). Alpha rhythm of the EEG modulates visual detection performance in humans. *Cognitive Brain Research*, *20*(3), 376–383. https://doi.org/10.1016/j.cogbrainres.2004.03.009

Eskew, R. T., Stromeyer, C. F., & Kronauer, R. E. (1994). Temporal properties of the red-green chromatic mechanism. *Vision Research*, *34*(23), 3127–3137. https://doi.org/10.1016/0042-6989(94)90078-7

Estévez, O., & Spekreijse, H. (1982). The 'silent substitution' method in visual research. *Vision Research*, *22*(6), 681–691.

Farrant, M., & Nusser, Z. (2005). Variations on an inhibitory theme: Phasic and tonic activation of GABA(A) receptors. *Nature Reviews. Neuroscience*, *6*(3), 215–229. https://doi.org/10.1038/nrn1625

Farrell, J. E., Benson, B. L., Haynie, C. R., Packard, H., & Ca, P. A. (1987). Predicting Flicker Thresholds for Video Display Terminals. *Proc. SID*.

Faulkner, H. J., Traub, R. D., & Whittington, M. A. (1998). Disruption of synchronous gamma oscillations in the rat hippocampal slice: A common mechanism of anaesthetic drug action. *British Journal of Pharmacology*, *125*(3), 483–492. https://doi.org/10.1038/sj.bjp.0702113

Feig, S., & Harting, J. K. (1994). Ultrastructural studies of the primate lateral geniculate nucleus: Morphology and spatial relationships of axon terminals arising from the retina, visual cortex (area 17), superior colliculus, parabigeminal nucleus, and pretectum of Galago crassicaudatus. *The Journal of Comparative Neurology*, *343*(1), 17–34. https://doi.org/10.1002/cne.903430103

Feld, G. B., Wilhelm, I., Ma, Y., Groch, S., Binkofski, F., Mölle, M., & Born, J. (2013). Slow Wave Sleep Induced by GABA Agonist Tiagabine Fails to Benefit Memory Consolidation. *Sleep*, *36*(9), 1317–1326. https://doi.org/10.5665/sleep.2954

Fisahn, A., Pike, F. G., Buhl, E. H., & Paulsen, O. (1998). Cholinergic induction of network oscillations at 40 Hz in the hippocampus in vitro. *Nature*, *394*(6689), 186–189. https://doi.org/10.1038/28179

Fisahn, André. (2005). Kainate receptors and rhythmic activity in neuronal networks: Hippocampal gamma oscillations as a tool. *The Journal of Physiology*, *562*(Pt 1), 65–72. https://doi.org/10.1113/jphysiol.2004.077388

Foxe, J. J., & Snyder, A. C. (2011). The Role of Alpha-Band Brain Oscillations as a Sensory Suppression Mechanism during Selective Attention. *Frontiers in Psychology*, *2*. https://doi.org/10.3389/fpsyg.2011.00154

Fries, P., Reynolds, J. H., Rorie, A. E., & Desimone, R. (2001). Modulation of oscillatory neuronal synchronization by selective visual attention. *Science (New York, N.Y.)*, *291*(5508), 1560–1563. https://doi.org/10.1126/science.1055465

Fries, Pascal. (2009). Neuronal Gamma-Band Synchronization as a Fundamental Process in Cortical Computation. *Annual Review of Neuroscience*, *32*(1), 209–224. https://doi.org/10.1146/annurev.neuro.051508.135603

Gaetz, W., Edgar, J. C., Wang, D. J., & Roberts, T. P. L. (2011). Relating MEG measured motor cortical oscillations to resting γ-Aminobutyric acid (GABA) concentration. *NeuroImage*, *55*(2), 616–621. https://doi.org/10.1016/j.neuroimage.2010.12.077

Gardner, E. P., & Martin, J. H. (2000). *Coding of sensory information. Principles of Neural Science, 4, 411-429.*

Gieselmann, M. A., & Thiele, A. (2008). Comparison of spatial integration and surround suppression characteristics in spiking activity and the local field potential in macaque V1. *European Journal of Neuroscience*, *28*(3), 447–459. https://doi.org/10.1111/j.1460-9568.2008.06358.x

Gillies, M. J., Traub, R. D., LeBeau, F. E. N., Davies, C. H., Gloveli, T., Buhl, E. H., & Whittington, M. A. (2002). A Model of Atropine-Resistant Theta Oscillations in Rat Hippocampal Area CA1. *The Journal of Physiology*, *543*(3), 779–793. https://doi.org/10.1113/jphysiol.2002.024588

Gloveli, T., Dugladze, T., Rotstein, H. G., Traub, R. D., Monyer, H., Heinemann, U., Whittington, M. A., & Kopell, N. J. (2005). Orthogonal arrangement of rhythm-generating microcircuits in the hippocampus. *Proceedings of the National Academy of Sciences of the United States of America*, *102*(37), 13295–13300. https://doi.org/10.1073/pnas.0506259102

Glykys, J., & Mody, I. (2007). The main source of ambient GABA responsible for tonic inhibition in the mouse hippocampus. *The Journal of Physiology*, *582*(Pt 3), 1163–1178. https://doi.org/10.1113/jphysiol.2007.134460

Gonzalez-Burgos, G., & Lewis, D. A. (2012). NMDA receptor hypofunction, parvalbumin-positive neurons, and cortical gamma oscillations in schizophrenia. *Schizophrenia Bulletin*, *38*(5), 950–957. https://doi.org/10.1093/schbul/sbs010

Goodale, M. A., & Milner, A. D. (1992). Separate visual pathways for perception and action. *Trends in Neurosciences*, *15*(1), 20–25. https://doi.org/10.1016/0166-2236(92)90344-8

Gouwens, N. W., Zeberg, H., Tsumoto, K., Tateno, T., Aihara, K., & Robinson, H. P. C. (2010). Synchronization of Firing in Cortical Fast-Spiking Interneurons at Gamma Frequencies: A Phase-Resetting Analysis. *PLOS Computational Biology*, *6*(9), e1000951. https://doi.org/10.1371/journal.pcbi.1000951

Graaf, T. A. de, Gross, J., Paterson, G., Rusch, T., Sack, A. T., & Thut, G. (2013). Alpha-Band Rhythms in Visual Task Performance: Phase-Locking by Rhythmic Sensory Stimulation. *PLOS ONE*, *8*(3), e60035. https://doi.org/10.1371/journal.pone.0060035

Gray, C. M., König, P., Engel, A. K., & Singer, W. (1989). Oscillatory responses in cat visual cortex exhibit inter-columnar synchronization which reflects global stimulus properties. *Nature*, *338*(6213), 334–337. https://doi.org/10.1038/338334a0

Groppe, D. M., Bickel, S., Keller, C. J., Jain, S. K., Hwang, S. T., Harden, C., & Mehta, A. D. (2013). Dominant frequencies of resting human brain activity as measured by the electrocorticogram. *NeuroImage*, *79*, 223–233. https://doi.org/10.1016/j.neuroimage.2013.04.044

Gur, Moshe, Beylin, A., & Snodderly, D. M. (1997). Response Variability of Neurons in Primary Visual Cortex (V1) of Alert Monkeys. *Journal of Neuroscience*, *17*(8), 2914–2920. https://doi.org/10.1523/JNEUROSCI.17-08-02914.1997

Gur, Moshe, & Snodderly, D. M. (1997). A Dissociation Between Brain Activity and Perception: Chromatically Opponent Cortical Neurons Signal Chromatic Flicker that is not Perceived. *Vision Research*, *37*(4), 377–382. https://doi.org/10.1016/S0042-6989(96)00183-6

Hadjikhani, N., Liu, A. K., Dale, A. M., Cavanagh, P., & Tootell, R. B. (1998). Retinotopy and color sensitivity in human visual cortical area V8. *Nature Neuroscience*, *1*(3), 235–241. https://doi.org/10.1038/681

Hakim, R., Shamardani, K., & Adesnik, H. (2018). A neural circuit for gamma-band coherence across the retinotopic map in mouse visual cortex. *ELife*, *7*, e28569. https://doi.org/10.7554/eLife.28569

Hall, S. D., Stanford, I. M., Yamawaki, N., McAllister, C. J., Rönnqvist, K. C., Woodhall, G. L., & Furlong, P. L. (2011). The role of GABAergic modulation in motor function related neuronal network activity. *NeuroImage*, *56*(3), 1506–1510. https://doi.org/10.1016/j.neuroimage.2011.02.025

Hall, Stephen D., Holliday, I. E., Hillebrand, A., Singh, K. D., Furlong, P. L., Hadjipapas, A., & Barnes, G. R. (2005). The missing link: Analogous human and primate cortical gamma oscillations. *NeuroImage*, *26*(1), 13–17. https://doi.org/10.1016/j.neuroimage.2005.01.009

Hamann, M., Rossi, D. J., & Attwell, D. (2002). Tonic and spillover inhibition of granule cells control information flow through cerebellar cortex. *Neuron*, *33*(4), 625–633. https://doi.org/10.1016/s0896-6273(02)00593-7

Han, C.-H., Kim, Y.-W., Kim, D. Y., Kim, S. H., Nenadic, Z., & Im, C.-H. (2019). Electroencephalography-based endogenous brain–computer interface for online communication with a completely locked-in patient. *Journal of NeuroEngineering and Rehabilitation*, *16*(1), 18. https://doi.org/10.1186/s12984-019-0493-0

Hancock, P. A., & Warm, J. S. (1989). A dynamic model of stress and sustained attention. *Human Factors*, *31*(5), 519–537. https://doi.org/10.1177/001872088903100503

Hansen, T., Olkkonen, M., Walter, S., & Gegenfurtner, K. R. (2006). Memory modulates color appearance. *Nature Neuroscience*, *9*(11), 1367–1368. https://doi.org/10.1038/nn1794

Hanslmayr, S., Aslan, A., Staudigl, T., Klimesch, W., Herrmann, C. S., & Bäuml, K.-H. (2007). Prestimulus oscillations predict visual perception performance between and within subjects. *NeuroImage*, *37*(4), 1465–1473. https://doi.org/10.1016/j.neuroimage.2007.07.011

Harting, J. K., Huerta, M. F., Hashikawa, T., & van Lieshout, D. P. (1991). Projection of the mammalian superior colliculus upon the dorsal lateral geniculate nucleus: Organization of tectogeniculate pathways in nineteen species. *The Journal of Comparative Neurology*, *304*(2), 275–306. https://doi.org/10.1002/cne.903040210

Hartmann, E., Lachenmayr, B., & Brettel, H. (1979). The peripheral critical flicker frequency. *Vision Research*, *19*(9), 1019–1023. https://doi.org/10.1016/0042-6989(79)90227-x

Hecht, S., & Verrijp, C. D. (1933). The Influence of Intensity, Color and Retinal Location on the Fusion Frequency of Intermittent Illumination. *Proceedings of the National Academy of Sciences*, *19*(5), 522–535. https://doi.org/10.1073/pnas.19.5.522

Heinemann, L., Kleinschmidt, A., & Müller, N. G. (2009). Exploring BOLD Changes during Spatial Attention in Non-Stimulated Visual Cortex. *PLOS ONE*, *4*(5), e5560. https://doi.org/10.1371/journal.pone.0005560

Hendry, S. H., & Reid, R. C. (2000). The koniocellular pathway in primate vision. *Annual Review of Neuroscience*, *23*(1), 127–153.

Henrie, J. A., & Shapley, R. (2005). LFP power spectra in V1 cortex: The graded effect of stimulus contrast. *Journal of Neurophysiology*, *94*(1), 479–490. https://doi.org/10.1152/jn.00919.2004

Holcombe, A. O., & Cavanagh, P. (2001). Early binding of feature pairs for visual perception. *Nature Neuroscience*, *4*(2), 127–128. https://doi.org/10.1038/83945

Holt, A. B., Kormann, E., Gulberti, A., Pötter-Nerger, M., McNamara, C. G., Cagnan, H., Baaske, M. K., Little, S., Köppen, J. A., Buhmann, C., Westphal, M., Gerloff, C., Engel, A. K., Brown, P., Hamel, W., Moll, C. K. E., & Sharott, A. (2019). Phase-

Dependent Suppression of Beta Oscillations in Parkinson's Disease Patients. *Journal of Neuroscience*, *39*(6), 1119–1134. https://doi.org/10.1523/JNEUROSCI.1913-18.2018

Hömberg, V., Grünewald, G., & Grünewald-Zuberbier, E. (1981). The variation of p300 amplitude in a money-winning paradigm in children. *Psychophysiology*, *18*(3), 258–262. https://doi.org/10.1111/j.1469-8986.1981.tb03030.x

Honkanen, R., Rouhinen, S., Wang, S. H., Palva, J. M., & Palva, S. (2015). Gamma Oscillations Underlie the Maintenance of Feature-Specific Information and the Contents of Visual Working Memory. *Cerebral Cortex (New York, N.Y.: 1991)*, *25*(10), 3788–3801. https://doi.org/10.1093/cercor/bhu263

Huk, A. C., & Heeger, D. J. (2002). Pattern-motion responses in human visual cortex. *Nature Neuroscience*, *5*(1), 72–75. https://doi.org/10.1038/nn774

Jensen, O., & Mazaheri, A. (2010). Shaping Functional Architecture by Oscillatory Alpha Activity: Gating by Inhibition. *Frontiers in Human Neuroscience*, *4*. https://doi.org/10.3389/fnhum.2010.00186

Jiang, Y., Zhou, K., & He, S. (2007). Human visual cortex responds to invisible chromatic flicker. *Nature Neuroscience*, *10*(5), 657–662. https://doi.org/10.1038/nn1879

Kaiser, P. K., Lee, B. B., Martin, P. R., & Valberg, A. (1990). The physiological basis of the minimally distinct border demonstrated in the ganglion cells of the macaque retina. *The Journal of Physiology*, *422*(1), 153–183. https://doi.org/10.1113/jphysiol.1990.sp017978

Kastner, S., Pinsk, M. A., De Weerd, P., Desimone, R., & Ungerleider, L. G. (1999). Increased Activity in Human Visual Cortex during Directed Attention in the Absence of Visual Stimulation. *Neuron*, *22*(4), 751–761. https://doi.org/10.1016/S0896-6273(00)80734-5

Keeley, S., Fenton, A. A., & Rinzel, J. (2016). Modeling fast and slow gamma oscillations with interneurons of different subtype. *Journal of Neurophysiology*, *117*(3), 950–965. https://doi.org/10.1152/jn.00490.2016

Keitel, C., Quigley, C., & Ruhnau, P. (2014). Stimulus-Driven Brain Oscillations in the Alpha Range: Entrainment of Intrinsic Rhythms or Frequency-Following Response? *The Journal of Neuroscience*, *34*(31), 10137–10140. https://doi.org/10.1523/JNEUROSCI.1904-14.2014

Kelly, D. H. (1983). Spatiotemporal variation of chromatic and achromatic contrast thresholds. *Journal of the Optical Society of America*, *73*(6), 742–750. https://doi.org/10.1364/josa.73.000742

Kelly, S. P., Lalor, E. C., Reilly, R. B., & Foxe, J. J. (2006). Increases in Alpha Oscillatory Power Reflect an Active Retinotopic Mechanism for Distracter Suppression During Sustained Visuospatial Attention. *Journal of Neurophysiology*, *95*(6), 3844–3851. https://doi.org/10.1152/jn.01234.2005

King, J.-R., & Dehaene, S. (2014). Characterizing the dynamics of mental representations: The temporal generalization method. *Trends in Cognitive Sciences*, *18*(4), 203–210. https://doi.org/10.1016/j.tics.2014.01.002

Kleiner, M., Brainard, D., Pelli, D., Ingling, A., Murray, R., & Broussard, C. (2007). What's new in psychtoolbox-3. *Perception*, *36*(14), 1–16.

Klimesch, W. (2012). Alpha-band oscillations, attention, and controlled access to stored information. *Trends in Cognitive Sciences*, *16*(12), 606–617. https://doi.org/10.1016/j.tics.2012.10.007

Klimesch, W., Sauseng, P., & Hanslmayr, S. (2007). EEG alpha oscillations: The inhibition-timing hypothesis. *Brain Research Reviews*, *53*(1), 63–88. https://doi.org/10.1016/j.brainresrev.2006.06.003

Kohus, Z., Káli, S., Rovira-Esteban, L., Schlingloff, D., Papp, O., Freund, T. F., Hájos, N., & Gulyás, A. I. (2016). Properties and dynamics of inhibitory synaptic communication within the CA3 microcircuits of pyramidal cells and interneurons

expressing parvalbumin or cholecystokinin. *The Journal of Physiology*, *594*(13), 3745–3774. https://doi.org/10.1113/JP272231

Koike, T., & Saiki, J. (2006). Stochastic saliency-based search model for search asymmetry with uncertain targets. *Neurocomputing*, *69*(16), 2112–2126. https://doi.org/10.1016/j.neucom.2005.09.009

Kourtzi, Z., & Kanwisher, N. (2000). Activation in human MT/MST by static images with implied motion. *Journal of Cognitive Neuroscience*, *12*(1), 48–55. https://doi.org/10.1162/08989290051137594

Kremers, J., Lee, B. B., Pokorny, J., & Smith, V. C. (1993). Responses of macaque ganglion cells and human observers to compound periodic waveforms. *Vision Research*, *33*(14), 1997–2011. https://doi.org/10.1016/0042-6989(93)90023-p

Kuai, S., Zhang, J.-Y., Klein, S., Levi, D., & Yu, C. (2005). The essential role of stimulus temporal patterning in enabling perceptual learning. *Nature Neuroscience*, *8*, 1497–1499. https://doi.org/10.1038/nn1546

Kujala, J., Jung, J., Bouvard, S., Lecaignard, F., Lothe, A., Bouet, R., Ciumas, C., Ryvlin, P., & Jerbi, K. (2015). Gamma oscillations in V1 are correlated with $GABA_A$ receptor density: A multi-modal MEG and Flumazenil-PET study. *Scientific Reports*, *5*, 16347. https://doi.org/10.1038/srep16347

Kuramoto, Y. (1984). Method of Phase Description I. In Y. Kuramoto (Ed.), *Chemical Oscillations, Waves, and Turbulence* (pp. 22–34). Springer. https://doi.org/10.1007/978-3-642-69689-3_3

Kuznetsova, A., Brockhoff, P. B., & Christensen, R. H. B. (2017). lmerTest Package: Tests in Linear Mixed Effects Models. *Journal of Statistical Software*, *82*(1), 1–26. https://doi.org/10.18637/jss.v082.i13

Lakatos, P., Shah, A., Knuth, K., Ulbert, I., Karmos, G., & Schroeder, C. (2005). Lakatos P, Shah AS, Knuth KH, Ulbert I, Karmos G, Schroeder CEAn oscillatory hierarchy controlling neuronal excitability and stimulus processing in the auditory

cortex. J Neurophysiol 94:1904-1911. *Journal of Neurophysiology*, *94*, 1904–1911. https://doi.org/10.1152/jn.00263.2005

Lee, B B, Martin, P. R., & Valberg, A. (1988). The physiological basis of heterochromatic flicker photometry demonstrated in the ganglion cells of the macaque retina. *The Journal of Physiology*, *404*(1), 323–347. https://doi.org/10.1113/jphysiol.1988.sp017292

Lee, B. B., Pokorny, J., Smith, V. C., Martin, P. R., & Valberg, A. (1990). Luminance and chromatic modulation sensitivity of macaque ganglion cells and human observers. *Journal of the Optical Society of America. A, Optics and Image Science*, *7*(12), 2223–2236. https://doi.org/10.1364/josaa.7.002223

Lee, Barry B. (2011). Visual pathways and psychophysical channels in the primate. *The Journal of Physiology*, *589*(1), 41–47. https://doi.org/10.1113/jphysiol.2010.192658

Lee, Barry B., & Sun, H. (2009). The chromatic input to cells of the magnocellular pathway of primates. *Journal of Vision*, *9*(2), 15.1-1518. https://doi.org/10.1167/9.2.15

Lee, J., & Stromeyer, C. F. (1989). Contribution of human short-wave cones to luminance and motion detection. *The Journal of Physiology*, *413*, 563–593.

Lee, R. J., & Mather, G. (2019). Chromatic adaptation from achromatic stimuli with implied color. *Attention, Perception, & Psychophysics*, *81*(8), 2890–2901. https://doi.org/10.3758/s13414-019-01716-5

Leopold, D. A., Murayama, Y., & Logothetis, N. K. (2003). Very slow activity fluctuations in monkey visual cortex: Implications for functional brain imaging. *Cerebral Cortex (New York, N.Y.: 1991)*, *13*(4), 422–433. https://doi.org/10.1093/cercor/13.4.422

Leszczynski, M., & Schroeder, C. E. (2019). The Role of Neuronal Oscillations in Visual Active Sensing. *Frontiers in Integrative Neuroscience*, *13*. https://doi.org/10.3389/fnint.2019.00032

Leventhal, A. G., Rodieck, R. W., & Dreher, B. (1981). Retinal ganglion cell classes in the Old World monkey: Morphology and central projections. *Science (New York, N.Y.)*, *213*(4512), 1139–1142. https://doi.org/10.1126/science.7268423

Lima, B., Singer, W., Chen, N.-H., & Neuenschwander, S. (2010). Synchronization dynamics in response to plaid stimuli in monkey V1. *Cerebral Cortex (New York, N.Y.: 1991)*, *20*(7), 1556–1573. https://doi.org/10.1093/cercor/bhp218

Limbach, K., & Corballis, P. (2016). Prestimulus alpha power influences response criterion in a detection task. *Psychophysiology*, *53*. https://doi.org/10.1111/psyp.12666

Little, S., & Brown, P. (2014). The functional role of beta oscillations in Parkinson's disease. *Parkinsonism & Related Disorders*, *20 Suppl 1*, S44-48. https://doi.org/10.1016/S1353-8020(13)70013-0

Liu, J., & Wandell, B. A. (2005a). Specializations for chromatic and temporal signals in human visual cortex. *The Journal of Neuroscience: The Official Journal of the Society for Neuroscience*, *25*(13), 3459–3468. https://doi.org/10.1523/JNEUROSCI.4206-04.2005

Liu, J., & Wandell, B. A. (2005b). Specializations for Chromatic and Temporal Signals in Human Visual Cortex. *The Journal of Neuroscience*, *25*(13), 3459–3468. https://doi.org/10.1523/JNEUROSCI.4206-04.2005

Livingstone, M. S., & Hubel, D. H. (1987). Psychophysical evidence for separate channels for the perception of form, color, movement, and depth. *The Journal of Neuroscience: The Official Journal of the Society for Neuroscience*, *7*(11), 3416–3468.

Lozano-Soldevilla, D., ter Huurne, N., Cools, R., & Jensen, O. (2014). GABAergic Modulation of Visual Gamma and Alpha Oscillations and Its Consequences for Working Memory Performance. *Current Biology*, *24*(24), 2878–2887. https://doi.org/10.1016/j.cub.2014.10.017

Luck, S. J., Chelazzi, L., Hillyard, S. A., & Desimone, R. (1997). Neural mechanisms of spatial selective attention in areas V1, V2, and V4 of macaque visual cortex. *Journal of Neurophysiology*, *77*(1), 24–42. https://doi.org/10.1152/jn.1997.77.1.24

Lundqvist, M., Herman, P., & Lansner, A. (2011). Theta and Gamma Power Increases and Alpha/Beta Power Decreases with Memory Load in an Attractor Network Model. *Journal of Cognitive Neuroscience*, *23*(10), 3008–3020. https://doi.org/10.1162/jocn_a_00029

Macdonald, R. L., & Olsen, R. W. (1994). GABAA receptor channels. *Annual Review of Neuroscience*, *17*, 569–602. https://doi.org/10.1146/annurev.ne.17.030194.003033

MacLeod, D. I. A., & Boynton, R. M. (1979). Chromaticity diagram showing cone excitation by stimuli of equal luminance. *JOSA*, *69*(8), 1183–1186. https://doi.org/10.1364/JOSA.69.001183

Magazzini, L., Muthukumaraswamy, S. D., Campbell, A. E., Hamandi, K., Lingford-Hughes, A., Myers, J. F. M., Nutt, D. J., Sumner, P., Wilson, S. J., & Singh, K. D. (2016). Significant reductions in human visual gamma frequency by the gaba reuptake inhibitor tiagabine revealed by robust peak frequency estimation. *Human Brain Mapping*, *37*(11), 3882–3896. https://doi.org/10.1002/hbm.23283

Makeig, S., Westerfield, M., Jung, T.-P., Enghoff, S., Townsend, J., Courchesne, E., & Sejnowski, T. J. (2002). Dynamic Brain Sources of Visual Evoked Responses. *Science*, *295*(5555), 690–694. https://doi.org/10.1126/science.1066168

Mann, E. O., & Mody, I. (2010). Control of hippocampal gamma oscillation frequency by tonic inhibition and excitation of interneurons. *Nature Neuroscience*, *13*(2), 205–212. https://doi.org/10.1038/nn.2464

Martin, D. L., & Rimvall, K. (1993). Regulation of gamma-aminobutyric acid synthesis in the brain. *Journal of Neurochemistry*, *60*(2), 395–407. https://doi.org/10.1111/j.1471-4159.1993.tb03165.x

Matin, L. (1968). Critical Duration, the Differential Luminance Threshold, Critical Flicker Frequency, and Visual Adaptation: A Theoretical Treatment*. *JOSA*, *58*(3), 404–415. https://doi.org/10.1364/JOSA.58.000404

Maunsell, J. H., Nealey, T. A., & DePriest, D. D. (1990). Magnocellular and parvocellular contributions to responses in the middle temporal visual area (MT) of the macaque monkey. *The Journal of Neuroscience: The Official Journal of the Society for Neuroscience*, *10*(10), 3323–3334.

McKeefry, D. J., Burton, M. P., & Morland, A. B. (2010). The contribution of human cortical area V3A to the perception of chromatic motion: A transcranial magnetic stimulation study. *European Journal of Neuroscience*, *31*(3), 575–584. https://doi.org/10.1111/j.1460-9568.2010.07095.x

McKeefry, D. J., Russell, M. H., Murray, I. J., & Kulikowski, J. J. (1996). Amplitude and phase variations of harmonic components in human achromatic and chromatic visual evoked potentials. *Visual Neuroscience*, *13*(4), 639–653. https://doi.org/10.1017/s0952523800008543

McKeefry, D. J., & Zeki, S. (1997). The position and topography of the human colour centre as revealed by functional magnetic resonance imaging. *Brain: A Journal of Neurology*, *120 (Pt 12)*, 2229–2242. https://doi.org/10.1093/brain/120.12.2229

Meador, K. J., Ray, P. G., Echauz, J. R., Loring, D. W., & Vachtsevanos, G. J. (2002). Gamma coherence and conscious perception. *Neurology*, *59*(6), 847–854. https://doi.org/10.1212/wnl.59.6.847

Mishkin, M., & Ungerleider, L. G. (1982). Contribution of striate inputs to the visuospatial functions of parieto-preoccipital cortex in monkeys. *Behavioural Brain Research*, *6*(1), 57–77. https://doi.org/10.1016/0166-4328(82)90081-X

Mishkin, M., Ungerleider, L. G., & Macko, K. A. (1983). Object vision and spatial vision: Two cortical pathways. *Trends in Neurosciences*, *6*, 414–417. https://doi.org/10.1016/0166-2236(83)90190-X

Monto, S., Palva, S., Voipio, J., & Palva, J. M. (2008). Very Slow EEG Fluctuations Predict the Dynamics of Stimulus Detection and Oscillation Amplitudes in Humans. *Journal of Neuroscience*, *28*(33), 8268–8272. https://doi.org/10.1523/JNEUROSCI.1910-08.2008

Morand, S., Thut, G., de Peralta, R. G., Clarke, S., Khateb, A., Landis, T., & Michel, C. M. (2000). Electrophysiological Evidence for Fast Visual Processing through the Human Koniocellular Pathway when Stimuli Move. *Cerebral Cortex*, *10*(8), 817–825. https://doi.org/10.1093/cercor/10.8.817

Morgan, H. M., Muthukumaraswamy, S. D., Hibbs, C. S., Shapiro, K. L., Bracewell, R. M., Singh, K. D., & Linden, D. E. J. (2011). Feature integration in visual working memory: Parietal gamma activity is related to cognitive coordination. *Journal of Neurophysiology*, *106*(6), 3185–3194. https://doi.org/10.1152/jn.00246.2011

Mullen, K. T., Thompson, B., & Hess, R. F. (2010). Responses of the human visual cortex and LGN to achromatic and chromatic temporal modulations: An fMRI study. *Journal of Vision*, *10*(13), 13. https://doi.org/10.1167/10.13.13

Muthukumaraswamy, S. D., Myers, J. F. M., Wilson, S. J., Nutt, D. J., Lingford-Hughes, A., Singh, K. D., & Hamandi, K. (2013). The effects of elevated endogenous GABA levels on movement-related network oscillations. *NeuroImage*, *66*, 36–41. https://doi.org/10.1016/j.neuroimage.2012.10.054

Muthukumaraswamy, Suresh D. (2010). Functional properties of human primary motor cortex gamma oscillations. *Journal of Neurophysiology*, *104*(5), 2873–2885. https://doi.org/10.1152/jn.00607.2010

Muthukumaraswamy, Suresh D., Edden, R. A. E., Jones, D. K., Swettenham, J. B., & Singh, K. D. (2009). Resting GABA concentration predicts peak gamma frequency and fMRI amplitude in response to visual stimulation in humans. *Proceedings of the National Academy of Sciences*, *106*(20), 8356–8361. https://doi.org/10.1073/pnas.0900728106

Nealey, T. A., & Maunsell, J. H. (1994). Magnocellular and parvocellular contributions to the responses of neurons in macaque striate cortex. *Journal of*

Neuroscience, *14*(4), 2069–2079. https://doi.org/10.1523/JNEUROSCI.14-04-02069.1994

Nestares, O., & Heeger, D. J. (2000). Robust multiresolution alignment of MRI brain volumes. *Magnetic Resonance in Medicine*, *43*(5), 705–715.

Nobre, A. C., Coull, J. T., Maquet, P., Frith, C. D., Vandenberghe, R., & Mesulam, M. M. (2004). Orienting attention to locations in perceptual versus mental representations. *Journal of Cognitive Neuroscience*, *16*(3), 363–373. https://doi.org/10.1162/089892904322926700

Norcia, A. M., Appelbaum, L. G., Ales, J. M., Cottereau, B. R., & Rossion, B. (2015). The steady-state visual evoked potential in vision research: A review. *Journal of Vision*, *15*(6), 4. https://doi.org/10.1167/15.6.4

Nusser, Z., & Mody, I. (2002). Selective modulation of tonic and phasic inhibitions in dentate gyrus granule cells. *Journal of Neurophysiology*, *87*(5), 2624–2628. https://doi.org/10.1152/jn.2002.87.5.2624

Oken, B. S., Salinsky, M. C., & Elsas, S. M. (2006). Vigilance, alertness, or sustained attention: Physiological basis and measurement. *Clinical Neurophysiology : Official Journal of the International Federation of Clinical Neurophysiology*, *117*(9), 1885–1901. https://doi.org/10.1016/j.clinph.2006.01.017

Olkkonen, M., Hansen, T., & Gegenfurtner, K. R. (2008). Color appearance of familiar objects: Effects of object shape, texture, and illumination changes. *Journal of Vision*, *8*(5), 1–16. https://doi.org/10.1167/8.5.13

Olsen, R. W., & DeLorey, T. M. (1999). GABA Receptor Physiology and Pharmacology. *Basic Neurochemistry: Molecular, Cellular and Medical Aspects. 6th Edition*. https://www.ncbi.nlm.nih.gov/books/NBK28090/

Olsen, R. W., & Sieghart, W. (2008). International Union of Pharmacology. LXX. Subtypes of γ-Aminobutyric AcidA Receptors: Classification on the Basis of Subunit Composition, Pharmacology, and Function. Update. *Pharmacological Reviews*, *60*(3), 243–260. https://doi.org/10.1124/pr.108.00505

Oostenveld, R., Fries, P., Maris, E., & Schoffelen, J.-M. (2011). *FieldTrip: Open Source Software for Advanced Analysis of MEG, EEG, and Invasive Electrophysiological Data* [Research Article]. Computational Intelligence and Neuroscience. https://doi.org/10.1155/2011/156869

Palva, S., & Palva, J. M. (2011). Functional Roles of Alpha-Band Phase Synchronization in Local and Large-Scale Cortical Networks. *Frontiers in Psychology*, *2*. https://doi.org/10.3389/fpsyg.2011.00204

Pang, D., Kimura, A., Takeuchi, T., Yamato, J., & Kashino, K. (2008). *A stochastic model of selective visual attention with a dynamic Bayesian network*. 1073–1076. https://doi.org/10.1109/ICME.2008.4607624

Pelli, D. G. (1997). The VideoToolbox software for visual psychophysics: Transforming numbers into movies. *Spatial Vision*, *10*(4), 437–442.

Perry, V. H., Oehler, R., & Cowey, A. (1984). Retinal ganglion cells that project to the dorsal lateral geniculate nucleus in the macaque monkey. *Neuroscience*, *12*(4), 1101–1123. https://doi.org/10.1016/0306-4522(84)90006-x

Pessoa, L., Kastner, S., & Ungerleider, L. G. (2003). Neuroimaging Studies of Attention: From Modulation of Sensory Processing to Top-Down Control. *Journal of Neuroscience*, *23*(10), 3990–3998. https://doi.org/10.1523/JNEUROSCI.23-10-03990.2003

Petrov, A. A., Dosher, B. A., & Lu, Z.-L. (2006). Perceptual learning without feedback in non-stationary contexts: Data and model. *Vision Research*, *46*(19), 3177–3197. https://doi.org/10.1016/j.visres.2006.03.022

Pfurtscheller, G. (2001). Functional brain imaging based on ERD/ERS. *Vision Research*, *41*(10–11), 1257–1260. https://doi.org/10.1016/s0042-6989(00)00235-2

Pfurtscheller, G. (2003). Induced Oscillations in the Alpha Band: Functional Meaning. *Epilepsia*, *44*(s12), 2–8. https://doi.org/10.1111/j.0013-9580.2003.12001.x

Pfurtscheller, G., & Lopes da Silva, F. H. (1999). Event-related EEG/MEG synchronization and desynchronization: Basic principles. *Clinical Neurophysiology: Official Journal of the International Federation of Clinical Neurophysiology*, *110*(11), 1842–1857. https://doi.org/10.1016/s1388-2457(99)00141-8

Pfurtscheller, G., Neuper, C., & Krausz, G. (2000). Functional dissociation of lower and upper frequency mu rhythms in relation to voluntary limb movement. *Clinical Neurophysiology: Official Journal of the International Federation of Clinical Neurophysiology*, *111*(10), 1873–1879. https://doi.org/10.1016/s1388-2457(00)00428-4

Popescu, F., Fazli, S., Badower, Y., Blankertz, B., & Müller, K.-R. (2007). Single trial classification of motor imagination using 6 dry EEG electrodes. *PloS One*, *2*(7), e637. https://doi.org/10.1371/journal.pone.0000637

Porcello, D. M., Huntsman, M. M., Mihalek, R. M., Homanics, G. E., & Huguenard, J. R. (2003). Intact Synaptic GABAergic Inhibition and Altered Neurosteroid Modulation of Thalamic Relay Neurons in Mice Lacking δ Subunit. *Journal of Neurophysiology*, *89*(3), 1378–1386. https://doi.org/10.1152/jn.00899.2002

Puts, N. A. J., & Edden, R. A. E. (2012). In vivo magnetic resonance spectroscopy of GABA: A methodological review. *Progress in Nuclear Magnetic Resonance Spectroscopy*, *60*, 29–41. https://doi.org/10.1016/j.pnmrs.2011.06.001

Rajabi, K., B.Monajemi, M., Setareh, S., & Setareh, J. (2017). Variability of Frontal Alpha Wave in Response to Mood Induction via Visual Stimulus: A Quantitative Electroencephalographic Study. *Iranian Journal of Psychiatry and Behavioral Sciences*, *11*. https://doi.org/10.5812/ijpbs.5482

Rasch, B., & Born, J. (2013). About sleep's role in memory. *Physiological Reviews*, *93*(2), 681–766. https://doi.org/10.1152/physrev.00032.2012

Ray, S., & Maunsell, J. H. R. (2011). Different Origins of Gamma Rhythm and High-Gamma Activity in Macaque Visual Cortex. *PLOS Biology*, *9*(4), e1000610. https://doi.org/10.1371/journal.pbio.1000610

Regan, M. P., & Regan, D. (1988). A frequency domain technique for characterizing nonlinearities in biological systems. *Journal of Theoretical Biology*, *133*(3), 293–317. https://doi.org/10.1016/S0022-5193(88)80323-0

Reid, R. C., & Shapley, R. M. (2002). Space and Time Maps of Cone Photoreceptor Signals in Macaque Lateral Geniculate Nucleus. *The Journal of Neuroscience*, *22*(14), 6158–6175.

Richardson, B. D., Ling, L. L., Uteshev, V. V., & Caspary, D. M. (2011). Extrasynaptic GABAA Receptors and Tonic Inhibition in Rat Auditory Thalamus. *PLOS ONE*, *6*(1), e16508. https://doi.org/10.1371/journal.pone.0016508

Rider, A. T., Henning, G. B., Eskew, R. T., & Stockman, A. (2018). Harmonics added to a flickering light can upset the balance between ON and OFF pathways to produce illusory colors. *Proceedings of the National Academy of Sciences*, *115*(17), E4081–E4090. https://doi.org/10.1073/pnas.1717356115

Rock, I., Linnett, C. M., Grant, P., & Mack, A. (1992). Perception without attention: Results of a new method. *Cognitive Psychology*, *24*(4), 502–534. https://doi.org/10.1016/0010-0285(92)90017-v

Roepstorff, A., & Lambert, J. D. (1994). Factors contributing to the decay of the stimulus-evoked IPSC in rat hippocampal CA1 neurons. *Journal of Neurophysiology*, *72*(6), 2911–2926. https://doi.org/10.1152/jn.1994.72.6.2911

Romei, V., Brodbeck, V., Michel, C., Amedi, A., Pascual-Leone, A., & Thut, G. (2008). Spontaneous Fluctuations in Posterior α-Band EEG Activity Reflect Variability in Excitability of Human Visual Areas. *Cerebral Cortex (New York, NY)*, *18*(9), 2010–2018. https://doi.org/10.1093/cercor/bhm229

Rosen, A. C., Rao, S. M., Caffarra, P., Scaglioni, A., Bobholz, J. A., Woodley, S. J., Hammeke, T. A., Cunningham, J. M., Prieto, T. E., & Binder, J. R. (1999). Neural basis of endogenous and exogenous spatial orienting. A functional MRI study. *Journal of Cognitive Neuroscience*, *11*(2), 135–152. https://doi.org/10.1162/089892999563283

Roy, N., Bak, J. H., Akrami, A., Brody, C., & Pillow, J. (2018, January 1). *Efficient inference for time-varying behavior during learning*.

Samaha, J., Iemi, L., & Postle, B. R. (2017). Prestimulus alpha-band power biases visual discrimination confidence, but not accuracy. *Consciousness and Cognition*, *54*, 47–55. https://doi.org/10.1016/j.concog.2017.02.005

Samaha, J., & Postle, B. R. (2015). The Speed of Alpha-Band Oscillations Predicts the Temporal Resolution of Visual Perception. *Current Biology: CB*, *25*(22), 2985–2990. https://doi.org/10.1016/j.cub.2015.10.007

Samonds, J. M., & Bonds, A. B. (2005). Gamma oscillation maintains stimulus structure-dependent synchronization in cat visual cortex. *Journal of Neurophysiology*, *93*(1), 223–236. https://doi.org/10.1152/jn.00548.2004

Santhakumar, V., Jones, R. T., & Mody, I. (2010). Developmental regulation and neuroprotective effects of striatal tonic GABAA currents. *Neuroscience*, *167*(3), 644–655. https://doi.org/10.1016/j.neuroscience.2010.02.048

Sauseng, P., Klimesch, W., Stadler, W., Schabus, M., Doppelmayr, M., Hanslmayr, S., Gruber, W. R., & Birbaumer, N. (2005). A shift of visual spatial attention is selectively associated with human EEG alpha activity. *European Journal of Neuroscience*, *22*(11), 2917–2926. https://doi.org/10.1111/j.1460-9568.2005.04482.x

Sauseng, Paul, Klimesch, W., Doppelmayr, M., Pecherstorfer, T., Freunberger, R., & Hanslmayr, S. (2005). EEG alpha synchronization and functional coupling during top-down processing in a working memory task. *Human Brain Mapping*, *26*(2), 148–155. https://doi.org/10.1002/hbm.20150

Saxena, N., Muthukumaraswamy, S. D., Diukova, A., Singh, K., Hall, J., & Wise, R. (2013). Enhanced stimulus-induced gamma activity in humans during propofol-induced sedation. *PloS One*, *8*(3), e57685. https://doi.org/10.1371/journal.pone.0057685

Sayers, B. M., Beagley, H. A., & Henshall, W. R. (1974). The mechansim of auditory evoked EEG responses. *Nature*, *247*(5441), 481–483.

Scanziani, M. (2000). GABA Spillover Activates Postsynaptic GABAB Receptors to Control Rhythmic Hippocampal Activity. *Neuron*, *25*(3), 673–681. https://doi.org/10.1016/S0896-6273(00)81069-7

Schanze, T., & Eckhorn, R. (1997). Phase correlation of cortical rhythms at different frequencies: Higher-order spectral analysis of multiple-microelectrode recordings from cat and monkey visual cortex. *International Journal of Psychophysiology*, *26*(1), 171–189. https://doi.org/10.1016/S0167-8760(97)00763-0

Schiller, P. H., & Colby, C. L. (1983). The responses of single cells in the lateral geniculate nucleus of the rhesus monkey to color and luminance contrast. *Vision Research*, *23*(12), 1631–1641. https://doi.org/10.1016/0042-6989(83)90177-3

Schoffelen, J.-M., Oostenveld, R., & Fries, P. (2005). Neuronal Coherence as a Mechanism of Effective Corticospinal Interaction. *Science*, *308*(5718), 111–113. https://doi.org/10.1126/science.1107027

Schroeder, C. E., & Lakatos, P. (2009). Low-frequency neuronal oscillations as instruments of sensory selection. *Trends in Neurosciences*, *32*(1), 9–18. https://doi.org/10.1016/j.tins.2008.09.012

Schwartz, G., & Rieke, F. (2011). Nonlinear spatial encoding by retinal ganglion cells: When 1 + 1 ≠ 2. *The Journal of General Physiology*, *138*(3), 283–290. https://doi.org/10.1085/jgp.201110629

Sellers, E. W., & Donchin, E. (2006). A P300-based brain-computer interface: Initial tests by ALS patients. *Clinical Neurophysiology: Official Journal of the International Federation of Clinical Neurophysiology*, *117*(3), 538–548. https://doi.org/10.1016/j.clinph.2005.06.027

Seidemann, E., Poirson, A. B., Wandell, B. A., Newsome, W.T. (1999). Color signals in area MT of the macaque monkey. *Neuron*, 24(4): 911-7. https://doi.org/10.1016/s0896-6273(00)81038-7

Sewards, T. V., & Sewards, M. A. (1999). Alpha-band oscillations in visual cortex: Part of the neural correlate of visual awareness? *International Journal of Psychophysiology*, *32*(1), 35–45. https://doi.org/10.1016/S0167-8760(98)00062-2

Shady, S., MacLeod, D. I. A., & Fisher, H. S. (2004). Adaptation from invisible flicker. *Proceedings of the National Academy of Sciences of the United States of America*, *101*(14), 5170–5173. https://doi.org/10.1073/pnas.0303452101

Shapley, R., & Perry, V. H. (1986). Cat and monkey retinal ganglion cells and their visual functional roles. *Trends in Neurosciences*, *9*, 229–235.

Silvoni, S., Volpato, C., Cavinato, M., Marchetti, M., Priftis, K., Merico, A., Tonin, P., Koutsikos, K., Beverina, F., & Piccione, F. (2009). P300-Based Brain-Computer Interface Communication: Evaluation and Follow-up in Amyotrophic Lateral Sclerosis. *Frontiers in Neuroscience*, *3*, 60. https://doi.org/10.3389/neuro.20.001.2009

Sincich, L. C., & Horton, J. C. (2005). The circuitry of V1 and V2: Integration of color, form, and motion. *Annual Review of Neuroscience*, *28*, 303–326. https://doi.org/10.1146/annurev.neuro.28.061604.135731

Small, D. M., Gitelman, D. R., Gregory, M. D., Nobre, A. C., Parrish, T. B., & Mesulam, M.-M. (2003). The posterior cingulate and medial prefrontal cortex mediate the anticipatory allocation of spatial attention. *NeuroImage*, *18*(3), 633–641. https://doi.org/10.1016/s1053-8119(02)00012-5

Solomon, S. G., Peirce, J. W., Dhruv, N. T., & Lennie, P. (2004). Profound Contrast Adaptation Early in the Visual Pathway. *Neuron*, *42*(1), 155–162. https://doi.org/10.1016/S0896-6273(04)00178-3

Solomon, S. G., White, A. J. R., & Martin, P. R. (1999). Temporal contrast sensitivity in the lateral geniculate nucleus of a New World monkey, the marmoset Callithrix jacchus. *The Journal of Physiology*, *517*(3), 907–917. https://doi.org/10.1111/j.1469-7793.1999.0907s.x

Spaak, E., de Lange, F. P., & Jensen, O. (2014). Local entrainment of α oscillations by visual stimuli causes cyclic modulation of perception. *The Journal of Neuroscience: The Official Journal of the Society for Neuroscience*, *34*(10), 3536–3544. https://doi.org/10.1523/JNEUROSCI.4385-13.2014

Spitschan, M., Aguirre, G. K., & Brainard, D. H. (2015). Selective Stimulation of Penumbral Cones Reveals Perception in the Shadow of Retinal Blood Vessels. *PLOS ONE*, *10*(4), e0124328. https://doi.org/10.1371/journal.pone.0124328

Spitschan, M., Datta, R., Stern, A. M., Brainard, D. H., & Aguirre, G. K. (2016). Human Visual Cortex Responses to Rapid Cone and Melanopsin-Directed Flicker. *The Journal of Neuroscience: The Official Journal of the Society for Neuroscience*, *36*(5), 1471–1482. https://doi.org/10.1523/JNEUROSCI.1932-15.2016

Spitschan, M., Jain, S., Brainard, D. H., & Aguirre, G. K. (2014). Opponent melanopsin and S-cone signals in the human pupillary light response. *Proceedings of the National Academy of Sciences*, *111*(43), 15568–15572. https://doi.org/10.1073/pnas.1400942111

Stagg, C. J. (2014). Magnetic Resonance Spectroscopy as a tool to study the role of GABA in motor-cortical plasticity. *NeuroImage*, *86*, 19–27. https://doi.org/10.1016/j.neuroimage.2013.01.009

Stagg, C. J., Bachtiar, V., & Johansen-Berg, H. (2011a). What are we measuring with GABA magnetic resonance spectroscopy? *Communicative & Integrative Biology*, *4*(5), 573–575. https://doi.org/10.4161/cib.4.5.16213

Stagg, C. J., Bachtiar, V., & Johansen-Berg, H. (2011b). The role of GABA in human motor learning. *Current Biology: CB*, *21*(6), 480–484. https://doi.org/10.1016/j.cub.2011.01.069

Stagg, C. J., Best, J. G., Stephenson, M. C., O'Shea, J., Wylezinska, M., Kincses, Z. T., Morris, P. G., Matthews, P. M., & Johansen-Berg, H. (2009). Polarity-sensitive modulation of cortical neurotransmitters by transcranial stimulation. *The Journal of Neuroscience: The Official Journal of the Society for Neuroscience*, *29*(16), 5202–5206. https://doi.org/10.1523/JNEUROSCI.4432-08.2009

Steinmetz, P. N., Roy, A., Fitzgerald, P. J., Hsiao, S. S., Johnson, K. O., & Niebur, E. (2000). Attention modulates synchronized neuronal firing in primate somatosensory cortex. *Nature*, *404*(6774), 187–190. https://doi.org/10.1038/35004588

Stockman, A., Henning, G. B., & Rider, A. T. (2017). Linear–nonlinear models of the red–green chromatic pathway. *Journal of Vision*, *17*(13), 7–7. https://doi.org/10.1167/17.13.7

Stockman, A., MacLeod, D. I. A., & DePriest, D. D. (1991). The temporal properties of the human short-wave photoreceptors and their associated pathways. *Vision Research*, *31*(2), 189–208. https://doi.org/10.1016/0042-6989(91)90111-H

Stockman, A., & Sharpe, L. T. (2000). The spectral sensitivities of the middle-and long-wavelength-sensitive cones derived from measurements in observers of known genotype. *Vision Research*, *40*(13), 1711–1737.

Sun, H., Smithson, H. E., Zaidi, Q., & Lee, B. B. (2006). Specificity of cone inputs to macaque retinal ganglion cells. *Journal of Neurophysiology*, *95*(2), 837–849. https://doi.org/10.1152/jn.00714.2005

Sundberg, K. A., Mitchell, J. F., Gawne, T. J., & Reynolds, J. H. (2012). Attention Influences Single Unit and Local Field Potential Response Latencies in Visual Cortical Area V4. *The Journal of Neuroscience*, *32*(45), 16040–16050. https://doi.org/10.1523/JNEUROSCI.0489-12.2012

Supèr, H., van der Togt, C., Spekreijse, H., & Lamme, V. A. F. (2003). Internal State of Monkey Primary Visual Cortex (V1) Predicts Figure–Ground Perception. *The Journal of Neuroscience*, *23*(8), 3407–3414. https://doi.org/10.1523/JNEUROSCI.23-08-03407.2003

Swanson, W. H., Ueno, T., Smith, V. C., & Pokorny, J. (1987). Temporal modulation sensitivity and pulse-detection thresholds for chromatic and luminance perturbations. *Journal of the Optical Society of America A*, *4*(10), 1992. https://doi.org/10.1364/JOSAA.4.001992

Taranto-Montemurro, L., Sands, S. A., Edwards, B. A., Azarbarzin, A., Marques, M., de Melo, C., Eckert, D. J., White, D. P., & Wellman, A. (2017). Effects of Tiagabine on Slow Wave Sleep and Arousal Threshold in Patients With Obstructive Sleep Apnea. *Sleep*, *40*(2). https://doi.org/10.1093/sleep/zsw047

Thiele, A., Dobkins, K. R., & Albright, T. D. (1999). The Contribution of Color to Motion Processing in Macaque Middle Temporal Area. *Journal of Neuroscience*, *19*(15), 6571–6587. https://doi.org/10.1523/JNEUROSCI.19-15-06571.1999

Thompson, S. M., & Gähwiler, B. H. (1992). Effects of the GABA uptake inhibitor tiagabine on inhibitory synaptic potentials in rat hippocampal slice cultures. *Journal of Neurophysiology*, *67*(6), 1698–1701. https://doi.org/10.1152/jn.1992.67.6.1698

Thut, G., Nietzel, A., Brandt, S. A., & Pascual-Leone, A. (2006). Alpha-band electroencephalographic activity over occipital cortex indexes visuospatial attention bias and predicts visual target detection. *The Journal of Neuroscience: The Official Journal of the Society for Neuroscience*, *26*(37), 9494–9502. https://doi.org/10.1523/JNEUROSCI.0875-06.2006

Tognarelli, J. M., Dawood, M., Shariff, M. I. F., Grover, V. P. B., Crossey, M. M. E., Cox, I. J., Taylor-Robinson, S. D., & McPhail, M. J. W. (2015). Magnetic Resonance Spectroscopy: Principles and Techniques: Lessons for Clinicians. *Journal of Clinical and Experimental Hepatology*, *5*(4), 320–328. https://doi.org/10.1016/j.jceh.2015.10.006

Tolhurst, D. J., Movshon, J. A., & Dean, A. F. (1983). The statistical reliability of signals in single neurons in cat and monkey visual cortex. *Vision Research*, *23*(8), 775–785. https://doi.org/10.1016/0042-6989(83)90200-6

Traub, R. D., Whittington, M. A., Colling, S. B., Buzsáki, G., & Jefferys, J. G. (1996). Analysis of gamma rhythms in the rat hippocampus in vitro and in vivo. *The Journal of Physiology*, *493*(2), 471–484. https://doi.org/10.1113/jphysiol.1996.sp021397

Troscianko, T., Davidoff, J., Humphreys, G., Landis, T., Fahle, M., Greenlee, M., Brugger, P., & Phillips, W. (1996). Human colour discrimination based on a non-

parvocellular pathway. *Current Biology*, *6*(2), 200–210. https://doi.org/10.1016/S0960-9822(02)00453-0

Tyler, C. W. (1985). Analysis of visual modulation sensitivity. II. Peripheral retina and the role of photoreceptor dimensions. *Journal of the Optical Society of America. A, Optics and Image Science*, *2*(3), 393–398. https://doi.org/10.1364/josaa.2.000393

van Dijk, H., Schoffelen, J.-M., Oostenveld, R., & Jensen, O. (2008). Prestimulus oscillatory activity in the alpha band predicts visual discrimination ability. *The Journal of Neuroscience: The Official Journal of the Society for Neuroscience*, *28*(8), 1816–1823. https://doi.org/10.1523/JNEUROSCI.1853-07.2008

Van Essen, D. C., & Gallant, J. L. (1994). Neural mechanisms of form and motion processing in the primate visual system. *Neuron*, *13*(1), 1–10. https://doi.org/10.1016/0896-6273(94)90455-3

van Kerkoerle, T., Self, M. W., Dagnino, B., Gariel-Mathis, M.-A., Poort, J., van der Togt, C., & Roelfsema, P. R. (2014). Alpha and gamma oscillations characterize feedback and feedforward processing in monkey visual cortex. *Proceedings of the National Academy of Sciences of the United States of America*, *111*(40), 14332–14341. https://doi.org/10.1073/pnas.1402773111

van Pelt, S., & Fries, P. (2013). Visual stimulus eccentricity affects human gamma peak frequency. *NeuroImage*, *78*, 439–447. https://doi.org/10.1016/j.neuroimage.2013.04.040

Vanderwolf, C. H. (1969). Hippocampal electrical activity and voluntary movement in the rat. *Electroencephalography and Clinical Neurophysiology*, *26*(4), 407–418. https://doi.org/10.1016/0013-4694(69)90092-3

Vatansever, D., Menon, D. K., & Stamatakis, E. A. (2017). Default mode contributions to automated information processing. *Proceedings of the National Academy of Sciences*, *114*(48), 12821–12826. https://doi.org/10.1073/pnas.1710521114

Veit, J., Hakim, R., Jadi, M. P., Sejnowski, T. J., & Adesnik, H. (2017). Cortical gamma band synchronization through somatostatin interneurons. *Nature Neuroscience*, *20*(7), 951–959. https://doi.org/10.1038/nn.4562

Vogt, F., Klimesch, W., & Doppelmayr, M. (1998). High-frequency components in the alpha band and memory performance. *Journal of Clinical Neurophysiology: Official Publication of the American Electroencephalographic Society*, *15*(2), 167–172. https://doi.org/10.1097/00004691-199803000-00011

Vul, E., Hanus, D., & Kanwisher, N. (2009). Attention as inference: Selection is probabilistic; Responses are all-or-none samples. *Journal of Experimental Psychology. General*, *138*(4), 546. https://doi.org/10.1037/a0017352

Vul, E., & MacLeod, D. I. A. (2006). Contingent aftereffects distinguish conscious and preconscious color processing. *Nature Neuroscience*, *9*(7), 873–874. https://doi.org/10.1038/nn1723

Wade, A., Augath, M., Logothetis, N., & Wandell, B. (2008). FMRI measurements of color in macaque and human. *Journal of Vision*, *8*(10), 6.1-619. https://doi.org/10.1167/8.10.6

Wade, A. R., & Rowland, J. (2010). Early suppressive mechanisms and the negative blood oxygenation level-dependent response in human visual cortex. *The Journal of Neuroscience: The Official Journal of the Society for Neuroscience*, *30*(14), 5008–5019. https://doi.org/10.1523/JNEUROSCI.6260-09.2010

Wandell, B. A., Poirson, A. B., Newsome, W. T., Baseler, H. A., Boynton, G. M., Huk, A., Gandhi, S., & Sharpe, L. T. (1999). Color signals in human motion-selective cortex, *Neuron*, 24(4), 901-9. https://doi.org/ 10.1016/s0896-6273(00)81037-5

Wehr, M., & Zador, A. M. (2003). Balanced inhibition underlies tuning and sharpens spike timing in auditory cortex. *Nature*, *426*(6965), 442–446. https://doi.org/10.1038/nature02116

Werner, G., & Mountcastle, V. B. (1963). The variability of central neural activity in a sensory system, and its implications for the central reflection of sensory events. *Journal of Neurophysiology*, *26*, 958–977. https://doi.org/10.1152/jn.1963.26.6.958

Whittington, M. A., Jefferys, T. G. R., & Traub, R. D. (1996). Effects of intravenous anaesthetic agents on fast inhibitory oscillations in the rat hippocampus in vitro. *British Journal of Pharmacology*, *118*(8), 1977–1986. https://doi.org/10.1111/j.1476-5381.1996.tb15633.x

Whittington, M. A., Traub, R. D., Faulkner, H. J., Jefferys, J. G. R., & Chettiar, K. (1998). Morphine disrupts long-range synchrony of gamma oscillations in hippocampal slices. *Proceedings of the National Academy of Sciences*, *95*(10), 5807–5811. https://doi.org/10.1073/pnas.95.10.5807

Whittington, M. A., Traub, R. D., & Jefferys, J. G. (1995). Synchronized oscillations in interneuron networks driven by metabotropic glutamate receptor activation. *Nature*, *373*(6515), 612–615. https://doi.org/10.1038/373612a0

Whittington, M. A., Traub, R. D., Kopell, N., Ermentrout, B., & Buhl, E. H. (2000). Inhibition-based rhythms: Experimental and mathematical observations on network dynamics. *International Journal of Psychophysiology*, *38*(3), 315–336. https://doi.org/10.1016/S0167-8760(00)00173-2

Winawer, J., Huk, A. C., & Boroditsky, L. (2008). A Motion Aftereffect From Still Photographs Depicting Motion: *Psychological Science*. https://journals.sagepub.com/doi/10.1111/j.1467-9280.2008.02080.x

Wisowaty, J. J. (1981). Estimates for the temporal response characteristics of chromatic pathways. *Journal of the Optical Society of America*, *71*(8), 970–977. https://doi.org/10.1364/josa.71.000970

Womelsdorf, T., & Fries, P. (2007). The role of neuronal synchronization in selective attention. *Current Opinion in Neurobiology*, *17*(2), 154–160. https://doi.org/10.1016/j.conb.2007.02.002

Womelsdorf, T., Fries, P., Mitra, P. P., & Desimone, R. (2006). Gamma-band synchronization in visual cortex predicts speed of change detection. *Nature*, *439*(7077), 733–736. https://doi.org/10.1038/nature04258

Womelsdorf, T., Schoffelen, J.-M., Oostenveld, R., Singer, W., Desimone, R., Engel, A. K., & Fries, P. (2007). Modulation of Neuronal Interactions Through Neuronal Synchronization. *Science*, *316*(5831), 1609–1612. https://doi.org/10.1126/science.1139597

Worden, M. S., Foxe, J. J., Wang, N., & Simpson, G. V. (2000). Anticipatory biasing of visuospatial attention indexed by retinotopically specific alpha-band electroencephalography increases over occipital cortex. *Journal of Neuroscience*, 63.

Wróbel, A. (2000). Beta activity: A carrier for visual attention. *Acta Neurobiologiae Experimentalis*, *60*(2), 247–260.

Wu, S. M., & Maple, B. R. (1998). Amino acid neurotransmitters in the retina: A functional overview. *Vision Research*, *38*(10), 1371–1384. https://doi.org/10.1016/s0042-6989(97)00296-4

Wyss, C., Tse, D. H. Y., Kometer, M., Dammers, J., Achermann, R., Shah, N. J., Kawohl, W., & Neuner, I. (2017). GABA metabolism and its role in gamma-band oscillatory activity during auditory processing: An MRS and EEG study. *Human Brain Mapping*, *38*(8), 3975–3987. https://doi.org/10.1002/hbm.23642

Yan, l., Imbrosci, B., Zhang, W., Neubacher, U., Hatt, H., Eysel, U. & Mittmann, T. (2011). Changes in NMDA-Receptor Function in the First Week Following Laser-Induced Lesions in Rat Visual Cortex. *Cerebral Cortex,* 22, 2392-403. https://doi.org/10.1093/cercor/bhr318

Yang, X.-L. (2004). Characterization of receptors for glutamate and GABA in retinal neurons. *Progress in Neurobiology*, *73*(2), 127–150. https://doi.org/10.1016/j.pneurobio.2004.04.002

Young, M. P., Tanaka, K., & Yamane, S. (1992). On oscillating neuronal responses in the visual cortex of the monkey. *Journal of Neurophysiology*, *67*(6), 1464–1474. https://doi.org/10.1152/jn.1992.67.6.1464

Yuval-Greenberg, S., & Deouell, L. Y. (2009). The broadband-transient induced gamma-band response in scalp EEG reflects the execution of saccades. *Brain Topography*, *22*(1), 3–6. https://doi.org/10.1007/s10548-009-0077-6

Yuval-Greenberg, S., & Deouell, L. Y. (2011). Scalp-recorded induced γ-band responses to auditory stimulation and its correlations with saccadic muscle-activity. *Brain Topography*, *24*(1), 30–39. https://doi.org/10.1007/s10548-010-0157-7

Yuval-Greenberg, S., Tomer, O., Keren, A. S., Nelken, I., & Deouell, L. Y. (2008). Transient Induced Gamma-Band Response in EEG as a Manifestation of Miniature Saccades. *Neuron*, *58*(3), 429–441. https://doi.org/10.1016/j.neuron.2008.03.027

Zeki, S. (1990). A Century of Cerebral Achromatopsia. *Brain*, *113*(6), 1721–1777. https://doi.org/10.1093/brain/113.6.1721

Zhang, Y., Wang, X., Bressler, S. L., Chen, Y., & Ding, M. (2008). Prestimulus cortical activity is correlated with speed of visuomotor processing. *Journal of Cognitive Neuroscience*, *20*(10), 1915–1925. https://doi.org/10.1162/jocn.2008.20132

Zlody, R. L. (1965). The Relationship between Critical Flicker Frequency (CFF) and Several Intellectual Measures. *The American Journal of Psychology*, *78*(4), 596–602. JSTOR. https://doi.org/10.2307/1420921

Appendices

Table 3.6 *Details of linear regression model for each participant, averaged across all electrodes predicting binned scores from prestimulus alpha power.*

i. Subject: *AKS*

Variable	b	SE	β	*t*	p
Intercept (Constant)	0.52	0.54		.96	.368
Standardised alpha power	-0.95	0.87	-.36	-1.10	.305

ii. Subject: *ARW*

Variable	b	SE	β	*t*	p
Intercept (Constant)	-0.33	0.41		-.80	.447
Standardised alpha power	0.65	0.69	.30	.94	.371

iii. Subject: *AVB*

Variable	b	SE	β	*t*	p
Intercept (Constant)	-0.44	0.31		-1.41	.196
Standardised alpha power	0.98	0.59	.51	1.67	.133

iv. Subject: *MK*

Variable	b	SE	β	*t*	p
Intercept (Constant)	-0.99	0.29		-3.47	.007
Standardised alpha power	1.98	0.48	.81	4.10	.003

v. Subject: *PC*

Variable	b	SE	β	*t*	p
Intercept (Constant)	0.89	0.39		2.27	.049
Standardised alpha power	-1.78	0.66	-.67	-2.68	.025

vi. Subject: *RM*

Variable	b	SE	β	*t*	p
Intercept (Constant)	0.57	0.20		2.87	.018
Standardised alpha power	-1.14	0.34	-.75	-3.40	.008

vii. Subject: *TN*

Variable	b	SE	β	*t*	p
Intercept (Constant)	0.80	0.33		2.40	.040
Standardised alpha power	-1.61	0.57	-.69	-2.84	.019

Table 3.7 *Details of linear regression model for each participant, averaged across visual electrodes predicting binned scores from prestimulus alpha power.*

i. Subject: *AKS*

Variable	b	SE	β	*t*	p
Intercept (Constant)	-0.20	0.54		-0.38	.717
Standardised alpha power	0.38	.87	.15	0.43	.678

ii. Subject: *ARW*

Variable	b	SE	β	*t*	p
Intercept (Constant)	-0.12	0.58		-0.20	.846
Standardised alpha power	0.23	0.99	.08	0.24	.818

iii. Subject: *AVB*

Variable	b	SE	β	*t*	p
Intercept (Constant)	0.12	0.56		0.21	.837
Standardised alpha power	-0.26	1.04	-.09	-0.25	.808

iv. Subject: *MK*

Variable	b	SE	β	*t*	p
Intercept (Constant)	-1.27	0.23		-5.60	<.001
Standardised alpha power	2.53	0.38	.91	6.62	<.001

v. Subject: *PC*

Variable	b	SE	β	*t*	p
Intercept (Constant)	1.10	0.43		2.54	.032
Standardised alpha power	-2.19	0.73	-.71	-3.01	.015

vi. Subject: *RM*

Variable	b	SE	β	*t*	p
Intercept (Constant)	1.01	0.44		2.28	.049
Standardised alpha power	-2.01	0.75	-.67	-2.70	.025

vii. Subject: *TN*

Variable	b	SE	β	*t*	p
Intercept (Constant)	1.08	0.39		2.81	.020
Standardised alpha power	-2.16	0.65	-.74	-3.32	.009

Table 3.8 *Details of linear regression model for each participant, averaged across all electrodes predicting reaction time from prestimulus alpha power.*

i. Subject: *AKS*

Variable	b	SE	β	*t*	p
Intercept (Constant)	-1.26	0.28		-4.59	.001
Standardised alpha power	0.23	0.04	.86	5.42	<.001

ii. Subject: *ARW*

Variable	b	SE	β	*t*	p
Intercept (Constant)	-0.27	0.39		-0.69	.504
Standardised alpha power	0.05	0.06	.25	0.82	.432

iii. Subject: *AVB*

Variable	b	SE	β	*t*	p
Intercept (Constant)	0.36	0.34		1.05	.317
Standardised alpha power	-0.07	0.05	-.37	-1.24	.242

iv. Subject: *MK*

Variable	b	SE	β	*t*	p
Intercept (Constant)	-0.52	0.44		-1.17	.276
Standardised alpha power	0.08	0.06	.41	1.28	.237

v. Subject: *PC*

Variable	b	SE	β	*t*	p
Intercept (Constant)	-0.74	0.49		-1.53	.158
Standardised alpha power	0.13	0.08	.50	1.80	.102

vi. Subject: *RM*

Variable	b	SE	β	*t*	p
Intercept (Constant)	-0.44	0.28		-1.54	.154
Standardised alpha power	0.08	0.04	-.50	1.82	.099

vii. Subject: *TN*

Variable	b	SE	β	*t*	p
Intercept (Constant)	0.26	0.29		0.90	.389
Standardised alpha power	-0.05	0.05	-.32	-1.06	.312

Table 3.9 *Details of linear regression model for each participant, averaged across visual electrodes predicting reaction time from prestimulus alpha power.*

i. Subject: *AKS*

Variable	b	SE	β	*t*	p

Intercept (Constant)	-1.32	0.29		-4.58	.001
Standardised alpha power	0.24	0.04	.86	5.40	<.001

ii. Subject: *ARW*

Variable	b	SE	β	*t*	p
Intercept (Constant)	-0.16	0.47		-0.33	.745
Standardised alpha power	0.03	0.07	.12	0.40	.701

iii. Subject: *AVB*

Variable	b	SE	β	*t*	p
Intercept (Constant)	0.26	0.49		0.53	.605
Standardised alpha power	-0.07	0.08	-.20	-.63	.543

iv. Subject: *MK*

Variable	b	SE	β	*t*	p
Intercept (Constant)	-0.63	0.41		-1.55	.161
Standardised alpha power	0.10	0.06	.51	1.69	.130

v. Subject: *PC*

Variable	b	SE	β	*t*	p
Intercept (Constant)	-0.62	0.52		-1.19	.263
Standardised alpha power	0.11	0.08	.41	1.40	.192

vi. Subject: *RM*

Variable	b	SE	β	*t*	p
Intercept (Constant)	-0.74	0.43		-1.71	.118
Standardised alpha power	0.14	0.07	.54	2.02	.071

vii. Subject: *TN*

Variable	b	SE	β	*t*	p
Intercept (Constant)	0.66	0.29		2.26	.047
Standardised alpha power	-0.12	0.05	-.65	-2.67	.023

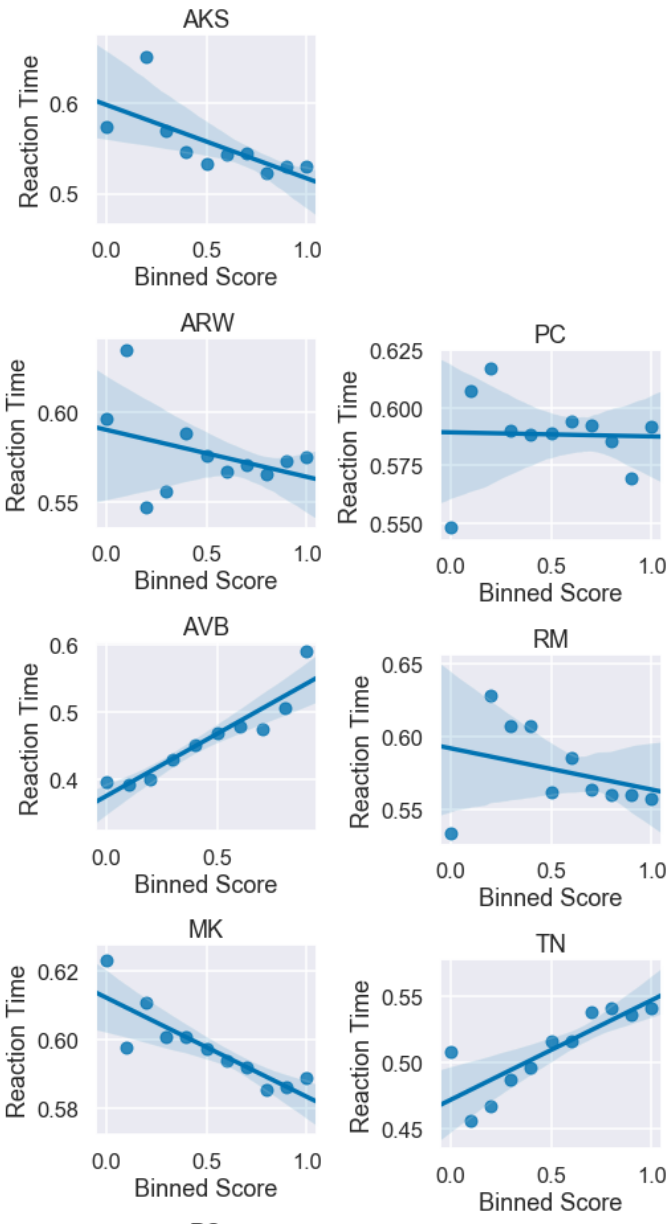

Fig. 3.8 *Reaction time plotted against binned scores. Positive correlation likely demonstrates a trade-off between taking longer to respond and being more accurate at the task. This might be a way to assess the autopilot mode in people: positive correlation could mean that the task takes up more conscious effort, and no positive correlation (or negative correlation) could indicate that scores are not due the fact that they're taking longer and being more careful.*

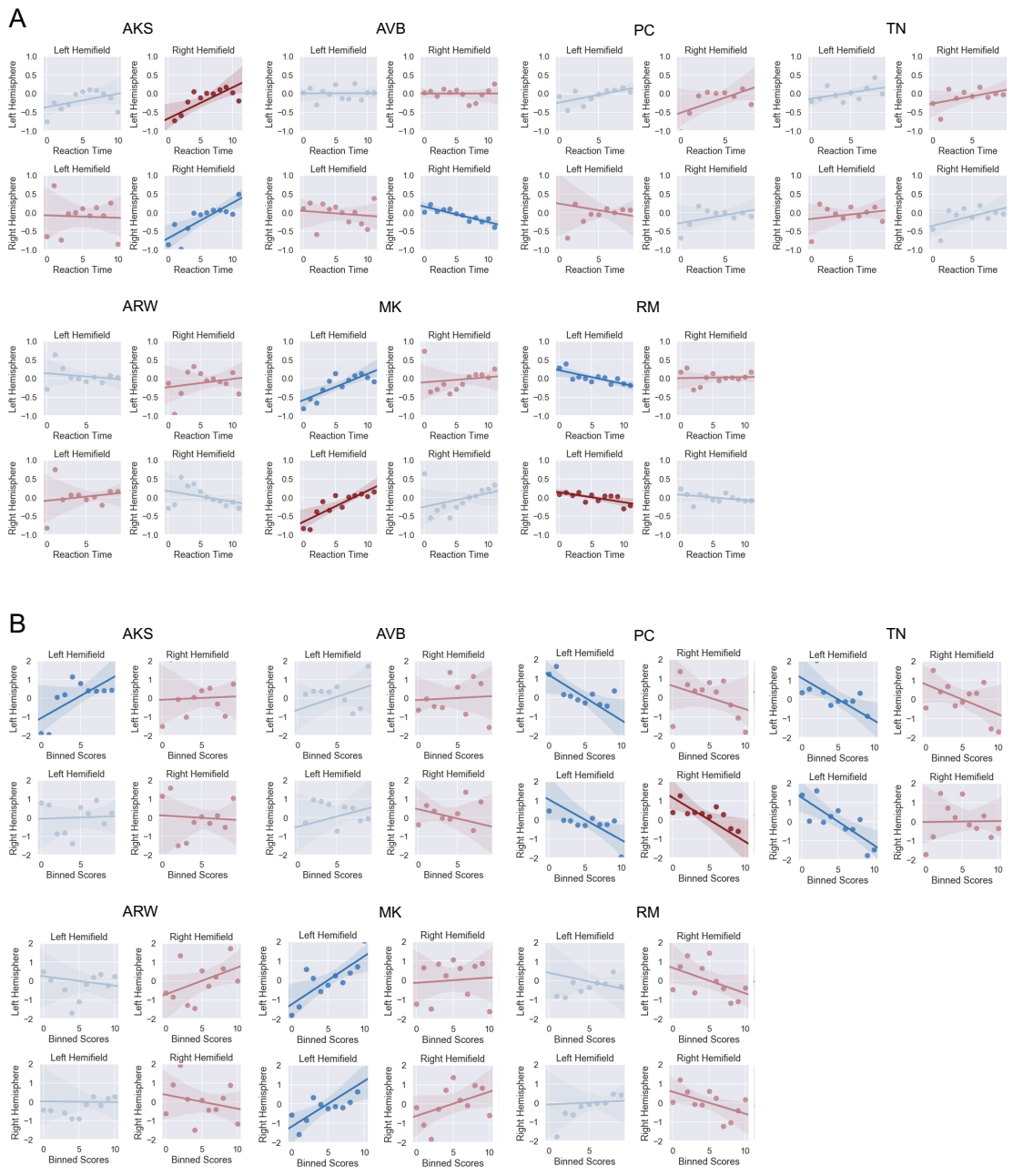

Fig. 3.9 *Scatterplots of the left hemisphere visual electrodes (top row) and right hemisphere visual electrodes (bottom row) with (A) binned scores and (B) reaction time. Data were grouped by whether the target in that particular trial appeared in the left visual field or the right. Blue denotes responses from ipsilateral electrodes and red denotes responses from contralateral electrodes in respect of the target location. Data that did not reach significance were paled out.*

Table 4.2 *Detail of ANOVAs showing significant effect of stimulus colour on individual frequency bins for coherently averaged EEG data with Bonferroni-corrected p-values. Last three columns show post-hoc tests analysing the difference between stimulus colours. Asterisks (*) denote significant differences between stimulus colours.*

Stimulus Frequency (Hz)	*Power Spectrum Frequency (Hz)*	*ANOVA*	*Luminance and S-cone isolating*	*Luminance and red-green*	*Red-green and S-cone isolating*
5	5	F(2, 32) = 6.04, p = .026	.277	.025 *	.483
	10	F(2, 32) = 5.82, p = .028	.046 *	.999	.043 *
	15	F(2, 32) = 5.65, p = .030	.894	.317	.145
	20	F(2, 32) = 17.78, p < .001	.299	.986	.230
	30	F(2, 32) = 8.76, p < .001	.020 *	.929	.007 *
	33	F(2, 32) = 4.58, p = .048	.001 *	.069	.185
	40	F(2, 32) = 9.70, p = .007	.005 *	.481	.085
	65	F(2, 32) = 7.62, p = .014	.013 *	.122	.607
12	12	F(2, 32) = 5.37, p = .034	.050 *	.233	.725
	24	F(2, 32) = 10.52, p = .005	< .001 *	.001 *	.747
	36	F(2, 32) = 14.65, p = .001	.660	.104	.454
	37	F(2, 32) = 5.89, p = .028	< .001 *	< .001 *	.762

	48	F(2, 32) = 19.76, p < .001	.021 *	.009 *	.942
	51	F(2, 32) = 4.62, p = .047	.066	.252	.770
	60	F(2, 32) = 4.55, p = .049	.006 *	.077	.583
16	16	F(2, 32) = 14.73, p = .001	< .001 *	< .001 *	.993
	24	F(2, 32) = 7.81, p = .013	< .001 *	.001 *	.934
	32	F(2, 32) = 13.04, p = .002	.103	.965	.059
	36	F(2, 32) = 7.35, p = .015	.126	.769	.405
	48	F(2, 32) = 15.80, p = .001	.034 *	.055	.979
	51	F(2, 32) = 3.55, p = .040	.702	.033 *	.183
	64	F(2, 32) = 5.96, p = .027	.032 *	.011 *	.916
	65	F(2, 32) = 4.87, p = .042	.103	.997	.121
	98	F(2, 32) = 5.02, p = .040	.298	.048 *	.625

Table 4.3 *Detail of ANOVAs showing significant effect of stimulus colour on individual frequency bins for incoherently averaged EEG data with Bonferroni-corrected p-values. Last three columns show post-hoc tests analysing the difference between stimulus colours. Asterisks (*) denote significant differences between stimulus colours.*

Stimulus Frequency (Hz)	*Power Spectrum Frequency (Hz)*	*ANOVA*	*Luminance and S-cone isolating*	*Luminance and red-green*	*Red-green and S-cone isolating*
5	5	F(2, 32) = 8.11, p = .012	.303	.151	.915
	10	F(2, 32) = 7.84, p = .013	.799	.965	.921
	12	F(2, 32) = 5.01, p = .040	.672	.782	.982
	15	F(2, 32) = 9.47, p = .007	.945	.441	.635
	20	F(2, 32) = 6.75, p = .019	.514	.882	.805
	21	F(2, 32) = 3.39, p = .046	.104	.953	.185
12	6	F(2, 32) = 5.88, p = .007	.511	.934	.730
	8	F(2, 32) = 6.96, p = .018	.619	.888	.884
	9	F(2, 32) = 6.17, p = .024	.582	.757	.956
	10	F(2, 32) = 10.04, p = .006	.788	.972	.902
	11	F(2, 32) = 12.23, p = .003	.892	.438	.219
	12	F(2, 32) = 5.53, p = .032	.429	.992	.363
	24	F(2, 32) = 7.38, p = .015	.644	.977	.769
	36	F(2, 32) = 10.07, p = .006	.066	.996	.055

16	8	F(2, 32) = 7.22, p = .016	.853	.819	.998
	10	F(2, 32) = 6.89, p = .018	.607	.718	.982
	15	F(2, 32) = 8.59, p = .010	.986	.910	.966
	16	F(2, 32) = 16.69, p = .001	.174	.809	.461
	18	F(2, 32) = 6.87, p = .018	.644	.856	.929
	24	F(2, 32) = 5.14, p = .012	.150	.272	.939
	32	F(2, 32) = 9.36, p = .007	.739	.839	.983
	40	F(2, 32) = 6.80, p = .003	.915	.917	.999

Table 5.1 *Details of one-sample t-tests comparing BOLD amplitudes of each condition to null for participant ARW.*

Colour	Temporal Frequency (Hz)	V1	V3a	V4
Luminance	*2*	t(16) = 1.71, p = .107	t(16) = 2.35, p = .032	t(16) = 2.29, p = .036
	8	t(12) = 4.19, p = .001	t(12) = 4.59, p < .001	t(12) = 5.10, p < .001
	32	t(12) = 2.68, p = .020	t(12) = 2.65, p = .021	t(12) = 3.91, p = .002
	64	t(15) = 3.39, p = .004	t(15) = 2.56, p = .022	t(15) = 5.10, p < .001

	125	t(14) = 0.39, p = .704	t(14) = 0.79, p = .441	t(14) = 3.71, p = .002
	2 (subthreshold contrast)	t(10) = 1.88, p = .260	t(10) = 3.21, p = .009	t(10) = 3.03, p = .013
S-cone isolating	*2*	t(13) = 4.06, p = .001	t(13) = 5.67, p < .001	t(13) = 8.00, p < .001
	8	t(11) = 2.00, p = .071	t(11) = 2.59, p = .025	t(11) = 4.60, p<.001
	32	t(14) = 1.69, p = .114	t(14) = 1.98, p = .068	t(14) = 2.09, p = .055
	64	t(16) = 3.57, p = .003	t(16) = 2.63, p = .018	t(16) = 2.92, p = .010
	125	t(20) = -0.14, p = .888	t(20) = 0.30, p = .766	t(20) = 0.70, p = .490
	2 (subthreshold contrast)	t(15) = 1.90, p = .077	t(15) = 1.56, p = .140	t(15) = 2.16, p = .048
Red-green	*2*	t(12) = 4.22, p = .001	t(12) = 3.58, p = .004	t(12) = 5.00, p<.001
	8	t(16) = 2.73, p = .015	t(16) = 1.73, p = .104	t(16) = 3.25, p = .005
	32	t(17) = 0.34, p = .735	t(17) = 1.26, p = .226	t(17) = 2.41, p = .028
	64	t(18) = 3.54, p = .002	t(18) = 3.05, p = .007	t(18) = 4.64, p < .001
	125	t(8) = 2.56, p = .034	t(8) = 1.98, p = .083	t(8) = 3.02, p = .017
	2 (subthreshold contrast)	t(14) = 2.21, p = .044	t(14) = 0.73, p = .475	t(14) = 1.35, p = .200

Table 5.2 *Details of one-sample t-tests comparing BOLD amplitudes of each condition to null for participant RE.*

Colour	Temporal Frequency (Hz)	V1	V3	V4
Luminance	*2*	t(10) = 2.46, p = .034	t(10) = 1.88, p = .090	t(10) = 2.27, p = .034
	8	t(13) = 3.09, p = .009	t(13) = 1.93, p = .075	t(13) = 0.67, p = .009
	32	t(13) = 3.02, p = .010	t(13) = 1.38, p = .190	t(13) = 0.85, p = .010
	64	t(14) = 0.29, p = .779	t(14) = 0.28, p = .787	t(14) = 0.02, p = .779
	125	t(14) = 0.39, p = .704	t(14) = -1.66, p = .119	t(14) = 0.58, p = .704
	2 (subthreshold contrast)	t(13) = -1.02, p = .847	t(13) = 2.85, p = .014	t(13) = 3.07, p = .009
S-cone isolating	*2*	t(12) = -1.02, p = .326	t(12) = -1.46, p = .170	t(12) = 0.47, p = .644
	8	t(12) = 2.32, p = .039	t(12) = 0.31, p = .765	t(12) = 0.99, p = .344
	32	t(14) = -0.03, p = .979	t(14) = -0.96, p = .353	t(14) = -1.36, p = .197
	64	t(13) = 1.08, p = .302	t(13) = 0.20, p = .845	t(13) = 0.68, p = .510
	125	t(12) = 0.78, p = .450	t(12) = 1.77, p = .101	t(12) = 2.62, p = .022
	2 (subthreshold contrast)	t(14) = -0.98, p = .343	t(14) = -0.37, p = .717	t(14) = 0.30, p = .769
Red-green	*2*	t(13) = 5.50, p<.001	t(13) = 3.36, p = .005	t(13) = 5.42, p<.001
	8	t(13) = 0.18, p = .864	t(13) = -0.67, p = .518	t(13) = 2.69, p = .019
	32	t(14) = -0.78, p = .447	t(14) = -1.43, p = .174	t(14) = -0.58, p = .568

64	t(22) = 0.63, p = .538	t(22) = 0.74, p = .465	t(22) = 2.13, p = .045
125	t(14) = -0.34, p = .736	t(14) = -0.08, p = .938	t(14) = 1.25, p = .233
2 (subthreshold contrast)	t(14) = 0.06, p = .957	t(14) = 0.12, p = .903	t(14) = 0.73, p = .476

Table 5.3 *Details of one-sample t-tests comparing BOLD amplitudes of each condition to null for participant MS.*

Colour	*Temporal Frequency (Hz)*	*V1*	*V4*
Luminance	*2*	t(11) = 3.61, p = .004	t(11) = 4.59, p < .001
	8	t(15) = 0.11, p = .910	t(15) = 0.30, p = .769
	32	t(11) = 0.44, p = .667	t(11) = 1.54, p = .153
	64	t(15) = -1.94, p = .071	t(15) = -1.74, p = .102
	125	t(14) = 0.82, p = .429	t(14) = 0.90, p = .384
	2 (subthreshold contrast)	t(13) = -0.98, p = .344	t(13) = -0.34, p = .741
S-cone isolating	*2*	t(14) = 0.52, p = .611	t(14) = 2.02, p = .063
	8	t(11) = 0.46, p = .651	t(11) = -0.17, p = .872
	32	t(15) = -1.52, p = .150	t(15) = -0.82, p = .427
	64	t(15) = 0.48, p = .641	t(15) = 0.93, p = .367

	125	t(12) = 0.44, p = .667	t(12) = 0.77, p = .458
	2 (subthreshold contrast)	t(14) = -1.42, p = .177	t(14) = 0.10, p = .926
Red-green	*2*	t(14) = 2.76, p = .015	t(14) = 3.44, p = .004
	8	t(15) = 1.39, p = .184	t(15) = 1.72, p = .106
	32	t(15) = -1.98, p = .066	t(15) = -0.93, p = .367
	64	t(23) = -0.23, p = .818	t(23) = 0.15, p = .882
	125	t(14) = -0.69, p = .499	t(14) = 0.65, p = .526
	2 (subthreshold contrast)	t(14) = 0.12, p = .908	t(14) = 0.37, p = .718

Table 5.4 *Mean and standard deviations of BOLD responses (averaged across all participants) for all stimulus colours, contrast and frequencies in V1, V3a and V4.*

Stimulus Colour	*Contrast*	*Stimulus Frequency (Hz)*	*V1*	*V3a*	*V4*
Luminance	*Subthreshold*	*2*	0.06 (0.03)	0.17 (0.01)	0.13 (0.06)
	Full	*2*	0.24 (0.12)	0.30 (0.18)	0.24 (0.06)
		8	0.24 (0.06)	0.33 (0.04)	0.21 (0.11)
		32	0.18 (0.04)	0.21 (0.04)	0.20 (0.09)
		64	0.11 (0.11)	0.21 (0.03)	0.15 (0.15)
		125	0.05 (0.06)	0.01 (0.10)	0.12 (0.08)
S-cone isolating	*Subthreshold*	*2*	0.02 (0.10)	0.04 (0.12)	0.08 (0.09)
	Full	*2*	0.21 (0.15)	0.24 (0.20)	0.30 (0.13)
		8	0.11 (0.08)	0.16 (0.10)	0.16 (0.14)

Red-green		*32*	0.05 (0.11)	0.09 (0.14)	0.06 (0.12)
		64	0.13 (0.08)	0.18 (0.06)	0.15 (0.06)
		125	0.04 (0.07)	0.14 (0.02)	0.09 (0.10)
	Subthreshold	*2*	0.08 (0.05)	0.10 (0.01)	0.12 (0.04)
	Full	*2*	0.27 (0.06)	0.33 (< 0.01)	0.34 (0.06)
		8	0.15 (0.09)	0.17 (0.10)	0.23 (0.09)
		32	0.06 (0.05)	0.12 (0.08)	0.14 (0.06)
		64	0.14 (0.10)	0.20 (< 0.01)	0.17 (0.12)
		125	0.13 (0.13)	0.15 (0.15)	0.21 (0.11)